THE FLOW BEHAVIOUR OF XANTHAN BIOPOLYMER IN POROUS MEDIA

By

Yaduo Huang B.Sc. M.Eng.

Thesis Submitted for the Degree of Doctor of Philosophy

Department of Petroleum Engineering
Heriot-Watt University
Edinburgh, United Kingdom
June 1993

TABLE OF CONTENTS

LIST OF TABLES

LIST OF FIGURES

NOMENCLATURE

A	column cross-sectional area
ALA	aggregation limited adsorption model
a	particle diameter
a, b	empirical constants
C	polymer concentration
	constant for estimating average hydraulic radius, 25/12
CLA	collosion limited adsorption model
C_0, C_b	injected or bulk polymer concentration
C_{cs}	concentration or solubility of dissolved colloidal species
C_e	equilibrium polymer concentration
C_{ce}	equivalence equilibrium concentration, C_e/R
C_p	polymer concentration
C_w	wall polymer concentration
D	dispersion coefficient
DSM	dissolved species model
D_0	diffusion coefficient
D_r	ratio of polymer to tracer dispersion coefficient
d	particle size
EOR	enhanced oil recovery
F_ϕ	exclusion factor
HPAM	partially hydrolysed polyacrylamide
I	ionic strength
IPV	inaccessible pore volume
K	power law constant
k	permeability
k	depletion concentration constant
k_o	oil phase effective permeability

k_w	water phase effective permeability
k'	Huggins constant
l, L	rod length of xanthan molecule
L	column lenth
	liquid volume or originnal liquid volume
LL	linear layer model
L_b	bulk (after adsorption) liquid volume
L_{dl}	depleted layer liquid volume
M	mobility ratio
	polymer molecular weight
m	mass of ballotini beads
N_A	Avogadro's number, $6.023x10^{23}$
n	power law index
P_e	Peclet number
PRF	Permeability reduction factor, k/k_0
PV	pore volume
PV_p	effective pore volume corresponding to polymer flooding
PV_ϕ	relative exclusion volume, $1-F_\phi$
p	length-to-diameter ratio of rigid particles
Q	volumetric flow rate
R	solid/liquid ratio
R_G	polymer radius of gyration
R_{max}	upper limit of the radius distribution
R_{min}	lower limit of the radius distribution
r	cylindrical pore radius or average hydraulic radius
r^2	regression coefficient
S	solid mass
S/L	solid/liquid ratio
SSA	specific surface area
TF	two fluid flow model

U	average frontal velocity
V, v	total volume of polymer solution
v	frontal velocity
x	collision limited distance
α	apparent shear rate constant
	geometric factor in CLA model
α , β	concentration ratio, C_w/C_b
β	constant in dissolved species model
β'	concentration ratio, C_w/C_b^x
Γ	polymer adsorption level
Γ_0	full polymer adsorption level
Γ_a	average polymer adsorption level
	apparent polymer adsorption level
$\dot{\gamma}$	shear rate
$\dot{\gamma}_{pm}$	porous medium shear rate
ΔP	differential pressure
δ	depleted layer thickness
δ/r	relative depleted layer thickness
ϕ	porosity
ϕ_p	effective porosity corresponding to polymer flooding
η	viscosity
η_0	zero shear rate viscosity
η_{app}	apparent viscosity
η_b	bulk viscosity
η_{in}	injection (inlet) viscosity
η_o	oil phase viscosity
η_{out}	effluent (outlet) viscosity
η_r	relative viscosity
η_s	solvent viscosity

η_{sp}	specific viscosity
η_w	wall viscosity
	water phase viscosity
η_∞	infinite shear rate viscosity
$[\eta]$	intrinsic viscosity
$[\eta]_o$	intrinsic viscosity at low shear rate
$[\eta]_\infty$	intrinsic viscosity at infinite ionic strength
κ	Haring-Greenkorn distribution constant
$\kappa_1, \kappa_2, \kappa_3$	constants in dissolved species model
λ	time constant
λ_o	oil phase mobility
λ_w	water phase mobility
ρ	solid density
σ	value related to the spread of the Haring-Greenkorn distribution function
	specific surface area of solid, SSA
υ	fluid superficial velocity
	viscosity factor
υ_{sp}	specific volume
ξ	constant in dissolved species model

ACKNOWLEDGEMENTS

I am very grateful to my supervisor Prof. Kenneth S. Sorbie for his continuous interest, sincere support, and excellent guidance throughout my study period. His scientific way of thinking, rich experience, strickness to his work and amiability to his students are valuable assets for me in completing this research project.

My sincere thanks are extended to all people both within and outside the Petroleum Engineering Department for their help and encouragement during this study. Special mentions are given to Mr. Walter Crawford, workshop technician at the Department of Petroleum Engineering for the manufacture and maintenance of the test columns and to Mme. Christine Noïk of Institut Français du Pétrole for the preparation and supply of the experimental scleroglucan samples.

I am indebted to Dr. Guy Chauveteau of Institut Français du Pétrole for many interesting and stimulating discussions on this research. Thanks are also given to Dr. Jacqueline Lecourtier of Institut Français du Petrole, Dr. Alistair Fletcher of the Petroleum Science and Technology Institute, Dr. Guy Muller of Universite de Rouen, Dr. Ian Sutherland of Edinburgh University, and Prof Edwin Morris of Silsoe College for their helpful comments on this work.

The financial supports of this project were partly provided by the Petroleum Science and Technology Institute (PSTI), Edinburgh and Institut Français du Petrole (IFP), and are also gratefully acknowledged.

Finally, I express my heartfelt gratitude to my wife, Jin Zhang, and my parents for their warm concern and encouragement, and sincere understanding and support. To them I dedicate this thesis.

ABSTRACT

Xanthan biopolymer solutions have been used on many occasions in enhanced oil recovery operations. The flow behaviour of this biopolymer within the porous medium has a significant bearing on the success of xanthan injection in such processes. This thesis describes some important aspects of the flow behaviour, such as transport, adsorption and rheology, of xanthan biopolymer solution through porous media. Results are related to the depleted layer effect where macromolecules are excluded from the pore wall due to steric hinderance. The experiments include measurement of both the in situ polymer rheology and the advancement of the polymer molecules relative to the tracer in propagation through non-adsorbing or slightly adsorbing ballotini glass bead packed columns. In total, 100 independent experiments have been run and accurate results have been obtained. These results show a clear apparent slip effect on the in situ rheology of the xanthan which is consistent with the observed exclusion factors in the transport behaviour. The rheological data was analysed using a simple mathematical expression (the *two fluid model*) as well as a analytical model (the *linear layer model*). The results indicate that the depleted layer thickness is affected more or less by polymer concentration, pH and salinity. Xanthan static adsorption level is much higher than dynamic adsorption and the adsorption effect on its in situ rheology is not important. This thesis also presents work on another biopolymer, scleroglucan, which displays different flow behaviour from xanthan in some respects.

CHAPTER 1

INTRODUCTION

Polymer enhanced oil recovery is one of a number of ways to produce the oil remaining trapped after primary and secondary recovery processes. The development of polymer enhanced oil recovery is strongly dependent on both thchnical and economic considerations. However, it is generally recognized that oil will remain a major and difficult-to-replace source of energy. As a consequence, the development of polymer enhanced oil recovery technology appears to be quite probable, in so far as significant technical advances continue to improve its efficiency.

Most principles applied in polymer enhanced oil recovery have been known for a long time. Numerous laboratory studies and field pilots have been carried out especially over the last two decades. This has resulted in a great increase in knowledge and the understanding of mechanisms involved in polymer enhanced oil recovery processes. However, many problems still remain to be solved. One very important aspect which must be understood in more detail is the flow behaviour of polymer solutions through porous media. As might be expected, the molecular structure plays an important role in determining the in-situ flow behaviour. Another important factor is the microscopic structure and geometry of the porous medium itself. Clearly, the flows through a porous medium will be much more tortuous and complex than those found in rheometers where flows are well-defined.

In this work, some important aspects of the flow behaviour of non-Newtoian xanthan and scleroglucan biopolymer solutions through porous media are investigated and studied experimentally and theoretically. Most work is performed with xanthan samples and ballotini glass bead packed columns although some results on scleroglucan are also

presented. Many new findings and interesting results are presented in the thesis and these are summarised briefly as follows.

Following this chapter, Chapter 2 reviews the published literature on the flow behaviour of xanthan biopolymer through porous media which gives a general context for the work which is presented later.

A description of the experimental materials and apparatus used in this work is given in Chapter 3. A new method for determining biopolymer concentration is introduced by measuring the polymer Newtonian bulk viscosity. Also a modified method is developed to measure the surface charges on ballotini glass beads. Another new observation in this chapter is that the Huggins constant of the polymer solution is found to be very sensitive to the method of fitting the rheological data. A systematic experimental procedure for measuring the in situ biopolymer rheology is developed and described in this chapter.

The effect of xanthan concentration on its flow behaviour in porous media is studied in Chapter 4. The main finding is that the apparent depleted layer thickness determined by different theoretical models decreases with increasing xanthan concentration over the low concentration range and tends to a constant value at higher concentration. Some interpretation of this result is presented.

Chapter 5 focuses on the effect of pH and salinity on xanthan flow behaviour through porous media. The most important results display the dependence of relative depleted layer thickness on pH and salinity which relate to the xanthan conformation and the surface charge on the pore wall.

Xanthan adsorption at the solid-liquid interface and adsorption effects on in situ rheological behaviour are discussed in Chapter 6. Several models are proposed for explaining the effect of solid/liquid ratio on adsorption level. The effect of xanthan dynamic adsorption on in situ rheological behaviour is not very significant.

The flow behaviour of a nonionic polysaccharide, scleroglucan is investigated in Chapter 7 where it is compared with xanthan flow behaviour. Scleroglucan shows a much higher dynamic adsorption level, not very important concentration effect and ignorable pH influence. The apparent slip effect is clearly visible. A number of results on scleroglucan flow in sandpacks are also presented.

The overall conclusions of this study are given in Chapter 8, although the staged conclusions are also shown at the end of each chapter. The many interesting findings lead to a number of recommendations for future work which are also suggested in this chapter.

CHAPTER 2

A REVIEW ON THE FLOW BEHAVIOUR OF XANTHAN BIOPOLYMER THROUGH POROUS MEDIA

2.1 Introduction

Xanthan biopolymer solutions have been applied in enhanced oil recovery (EOR) operations where low concentrations of high molecular weight polymer are added to the displacing fluid in order to increase its viscosity and hence improve the efficiency of oil displacement. The xanthan biopolymer system has several unique properties for oilfield application, such as good injectivity arising from its pseudoplastic behaviour, good thermal and mechanical stability, and a relative insensitivity of viscosity to salinity. With the growing role for biopolymer solutions in EOR processes, it becomes increasingly important to develop an accurate description of the flow characteristics and rheological behaviour of such solutions in porous media. In principle, this behaviour can be determined in flow experiments using consolidated porous rock or unconsolidated bead or sand packs. However, the interpretation of the experimental results is complicated by the influence of several factors, such as non-Newtonian flow behaviour of polymer fluids (Savins, 1969; Bird et al, 1987), pore size/heterogeneity (Chauveteau, 1982), viscous and transport effects in the propagation of polymer slugs (Sorbie et al, 1987; Kolodziej, 1988), potential plugging of the pores by microgel existing in commercial xanthan solutions (Kohler and Chauveteau, 1981; Chauveteau and Kohler, 1984; Kolodziej, 1987), and the effect of polymer retention (Sorbie, 1991).

In this chapter, the important aspects of xanthan flow behaviour in porous media will be reviewed briefly, which relate to xanthan transport, retention, and rheology in porous media. The rheological behaviour of polymer solutions within the porous medium is

refered to in this thesis as the solution *in situ rheology*. In addition, the basic concepts of polymer enhanced oil recovery are also discussed. It is necessary to understand these aspects of xanthan flow in porous media in order to have access to an oil recovery process using this polymer.

2.2 Polymer Enhanced Oil Recovery

It is generally recognized that oil will remain a major and difficult-to-replace source of energy and the leading energy source at least during the first half of the 21st century. However, after the application of primary oil recovery (by natural reservoir pressure depletion) and secondary oil recovery (usually by waterflooding), much oil still remains in a reservoir. That is, these now conventional techniques still leave in the ground about two-thirds of the original oil in place (OOIP). This is an enormous incentive for development of enhanced methods, i.e. techniques for improving displacement efficiency or sweep efficiency, of recovering this remaining oil. The use of such techniques is called enhanced oil recovery (EOR). Overall reviews of EOR are presented in books by Lake (1989) and Baviére (1991), and a specific review of polymer flooding is given by Sorbie (1991).

To analyze the way in which EOR methods operate, two separate aspects of oil recovery efficiency are normally distinguished: (1) the displacement efficiency of oil at the pore scale, and (2) the sweep efficiency at the macroscopic scale. Figure 2.1 summarizes the main EOR methods (chemical, miscible and thermal methods) which are usually used to improve the oil displacement efficiency or/and the sweep efficiency. Some EOR methods act mainly on one of these aspects of oil recovery efficiency while others act on both aspects. Polymer flooding, for example, mainly affects the sweep efficiency at a macroscopic scale by increasing the displacing fluid viscosity, although in author's opinion (Huang et al, 1989) polymer might also be used to enhance the displacement efficiency of oil in some cases.

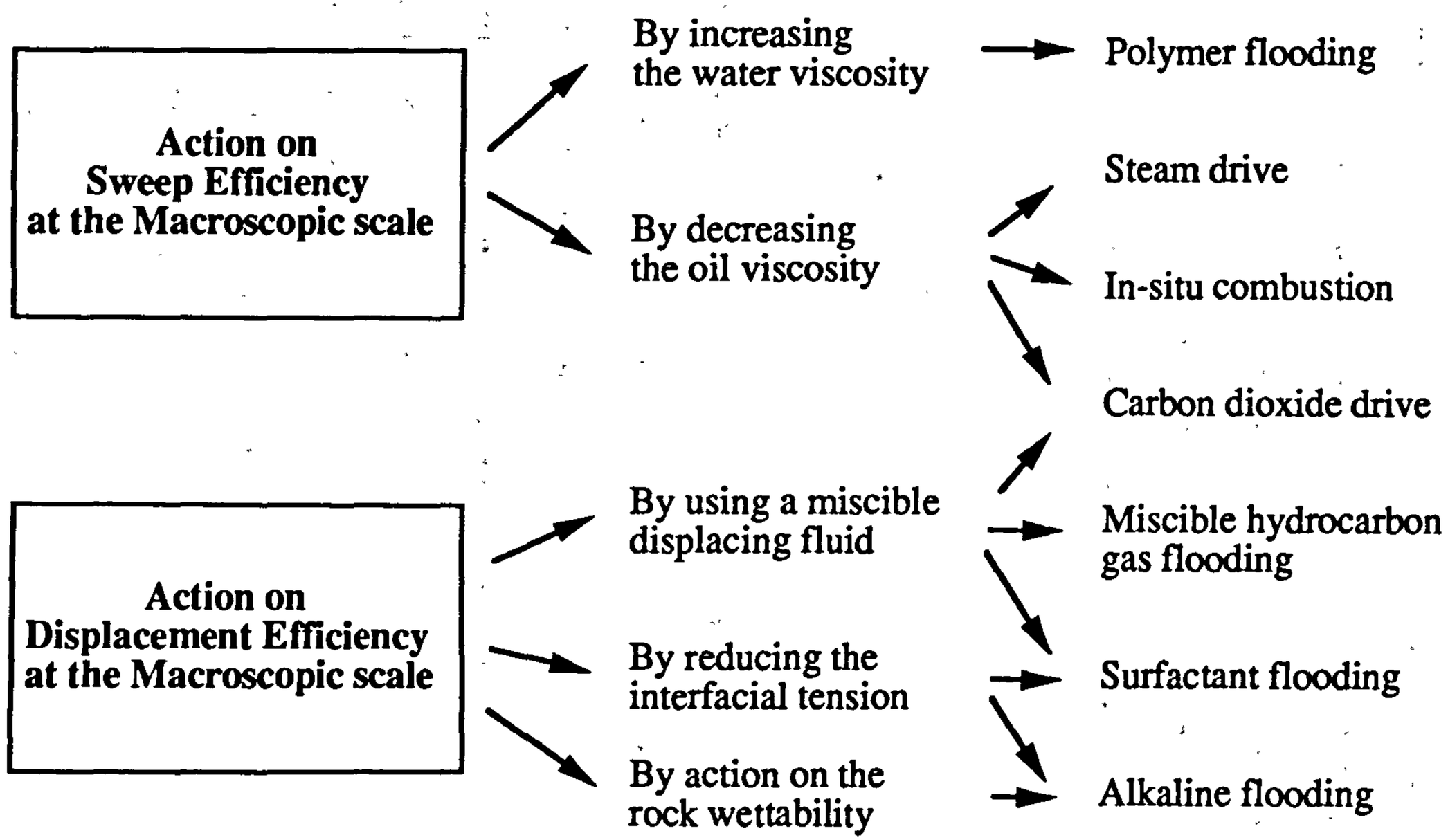

Figure 2.1 Factors on which the main types of enhanced oil recovery methods act.
(From Marle, 1991)

Polymers were first suggested as a means of increasing the flooding water viscosity and, also of reducing formation permeability in the early 1960s (Pye, 1964; Sandiford, 1964 and Gogarty, 1967). Since that time, a large number of polymer field applications have been carried out with varying degrees of success especially during the 1960s and 1970s (Chang, 1978). A series of novel polymers for oil recovery application have been developed and the understanding of phenomena related to polymer behaviour in the field of EOR has been greatly improved during the last two decades. At present, for many reservoirs, polymer flooding can be used without excessive risk and this process may now, in some circumstances, be economically attractive. Indeed, polymer flooding is the most successful EOR method in the whole chemical flooding "family" up to now. However, progress still remains to be achieved; additional laboratory studies, research in applied chemistry and field experiments are needed in order to decrease the technical risks, improve profitability, reduce operating costs, and to extend the range of applicability of the process.

When waterflooding a reservoir proves to be inefficient, in the sense that there is early water production and low oil recovery at breakthrough, polymer flooding may be considered as a possible remedy. Oil is left behind in a waterflood either because it is trapped by the capillary forces (residual oil) or because it is in some way bypassed. The bypassed oil may arise due to the unfavourable mobility ratio in the flood or the large-scale heterogeneity in the reservoir so that a poor linear, areal and vertical waterflooding efficiency may occur. The target for polymer flooding is mainly considered to be any oil that is bypassed in the waterflood. That is, the application of polymers may be considered for both unfavorable mobility ratio waterfloods and/or in reservoirs where there is excessive heterogeneity.

Central to all polymer oil recovery mechanisms is the idea of mobility ratio, M, defined as:

$$M = \frac{\lambda_o}{\lambda_w} = \frac{(\eta_o / k_o)}{(\eta_w / k_w)} \qquad [2.1]$$

where λ, η and k are mobility, viscosity and effective permeability respectively and the subscripts o and w refer to oil and water. For an unfavourable mobility ratio waterflood (M>1), the role of polymer is basically to remedy the poor waterflooding situation by reducing M. Polymer increases the aqueous-phase viscosity and may decrease the permeability to the aqueous phase. This improves the inefficient microscopic (linear) displacement efficiency for M>1, and inefficiency in the areal sweep of the waterflood as a result of (immiscible) viscous fingering, thus leading to improved oil recovery. For excessive reservoir heterogeneity, Polymers can act through a combination of two mechanisms (Chauveteau and Sorbie, 1991; Sorbie, 1991) as follows:

(1) mobility control in which the polymer slug viscosity changes fluid flow patterns within the reservoir;

(2) adsorption, leading to local reductions in permeability, which again alter fluid flow.

These effects may lead to an improvement of waterflooding performance in highly heterogeneous (layered) reservoirs. In particular, polymer can reduce the harmful effects of high-permeability layers in a vertically stratified system and so reduce watercut and improve vertical sweep efficiency.

The two most commercially used polymers in EOR applications are the synthetic material, polyacrylamide, in its partially hydrolysed form (HPAM) and the biopolymer, xanthan. Polymer molecules are long chains of repeating units (monomers) linked by covalent bonds. Figure 2.2 displays both the primary chemical structures of HPAM and xanthan. HPAM has a flexible coil structure in aqueous solution. It has been used in oil recovery processes far more frequently than xanthan biopolymer due to its longer history of use and its relative low cost. Like xanthan, HPAM is a polyelectrolyte, and as such it will interact quite strongly with ions in solution. However, since the polyacrylamide chain is

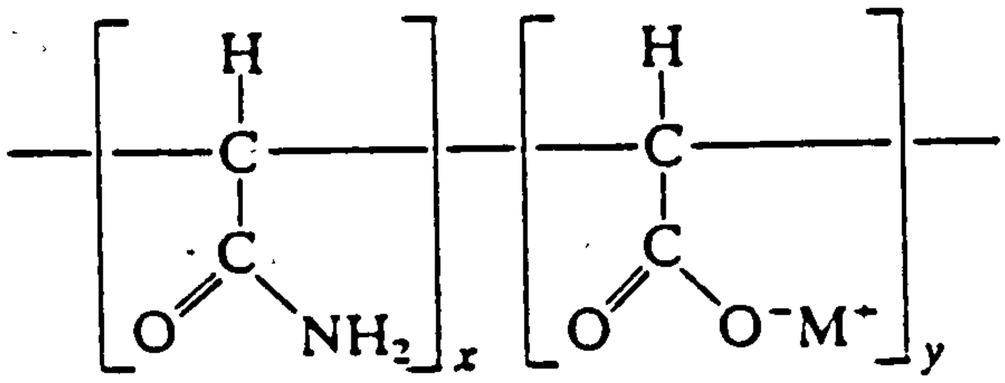

(a) Chemical structure of HPAM

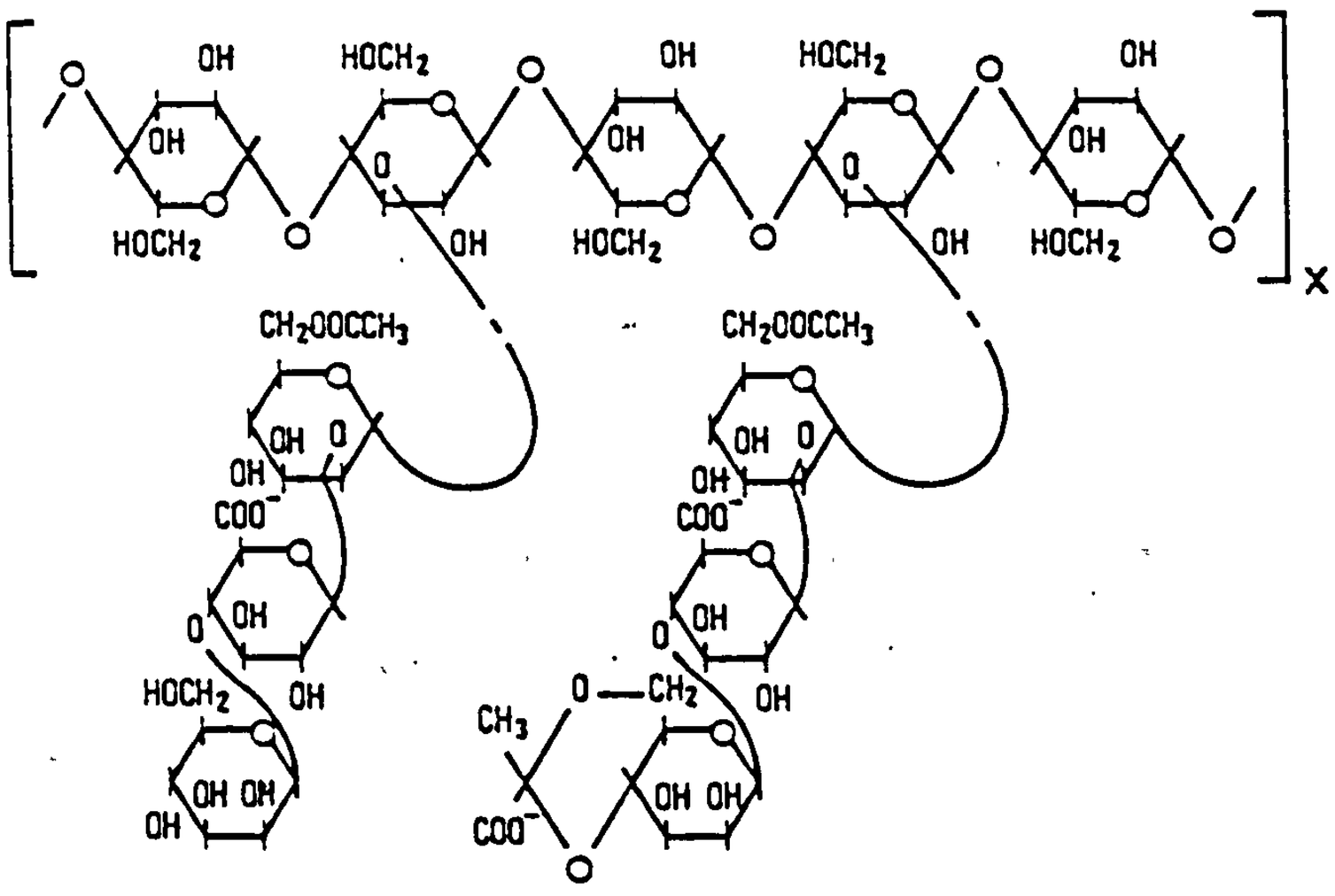

(b) Chemical structure of xanthan

Figure 2.2 The primary chemical structures of HPAM and xanthan

flexible, it may respond much more to the ionic strength of the aqueous solvent, and its solution properties are much more sensitive to salt/hardness than are those of xanthan.

Xanthan biopolymer shows the characteristics of a more rigid molecule. It is produced by the micro-organism xanthomonas campestris. The higher order molecular stucture has most bearing on the solution properties of the polymer. In the simplest model, xanthan has been considered to be a rigid rod (Rinaudo and Milas, 1978; Whitcomb and Macosko, 1978). The relative insensitivity of xanthan flow behaviour to temperature, pH and ionic strength of solution (salinity/hardness) is expected for a rigid rod, in contrast to the behaviour of random coil HPAM molecules. The strong pseudoplastic behaviour is also expected for long rod-like molecules. Other types of polymers have been proposed for use in high temperature and high salinity environments. Among these polymers, scleroglucan, a nonionic polysaccharide with a triple-stranded conformation (Rivenq et al, 1989) seems to be the most promising and part of this work will study this polymer.

In the follow sections of this chapter, the flow behaviour of xanthan biopolymer through porous media will be reviewed. A thorough discussion may be found in Sorbie's book (1991) which provides a detailed state-of-the-art review of polymer-improved oil recovery.

2.3 Xanthan Retention in Porous Media

When xanthan solution is injected into a reservoir, there may be significant interactions between the transported xanthan molecules and the porous medium. Such interactions will cause the polymer to be retained by the porous medium. Polymer retention has two main effects: (1) a decrease in the concentration of flowing polymer and in the velocity of the polymer front, and (2) a possible reduction in the permeability of rock where polymer is retained. The first effect is always detrimental to polymer flooding efficiency whereas the second is sometimes expected to be beneficial since it contributes to the reduction of the mobility of both the polymer slug and chase brine. Generally, polymer retention will

reduce the efficiency of the polymer flood despite the potential permeability reduction contribution. In fact, the level of polymer retention is one of the key factors in determing the economic viability of a polymer flood (Sorbie, 1991).

Three main mechanisms, as shown schematically in Figure 2.3, can lead to the retention of macromolecules in flow through porous media: (1) polymer adsorption, (2) mechanical entrapment, and (3) hydrodynamic retention. Although a clear distinction of the contributions from the three mechanisms cannot be made, the contribution from adsorption is a key mechanism that is relevant in well-dispersed polymer solutions. More recently, a wide variety of polymer retention mechanises have been identified and discussed (Chauveteau et al, 1991).

A fairly limited amount of data is available on xanthan adsorption in the oil literture. It seems that xanthan adsorption in porous media is rather less than that of HPAM and also tends to show less sensitivity to the salinity/hardness condition of the solvent. For comparison, the xanthan retention levels obtained by Sorbie et al (1987) in high permeability Clashach sandstone cores (0.8 to 1.8 D) range from 0.2 to 3 μg/g of rock. Those measured by other workers (Lecourtier and Chauveteau, 1985; Chauveteau and Lecourtier, 1988) for a sand pack with 2% clay and for pure sand pack were 28 and 5.4 μg/g of rock, respectively. Recent results from Huang and Sorbie (1992) showed that in high permeability (~ 1 D) and relative homogeneous ballotini glass bead pack, the xanthan loss is about 5 μg/g and is not significantly changed by salinity variation (0.1 to 35 g/l NaCl). Polymer retention in porous media of such high permeability should be due mainly to adsorption. However, the retention of xanthan biopolymer in field tests has been found to be significantly highter than expected from conventional analysis of core flood data. For example, in a surfactant-polymer flood pilot test operated at the Loudon field, Illinois (Reppert et al, 1990), xanthan biopolymer was injected and exhibited significantly higher retention by the reservoir than did the surfactant. The poor propagation, at least over the relatively short pilot distances, did not adversely affect process performance and the whole pilot test was successful. The recent result reported

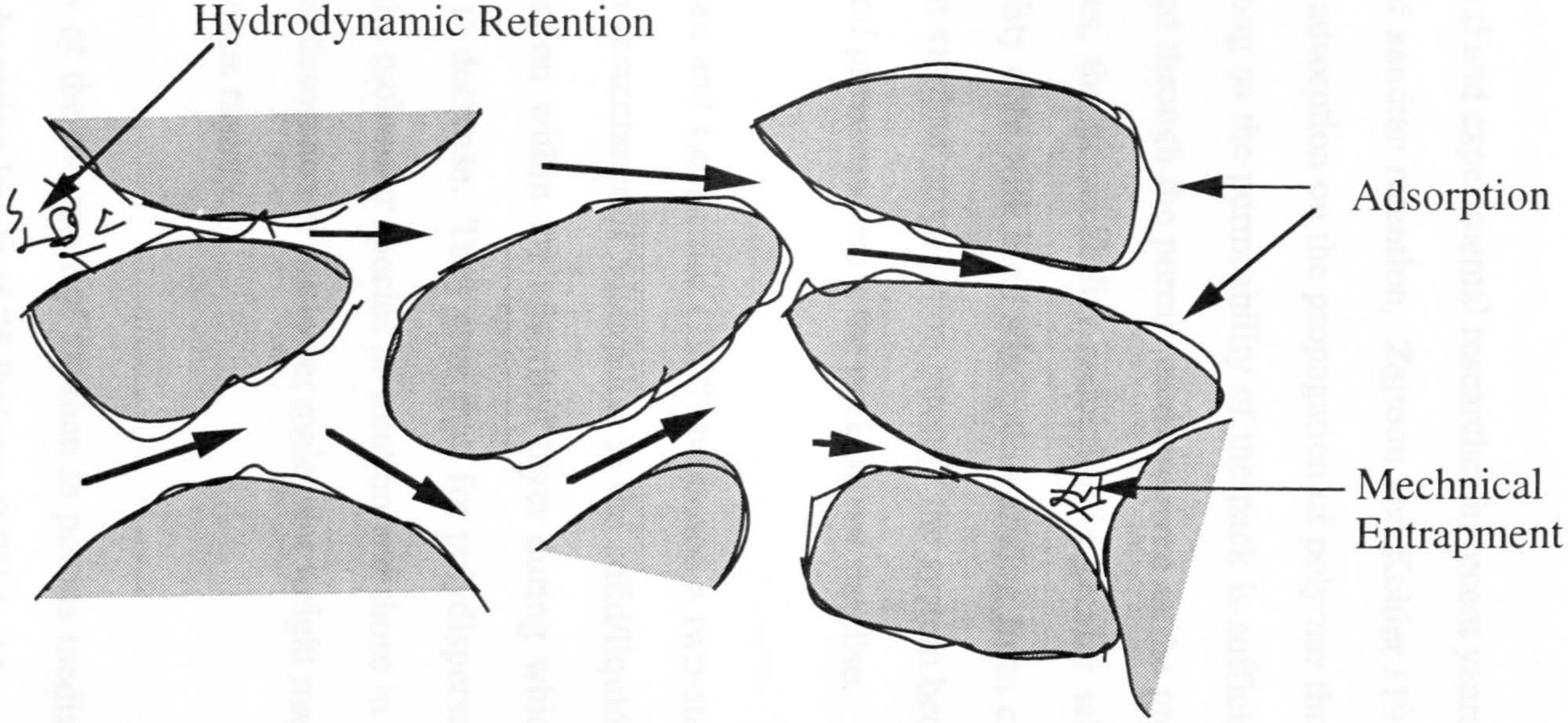

Figure 2.3 Schematic diagram of polymer retention mechanisms in porous media

by Littmann et al (1992) seems more encouraging. The polymer flood pilot project performed in the Eddesse-Nord sandstone reservoir (Germany) can be regarded as successful in terms of injection and production performance. Reservoir simulation results as well as laboratory studies have shown an adsorption of xanthan of 30-40 μg/g. The xanthan produced in one well, after it had been in the reservoir for about three years, showed no degradation.

Theoretical and experimental researches in recent years have displayed many interesting aspects of xanthan retention. Zaitoun and Kohler (1987) studied the effect of xanthan dynamic adsorption on the propagation of polymer through porous media. They found that, as long as the permeability of the pack is sufficiently high, the polymer is easily propagated through the porous medium even in the present of clays. However, even in such cases, the permeability reduction is greater when clays are present. In low-permeability core with high adsorption arising from clays, Zaitoun and Kohler (1987) found that xanthan propagation through the system becomes very poor and the effluent profiles and pressures across the pack do not stabilise.

Chauveteau and Lecourtier (1988) proposed a two-stage polymer adsorption process: firstly, an instantaneous adsorption at the solid/liquid interface followed by a slower reorganisation within the adsorbed layer during which the thickness of this layer is expected to decrease. They note that, for polydisperse polymers, there is an exchange between the molecular species in solution and those in the adsorbed layer, resulting in a preferential desorption of the lower molecular weight macromolecules which were initially adsorbed quite rapidly.

In a study of the transport of xanthan in porous media, Kolodziej (1988) obtained the xanthan adsorption levels of 75 lbs/acre-ft PV (~ 11 μg/g) at 100% brine saturation and 40 lbs/acre-ft PV (~ 6 μg/g) at residual oil. He conjectured that the somewhat unexpected lower level of xanthan adsorption at residual oil saturation may result from pore wall exclusion effects. Similar work was carried out by Lund and coworkers (1991). They

measured the retention of a xanthan biopolymer in Brent shaly sandstones. The cores were cleaned with different solvents and therefore had different wettabilities. They were then flooded to residual oil saturation with crude oil. In a core rendered oil/mixed wet by cleaning with depolarized kerosene, a retention as low as 5 μg/g was measured, while retention increased to 30 μg/g in a similar core rendered water-wet by cleaning with toluene and methanol. In the latter core (same type of cleaning), the absence of oil led to a retention as high as 50 μg/g. These effects may be explained (Broseta et al, 1992) in terms of water/rock and water/oil interfacial area distribution within the pore space, which is governed by wettability. In water-wet cores, droplets of residual oil offer an additional adsorbing surface to the polymer, whereas in oil-wet cores the oil wetting film offers the polymer a small adsorbing surface compared to the no longer accessible rock surface. Broseta et al (1992) found that adsorption increases with surface hydrophobicity, with the effect being stronger for polysaccharides (xanthan) than for anionic synthetic polymers (HPAM). From their results, xanthan adsorption levels increase greatly after substrate silanation, from 11 μg/g to 73 μg/g, in 100 % brine saturated (20 g/l NaCl) porous media. If the ideas of Broseta et al (1992) are correct, then, in Kolodziej's experiments (Kolodziej, 1988) mentioned above, the core wettability should have been changed to somewhat oil-wet after oil saturation. Reservoir wettability should be taken into account when planning a polymer flood, as polymer loss by retention seems to be significantly affected by wettability.

Huh et al (1990) developed a kinetic expression for polymer retention. First, a pore-level description of the polymer trapping phenomenon in a simplified model porous medium was attempted. Based on these pore-level considerations, a phenomenological polymer retention model was then proposed that accounted for both the adsorption of polymer molecules on rock surfaces and the mechanical entrapment in pore matrices. This model can be used to predict the effect of parameters such as flow rate and polymer concentration on retention. Finally, the validity of the model was tested by comparison with experimental data on the transport of xanthan biopolymer through low-permeability

sandstones. They generally supported the proposed model as a reasonable representation of the retention phenomenon.

In the measurements of polysaccharide polymer properties in porous media, Fletcher et al (1991) found polymer retention was a function of polymer type and molecular association. Polymer retention is also strongly dependent on rock type and preparation procedures. The total retention levels of xanthan (Flocon 4800MXC) are reported as ~40 μg/g in Berea core and < 10 μg/g in Clashach core with 100% sea water saturation; and 35-50 μg/g in Brent reservoir core with residual oil saturation. The significant retention of unfired Berea compared with Clashach was attributed to the higher clay content of Berea. The effect of Residual oil saturation is not very clear on xanthan retention, but very marked on polymer reological behaviour in porous media. They thought that inaccessible pore volume (IPV) should be measured so that corrections to the polymer retention can be made especially in low retention coreflood systems.

Chauveteau et al (1991) overviewed the mechanisms of polymer retention in porous media. They proposed that flow-induced retention may affect polymer propagation through reservoir more significantly than pure adsorption. A new and more precise terminology is introduced to make the distinction between the different types of retention which have their own characteristics and sensitivity to various parameters, in which the classification are described by fifteen different mechanisms based on both the location (in bulk flow, at the interfaces and in pore constrictions) and the nature of the dominant concerned phenomenon (hydrodynamic, physico-chemical or steric).

Very recent work by Huang and Sorbie (1992) concentrated on xanthan dynamic adsorption and its effect on the in situ polymer rheology in porous media. They found that xanthan dynamic adsorption process is fairly slow, and the adsorption levels are lower and not noticeably changed with salinity. However, the adsorption levels were much higher for higher xanthan concentration (21 μg/g for 400 ppm sample compared to ~ 5μg/g for 100 ppm samples). Experimental results also showed that the effect of

xanthan adsorption on in situ rheological behaviour is not very significant, which indicates that, when xanthan molecules adsorb onto the pore walls, the hydraulic radius of the porous medium is not very considerably affected and, therefore, that the rigid xanthan molecules are adsorbed very flat up against the pore wall.

To design a polymer project and assess its economic viability, it is necessary to estimate the polymer retention level in the native rock at deep reservoir flow rates. Goodyear et al (1992) recently tried to develop a pyrolysis/beta scintillation counting technique for the measurement of xanthan biopolymer retention levels in sandtone rock samples. The ^{14}C-labelled polymer used in such measurements must exhibit the same retention properties as the polymer to be used in the field. However, the xanthan used in their study does not meet this requirement, therefore a new source of ^{14}C-labelled xanthan is required. They thought this technique is a viable method for the measurement of ^{14}C retention levels in sandstone cores in the presence of residual oil.

Finally, xanthan plugging behaviour in porous media is mentioned here. This is not a mechanical entrapment problem although mechanical entrapment is a filtration-like mechanism in which the larger polymer species are thought to be "strained out" in the smaller pores. Formation plugging is characterized as causing a decrease in injectivity, which exceeds that due to the lower polymer mobility. This formation plugging can be attributed either to residual bacterial cell debris coming from the fermentation process or to multimolecular aggregates of biopolymer molecules known as microgels. The first cause are better understood, and post-mixing treatments have been devised to alleviate this. The second cause, microgels, has been given more attention in the last decade. Kohler and Chauveteau (1981) compared the flow properties of various industrial products or laboratory samples through porous media. The best way, they thought, to avoid plugging phenomena was through the use of fermentation broths specially prepared rather than powder form polymer for enhanced oil recovery and to inject them after dilution and clarification. In their later work (Chauveteau and Kohler, 1984), an efficient laboratory filtration technique was developed for removing all the microgels existing in an industrial

fermentation broth. Microgel plugging behaviour was illustrated by Chauveteau and Kohler (1984) using various types of porous media ranging from Millipore filter membranes to sandtone cores. Their work has also shown that microgels can significantly alter the rheological behaviour of the xanthan solutions in low permeability porous media. Kolodziej (1987) investigated the effects of brine salinity, enzyme treatments, core floods, added surfactants, various isopropyl alcohol precipitation and drying treatments, and different protein removal treatments on the formation of microgels. A consistent mechanism of microgel formation was proposed, which involves a salinity-induced association between denatured proteins and biopolymer molecules. These denatured protein-biopolymer molecule associations establish nucleation sites for the biopolymer molecules to form a microgel aggregate. It is clear, if the polymer sample contains microgels, a gel-like cake can be formed on the core inlet and even inside pore structure, possibly leading to severe core plugging. A polymer that demonstrates such properties should not be selected for field polymer flooding.

2.4 Xanthan Transport in Porous Media

A knowledge of the polymer transport properties in porous media is important for the prediction of polymer flooding. The transport of small noninteracting molecules or tracers is generally described by the convection-dispersion (CD) equation (Fried and Combarnous, 1971; Van Geneuchten, 1981), as follows:

$$\left(\frac{\partial c}{\partial t}\right) = D\left(\frac{\partial^2 c}{\partial x^2}\right) - \upsilon\left(\frac{\partial c}{\partial x}\right) \qquad [2.2]$$

where c is the solute concentration (g/cm^3), D is the dispersion coefficient (cm^2/s) and υ is the fluid superficial velocity (cm/s). However, to describe the transport of polymer, several extensions to equation 2.2 are required to take into account the following phenomena: (1) hydrodynamic dispersion, (2) excluded / inaccessible pore volume (IPV) effects, (3) Adsorption/retention, (4) Viscous fingering, (5) Non-equilibrium behaviour, (6) permeability heterogeneities, and (7) polydispersity. It has been found that terms

describing these effects may be included in generalised convection-dispersion equations which appear to give a satisfactory macroscopic description of the processes in that they reproduce the main features observed in laboratory core flood experiments.

Van Genuchten (1981) reported a least-squares computer model which provides a convenient, efficient and accurate means of fitting various transport parameters to column effluent data. Both equilibrium and non-equilibrium type transport models can be used alternatively in the curve-fitting program. The conceptually more complex non-equilibrium models may contain up to four unknown parameters if only the break-through side of the effluent curve is considered. Van Genuchten (1981) focused on solute transport in soils for agricultural science application but the approach has been used widely to analyse several aspects of polymer transport through porous media.

An extensive experimental and theoretical study was presented by Sorbie et al (1987) on the single-phase flow of xanthan/tracer slugs in a consolidated sandstone. The phenomena studied include almost all of the main effects on polymer transport through porous media, such as polymer/tracer dispersion, excluded/inaccessible-pore volume, and viscous fingering, as well as nonequilibrium effects in some floods. Macroscopic flow equations were derived that considered terms to model all of the behaviour listed adove. Sorbie et al (1987) also developed a microscopic approach to describe certain features of polymer flow in porous media.

Research on xanthan transport in porous media has in recent years focused on several topics. One of them is the hydrodynamic dispersion effect. Dispersion, as defined by Fried (1975), is the occurrence and evolution of a transition zone between two domains of a fluid phase with different composition. Most of experimental results have shown that the dispersion coefficient of polymer is larger than that of tracer over a range of flow rates. Sorbie et al (198^{7}) found that, at 100% brine saturation in the core, polymer dispersion is consistently above that of the chloride tracer by a factor of between 2 and 4, both for high-(400 mg/l) and low-(50 mg/l) concentration xanthanfloods. A typical

example of their results is shown for a low-concentration pulse of polymer solution labelled with ^{36}Cl in Figure 2.4. Kolodzjej (1988) found in his experiments that the dispersion of xanthan biopolymer solutions in 100% brine and residual oil Berea core floods is greater than that of a solvent tracer. Sorbie and Huang (1991) noted that the xanthan dispersion coefficient is greater than that of the tracer by a factor of ~2 or more in the low concentration region of 30 to 100 ppm. They also found a ratio of polymer to tracer dispersion coefficient by a factor of around 2 to 3 at various pH (1 to 10) in analysing the experimental transport results by fitting the effuent profiles to analytical solutions of the 1D convection-dispersion equation (van Genuchten et al, 1982; Sorbie et al, 1987).

Lecourtier and Chauveteau (1984 b) thought that hydrodynamic dispersion increases the spreading out of the concentration profile at both the leading and trailing edges of the slug. Hydrodynamic dispersion depends on both porous media properties (packing quality and grain diameter distribution) and flow rate through the Peclet number $P_e=vd/D_0$, where v is the frontal velocity, d is the particle size and D_0 is the diffusion coefficient. In Kolodzjej's opinion (1988), the above results are consistent with the polymer being a flow regime at a much higher Peclet number than the tracer, which results from the extremely low molecular diffusion coefficient of the polymer. The explanation for the larger dispersion coefficient of the polymer compared with that of the tracer is thought to be due to the magnitude of molecular diffusion constant and is explained in a recent paper by Sorbie and Clifford (1991). In this paper, a network model describing the transport statistics of both polymer and tracer has been constructed, in which the proper allowance has been made with the very different magnitudes of the molecular diffusion constant: for xanthan $D_0 = 2.5 \times 10^{-8}$ cm^2/s, and for chloride $D_0 = 2.0 \times 10^{-5}$ cm^2/s. The fact that the molecular diffusion constant of the xanthan is about three orders of magnitude less than of the tracer, thus implying that the macromolecules and the tracer particles are in quite different local flow regimes as decribed by the local Peclet number, and hence their transport statistics through the porous medium are rather different.

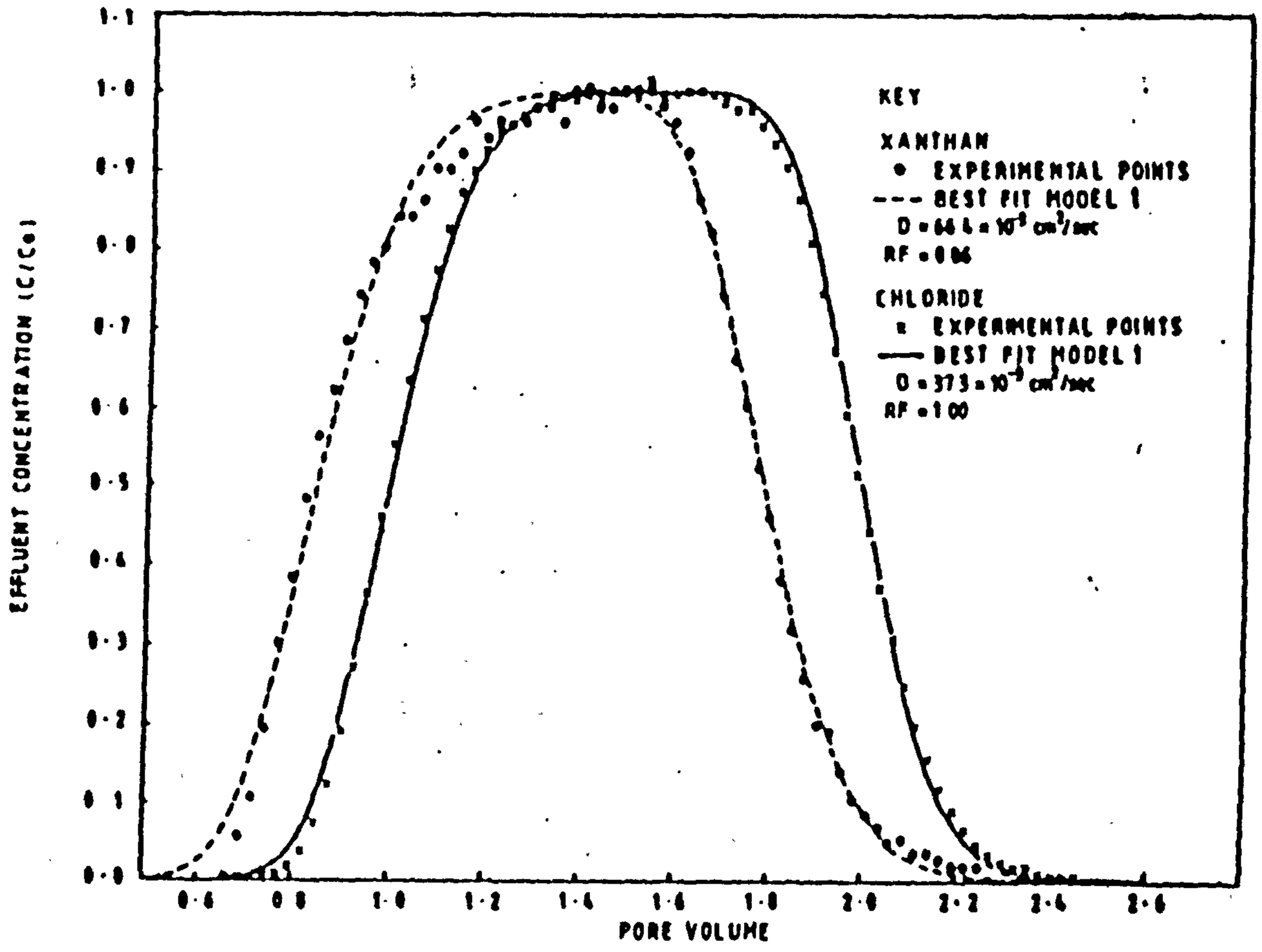

Figure 2.4 Effluent profiles for a 1-pv slug of 50 ppm xanthan in brine labelled with ^{36}Cl through a 1-m sandstone core (From Sorbie et al., 1987)

Another important aspect for xanthan transport through porous media is excluded / inaccessible pore volume effects. For example, the velocity of polymer molecules through porous media generally differs from that of inert tracer species such as lithium. Many observations have confirmed that, in non-adsorbing (or "satisfied adsorption-level") porous media, the polymer propagate consistently faster than the tracer. An example of this polymer velocity enhancement can be seen in Figure 2.4 for a low-concentration xanthan/tracer pulse. This has been explained in the literature by the following two possible mechanisms:

(i) Inaccessible pore volume effect (IPV) (Dawson and Lantz, 1972; Shah et al, 1978; Liauh et al, 1982); in this view, the polymer is thought to be too large to enter certain of the smaller pores and hence a fraction of the pore space - both in these smaller pores themselves and those larger pores to which they give access - is not accessible to the macromolecules. This phenomenon was originally reported in the oil literature by Dawson and Lantz (1972), who called it "inaccessible pore volume" (IPV). Gupta and Trushenski's results (1978) indicated that the polymer/chase-water mixing-zone volume at a given mobility ratio is the same for glycerine (classical miscible fluid), biopolymer, and polyacrylamide. However, the propagation rate of the mixing zone is much higher for polymer than for glycerine because of IPV. IPV increased as polymer concentration decresed over the investigated range. A micellar fluid ahead of the polymer bank increased IPV. Kolodziej (1988) investigated the effects of IPV in a two-phase xanthan biopolymer flooding experiment in an initial oil-saturated core. He obtained IPV values in the range 12-26 % PV in oil-free and residual oil Berea core floods. These values were found to decrease with increasing polymer concentration, and were greater in the residual oil core floods than in the 100% brine core floods. Kolodziej (1988) thought that the IPV concentration dependence may be due to a decrease in molecular size of the biopolymer, or the more uniform non-Newtonian flow field with increasing polymer concentration. He believed that the greater IPV values for the residual oil floods is due to the polymer flow being restricted to smaller pores in a residual oil Berea core, which increase the IPV.

It is possible that the IPV mechanism may operate in very low permeability porous media where some of the pores are extremely small.

(ii) Surface exclusion / depleted layer effect (Auvray, 1981; Chauveteau and Zaitoun, 1981; Lecourtier and Chauveteau, 1984); in this model, the polymer is viewed as being sterically excluded from the pore wall. Essentially the macromolecule has more orientational entropy in the central streamlines of a narrow channel than close to the wall as shown in Figure 2.5. Since the streamlines away from the wall are associated with the higher velocities, the polymer tends to move on average faster than any tracer species, which may be distributed evenly over all streamlines flowing through the pore. Although this mechanism will be present in all porous media irrespective of pore size, the surface exclusion phenomenon is of particular significance when the dimensions of the macromolecule approach those of a typical pore size. The effect has been reported by Chauveteau and coworkers in the analysis of several experiments in both non-adsobing (Chauveteau, 1982; Chauveteau and Zaitoun, 1981; Lecourtier and Chauveteau, 1984) and adsorbing (Chauveteau et al, 1984; Chauveteau, 1986) porous media. Sorbie et al. (1987) studied two different xanthan polymers with different effective rod lengths of about 0.5 and 1.0 μm in higher permeability outcrop sandstone cores (850-1850 md) and enhancements of between 6 and 17% were observed. Larger velocity enhancements were observed for the larger polymer molecule and in the lower permeability core, as would be expected. For high- permeability material, such as most unconsolidated sandpacks and in higher permeability outcrop cores, such as those used in Sorbie et al (1987) and in the bead pack studies of Sorbie and Huang (1991; 1992), the polymer velocity enhancement effect is more likely to be associated with the surface exclusion phenomenon.

Note that *both* of the above mechanisms would lead to a relative advancement of the polymer compared with the tracer molecules in non adsorbing porous media as well as some rheological effects. It is probable that either of the above physical causes may be in play in different experimental situations. Fletcher et al (1991) defined the IPV as a pore volume in porous media which is inaccessible to the polymer, which is on account of two

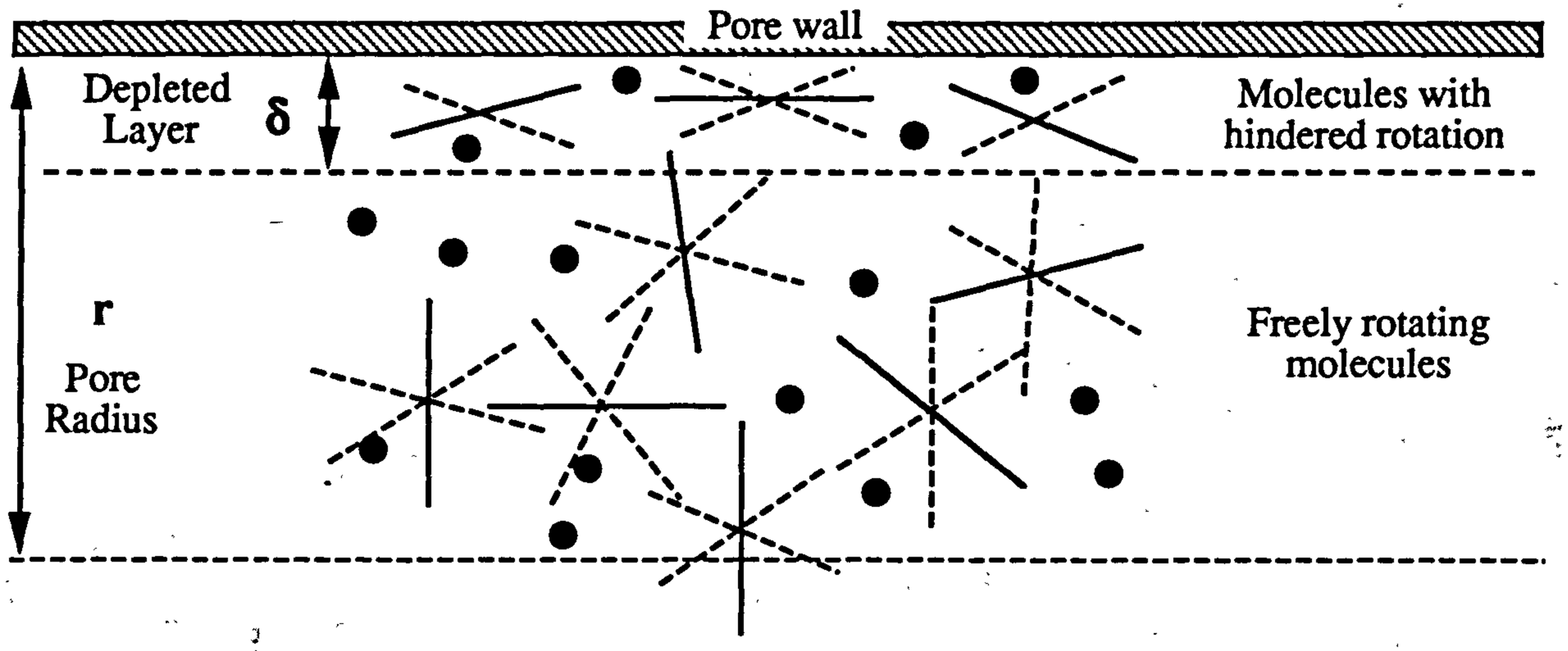

Figure 2.5 Molecular origin of the polymer surface depletion effect

separate effects: surface exclusion and original IPV. In the case of the surface exclusion mechanism, the rheological behaviour in the porous medium should show an apparent slip effect which will be discussed in detail in next section. However, the rheological implications of the IPV effect are rather more difficult to predict since, although the polymer concentration in certain small (low flow) pores is zero, the polymer concentration in the main flowing pores is higher than the input bulk polymer concentration.

We now consider the effect of the polydispersity on polymer transport through porous media. When polymer is passed through a porous material, the molecular weight separation within a porous medium may happen. The larger molecular weight species propagate faster than smaller fragments through the pore structure because the larger fragments are excluded from the smaller pores which is very similar to the IPV phenomenon or/and from the pore walls which is according to the excluded volume/surface exclusion mechanism. Lecourtier and Chauveteau (1984 a) studied the effects of shear rate and polymer concentration on the efficiency of xanthan fraction by hydrodynamic chromatography. They attribute all of the frontal spreading in the polymer effluent to the polydispersity effect and thought that the term "surface exclusion chromatography" seems more suitable than "hydrodynamic chromatography" in order to outline the physical mechanisms responsible for the separation process. At sufficiently low shear rates and polymer concentrations, efficient separation is reached and the complete molecular weight distribution can be determined. In their later work, Lecourtier and Chauveteau (1984 b) determined the optimum conditions to obtain the molecular weight distribution of xanthan by using wall exclusion chromatography. Brown and Sorbie (1989) thought that it is necessary to use a multicomponent representation of the polymer molecular weight distribution describing the polymer behaviour adequately when polydispersity effects are important. They used this approach to model the Lecourtier-Chauveteau results quantitatively and found that the data interpretation in such experiments is complicated somewhat by the presence of dispersion.

Other important factors affecting polymer transport in porous media are the adsorption / retention and the viscous fingering on xanthan transport in porous media. In the last section, the xanthan adsorption/retention in porous media has been discussed in detail. This section is more concerned with their effects on dynamic displacement effluent profiles. Polymer adsorption will always have the same gross effect on the position of the effluent compared with that of an inert tracer. The effluent will be retarded relative to the tracer because of the retention process, although this also depends on the magnitude of the IPV/excluded volume effect as discussed above. Huh et al (1990) studied polymer retention in porous media. Two characteristic features observed in the effluent profiles of xanthan from many corefloods were a frontal delay and a prolonged delay in attaining the feed concentration. They explained it as that the adsorption contribution largely produces the frontal delay, whereas mechanical entrapment is mainly responsible for the slow approach to feed concentration. Kolodziej (1988) also observed a characteristic tailing in the effluent profiles of xanthan solution for normalized concentrations greater than 70%. This result, he believed, is not a purely dispersive effect, and is due to a slow diffusion of polymer into dead-end regions of the pore space. Huang and Sorbie (1992) performed a series of experiments in which, after full and also early to tracer breakthrough of xanthan polymer, the flood column was shut in for 5 days and then was reopened. The xanthan adsorption in the porous medium is clearly visible immediately after the shut in, which was considered as resulting from the effect of slow adsorption to establish thermodynamic equilibrium. In an innovative polymer flooding simulator based on advanced concepts in polymer physics by Lecourtier et al (1992), the competitive effects of surface exclusion and adsorption chromatography were simulated. The results indicate that the preferential adsorption is dominant at the leading edge. The exclusion effects become become more effective at the trailing edge, because adsorption is not reversible in this case.

Viscous fingering is the phenomenon associated with displacement processes where displacing fluids used have lower viscosity than the displaced fluids. The less viscous displacing fluid will generally flow more easily than the higher viscosity displaced

material and tends to "finger" through the system in an irregular pattern and lead to early breakthrough of the displacing fluid and low sweep efficiency. The phenomenon of viscous fingering has received much attention in the literature and many studies. The general effect of viscous fingering on polymer transport experiments in porous media is displayed at the rear end of all the higher-viscosity polymer effluent profiles. The spreading out of the trailing edge of the xanthan polymer may easily be observed. Lecourtier and Chauveteau (1984 b) showed that the long tailing caused by viscous fingering strongly depends on polymer concentration. Sorbie et al (1987) found that, for a given series of floods, the lengths of the effluent tails show little dependence on flow rate, indicating that the pseudoplastic behaviour of the polymer did not have a very significant effect. To avoid viscous fingering in polymer flooding, Claridge (1978) proposed an idea of graded viscosity banks. The basic principle of this method is to reduce gradually the injected polymer concentration (and hence viscosity) in a series of steps or "bank". Pragmatic variants of this procedure have been used in field polymer floods since then.

2.5 Xanthan Rheology in Porous Media

2.5.1 Pseudoplastic Behaviour

Xanthan is a pseudoplastic (shear-thinning) polymer, i.e. the viscosity appears to be less at increasing shear rates. A more common way to plot its simple rheological behaviour is as viscosity against shear rate. The most commonly encountered analytical form of the viscosity-shear rate relationship is the power law model (Bird *et al.*, 1960), which describes the pseudoplastic region and is given by the expression:

$$\eta(\dot{\gamma}) = K\dot{\gamma}^{n-1} \qquad [2.3]$$

where K and n are constants. In the pseudoplastic region $n \leq 1$. For a Newtonian fluid n = 1 and K is the constant viscosity. This equation is quite satisfactory for describing the

psedoplastic region. However, xanthan tends to show Newtonian flow behaviour over a range of low shear rates. A more satisfactory model is the Carreau equation (Carreau, 1972). Here the viscosity function is given by:

$$\eta(\dot{\gamma}) = \eta_\infty + (\eta_0 - \eta_\infty)[1 + (\lambda\dot{\gamma})^2]^{(n-1)/2} \qquad [2.4]$$

where η_∞ and η_0 are infinite (often as solvent) and zero shear rate viscosities respectively; λ and n are a time constant and power law index as shown in equation 2.3 respectively. Figure 2.6 shows the improved behaviour of the Carreau model compared with the power law model. It is clear that Carreau model provides a very good whole range $\eta/\dot{\gamma}$ fit for many polymer systems.

The rheological behaviour of xanthan solutions in both viscometers and porous media has been studied by a number of investigators (Teeuw and Hesselink, 1980; Chauveteau and Zaitoun, 1981; Chauveteau, 1982; Chauveteau et al, 1984; Greaves and Patel, 1985; Willhite and Uhl, 1986; Hejri et al, 1988; Cannella et al, 1988; Fletcher et al, 1991). The main objective for these workers has been to develop simple semi-empirical equations which can be used to predict rheological behaviour in porous media from fairly easily obtained viscometric data. Apparent viscosity within the porous medium, η_{app}, is usually determined at each velocity (flow rate) using Darcy's law as follows:

$$\eta_{app} = \frac{kA\Delta P}{QL} \qquad [2.5]$$

where Q is the volumetric flow rate, $\Delta P/L$ is the pressure gradient, k is the permeability, and A is the total cross-sectional area of the porous medium. Expressions based on simple capillary bundle models of the porous medium where the permeability (k) and porosity (ϕ) are usually used to estimate a " pore radius " or " effective hydraulic radius ". From this pore length scale, the flow rate is then converted into an "apparent shear rate" within the porous medium, $\dot{\gamma}_{pm}$, which usually has the form (Savins, 1969; Chauveteau, 1982; Chauveteau, 1986; Sorbie et al, 1989) :

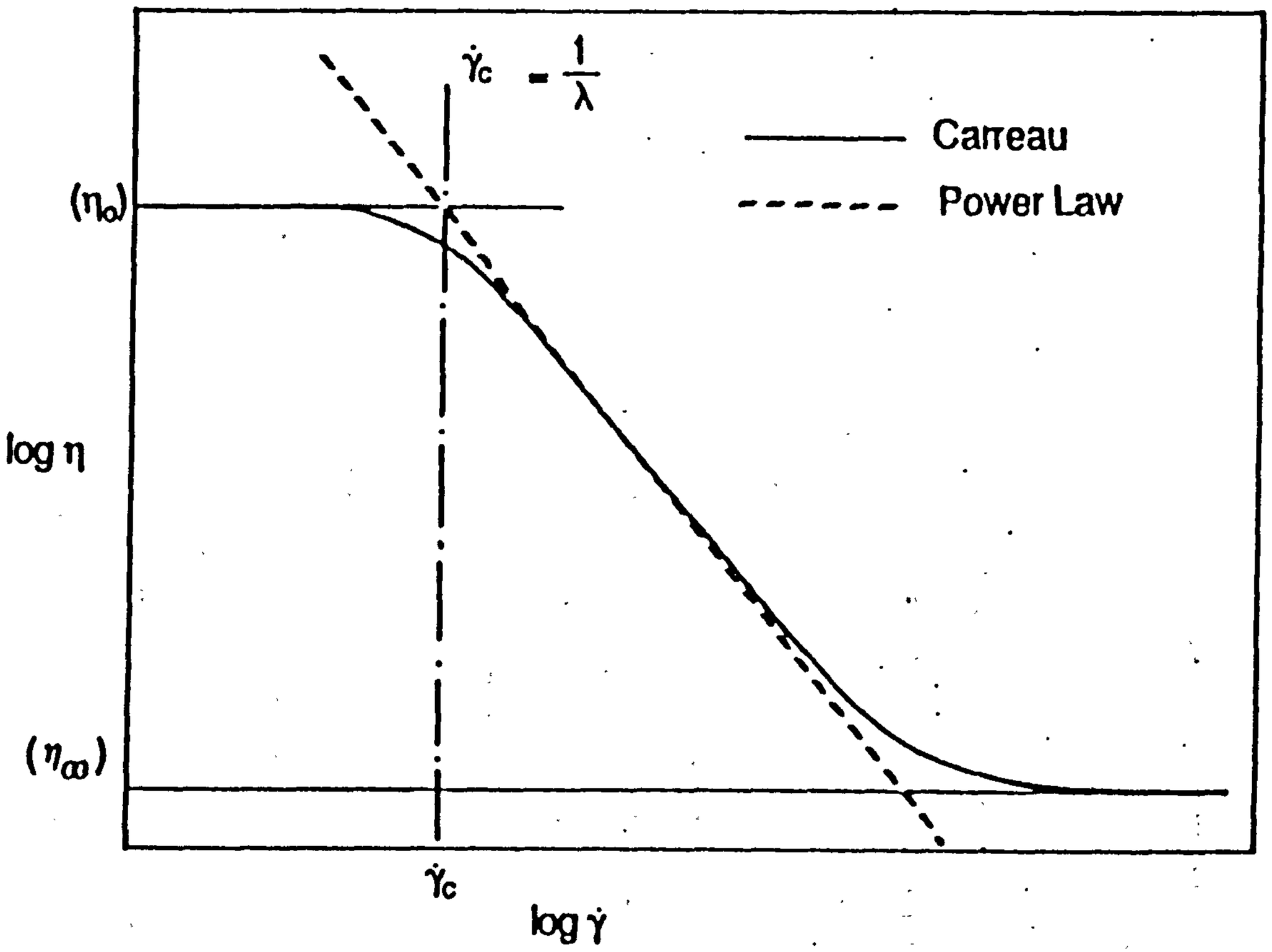

Figure 2.6 Comparison of the Carreau and power law models for $\eta/\dot{\gamma}$; the critical shear rate, $\dot{\gamma}_c$, defined as in the figure, is related to the Carreau relaxation time, λ, as shown. (From Sorbie, 1991)

$$\dot{\gamma}_{pm} = \alpha \frac{4U}{\sqrt{8k\phi}} \qquad [2.6]$$

where $U = Q/(A\phi)$ is the average frontal velocity and α is a constant which depends on the porous medium under study and may vary from ~1 in regular unconsolidated packs up to ~10 in consolidated sandstones (Chauveteau, 1982; Fletcher et al, 1991). Although these models are very elementary, they have been used quite successfully to correlate in situ rheological results for inelastic, pseudoplastic fluids such as xanthan biopolymer. The reason for the success of such simple models has been analyzed and explained using more fundamental network calculations by Sorbie et al (Sorbie et al, 1989; Sorbie, 1989).

When xanthan solution flows through porous media, a number of interesting rheological effects can be observed. Generally, theoretical and experimental research has focused on developing an accurate description of the flow characteristics and rheological behaviour of such solution in porous media since the 1980s. Teeuw and Hesselink (1980) derived a flow equation taking into account the effect of tortuosity on both shear stress and shear rate. This equation was applied in flow experiments in Bentheim sandstone core. They observed that biopolymer solutions exhibit the same shear-thinning characteristics in core flow as in rotary viscometers and the power-law exponents in the viscometer and porous media are in fair agreement. It was found, however, that the flow coefficient K in core flow was approximately half that of the corresponding value in bulk solution. In contrast to Teeuw and Hesselink's results, Willhite and coworkers (Willhite and Uhl, 1986, 1988; Hejri et at, 1988) reported that the measured power-law exponents for flow of xanthan solution in Berea sandstone cores and Ottawa sandpacks were lower than the values obtained in a viscometer. A linear relationship was developed between the two parameters. Like Teeuw and Hesselink (1980), they also found that the effective polymer viscosities are overestimated by the capillary bundle models.

Greaves and Patel (1985) studies the flow of xanthan at two concentrations (500 ppm and 1000 ppm) in higher permeability Elginshire sandstone cores. They suggest a hybrid

procedure for estimating $\dot{\gamma}_{pm}$ via the capillary bundle/power law approach and then predicting the in-situ viscosity using the actual viscosity/shear rate curve measured in their low-shear Contraves viscometer. This approach underpredicts the observed viscosity within the porous medium, possibly by overestmating the apparent shear in the porous medium.

An experimental and theoretical study of xanthan rheology in porous media has been reported by Cannella et al (1988). The results obtained in their study show that, although a low-shear Newtonian plateau is observed in the porous medium apparent viscosity for xanthan concentration of 300 ppm, none is seen for polymer concentration of 600 ppm and above. The fact that higher concentration solutions continue to exhibit power law behaviour is attributed by Cannella et al partly to intermolecular non-alignment at low flow rate in the narrow pore channels. It is suggested that the 300 ppm solution is close to the overlap concentration ($C^* = C[\eta]$) below which interactions between polymer molecules are very small. Cannella et al developed an apparent shear rate equation having no adjustable parameters. The apparent viscosity for a power-law fluid flowing in a porous medium was derived using effective medium theory and the porous medium was modeled as a network of capillary tubes. They found that the apparent viscosity expression obtained is similar to that from the capillary bundle model, but the coefficient values are different, as observed experimentally. This difference was thought to be a consequence of the connectivity of flow channels and their varible cross-section. Due to its shear-thinning nature, a power-law fluid flows mainly through the wide channels of porous media, and largely bypasses small-scale pore channels of the porous body. The capillary bundle model cannot describe this tendency of a shear-thinning fluid.

2.5.2 Apparent Slip Effects

In recent years, some workers have found that the in-situ behaviour of xanthan is inconsistent with that of the bulk fluid in the low flow rate (pseudo-Newtonian) regime. One very interesting aspect of the in situ rheology of this biopolymer is that, under certain

circumstance, an apparent slip effect is observed where the low flow Newtonian viscosity may be *below* the bulk fluid viscosity as shown in Figure 2.7. This finding has been interpreted in terms of a depleted layer/surface exclusion phenomenon where the macromolecules are excluded from a zone close to the pore wall due to steric hindrance effects. Under certain circumstances, the effects of surface exclusion may be observed on the macroscopic transport and rheological behaviour of the polymer in the porous medium. When a polymer solution labelled with an inert tracer is injected into a core or pack of non-adsorbing porous material, the average polymer molecule velocity is higher than that of the tracer, in the presence of this effect. This case has been discussed in detail in Section 2.4.

Such effects on polymer flow in porous media were first reported by Chauveteau and coworkers (Chauveteau and Zaitoun, 1981; Chauveteau, 1982) and in a number of papers since that time. Indeed, many other workers (Willhite and Uhl, 1986; Hejri et al, 1988; Cannella et al, 1988) have not found this type of behaviour, but this may be due to certain aspects of the solution preparation or may relate to the fact that most of Chauveteau's results are presented for lower concentration polymer solutions in the dilute regime where $C[\eta]<1$ and most other workers mainly present results for higher concentration solution.

Chauveteau and coworkers (Chauveteau and Zaitoun, 1981; Chauveteau, 1982; Chauveteau et al, 1984)) studied the influence of pore size on rheological behaviour of solutions of rodlike polymers (xanthan) flowing through fine pores. In small pores, the Newtonian apparent viscosity was found to decrease with pore size as long as pore diameters were larger than rod length. Such behaviour was interpreted as being due to the existence of a layer depleted in polymer close to the pore wall in which steric hindrances decrease the polymer segment concentration and thus the fluid viscosity near the wall. This situation is illustrated schematically in Figure 2.5, in which the quantity δ, is the effective thickness of the depleted layer and is of the order of the molecular size, *l*.

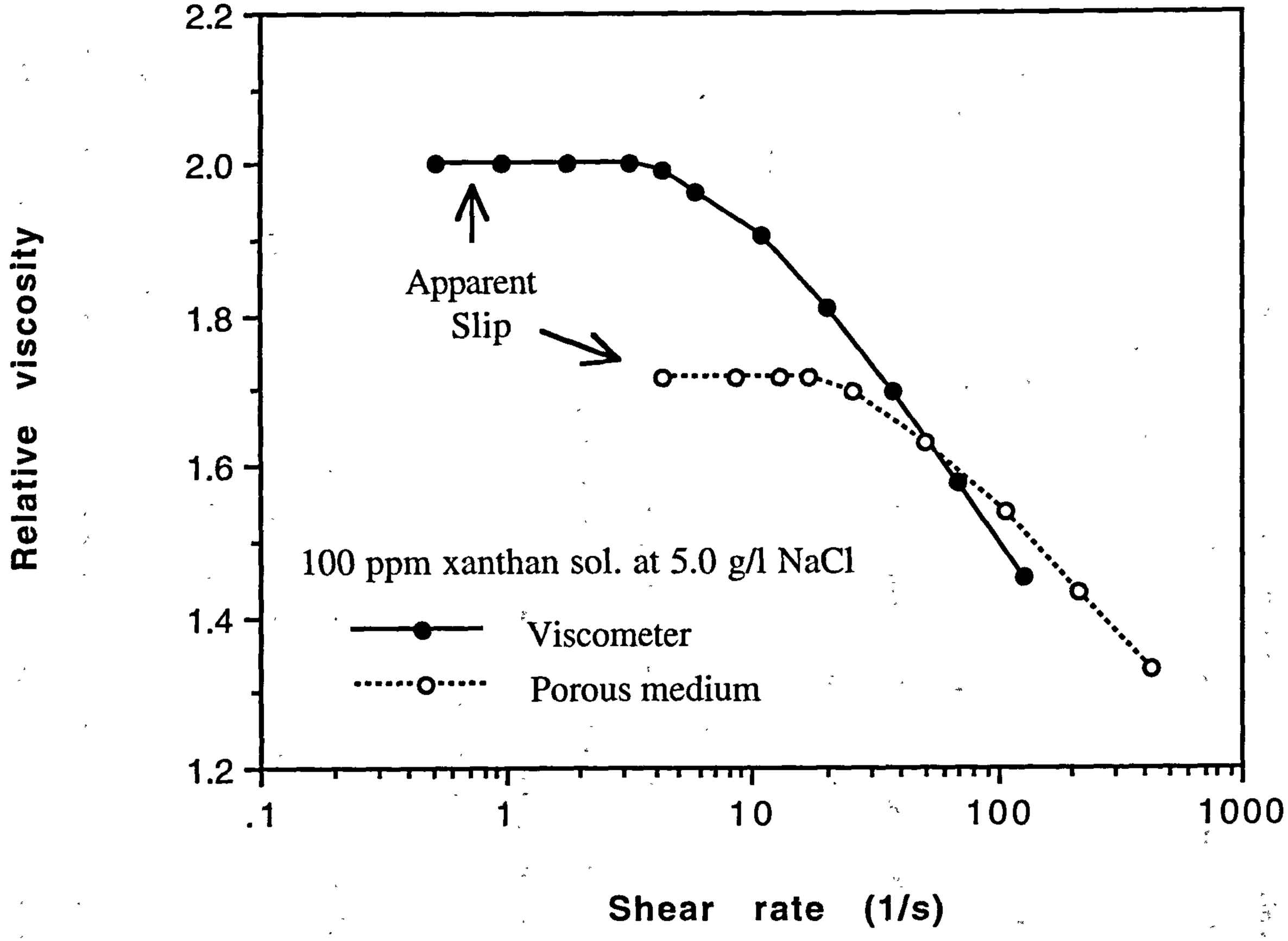

Figure 2.7 Observation on xanthan in situ rheology

Omari et al (1989) determined the apparent viscosity of dilute and semidilute xanthan solutions flowing through small cylindrical pores in Newtonian and shear-thinning regimes under conditions where there is no adsorption effect. The analysis of the results using a two-fluid flow model shows that the hydrodynamic thickness of the depletion layer near the pore wall is closely related to the equivalent rod length of the macromolecule, but seems to be insensitive to the persistence length. The hydrodynamic thickness does not depend on polymer concentration as expected for a semirigid polymer and decreases slightly as shear rate increases.

In contrast to Omari et al's results, Sorbie and Huang (1991) found in their experiments that the magnitude of the observed slip effect is a function of the polymer concentration. It appears that the *apparent* depleted layer thickness, (δ/r), decreases with increasing xanthan concentration over a range of low polymer concentration. They found no difficulty in reproducing the apparent slip effects arising from surface exclusion phenomena when the appropriate experimental precautions were taken. Sorbie and Huang's studies (1991; 1992a; 1992b) demonstrate that the in situ rheological behaviour of xanthan biopolymer (i.e. the effective depleted layer thickness) is affected by the polymer concentration, solution pH and salinity. These effects are interpreted in terms of the conformation of the xanthan molecule and the surface charge on the porous medium.

The xanthan rheological effect is very difficult to measure directly in a capillary because of the practical problems of working with very narrow capillaries and uncertainties resulting from end effects. Berge et al (1990) showed that the resistitive pulse technique (Coulter principle), which traditionally has been used for counting and sizing particles, also can be used to study xanthan solution flow in single pores of size relevant to flow in natural porous media. Autocorrelation analysis of the fluctuating signal across the pore and measured transit time distributions of polystyrene spheres suspended in the solution was used to study the flow. Ausserré et al. (1986; 1991) developed a optical evanescent-wave-induced fluorescence technique (EWIF) which can probe interfacial layers of sub-microscopic thicknesses. Using this method, they studied the hydronamic thickening of

depletion layers in colloidal solution and the variation of the depletion layer thickness was monitored optically.

2.5.3 Models for Flow in the Presence of Depleted Layers

The exclusion of macromolecules from the pore wall, as shown in Figure 2.5, results in a layer depleted in polymer in that region which will therefore have a lower effective viscosity than the bulk solution close to the centre of the pore. The distribution of polymer molecules in this region has been studied by several workers and some simple models exist that describe the concentration profiles across an idealised cylindrical capillary (Auvray, 1981; Chauveteau, 1982; Hoagland, 1988; Sorbie, 1990a). Two variants of this concentration distribution in a cylindrical pore are shown in Figure 2.8; the simple two fluid model of Chauveteau (1982) is shown in Figure 2.8(a) and a somewhat more realistic model - the linear layer model - is shown in Figure 2.8(b). For both models, the quantity , δ, (see Figures 2.5 and 2.8) is the effective thickness of the depleted layer which is of the order of the molecular size.

In the two fluid model shown in Figure 2.8(a), the polymer concentration in the region of the wall is taken to be constant which is well below the bulk injected value and the wall viscosity in this region, η_w , is consequently also a constant which lies between the bulk viscosity, η_b, and the solvent viscosity, η_s. The apparent viscosity, η_{app}, for the two fluid model will be below that of the bulk solution and can easily be calculated analytically to obtain the following expression:

$$\eta_{app} = \eta_w[1-(1-\frac{\eta_w}{\eta_b})(1-\frac{\delta}{r})^4]^{-1} \qquad [2.7]$$

where this model refers to the in situ apparent viscosity of the polymer in the low flow Newtonian regime; η_b and η_w are defined above and r is average pore radius in the porous medium. If the two fluid model were indeed an exact description of the physical situation, then Eq. [2.7] above would be exact. This is important in the light of the

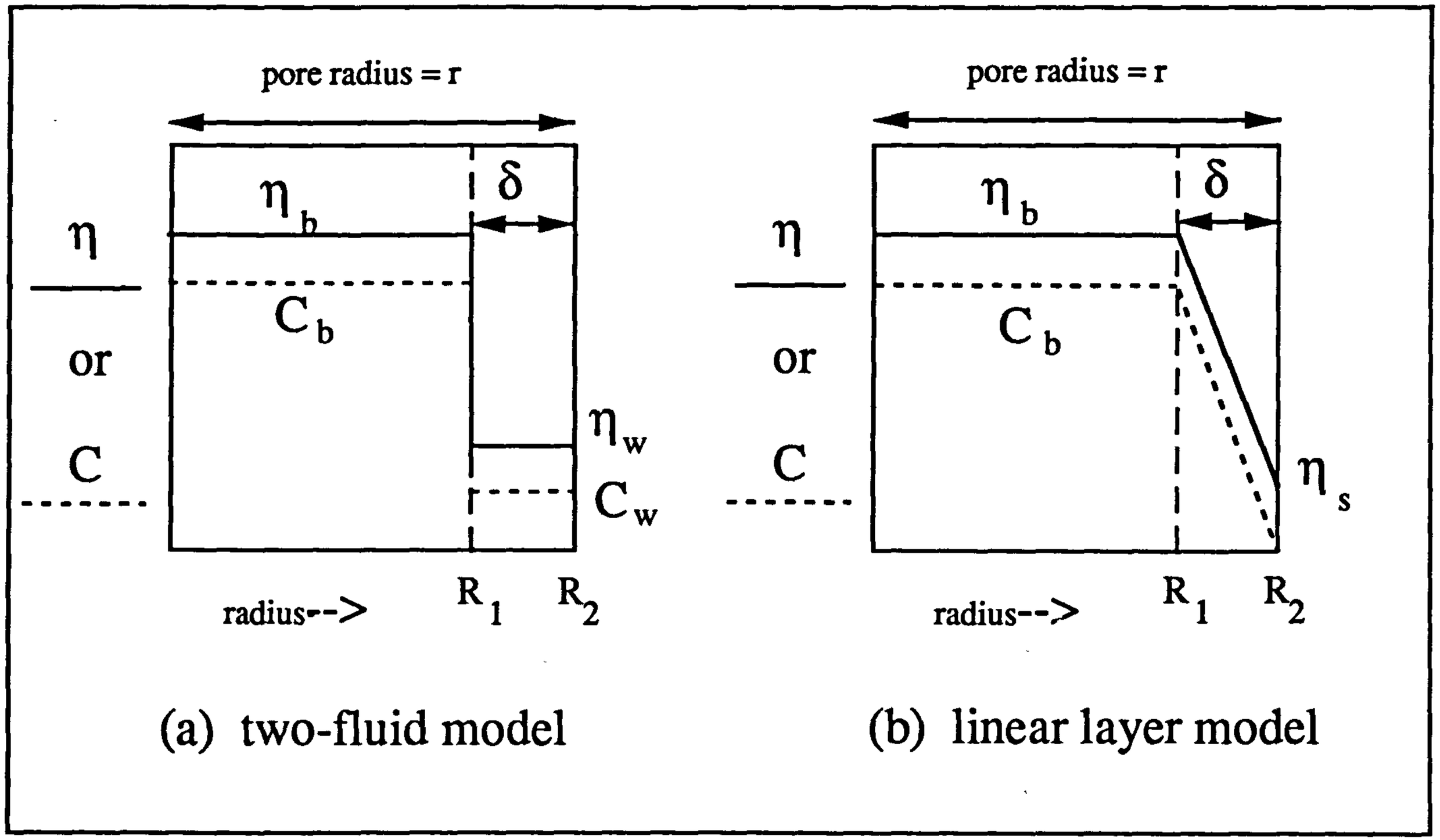

Figure 2.8 Depleted layer profiles across a capillary

further approximations that are made in the the practical application of the two fluid model as discussed below. In this model, there are further assumptions about how the wall viscosity, η_w, should be calculated and a method has been proposed by Chauveteau and coworkers (Chauveteau et al, 1984; Omari et al, 1989). These workers first simplify Eq. [2.7] and arrive at the expression:

$$\frac{\eta_b}{\eta_{app}} \approx 1+4\left(\frac{\eta_b}{\eta_w}-1\right)\frac{\delta}{r} \qquad [2.8]$$

based on the assumption that the depleted layer thickness is much less than the pore radius, i.e. $(\delta/r) << 1$. Further, using an expansion of the bulk and wall viscosities, η_b and η_w, in terms of concentrations, C_b and C_w, and retaining terms to first order in C_b gives:

$$\frac{\eta_b}{\eta_w} \approx \frac{1+C_b[\eta]_0+k'(C_b[\eta]_0)^2}{1+\beta C_b[\eta]_0+k'(\beta C_b[\eta]_0)^2} \qquad [2.9a]$$

$$\approx 1+(1-\beta)C_b[\eta]_0+0(C_b[\eta]_0)^2 \qquad [2.9b]$$

where β is the ratio (C_w/C_b) and k' is the Huggins constant. Substituting this approximate expansion into Eq. [2.8] above, then gives:

$$\frac{\eta_b}{\eta_{app}} \approx 1+4(1-\beta)C_b[\eta]_0\frac{\delta}{r} \qquad [2.10]$$

where, in order to apply the model, it remains only to evaluate the parameter β. This quantity is calculated by integrating the Auvray (1981) model for the polymer concentration profile in the capillary out to a distance from the wall where the concentration is taken arbitrarily to be $C = 0.95\ C_b$; this procedure gives $\beta = 0.64$ for a strictly rigid rod. The two fluid flow model, as used by Chauveteau and coworkers (Chauveteau et al, 1984; Omari et al, 1989), therefore implicitly contains two approximations relating to the small magnitudes of both (δ/r) and the concentration as

well as an arbitrary choice of the parameter β, which depends on the precise assumption made in the integration to determine the ratio (C_w/C_b). These various assumptions and approximations are very important since it is based on these, i.e. on Eq.[2.10], that the evidence for a constant (δ/r) with polymer concentration must rest. If Eq.[2.10] is correct and β is a constant, then we see immediately that if (η_b/η_{app}) is a linear function of $C_b[\eta]_0$, then this implies that (δ/r) is constant with polymer concentration.

The linear layer model for the concentration and viscosity profiles across the capillary has been investigated recently by Sorbie (1990a) who presents analytical expressions for the quantity η_{app}. In this model, analytical solution of the problem is still possible in the Newtonian low flow rate limit although the resulting expression for η_{app} is rather lengthy. The form of the apparent viscosity in this model is functionally as follows:

$$\eta_{app} = f(\eta_b, \eta_s; \{\delta/r\}) \qquad [2.11]$$

where only the bulk and solvent viscosities (η_b and η_s) are required along with the relative depleted layer thickness (δ/r). This expression is derived in reference (Sorbie, 1990a) but for completeness the main equations are presented in Appendix 1. The depleted layer thickness is given by $\delta = R_2 - R_1$ in the notation of Figure 2.8 and, in the formulae in Appendix 1, the simple functional relationship in Eq. [2.11] above may not be immediately apparent. Note that, in this model, the aspect of the two fluid model relating to the evaluation of η_w has now been replaced by the basic assumption of having a linear layer in concentration and viscosity in the depletion region close to the pore wall. This is expected to be a very good assumption especially in the lower concentration range where we do expect both profiles to be very close to linear and virtually all of our experimental results pertain to this case. Thus, in the application of the linear layer model to the analysis of experimental data, the only unknown is the relative depleted layer thickness, (δ/r), since η_b and η_s come from viscometric measurements and η_{app} is measured in the porous medium flow experiment. Thus, using this approach, we are in a position to calculate (δ/r) directly from our experimental data without further ancillary

calculations or assumptions and to check whether this quantity is constant with polymer concentration as has been argued previously (Omari et al, 1989) based on the apparent linearity of (η_b/η_{app}) vs. polymer concentration (from Eq.[2.10]).

Sorbie (1990b) also presented network calculations on depleted layer effects in polymer flow through porous media. The calculation of the effective viscosity in each bond, η_{eff}, in the presence of a depleted layer is rather more complex. Using input data based on xanthan, it was found that the macroscopic "apparent slip" effect can be quite substantial even for fairly low depleted layer thickness compared with average pore size in the network.

CHAPTER 3

EXPERIMENTAL DESCRIPTION

3.1 Materials and Solution Preparation

Brine: The solvents used in this work were NaCl brines with various salinities as follows: 0.1, 0.5, 5.0, 20, and 35 g/l NaCl. Unless otherwise stated, in Chapter 4 and 5, a solution of 35 g/l NaCl brine was used which is close to artificial sea water in ionic strength; in Chapter 6 and 7, the salinities of solutions are 0.1, 0.5, 5.0, and 35 g/l NaCl respectively; and in Chapter 8, 20 g/l NaCl was used for rather different experimental purposes.

Xanthan and Scleroglucan Solution Preparation: A fermentation broth of Flocon biopolymer 4800 C (assayed at 12.5 % active) was obtained from Pfizer Chemical Division. This broth was diluted to 3000 mg/kg (ppm) with two different salinities 0.1 and 35 g/l NaCl, and clarified by filtration through a 8 μm pore size Millipore filter held between two A-25 pre-filters in a 38 mm diameter (cross-sectional area, 11.3 cm^2) Millipore filter holder at 10 ml/hour ($2.5x10^{-4}$ cm/s). This procedure produced a clear solution without any viscosity loss. The clarified solution was then diluted with brine to a 2000 ppm stock solution containing 1000 ppm formaldehyde as biocide.

A similar method to that reported previously (Chauveteau and Kohler, 1984) was used to remove microgels from this clarified solution. Xanthan solution was filtered at a low flow rate of 5 ml/hour ($1.2x10^{-5}$ cm/s) through a filter holder containing three on-line Millipore filters with decreasing pore sizes 8 μm, 3 μm and 1.2 μm. The solution produced was then tested by monitoring the pressure drop across a 3 μm on-line Millipore filter while previously filtered solution passed through it at 15 ml/hour ($3.7x10^{-4}$ cm/s),

during which a stable pressure drop was observed. Using this procedure we obtained a microgel-free solution from which polymer bulk solutions were then prepared at concentrations of around 30 to 400 ppm by diluting the 2000 ppm microgel-free solution.

Scleroglucan samples were supplied by the Institut Français du Petrole (IFP). It is a nonionic polysaccharide biopolymer. These purified solutions had been treamented in IFP by the follow processes (Broseta et al, 1992): i) dissolution of power in the appropriate brine (20 g/l NaCl), ii) clarification of solutions through filter packs of 8 and 3 μm at 1 bar differential pressure, iii) ultrafiltration of solutions to remove small molecular weight impurities, iv) heating of solutions for disaggregation, and v) micro-gel filtration through a filter pack of 8, 5, and 3 μm filters at a flow rate of 6 ml/hour. In all solutions, NaN_3 (0.4 g/l) was added as a bactericide. Table 3.1 shows the charcteristics of scleroglucan samples supplied.

Table 3.1
Scleroglucan Intrinsic Viscosity and Huggins Constant

Sample No.	Concentration (ppm)	Newtonian Intrinsic Viscosity (cm^3/g)	Huggins Constant
1	236	7,800	0.4
2	257	7,800	0.5
3	497	11,000	0.6

3.2 η (C) Calibration

Viscosities of polymer samples measured at a given shear rate and temperature using a Contraves LS 30 viscometer were used to determined biopolymer concentration. This procedure must be carried out very carefully in a vibration free environment in order to obain accurate results. Figure 3.1 shows the bulk viscosities at different shear rates in various xanthan concentration. A Newtonian plateau at lower shear rates and a

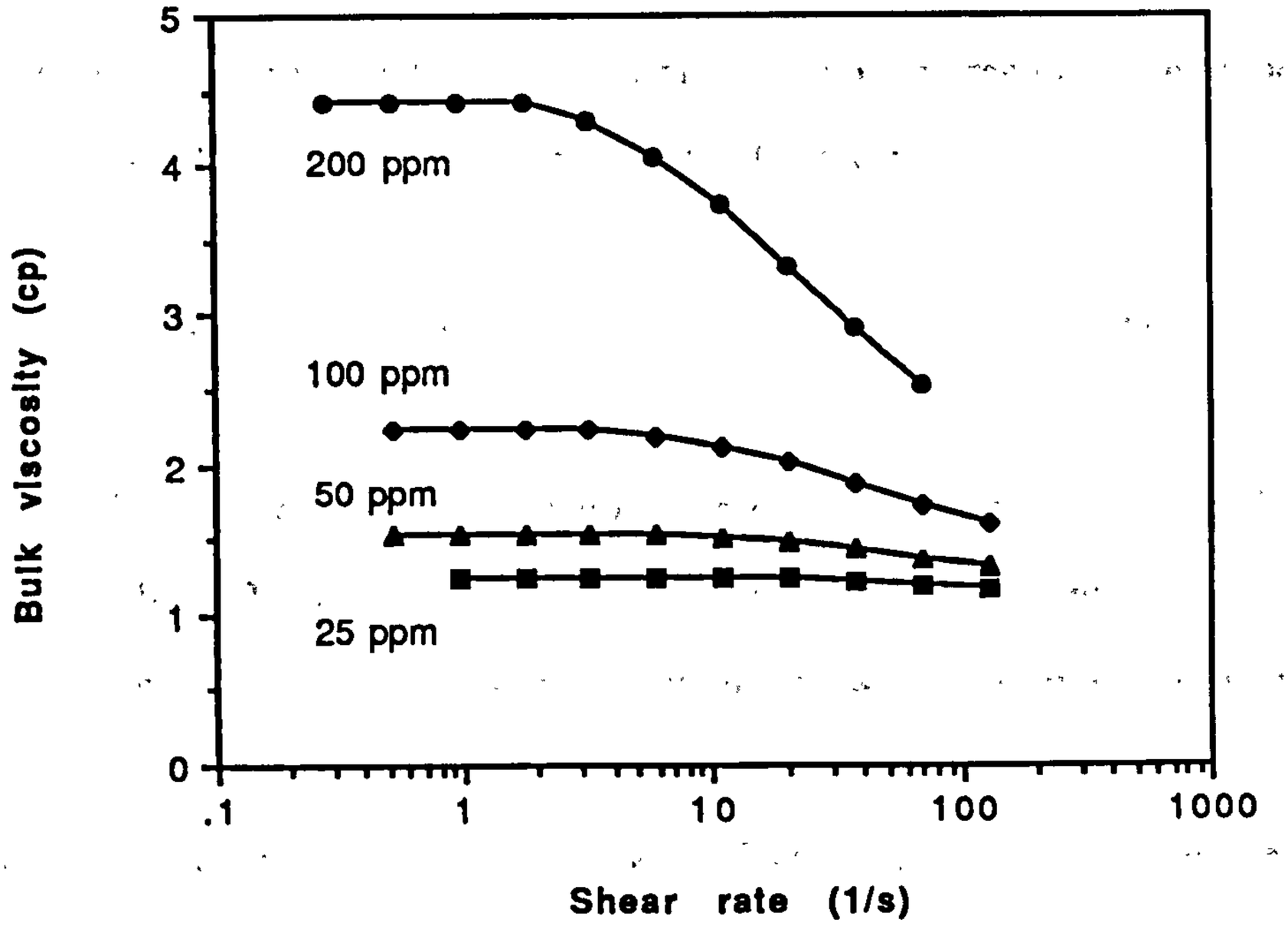

Figure 3.1 Bulk viscosities of xanthan solution at salinity 0.5 g/l NaCl, pH 5.0, temperature 20°C

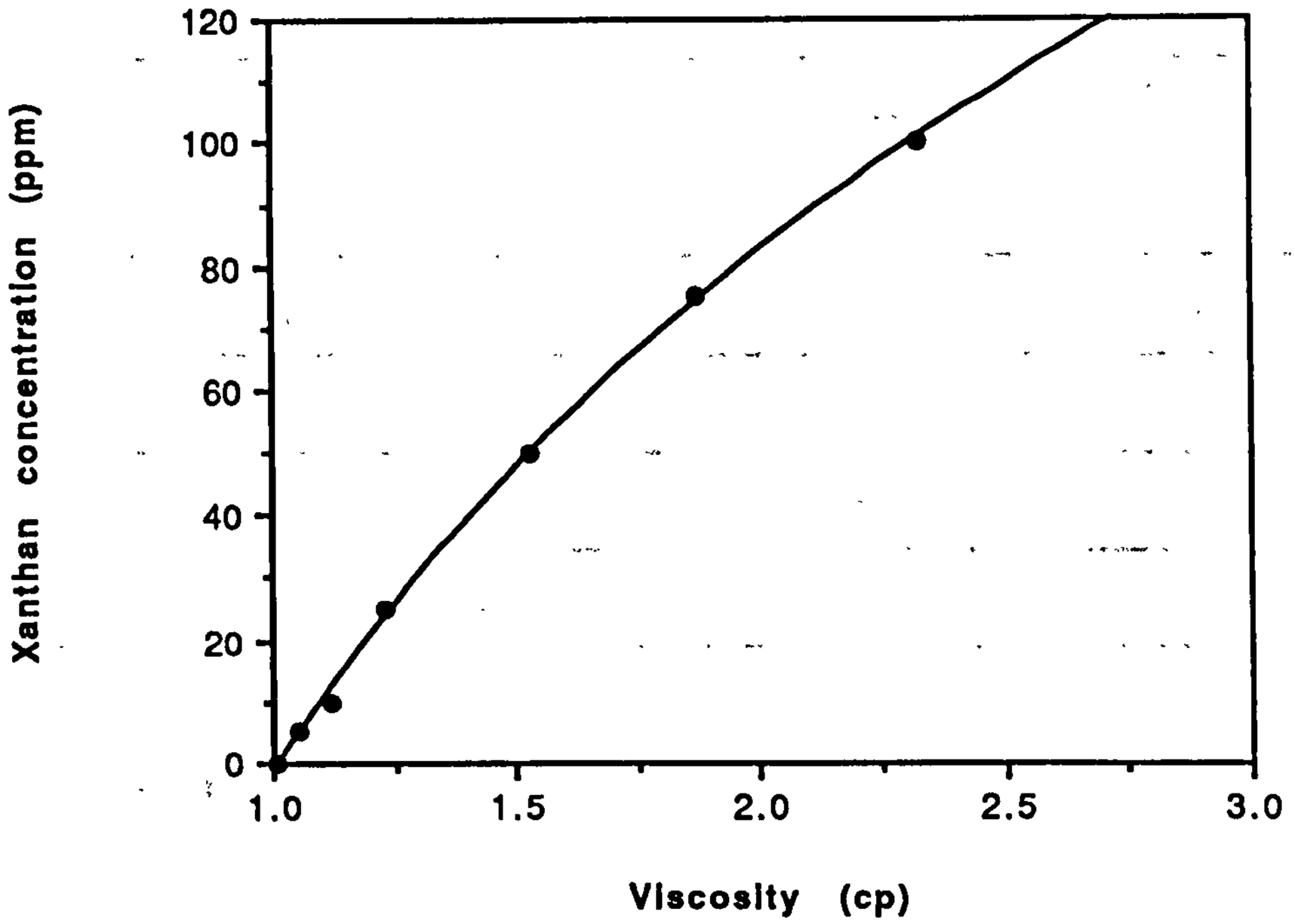

Figure 3.2 Calibration plot of viscosity vs xanthan concentration at Newtonian shear rate region at 21°C

pseudoplastic behaviour at higher shear rates are clearly observed. Based on the values of Newtonian viscosities shown on the plots, the calibration plot of viscosity vs. xanthan concentration is performed in the low shear rate (Newtonian) region. One of the results is shown in Figure 3.2. This relationship often has following form:

$$C_p = a + b \times \log \eta \qquad [3.1]$$

where a and b are constants; C_p is polymer concentration; and η is polymer bulk viscosity. Table 3.2 shows experimental results for 100 ppm xanthan solution for the constants a and b in different salinity systems, as well as corresponding regression coefficients, r^2, of the calibration plots. Where $r^2 \approx 0.999$ indicates a very good exponential (or logarithmic) relation between C_p and η. Generally, this measurement was done for each new xanthan sample. It is found to be a simple and accurate method for determining xanthan concentration.

Table 3.2

C/η Calibration Equation of Xanthan Solutions as Functions of Brine Salinity

Salinity (g/l NaCl)	Parameter a	Parameter b	Regression Coefficient r^2
0.1	-2.62	279	1.000
0.5	-3.35	295	1.000
5.0	-3.41	332	0.999
35	-25.1	390	0.998

3.3 Xanthan Intrinsic Viscosity [η] and Huggins Constant k′

The intrisic viscosity, [η], of a polymer solution is the limit of the reduced viscosity, η_{sp}/C, or inherent viscosity, $\ln\eta_r/C$, as the solution concentration, C, of polymer tends to zero, which may be determined according to the following equations:

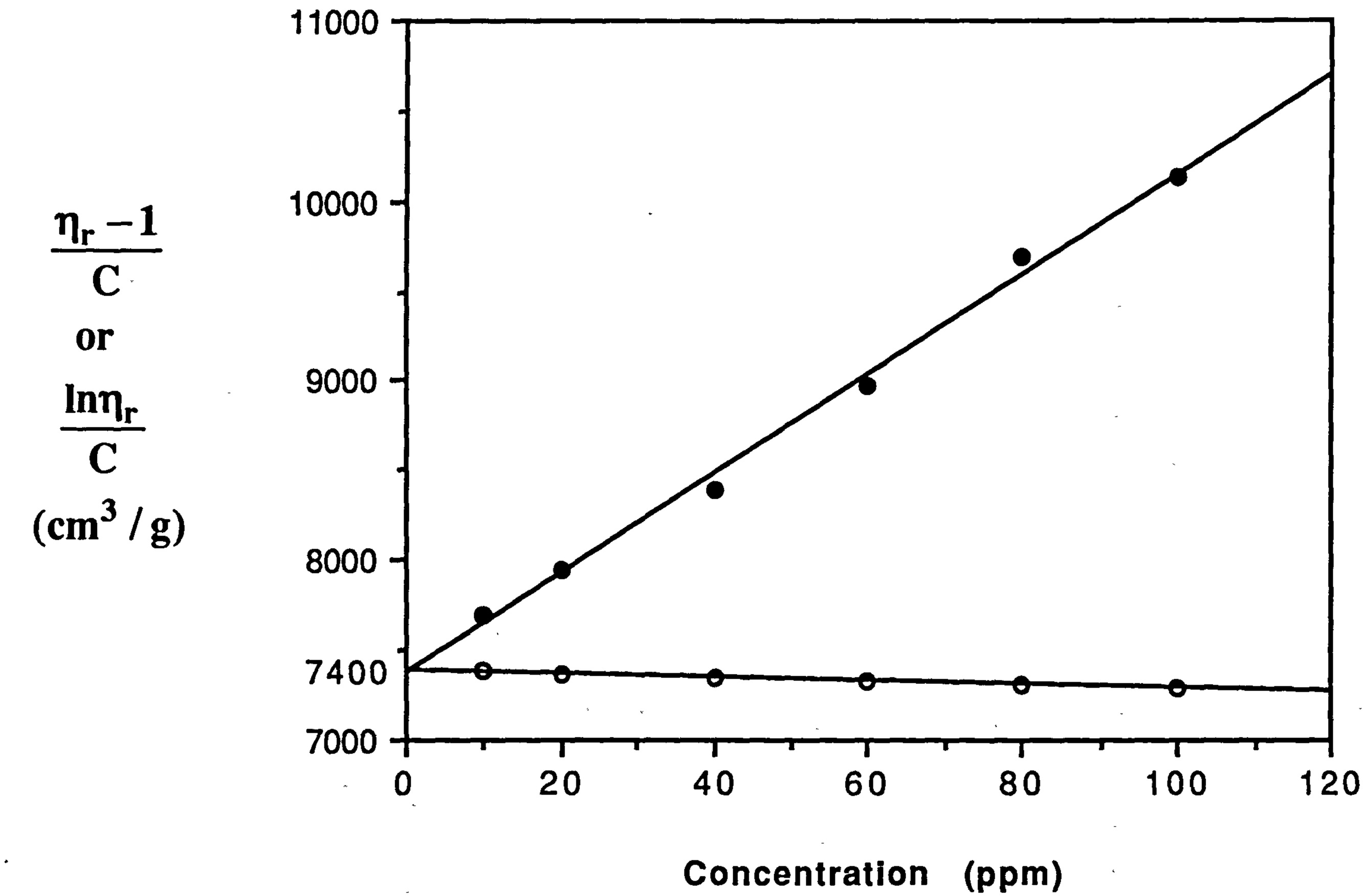

Figure 3.3 Determination of intrinsic viscosity for a xanthan sample at salinity 0.5 g/l NaCl, pH 5.0, temperature 21°C

$$\frac{\eta_{sp}}{C} = [\eta] + k'[\eta]^2 C \qquad [3.2]$$

where $\eta_{sp} = \eta_r - 1 = \eta/\eta_s - 1$; η_{sp}, η_r, η and η_s are specific, relative, polymer and solvent viscosities respectively. k′ is the Huggins constant. or

$$\frac{\ln \eta_r}{C} = [\eta] - k''[\eta]^2 C \qquad [3.3]$$

where k″ is a constant. In order to find the intrinsic viscosity, the specific or/and inherent viscosity is/are plotted against low polymer concentrations and is/are extrapolated to zero concentration as shown in Figure 3.3. The intrinsic viscosity is independent of polymer concentration, but depends on the molecular weight, volume and shape of the particles constituting the macromolecular solute.

Most of the data related to intrinsic viscosity in this work will be discussed or mentioned in the following chapters. It is well known that the Huggins constant (k′) is also an important factor for the properties of polymer solution, especially for polymer solubility in brine. Many our results show that the k′ values is 2 times or even 3 times higher than the normal value, ~0.4, even in good solvents. We are not very trusting of some of the k′ values, because it was found that the value of the Huggins constant is very sensitive to the method of fitting the rheological data. To illustrate this we present data from one set of the experimental measurements: Seven concentration points: 0, 10, 20, 40, 60, 80, and 100 ppm at pH 5.0, salinity 35 g/l NaCl, a η/C were taken and a calibration curve was obtain with the regression coefficient $r^2 = 0.999$ as discussed in the last section and the correlation corresponding to the curve is as follows:

$$\eta_r = \exp[2.87 \times 10^{-3} C_p] \qquad [3.4]$$

where η_r is relative viscosity and C_p is polymer concentration. Corresponding η_r may be obtained from various C_p using Eq. [3.4], and then [η] and k′ may be obtained from Eq. [3.2] through $(\eta_{sp}/C) / C$ plot. Calculated results are shown in Table 3.3 from which It

is easily seen that although [η] only changes slightly, k′ shows very large changes with different fitting concentration regions. For example, [η] changes from 6,500 to 6000 cm^3/g, i.e. 7.7%, with fitting C_p region changing from 10-100 ppm to 20-200 ppm. However, k′ changes from 0.664 to 1.007, i.e. 52%, with corresponding fitting C_p region change. Theoretically, the right side of Eq. [3.4] can be developed as a power series and k′ should be equal to 0.5. Note that, although these rasults are of theoretical concern to us, they do not significantly affect our later results or arguments. For this reason, we consider only the intrisic viscosity in some detail later.

Table 3.3

Fitting Data Effect on Xanthan Intrinsic Viscosity [η] and Huggins Constant k′*

Range calculated	Points calculated (ppm)	[η] (cm^3/g)	k′	r^{2**}
1-10 ppm	1,2,4,6,8,10	6607	0.512	1.000
5-50 ppm	5,10,20,30,40,50	6582	0.569	0.999
10-100 ppm	10,20,40,60,80,100	6494	0.664	0.997
20-200 ppm	20,40,80,120,160,200	6033	1.007	0.986
Theoretical value		6608	0.500	
Experimental value	10,20,40,60,80,100	6300	1.280	0.987

* Results calculated base on Eq. [3.4] at salinity 35 g/l NaCl;

** r^2 is the regression coefficient for corresponding (η_{sp}/C) / C plot.

3.4 Characterisation of the Porous Medium

Permeability: Ballotini glass beads having sizes in the range 45 to 90 μm were prewashed with dilute hydrochloric acid (0.1%) to remove any adsorbed impurities and were dried. After brine rinsing, they were then packed in a chromatography column with an inside diameter of 1 cm and a length of 50.3 cm with two pressure tappings positioned at the inlet, and the outlet of the packed column respectively. The porosity of the packed

column was obtained by weighing the dry and brine saturated column of ballotini and was found to be $\phi \approx 0.35$. The brine permeability was determined using Darcy's law from which we found that $k \approx 1.0$-1.2 Darcy for all of the packs prepared in this work.

Particle Size: The particle size and distribution of ballotini glass beads were determined using a Malvern MS20 Master Sizer. A relatively narrow size distribution was found, as shown in Figure 3.4, having average size 52 μm compared with the range 45 to 90 μm quoted by the supplier (The English Glass Co. Ltd.). The specific surface area (SSA) of ballotini, as well as a kind of natural sand (which was used in xanthan static adsorption experiments) from BDH Laboratory Supplies, was obtained from the above measurement or by a BET method.

Table 3.4
Specific Surface Area (SSA) of Ballotini Glass Bead and Sand

Sample	Method	Condition	SSA (m^2/g)	Average Size (μm)	Average SSA (m^2/g)
Ballotini	Malvern	Focal length: 100 mm	0.155	52	0.123
Ballotini	BET	Pressure: 708 mm Hg	0.091		
Sand	Malvern	Focal length: 300 mm	0.010	300	0.022
Sand	BET	Pressure: 708 mm Hg	0.034		

Table 3.4 shows the measuring data of SSA at room temprature. It seems that the SSA values are more or less changed with different measuring methods. Since it is not very important for this work, an average value of SSA is used.

Surface Charge: In this work, a modified Bolt's method (Bolt, 1957) was developed to measure the surface charge on ballotini glass beads. Ballotini was first prewashed with dilute hydrochloric acid (1.0%) until the pH was ≈ 2 and was then dried in an oven at 100°C, from which we obtained the ballotini sample with zero charge on the surface of

High Size	Under %	High Size	Under %	High Size	Under %	High Size	Under %	High Size	Under %	High Size	Under %	Span 0.74
180	100	64.4	80.5	23.0	4.3	8.25	3.2	2.95	3.1	1.06	2.3	D[4,3] 52.15µm
164	99.9	58.7	68.6	21.0	3.9	7.51	3.2	2.69	3.1	0.96	2.1	
149	99.9	53.4	54.4	19.1	3.7	6.84	3.2	2.45	3.1	0.88	1.9	
136	99.8	48.7	40.2	17.4	3.5	6.23	3.2	2.23	3.1	0.80	1.7	D[3,2] 14.14µm
124	99.7	44.3	28.6	15.9	3.4	5.67	3.2	2.03	3.0	0.73	1.6	
113	99.5	40.4	20.2	14.4	3.4	5.17	3.2	1.85	3.0	0.66	1.4	
103	99.0	36.8	14.3	13.2	3.3	4.71	3.2	1.68	2.9	0.60	1.3	D[v,0.9] 71.68µm
93.6	98.2	33.5	10.4	12.0	3.3	4.29	3.2	1.53	2.8	0.55	1.0	
85.2	96.6	30.5	7.7	10.9	3.3	3.91	3.2	1.40	2.7	0.50	0.7	
77.6	94.0	27.8	6.0	9.94	3.2	3.56	3.2	1.27	2.6			D[v,0.1] 33.13µm
70.7	89.1	25.3	5.0	9.05	3.2	3.24	3.2	1.16	2.5			
Source = :Sample Focal length = 100 mm Presentation = stnd				Beam length = 2.2 mm Residual = 0.611 % Obscuration = 0.2505 Volume distribution				Model indp Volume Conc. = 0.0881% Sp.S.A 0.1601 m^2/gm.				D[v,0.5] 51.95µm

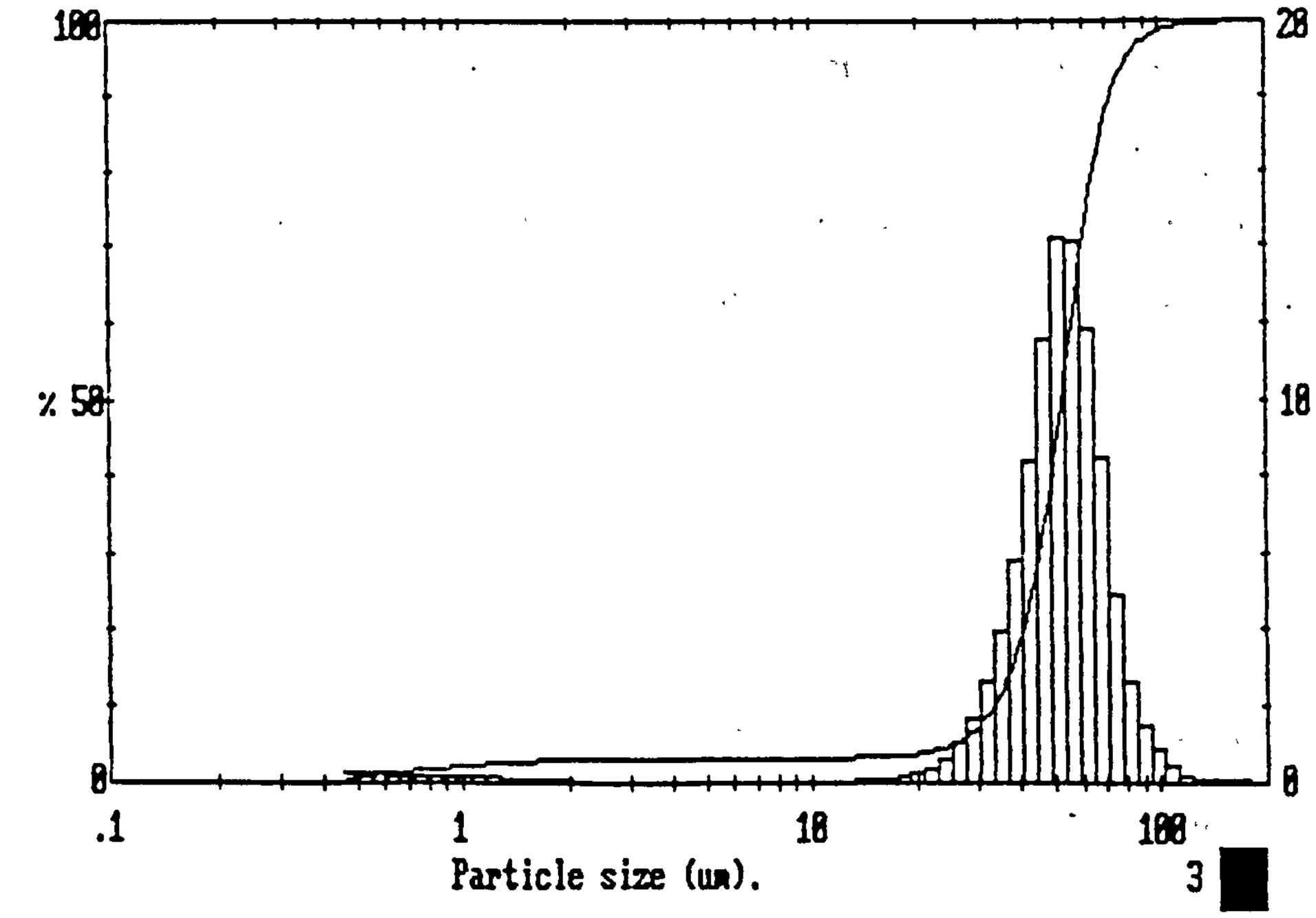

Figure 3.4 The particle size, distribution, and specific surface area of ballotini glass beads determined using a Malvern MS20 Master Sizer

the particles. The experimental sample with 20(w/w)% ballotini (i.e. solid:liquid ratio = 1:4) having pH=2.08 and 3.5% NaCl was titrated with NaOH. After each addition of NaOH the pH of the solution was measured. Following this, a solution sample without ballotini having the same pH, salinity and volume to the ballotini solution was titrated. The amount of NaOH used to produce a given pH value in the ballotini solution was then reduced by the amount necessary to produce this given pH value in the sample of the NaCl solution. This difference then constituted the amount of the OH^- ions adsorbed by the surface at the given pH value, and corresponded to the charge density on the ballotini surface.

3.5 Estimated Macromolecular and Pore Sizes

Polymer Rod Size: In order to make some estimate of the actual size of the depleted layer, we need to calculate the size of the xanthan molecule in solution and it is also helpful to estimate the average effective hydraulic radius (~ pore size) in the porous medium. Using relationships derived by Layec and Wolff (1974) and reported by Richards (1980) and Chauveteau (1982), the rod length, L, of the xanthan molecule may be estimated by follow equation:

$$L^3 = \frac{20}{\pi N_A}[\eta]M(\ln 2p - 0.5) \qquad [3.5]$$

where N_A is Avogadro's number, equal to 6.023 X 10^{23}; M is the polymer molecular weight; and p is the length-to-diameter ratio of rigid particles. For p >> 1, then:

$$\upsilon = \frac{[\eta]}{\upsilon_{sp}} = 0.159p^{1.801} \qquad [3.6]$$

where υ is the viscosity factor and υ_{sp} is the specific volume, equal to 0.620 for oligosaccharides. Therefore,

$$p^{1.801} = 10.14[\eta] \qquad [3.7]$$

Assuming that the molecular weight of xanthan is approximately $4x10^6$ (Broseta et al, 1992) and the intrinsic viscosity is 6,300 cm^3/g at salinity 35 g/l NaCl and pH 5.0, the rod length of the xanthan molecule is calculated to be ~1.2 μm and the diameter of the molecule is $2.6x10^{-3}$ μm.

Hydraulic Radius: In order to estimate the approximate magnitude of the pore size, an equivalent capillary bundle model of the porous medium may be used. Thus, an average hydraulic radius within the porous medium, r, may be defined as follows :

$$r = \sqrt{\frac{8kC}{\phi}} \qquad [3.8]$$

where C is a constant equal to 25 /12, and this leads to a characteristic capillary radius of approximately 7.00 μm.

3.6 Pack Flooding Methods

A schematic diagram of the porous medium flow apparatus used in this work is shown in Figure 3.5. The polymer fluid displacement system consisted of two pumps, a Pharmacia P-500 high precision pump was used for brine initial and postflush, and an ISCO μLC-500 micro flow pump was used for polymer injection. Some repeated experiments of polymer injection were performed by using a Harvard 940A (glass) syringe pump which display good repeatabilities of the apparent viscosities compared with those by using the ISCO pump implying that the effect of potential dissolved Fe+3 from the steel syringe of the ISCO pump on xanthan molecular conformation is negligible. The initial flooding experiment was a single-phase displacement of the brine by the lithium labelled xanthan solution in a ballotini packed column initially saturated by brine. The non-adsorbing

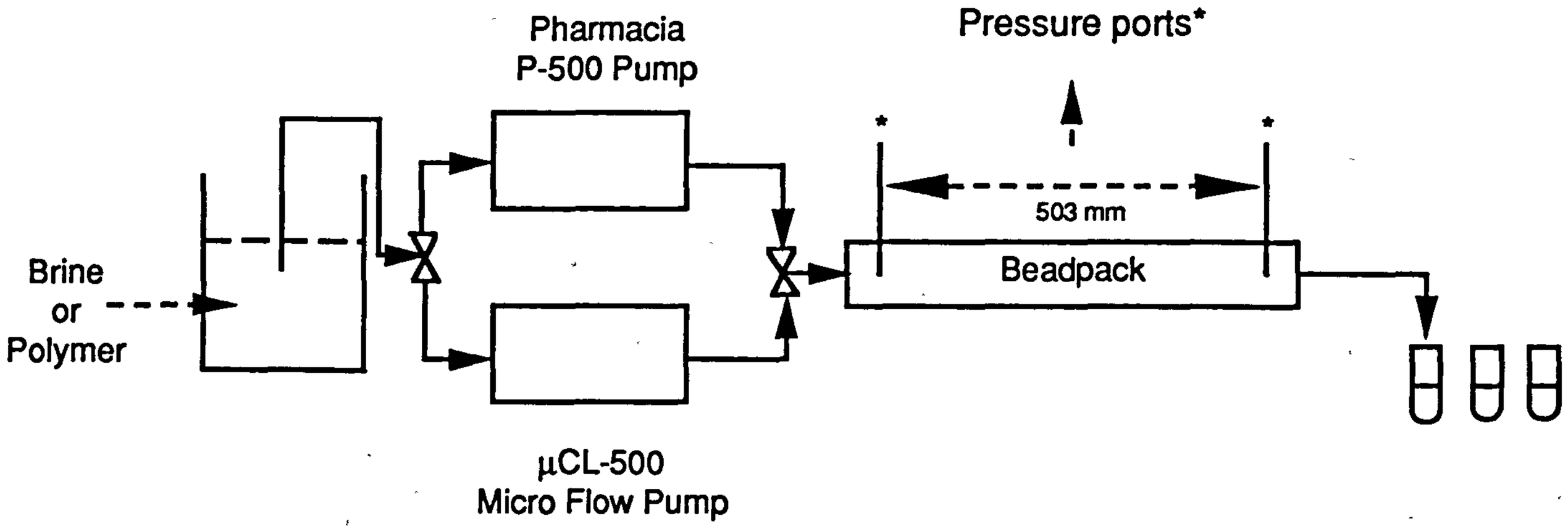

Figure 3.5 Schematic diagram of the porous medium flow apparatus

tracer (lithium) was added to the injected polymer solution to track the injected solvent profile.

For each polymer solution, the initially injected rate was 10 ml/hour. Effluent samples were collected by a Pharmacia LKB HeliFrac Fraction Collector and were analyzed using either a Contraves LS 30 Viscometer for polymer or a SpectrA-10 Atomic Absorption Spectrophotometer for lithium (Li^+) tracer until steady-state values of both polymer and tracer concentrations were reached. Also, a Philips PW9420 pH meter was used to measure the pH of the xanthan solutions in some cases. From the effluent profiles during this initial phase, the relative advancement of the xanthan to the lithium tracer was measured. After the steady state input concentration was reached in the effluent, the flow rate of injected polymer solution was normally varied over the range 3 μl/min to 300 μl/min corresponding to frontal advance rates of $1.8x10^{-4}$ to $1.8x10^{-2}$ cm/s.

Differential pressures at each flow rate were measured at the stabilised pressure drop using Druck pressure transducers having a precision of 0.1 mbar at the inlet and 0.01 mbar at outlet. Compared with the conrresponding water manometer, the pressure transducers at both inlet and outlet were calibrated and were confirmed to display the same reading at each given flow rate and the same linear relationship with various flow rates. The very good repeated data of pressure drop for each given flow rate were observed during a flooding process. The relative error of pressure drop was estimated to be less than ± 0.5%. In order to obtain the differential pressure data as accurate as possible, the effluent collecting point was kept to a position of about 30 cm higher than packed column, and the pressure indicators at both inlet and outlet must display the same number before each injection and after shut in. The dead volume of the packed test column, which is total 1.2 ml, also was fully considered during the effluent collection.

Apparent viscosities within the porous medium were determined at each velocity using Darcy's law as expressed by Eq. [2.5] and the corresponding porous medium shear rate was calculated from Eq. [2.6]. The results were then compared with those for the bulk

fluid. Brine permeability was determined following polymer flow at each xanthan concentration after a long brine postflush. All experiments were performed at 21°C (± 1°C).

CHAPTER 4

THE EFFECT OF XANTHAN CONCENTRATION ON ITS FLOW BEHAVIOR IN POROUS MEDIA

4.1 Introduction

The main concern in this Chapter relates to xanthan transport in porous media in the presence of depleted layer effects as described in Chapter 2 and illustrated in Figure 2.5. Both the transport (frontal advancement) and rheological (apparent slip) aspects of the effect are studied. Most previous experimental work which has examined these issues has focussed attention on higher xanthan concentrations (>300 ppm). In this Chapter, the rheology of lower concentration xanthan solutions (between 30 ppm and 200 ppm) in flow through porous media is mainly consider, and some new results from the experiments are presented. All of the experimental solutions used in this chapter have a salinity of 35 g/l NaCl and pH 5-6.

The experimental results show polymer advancement in porous media for all of the experimental polymer/tracer systems studied and lower observed in situ apparent viscosity than that of the bulk solution even for very low xanthan concentrations. It is certain that these results are due to the depleted layer effect in the experiments since the permeability of the bead packs used in this work are quite high (~ 1 Darcy; ~ 1 μm^2) and pore sizes are fairly large and uniform. The rheological data is analysed using a simple two fluid model due to Chauveteau and coworkers (Chauveteau, 1982; Chauveteau *et al.*, 1984) as well as a linear layer analytical model which has appeared recently (Sorbie, 1990a). Over the low polymer concentration range from 30 ppm to 200 ppm (which corresponds to values of the overlap parameter in the range, $c[\eta] = 0.19$ to 1.26), it is evident that the effective depleted layer thickness, (δ/r), apparently decreases with increasing polymer

concentration as estimated from both the simple two-fluid and the linear layer rheological models. However, at a higher concentration of 400 ppm, (δ/r), does not continue to decrease with increasing xanthan concentration.

In this chapter, it has also been found that the power law index is higher than the bulk value (i.e. the slope of the η_{app} vs. $\dot{\gamma}_{pm}$ is lower) for all polymer concentration values used in this work. This latter result is in accord with previous experimental findings (Chauveteau and Zaitoun, 1981; Chauveteau, 1982) and with theoretical predictions from network models of depleted layer flow in porous media (Sorbie, 1989; 1990).

4.2 Polymer / Tracer Separation

None of the previous studies on xanthan flow in porous media has reported results for both the polymer advancement during transport and the rheological behaviour for the same system. Results for both transport and rheological behaviour are presented in this Chapter. Several cycles of flood experiments were performed and each was carried out using the same packed column in order to make more consistent comparison of results. Almost no xanthan adsorption on the ballotini packs was observed from the measurement of both effluent concentration (material balance) and negligible permeability changes were observed between the polymer floods in each column The brine permeabilities between polymer floods were evaluated at five different flow rates and averaged.

The sequence of polymer injections began with 30 ppm solution followd by higher concentrations. Effluent polymer and tracer profiles for a typical core-flood experiment show the effects of dispersion and excluded volume at the leading edge of the slug and viscous fingering at the trailing edge. Viscous fingering is only clearly evident for the 150 ppm or higher concentration polymer slugs in this work. Since this phenomenon has been studied in some detail for xanthan propagation through porous media in previous work, we consider only the transport behaviour at the frontal parts of the xanthan and lithium slugs at the fixed flow rate of 10 ml/hour (frontal velocity = 1.0×10^{-2} cm/s).

Figures 4.1 - 4.4 show the frontal effluent profiles for 30 ppm, 50 ppm, 100 ppm, and 150 ppm xanthan solutions respectively in one of the ballotini packs. The earlier breakthrough of the polymer relative to the tracer is clearly visible for all floods. Such profiles have been measured for all of the polymer solutions studied and results are discussed below.

In assessing the amount of polymer advancement compared with tracer that is observed, an exclusion factor, F_ϕ, (sometimes referred to as a *retardation factor* (Van Genuchten, 1981; Sorbie *et al.*, 1987) may be defined as follows:

$$F_\phi = \frac{\phi_p}{\phi} = \frac{PV_p}{PV} \qquad [4.1]$$

where ϕ and PV are porosity and pore volume respectively, and ϕ_p and PV_p are the corresponding effective porosity and pore volume available to polymer. Calculations based on the effluent polymer and tracer profiles for all the floods are shown in Table 4.1 where estimates of the effective porosity values for polymer compared with tracer in the pack are presented. The quantity, F_ϕ, is approximately 0.91 in these experiments, which is similar to values measured in earlier work in high permeability outcrop sandstone cores (Sorbie et al, 1987), indicating that about 0.09 PV of the pack is excluded to the polymer. Note that two methods have been used to calculate F_ϕ based on (i) a straightforward evaluation of the area difference between the polymer and tracer profiles and (ii) fitting of these effluent profiles to analytical solutions of the 1D convection dispersion equation as described elsewhere (Van Genuchten, 1981; Van Genuchten and Alves, 1982; Sorbie et al, 1987). It is seen from Table 4.1 that both methods give quite similar estimates of F_ϕ.

In addition to the F_ϕ factor, the analytical method (ii) also gives a measurement of the polymer and tracer dispersion coefficients which are also presented in Table 4.1. It is noted that the polymer dispersion coefficient is greater than that of the tracer by a factor of ~2 or more which confirms earlier experimental results (Sorbie et al, 1987; Kolodziej,

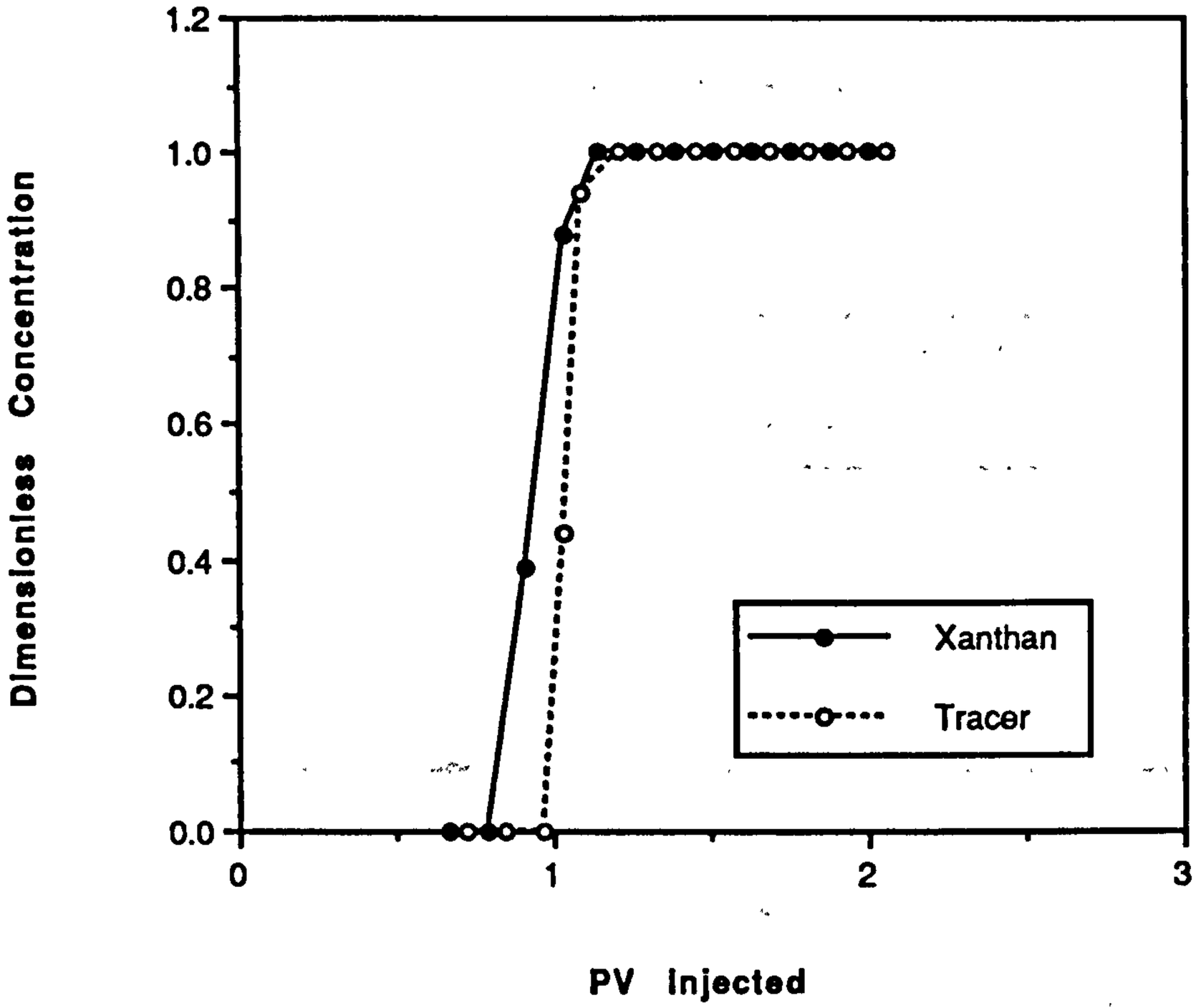

Figure 4.1 Frontal effluent profiles for 30 ppm xanthan solution in 35 g/l NaCl and lithium tracer

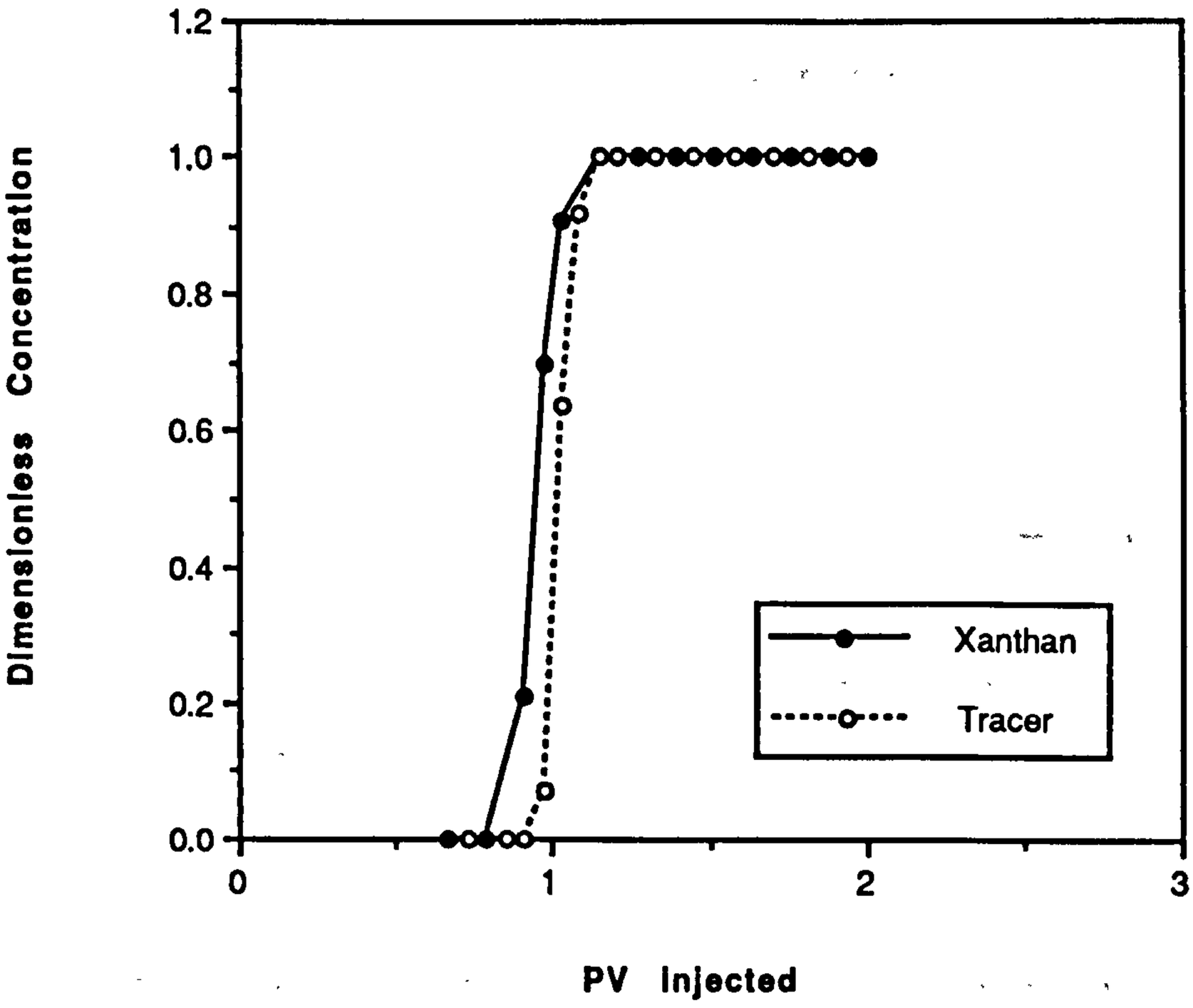

Figure 4.2 Frontal effluent profiles for 50 ppm xanthan solution in 35 g/l NaCl and lithium tracer

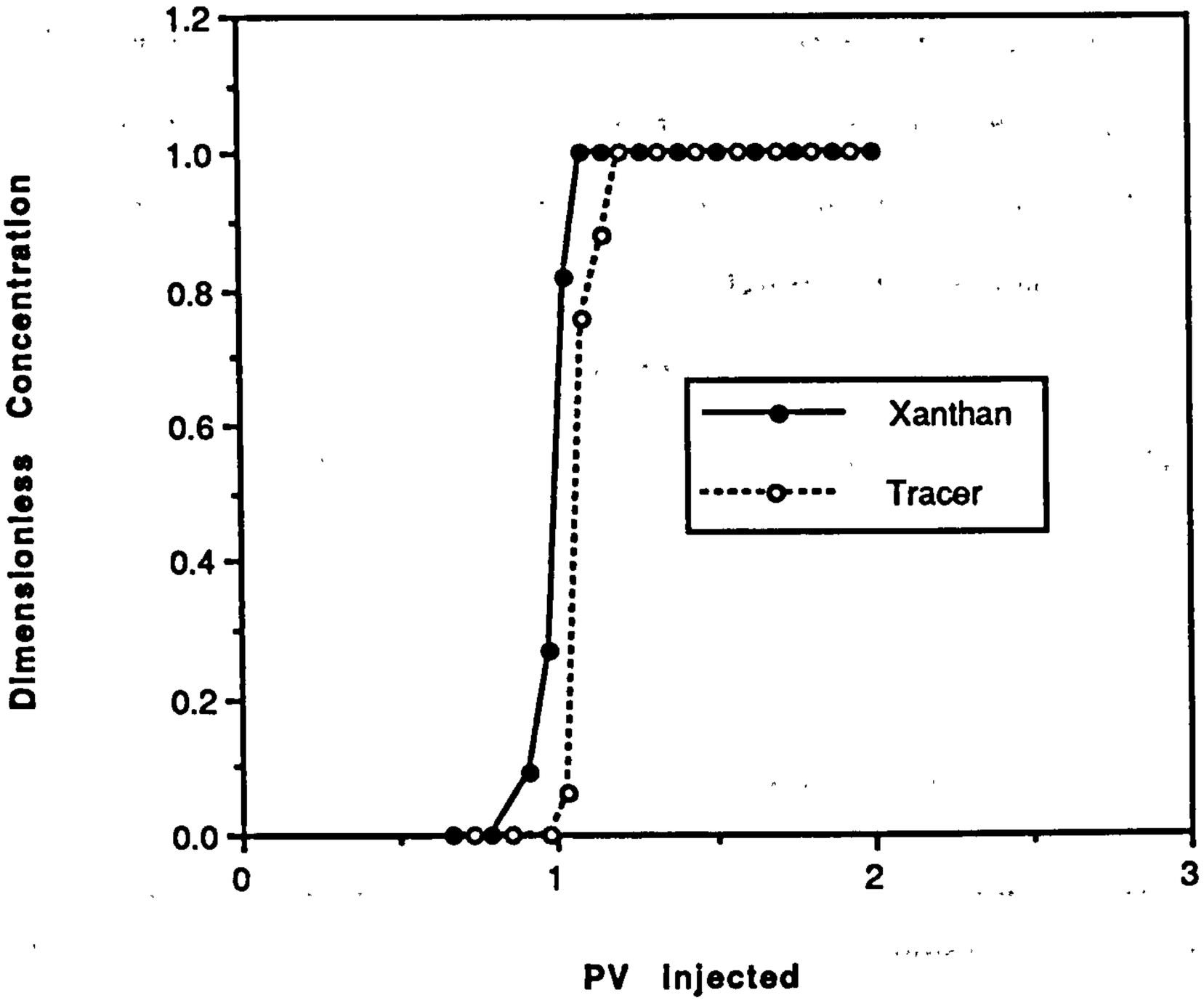

Figure 4.3 Frontal effluent profiles for 100 ppm xanthan solution in 35 g/l NaCl and lithium tracer

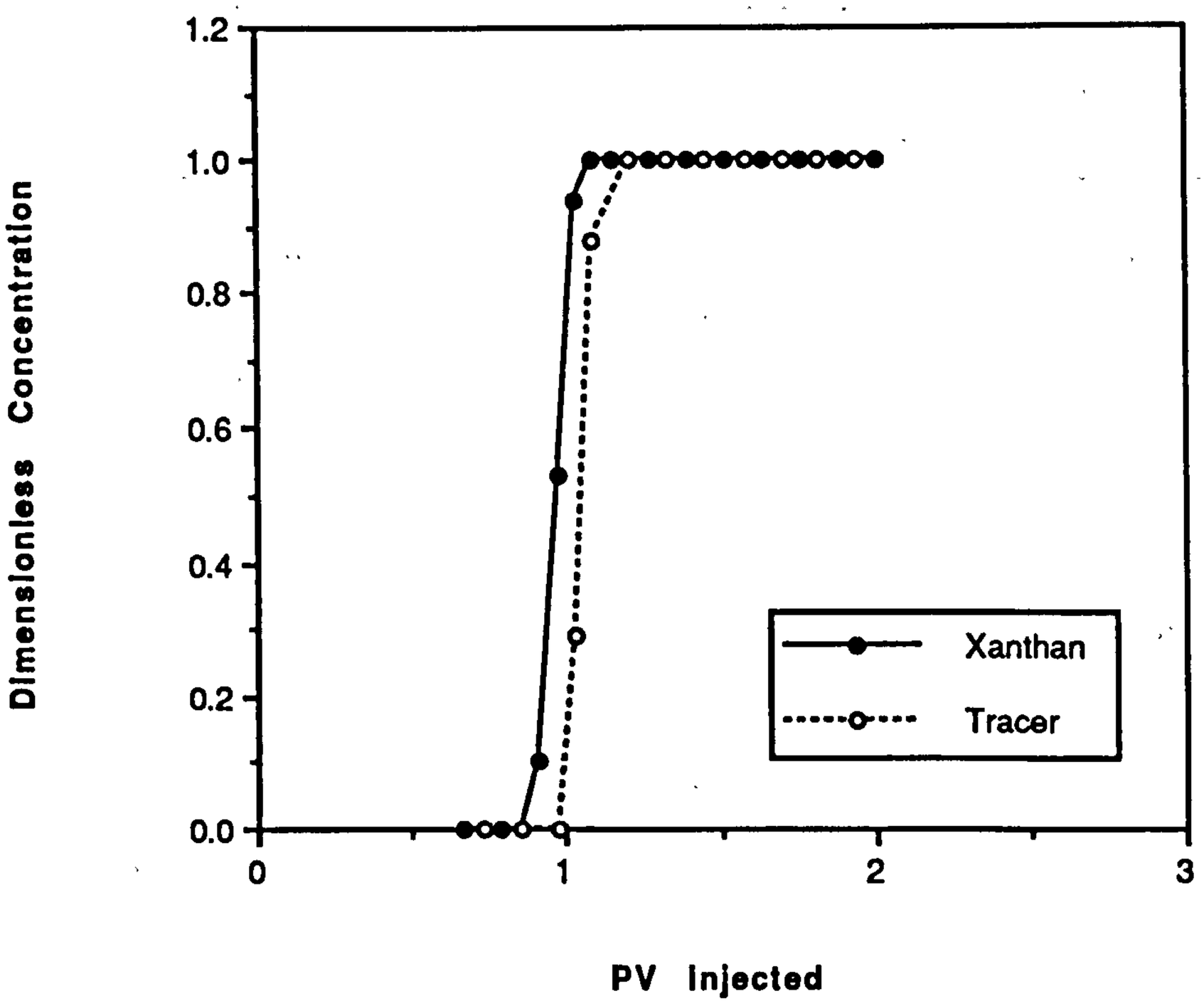

Figure 4.4 Frontal effluent profiles for 150 ppm xanthan solution in 35 g/l NaCl and lithium tracer

1988). There are two views as to why the polymer dispersion coefficient is greater than that of the tracer based on arguments relating to (a) the surface size exclusion effect leading to a molecular weight fractionation (Lecourtier and Chauveteau, 1984; Brown and Sorbie, 1989) or (b) the effective local Peclet number that determines the flow regime for tracer and macromolecular species which depends on the relative magnitude of the tracer and polymer diffusion coefficients (Sorbie and Clifford, 1991). However, this issue is beyond the scope of this thesis and will not be pursued further here.

Table 4.1

Frontal Analysis of Effluent Profiles[1]

Xanthan concentration (ppm)	Exclusion Factor (F_ϕ) from area difference	Exclusion Factor (F_ϕ) from direct fit to analytical solutions[2]	Polymer Dispersion Coefficient[2] ($x10^{-4}$ cm^2/s)	Tracer Dispersion Coefficient[2] ($x10^{-4}$ cm^2/s)
30	0.90	0.90	22.7	3.5
50	0.92	0.93	8.6	4.1
100	0.91	0.93	5.5	2.1
150	0.91	0.92	6.2	3.3

1. Data from experimental No. 4.1 in Table 4.2; flow rate is 10 cm^3/hour and the corresponding frontal velocity is 1.0×10^{-2} cm/s.
2. From analytical fitting method

The reason for the relative advancement of the polymer compared with the tracer species may, as discussed above, be due to either a surface exclusion or IPV mechanism. However, in this case, we conclude that pore wall exclusion is the main reason for the increased polymer velocity because of the higher permeability (~ 1.0 Darcy) and relative homogeneity of the ballotini glass packed column. The results in the following section on xanthan rheology will support this viewpoint.

4.3 In Situ Xanthan Rheology

As noted above, very low concentration xanthan solutions have been used in this work for the measurement of the in situ rheology of the polymer which has then been compared with the bulk fluid viscometric data. The measured η_{app} vs. $\dot{\gamma}_{pm}$ for a very careful sequence of experiments in one bead pack are shown in Figure 4.5 to 4.8 where they are compared with corresponding bulk fluid η vs. $\dot{\gamma}$ data. In these figures, the porous medium shear rate, $\dot{\gamma}_{pm}$, is determined with the factor $\alpha = 1$ (Eq. [2.6]) but, since we are primarily interested in the low flow rate Newtonian regime, the chosen value of α is not important here. It is clear that the low shear Newtonian in situ viscosities are below the bulk fluid viscosities even at very low xanthan concentrations (~30 ppm). A summary of some experimental results in the Newtonian flow regime is presented in Table 4.2. These in situ rheology results in the pseudo Newtonian regime provide a clear confirmation of the earlier experimental findings of Chauveteau and coworkers (Chauveteau and Zaitoun, 1981; Chauveteau, 1982; Chauveteau et al, 1984).

Much other work on xanthan flow in porous media has failed to detect apparent slip effects at low flow rate (Greaves and Patel, 1985; Willhite and Uhl, 1986; Hejri et al, 1988; Cannella et at, 1988). For example, Willhite and Uhl (1986) reported only power law behaviour of xanthan in flow through porous media and Cannella et al (1988) found that the low flow rate in situ apparent viscosity of xanthan was generally *above* the bulk fluid viscosity. However, in both of these studies, higher concentration polymer solutions (well into the semi-dilute regime, $[\eta]\, c > 5$) were used leading to a more significant contribution of polymer-polymer molecular interactions. Also, in those studies, microgel-free xanthan solutions were *not* used and this may also have affected the in situ rheological measurements. Chauveteau et al (1991) proposed a "reversible adsorption" explanation in which they thought that even a weak attractive interaction presented between polymer and interface may lead to effective viscosity higher than that predicted by the two fluid model, especially at high salinities. In this work, It tends to suggest that the apparent slip/surface exclusion effect is most clearly observable at low

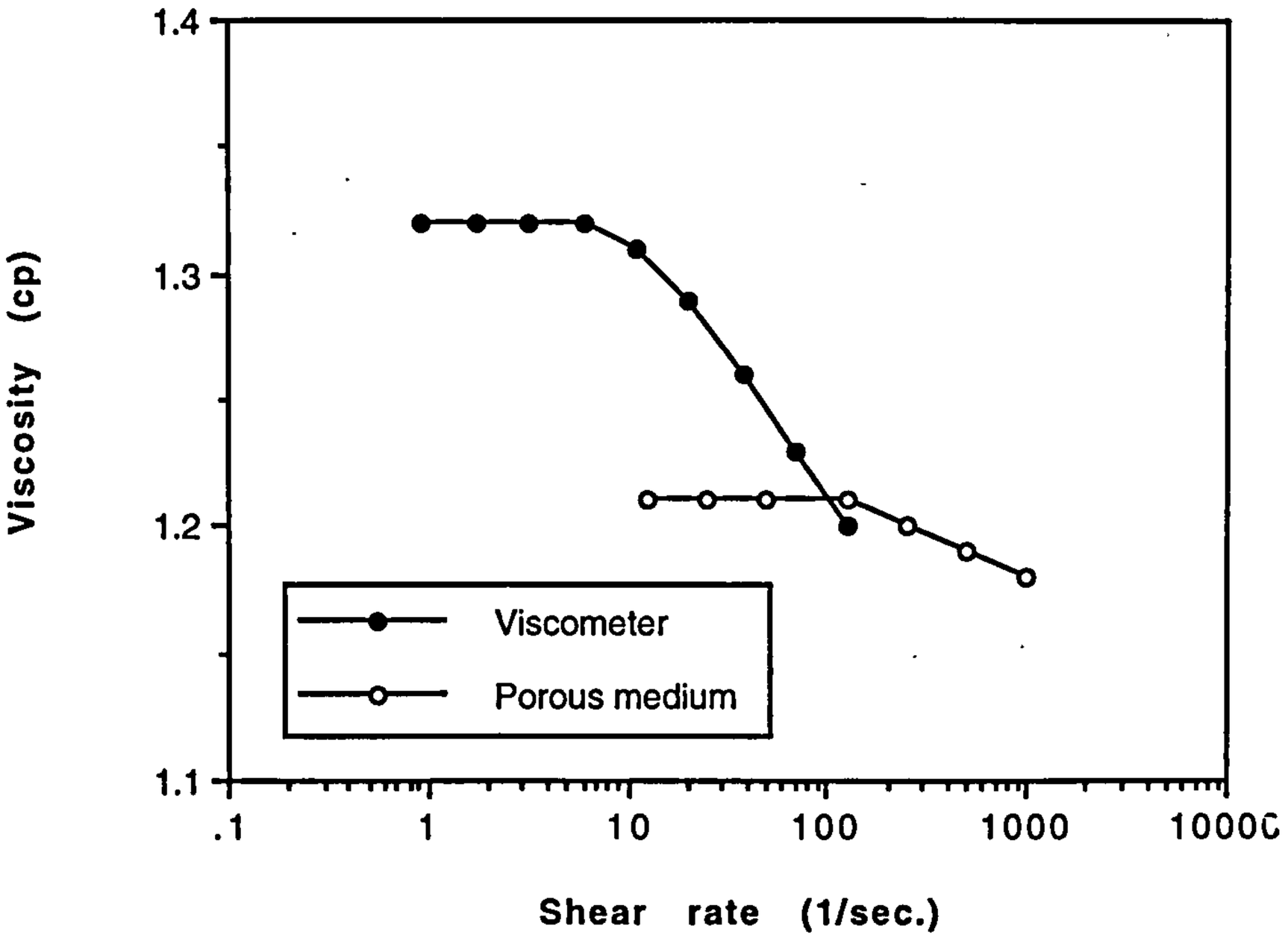

Figure 4.5 Comparison of in situ apparent viscosity and bulk viscosity for 30 ppm xanthan solution

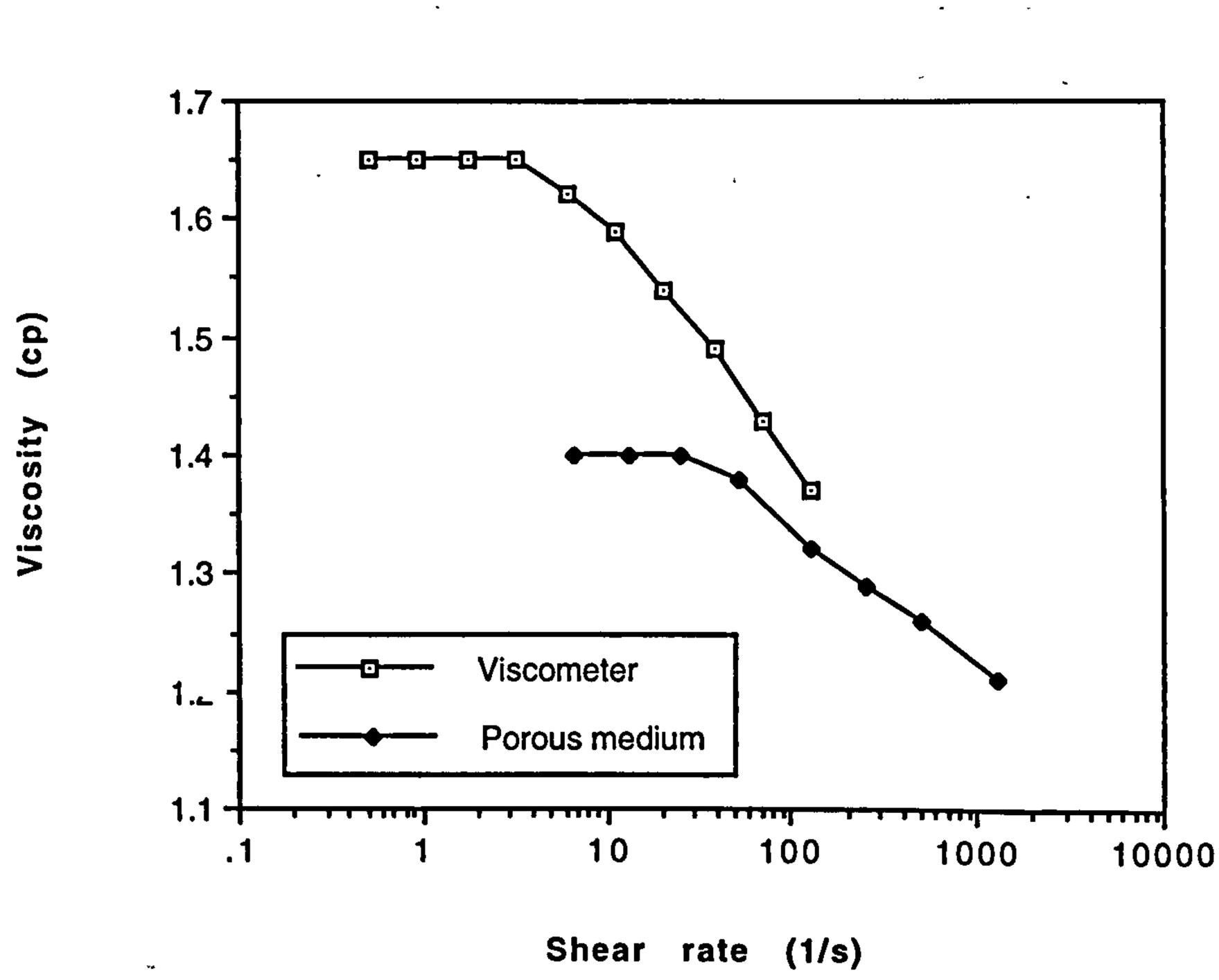

Figure 4.6 Comparison of in situ apparent viscosity and bulk viscosity for 50 ppm xanthan solution

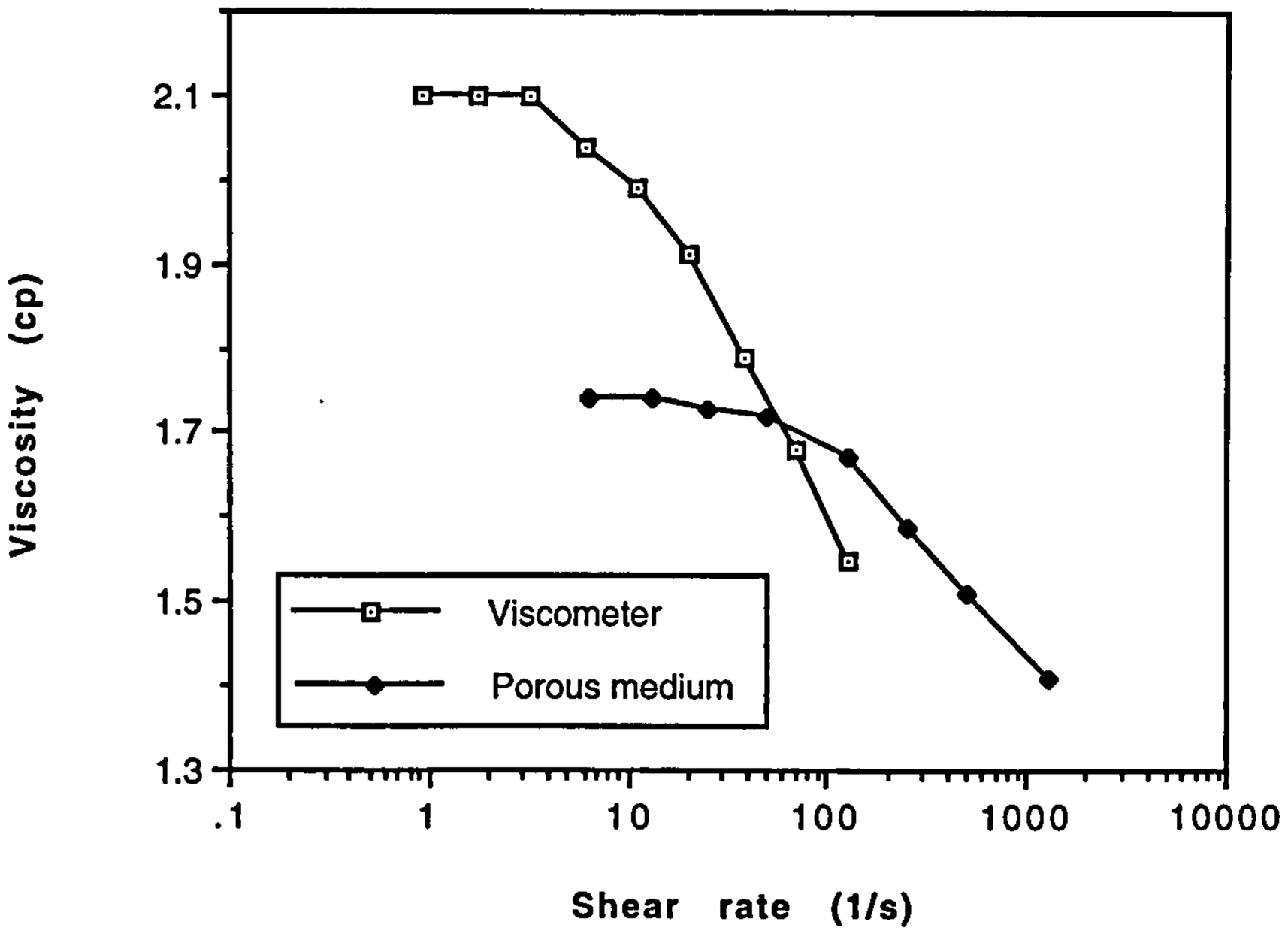

Figure 4.7 Comparison of in situ apparent viscosity and bulk viscosity for 100 ppm xanthan solution

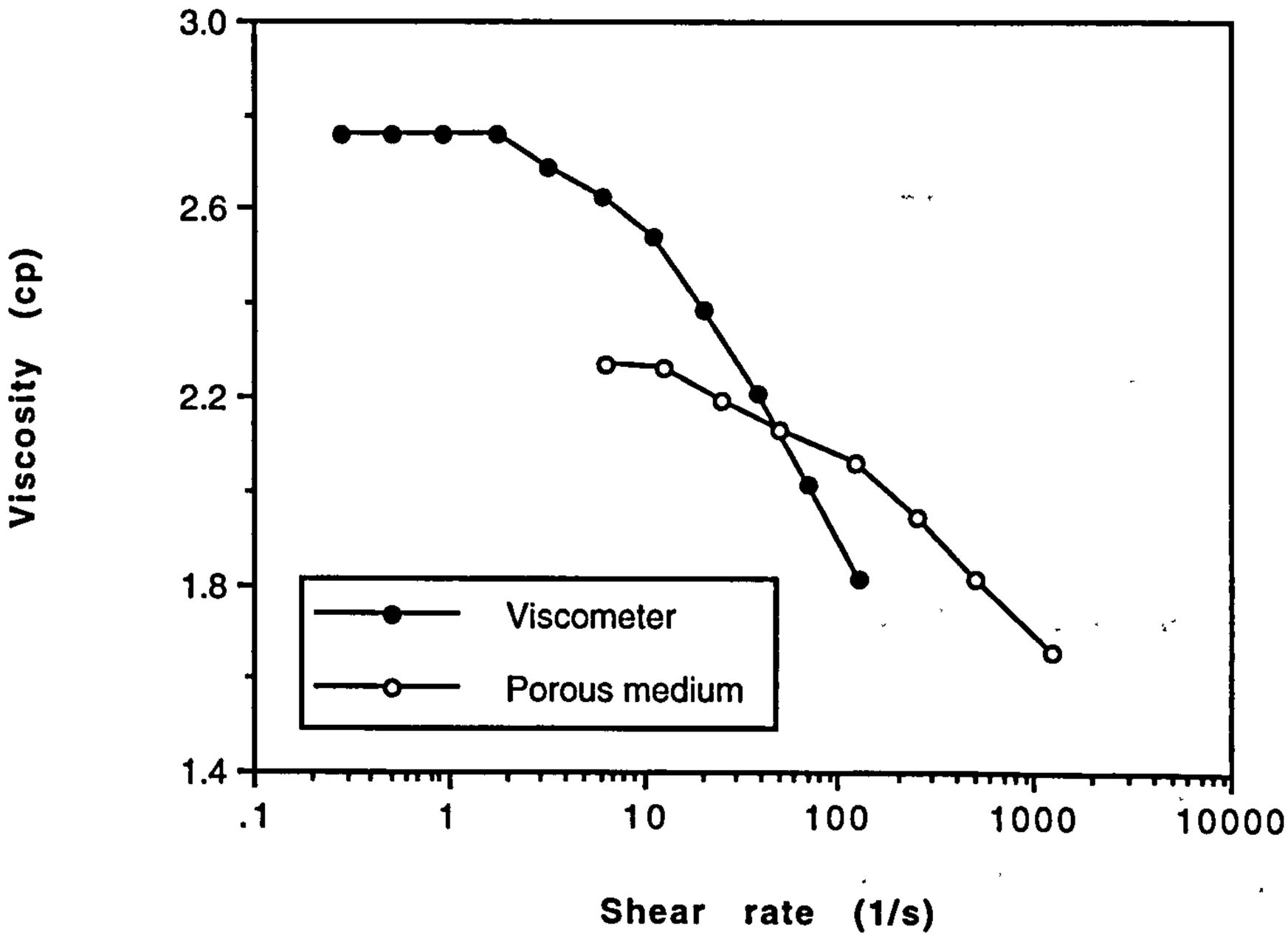

Figure 4.8 Comparison of in situ apparent viscosity and bulk viscosity for 150 ppm xanthan solution

polymer concentration for microgel-free solutions. In addition, we observe that the magnitude of this rheological effect is quite significant even in the high permeability packs used in this work (k ~ 1Darcy; ~ 1μm^2)

Table 4.2

Comparison of the Two-Fluid Depleted Layer Model with the Linear Layer Model

Exp. No.	Conc. (ppm)	η_b (cp)	η_{app} (cp)	% Viscosity decrease	δ/r Two-fluid model [A1]	δ/r Two-fluid model [A2]	δ/r Linear Layer model [A3]
4.1	30	1.32	1.21	8.33	0.330	0.334	0.241
	50	1.57	1.37	12.7	0.283	0.322	0.206
	100	2.10	1.80	14.3	0.159	0.184	0.120
	150	3.06	2.57	16.0	0.116	0.140	0.081
4.2	30	1.31	1.22	6.87	0.242	0.271	0.194
	50	1.65	1.40	15.1	0.334	0.394	0.226
	100	2.10	1.74	17.1	0.215	0.228	0.153
	150	2.76	2.27	17.8	0.151	0.159	0.105
4.3	50	1.53	1.37	10.5	0.219	0.257	0.171
	100	2.08	1.73	16.8	0.212	0.223	0.152
	200	3.90	3.20	17.9	0.112	0.121	0.073

4.4 (δ/r) as a Function of Low-Concentration Xanthan Solution

An example of the measured η_{app} vs. $\dot{\gamma}_{pm}$ for various polymer concentrations in one bead pack as well corresponding bulk data is shown in Figure 4.9. In order to analyse the results in Figure 4.9 and Table 4.2 in more detail, Both the linear layer model (Sorbie, 1990 & Appendix 1) and the two fluid model of Chauveteau et al (1981; 1982; 1984; 1989) have been used as described previously. In applying the linear layer model, the only unknown is the relative depleted layer thickness, (δ/r), since the bulk and solvent

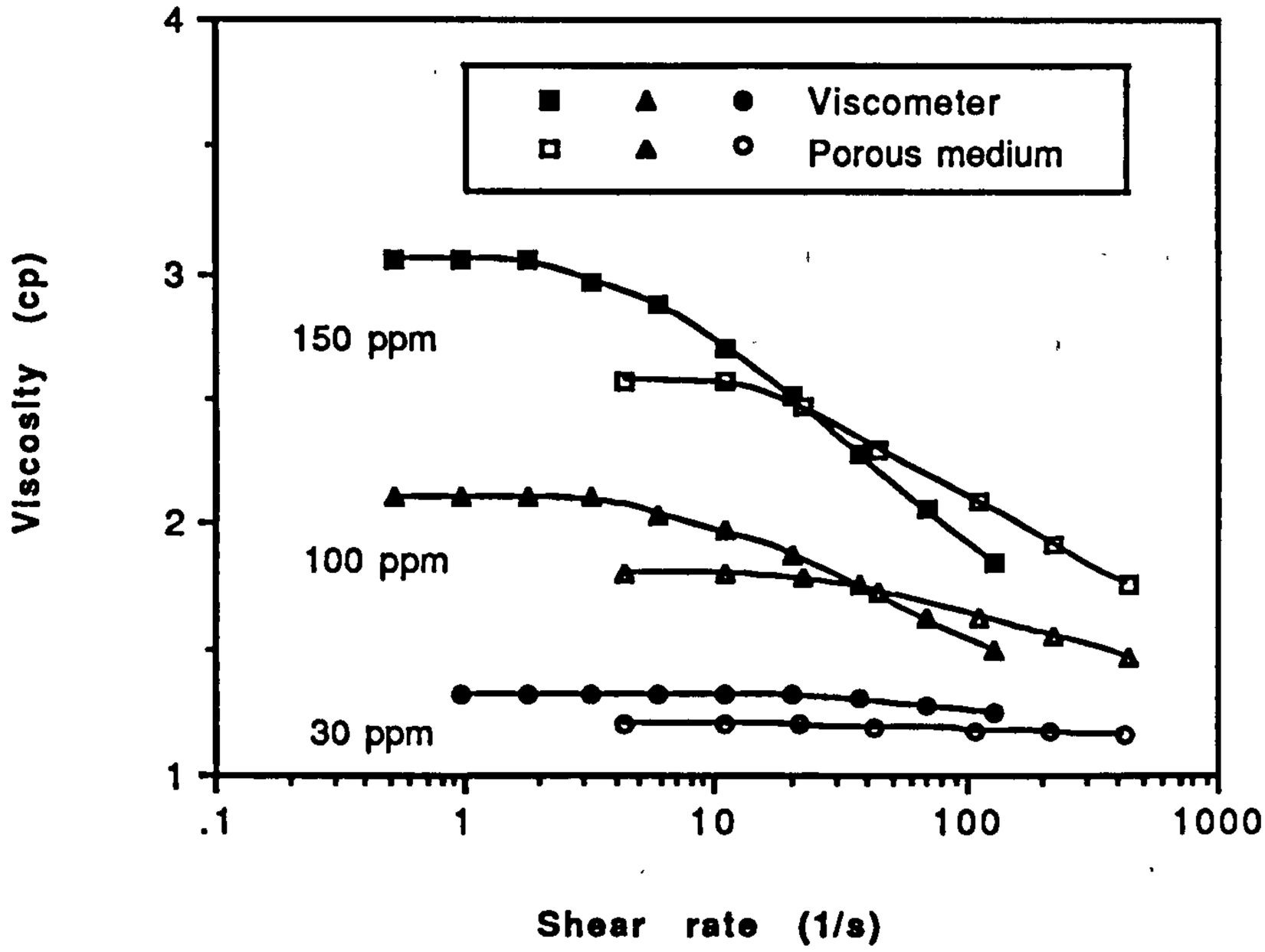

Figure 4.9 An example of the comparison of porous medium and viscometer rheologies for 30, 100, 150 ppm xanthan solution

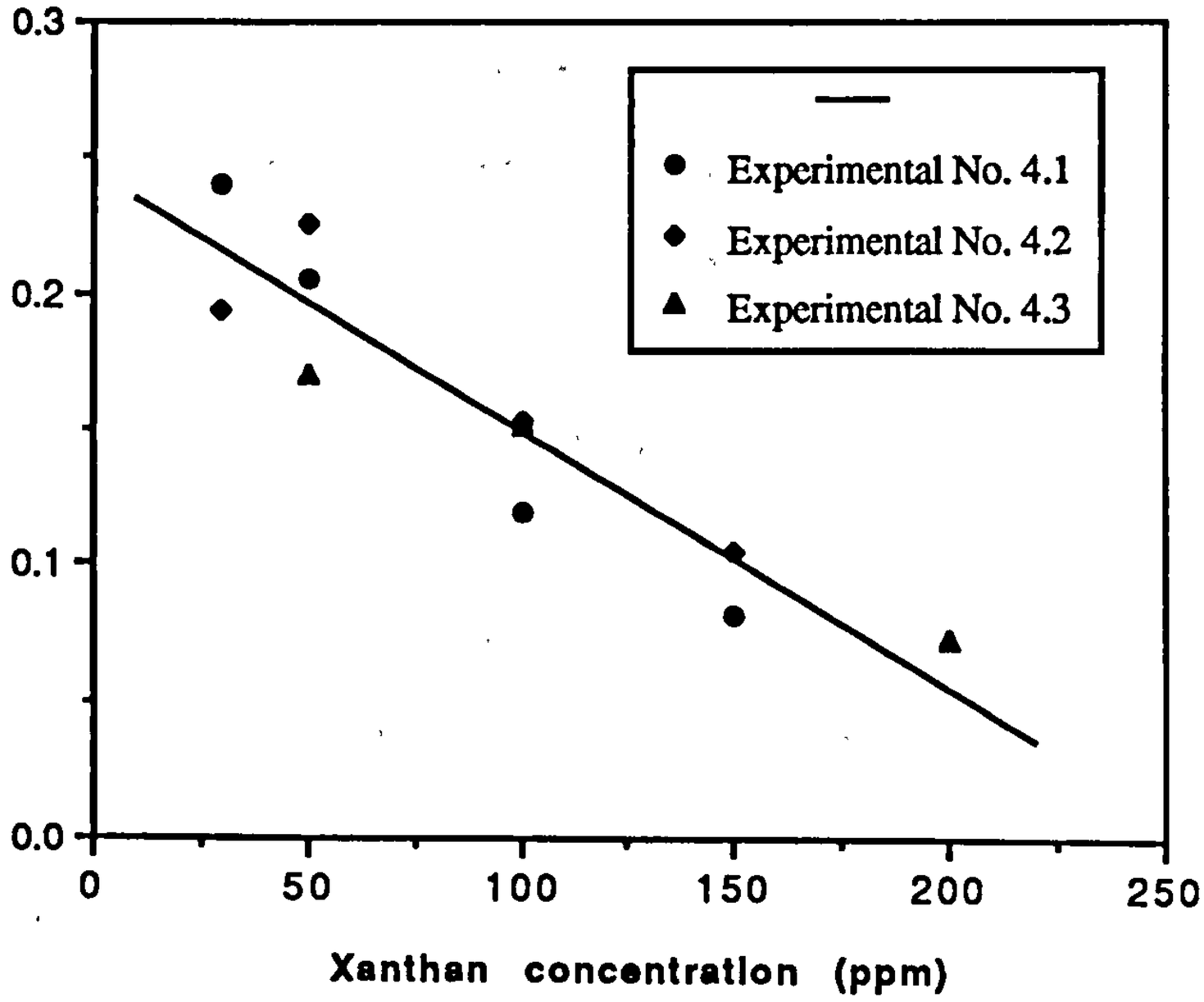

Figure 4.10 Dependence of the relative depleted layer thickness (δ/r) in the porous medium on xanthan concentration as calculated using the linear layer model

viscosities are known as discussed above. In the two fluid model, two assumptions on the evaluation of the viscosity, η_w, in the depleted layer region have been applied. Firstly, we have taken the model as proposed by Chauveteau et al (1984) with $\beta = 0.64$ and, secondly, we have also taken η_w to be the average of the bulk and solvent viscosities ($\eta_w = [\eta_b + \eta_s]/2$). Some approximate justification of the latter assumption is found in previous calculations comparing the two fluid and linear layer model (Sorbie, 1990).

The relative depleted layer thickness, (δ/r), was calculated for all the experimental data collected in this work (Table 4.2) using the linear layer model. The quantity, (δ/r), is shown as a function of polymer concentration in Figure 4.10. Our results indicate quite clearly that the depleted layer thickness decreases with increasing xanthan concentration over the low polymer concentration range studied in this work (30 - 200ppm). This is an interesting result which has been reproduced in several of our experiments using different packings of the same material, and which has not been found previously from viscometric measurements to our knowledge. Some resent results related to polymer concentration effect on depleted layer thickness are summarised in Table 4.3. Indeed, Omari et al (1989), using the two fluid model to analyse their results, state that (δ/r) is constant with concentration but we will return to their results below. Ausséré et al (1986), on the other hand, using a light scattering method, have also found that (δ/r) decreases with concentration over the range 100 to 1000 ppm for xanthan. In order to check the predictions of our model, we have reanalysed our data using the Chauveteau two fluid model under the two assumptions presented above (i.e. β=0.64 and η_w=$[\eta_b + \eta_s]/2$). Figure 4.11 shows (δ/r) as a function of polymer concentration as calculated using both variants of the two fluid model along with linear layer analysis from Figure 4.10 for comparison. Although there is some variation in the actual numerical values of the relative depleted layer thickness obtained from the different models, the trend is very similar and does certainly indicate a definite decrease in (δ/r) with polymer concentration. Thus, our conclusions on this matter appear to be confirmed and we are inclined to agree with the general findings of Ausséré et al (1986).

Table 4.3

A Reference on Concentration Dependent Changes of Apparent Slip in Polymer Solution Flow

Polymer	Concentration range	Results	References
PAM	0.005% - 0.05% (with 0.3% microgels in electrolyte-free aqueous solutions)	The width δ decreased with increasing c	Muller-Mohnssen et al (1990)
flexible-coil polymers HPAM	dilute regime semidilute regime (in 20g/l NaCl)	δ is constant δ diminishes with increasing concentration	Chauveteau et al (1984)
Xanthan $[\eta]_0$=4300 (cm^3/g)	dilute regime higher concentration (in 0.1 M NaCl)	δ is constant δ decreases rapidly	Ausserre et al (1986)
Xanthan $[\eta]_0$=4300 cm^3/g	C[η] = 1-7 (in 5g/l NaCl)	δ is constant	Chauveteau et al (1984)
Xanthan $[\eta]$=6900 cm^3/g	200-1600 ppm (in 5 g/l NaCl)	δ is change	Aubert et al (1982)
Xanthan $[\eta]_0$=4300 (cm^3/g)	272-519ppm (in 5 g/l NaCl)	δ is constant from η_{rb}/η_{rp}-$C_b[\eta]_0$ η decreases according to our calculation	Omari et al (1989)
Xanthan $[\eta]_0$=6400 cm^3/g	30-160 ppm (in 35 g/l NaCl)	δ decreases with increasing conc.	Sorbie and Huang (1991)

We now return to the assertion of Omari et al (1989) that the quantity (δ/r) is, in fact, constant with polymer concentration. Their findings are based on the linearity of (η_b/η_{app}) as a function of $C_b[\eta]_0$ as discussed above. However, their results are plotted for two xanthan samples over a fairly wide concentration range from ~70 to ~1000

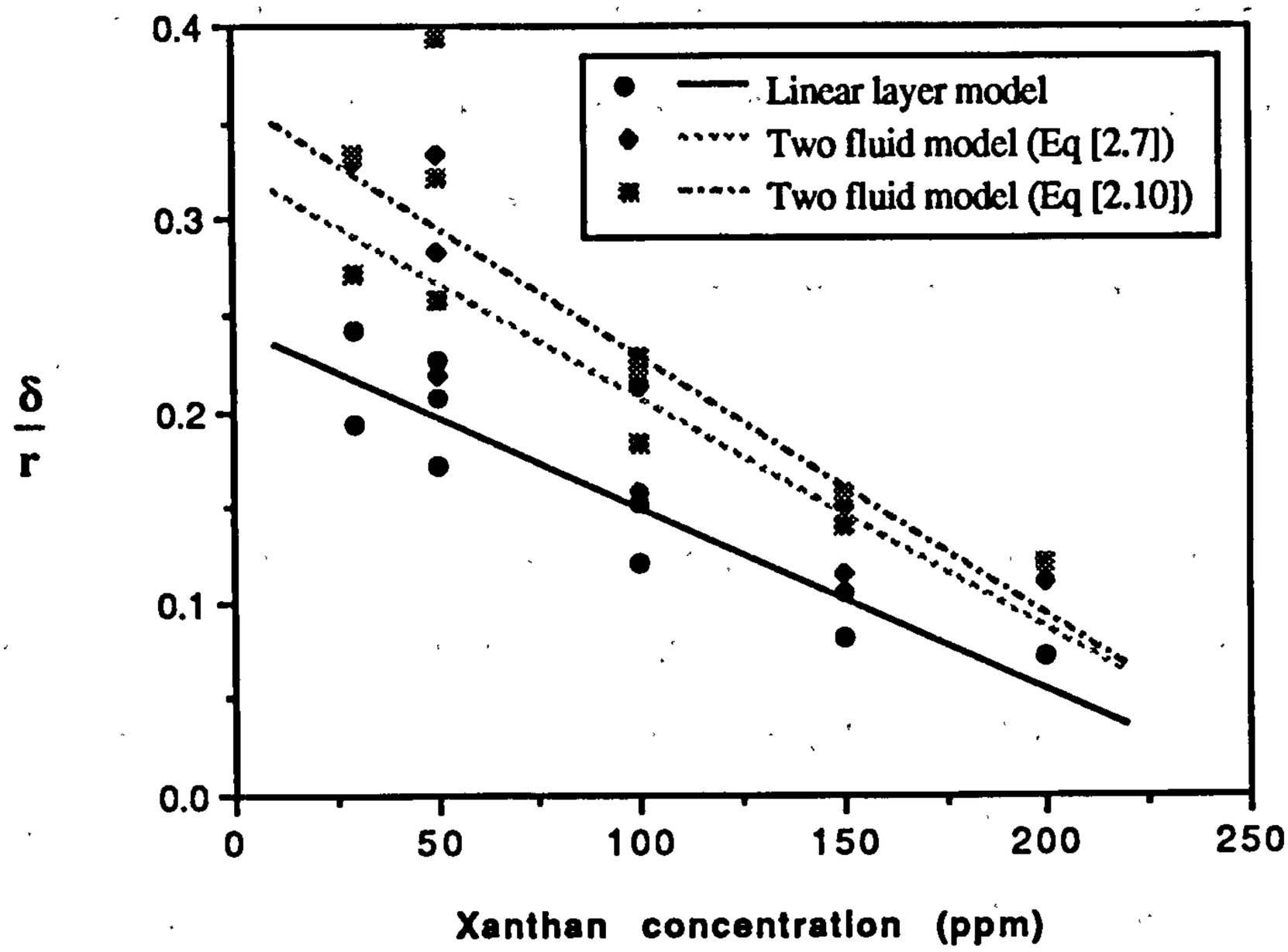

Figure 4.11 Dependence of the relative depleted layer thickness (δ/r) on xanthan concentration as calculated using both the two-fluid and the linear layer models

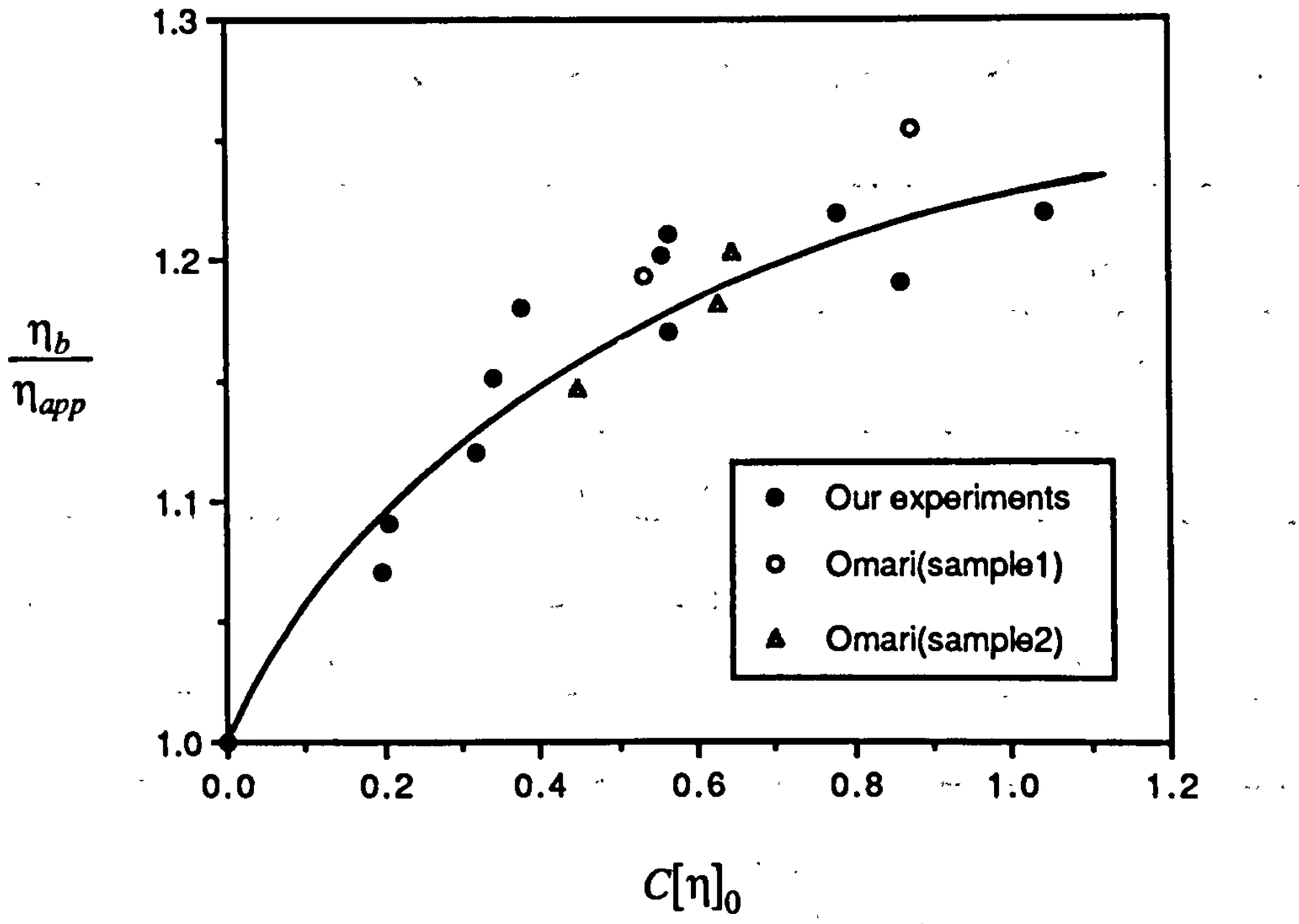

Figure 4.12 Plot of the quantities (η_b/η_{app}) vs $C_b[\eta]_0$ for the data from this work compared with the low concentration results ($C_b[\eta]_0 < 1$) from Omari et al. (1989)

ppm ($C_b[\eta]_0$ from ~ 0.4 to ~3.6) with only 5 data points presented for $C_b[\eta]_0 < 1$. The data presented in this work is replotted in this same manner in Figure 4.12 along with these 5 data points from Omari et al (1989). Clearly, the data of Omari et al (1989) shown in Figure 4.12 are broadly consistent with our results. However, their full set of results at higher concentration would appear in their work to give a linear slope in plot of the type in Figure 4.12

The (δ/r) data in Table 4.2 may be used to estimated the exclusion factor (F_ϕ) value by assuming the pore as a capillary tube. As discussed in section 3.5, supposing the rod length of the xanthan molecule is 1.2 μm and the capillary radius of the pore is 7.0 μm, the values of F_ϕ in porous medium from rheology data are calculated, which are shown and are compared with those from transport data in Table 4.4. The F_ϕ values from polymer rheology seem more or less lower than those from polymer/tracer transport implying a higher exclusion volume is demonstrated. It will be discussed in Section 4.6.

Table 4.4

Depleted Layer Thickness and Exclusion Factor[1]

Concentration (ppm)	Depleted layer thickness[2] δ (μm)	Exclusion factor (F_ϕ) from polymer rheology[3]	Exclusion factor (F_ϕ) from polymer / tracer transport[4]
30	1.69	0.76	0.90
50	1.44	0.79	0.92-0.93
100	0.84	0.88	0.91-0.93
150	0.57	0.92	0.91-0.92

1. Data based on experimental No. 4.1 in Table 4.1 and 4.2
2. Data calculated by Linear layer model at assmption of r = 7.0 μm from Eq. [3.8]
3. in low flow pseudo-Newtonian region (shear rate less than 11.0 s^{-1})
4. for high flow rate 10 cm^3/hour (shear rate around 220 s^{-1})

As noted above in the discussion of polymer transport, this apparent slip phenomenon is almost certainly a result of a wall exclusion effect. However, the dependence of the apparent depleted layer thickness on polymer concentration remains to be explained. It is possible that at the lowest concentration (30 ppm) where $c[\eta] \sim 0.19$ the intermolecular interaction is negligible whereas it becomes somewhat more significant at the highest concentration studied (200 ppm; $c[\eta] \sim 1.26$). Where the rotation of the xanthan semi-rigid rod is completely free (lower concentration), the depleted layer thickness will be larger. At the higher concentration, the hindrance to free rotation may lead to less of a difference in orientational entropy of the polymer molecules between the near-pore-wall region and the bulk region which may result in an effective reduction of the extent of the depleted layer close to the pore wall. However, at present, the precise origin of the decrese in (δ/r) with polymer concentration is not certain. A tentative suggestion which "correlates" these observations, rather than "explaining" them, is presented in appendix B (Huang et al, 1993) and work is still in progress to investigate this effect in more detail.

4.5 In Situ Xanthan Rheology at Higher Polymer Concentrations

A new series xanthan solutions in the concentration range 30 ppm to 400 ppm was used in the experiments reported here. The central problem in this section will be how the depleted layer thickness should vary at higher polymer concentrations. Figure 4.13 shows the rheological behavior of 400 ppm xathan solution. The whole experimental results are shown in Table 4.5 which display a clear apparent slip effect on the in situ rheology of xanthan. As in the last section, the relative depleted layer thickness (δ/r) decreases quite markedly with increasing polymer concentration over the low concentration range used in this work (30-200 ppm). However, at a higher concentration of 400 ppm, (δ/r), does not continue to decrease with increasing xanthan concentration. Figure 4.14 demonstrates the dependence of the relative depleted layer thickness on xanthan concentration as calculated using the linear layer model based on the data presented in Table 4.5. It appears that, at higher concentrations, (δ/r) tends to a constant value. This result is consistent with those of Chauveteau and coworkers (Chauveteau

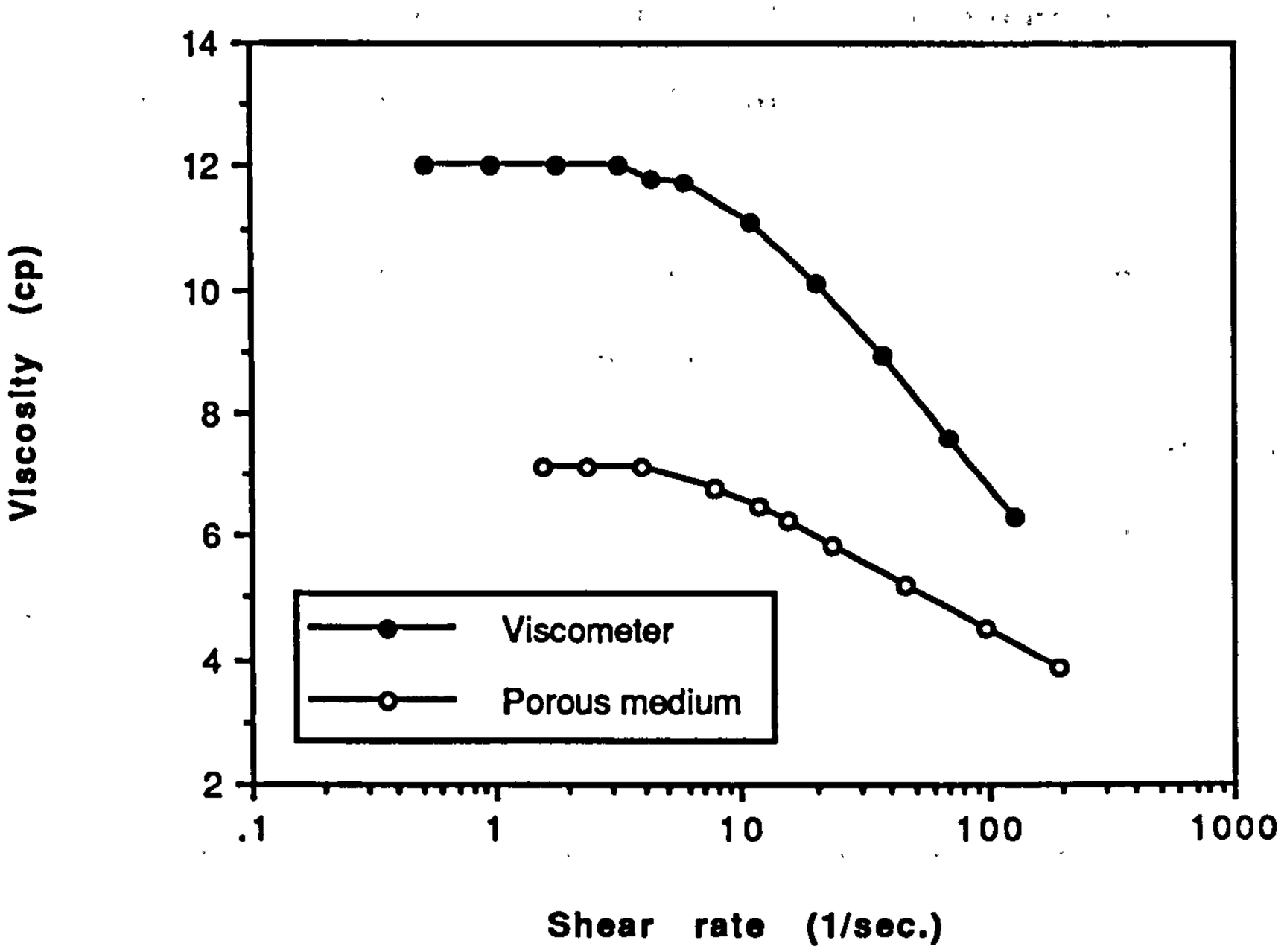

Figure 4.13 Comparison of porous medium and viscometer rheologies for 400 ppm xanthan solution

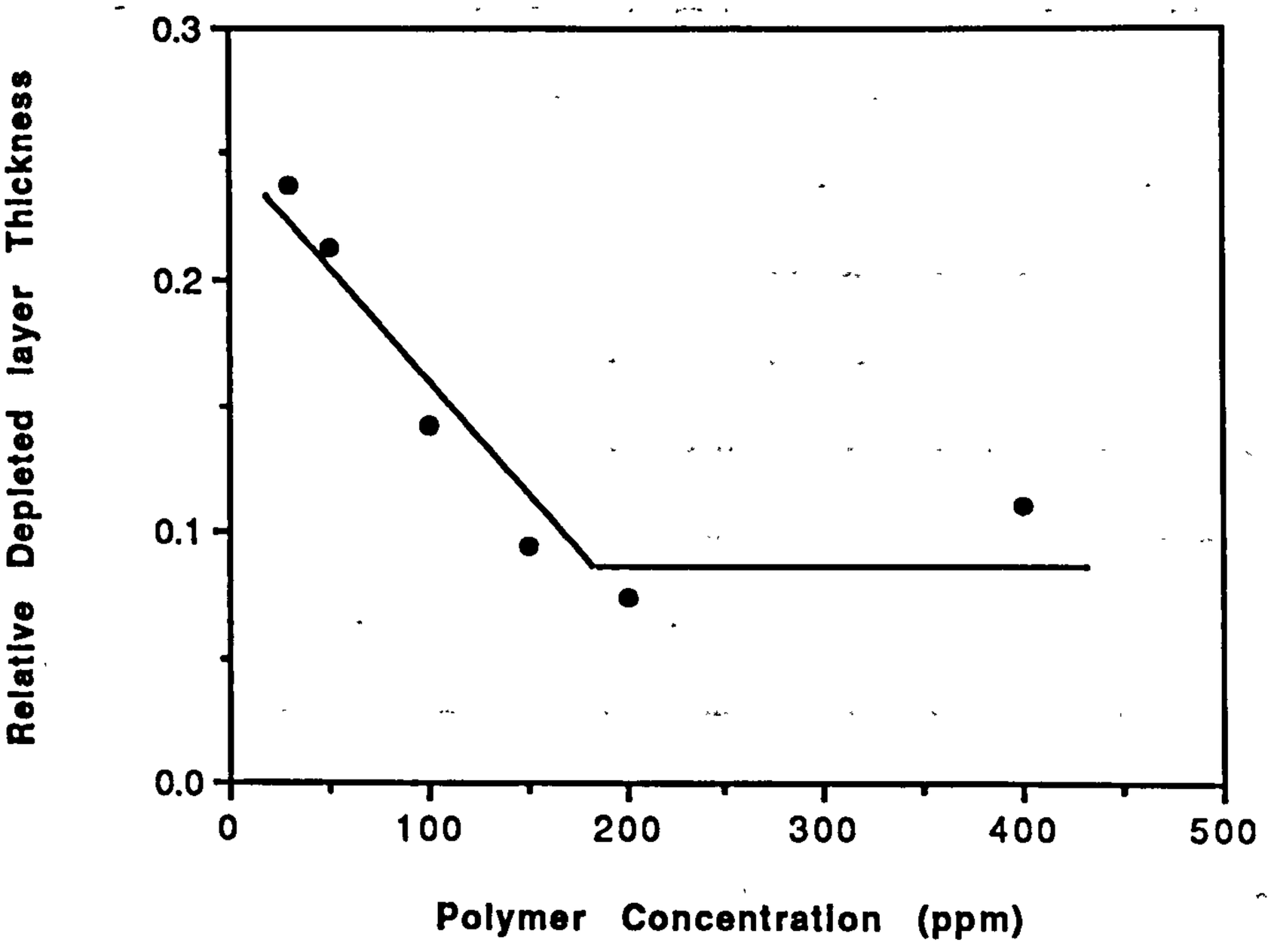

Figure 4.14 Higher polymer concentration effect on depleted layer thickness as calculated using the linear layer model

and Zaitoun, 1981; Aubert et al, 1982; Chauveteau et al, 1984; Omari et al, 1989), but is a little different from the results of Ausséré et al (1986) who found that (δ/r) decreases with concentration over the range 100 to 1000 ppm.

We would expect the depleted layer thickness to reduce to some constant value as the concentration increases above the values used in Section 4.4 and it is mainly this high concentration region to which the results of Omari et al (1989) refer. Further analysis of higher concentration results presented by Omari et al (1989) and Aubert et al (1982) are also presented in Table 4.5.

Table 4.5

Concentration Dependence of Depleted Layer Thickness for Xanthan

Example	Xanthan Conc. (ppm)	Bulk Viscosity η_b (cp)	Apparent Viscosity η_{app} (cp)	Relative Depleted Layer Thickness, (δ/r) (TF, Two fluid model; LL, Linear layer model)		
				TF (A1)*	TF (A2)*	LL (A3)*
Exp. No. 4.4	30	1.32	1.22	0.318	0.301	0.237
	50	1.58	1.38	0.295	0.320	0.213
	100	2.09	1.76	0.195	0.207	0.143
	150	2.91	2.42	0.134	0.149	0.094
	200	3.90	3.20	0.114	0.121	0.074
	400	12.00	7.14	0.343	0.188	0.110
Omari et al (1989)	272	2.56	1.83	0.453	0.237	0.219
	456	4.84	3.09	0.390	0.201	0.162
	519	6.02	3.81	0.341	0.181	0.139
Aubert et al (1982)	200	2.17	1.75	_	0.121	0.158
	400	4.00	2.45	_	0.159	0.220
	800	12.8	5.40	_	0.172	0.221
	1600	62.0	18.0	_	0.154	0.208

* see Appendix A

The Omari et al's results (concentration 272, 456 and 519 ppm; from Figure 2 in Ref. Omari et al, 1989) show that the calculated depleted layer does apparently decrease with polymer concentration whether the two fluid or linear layer models are used but that this decrease is considerably less marked that that observed for the low concentration data. Furthermore, the higher polymer concentration data of Aubert et al (1982) (200-1600ppm xanthan) shows that the quantity (δ/r) is virtually constant (for both linear layer and two fluid models) indicating that the apparent thickness of the depleted layer does tend to a constant value at higher concentrations. This result seems consistent with our result at higher concentration.

As explained in the last section, the intermolecular interaction becomes more significant with increasing concentration and therefore the hindrance to free rotation of polymer molecules may cause an effective compression of the extent of the depleted layer close to the pore wall. This kind of hindrance and compression will be become constant at much higher concentration (such as at 400 ppm or more) because the intrinsic space occupied by xanthan molecules close to the wall restricts further compression of the depleted layer.

More recently, an alternative mechanism for the apparent reduction in (δ/r) has been suggested by Chauveteau (private commucation) and this is currently being evaluated. Of course, for higher polymer concentrations, the situation is more complicated, and the simple analytical models, both two fluid and linear layer, have serious shortcomings due to the inherent approximations and assumptions which are involved in their formulation. The more viscous regime is probably best investigated theoretically using numerical solutions which retain all of the non-linearities in the depleted layer/capillary flow problem in conjunction with network models as have been described previously in the literature (Sorbie, 1989; 1990)

4.6 The In Situ Shear Thinning Region

Another specific finding from in situ rheology results is that the slopes of the apparent viscosity vs flow (shear) rate curve in the shear-thinning region are less steep (apparent power law indices are higher) in the presence of the depleted layer than in its absence and this quantity depends on the xanthan concentration. This can be seen quite clearly in the examples presented in Figure 4.9. Figure 4.15 shows power law index (n) as a function of xanthan concentration in the shear-thinning regime for both viscometric and porous medium flows. Power law indices tend to unity for both cases as the xanthan concentration tends to zero, which is the Newtonian fluid behaviour. The decrease of n value with the increase of xanthan concentration is fairly uniform and shows that increased shear-thinning character occurs for higher concentration. The power law exponent n is larger in the porous medium than in the viscometer, showing the approach of the xanthan viscosities in the porous medium and in the viscometer, which implies that the depleted layer thickness may decrease at higher flow rates. This may be due to the xanthan rod-like molecules orienting in the flow field allowing a closer approach of the macromolecule to the capillary wall. This interpretation would also explain the reason why the F_ϕ (see Table 4.4) resulting from the polymer-transport experiments is generally higher than that from the polymer-rheology experiments. The flow rate in the transport experiment is much higher than in the rheology experiments (by around a factor of 20), thus leading to a reduced apparent slip effect and a larger F_ϕ value in the former type of experiment.

4.7 Xanthan Apparent Viscosity in Field Polymer Flooding

It is usually necessary to have access to a field simulator which includes a polymer flooding option in order to set the design parameters for a given field application (Sorbie, 1991). Appropriately conducted laboratory experiments will give some of the relevant input for a simulation model. Polymer flood field tests may be significantly poorer than

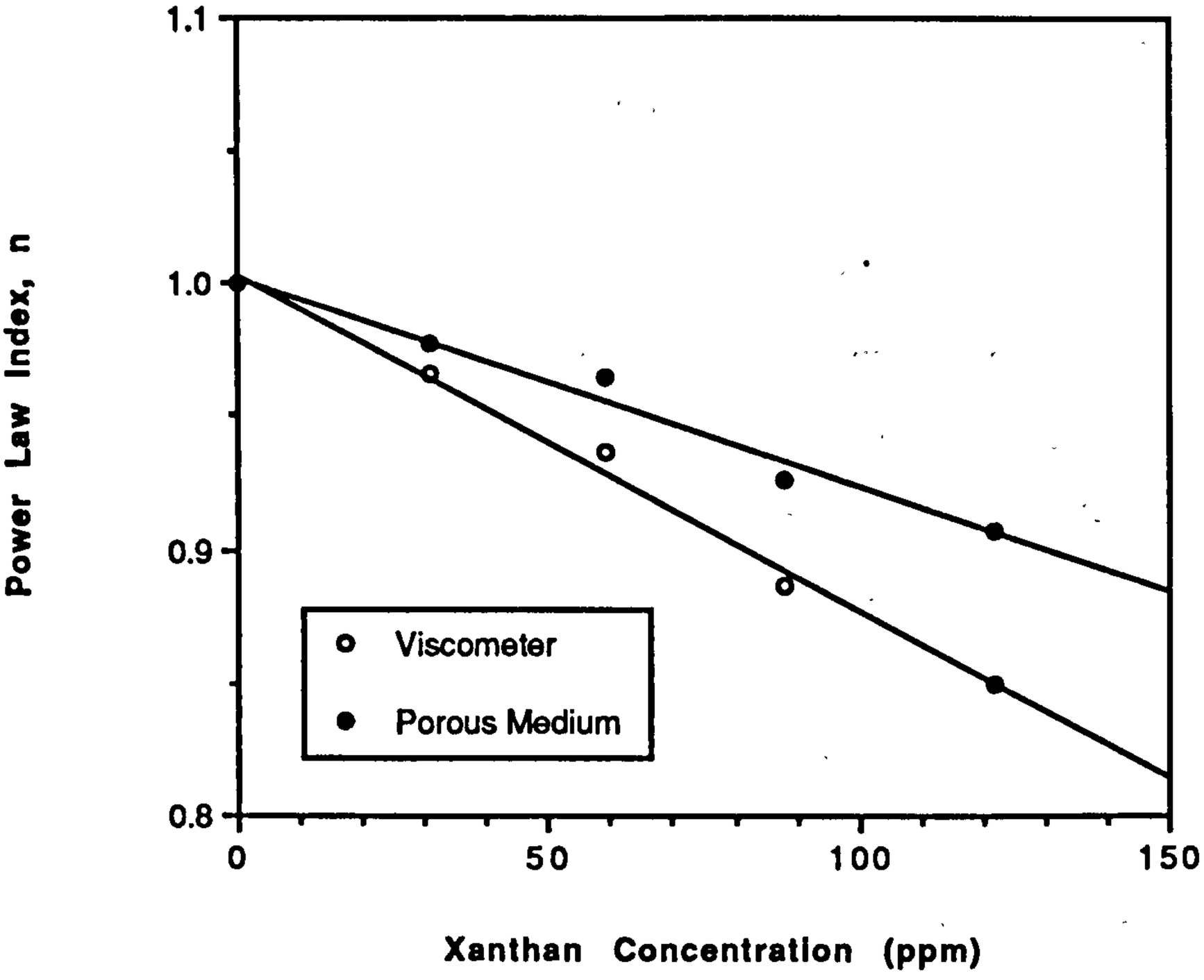

Figure 4.15 Power law index (n) as a function of xanthan concentration in the shear-thinning regime for both viscometric and porous media flows

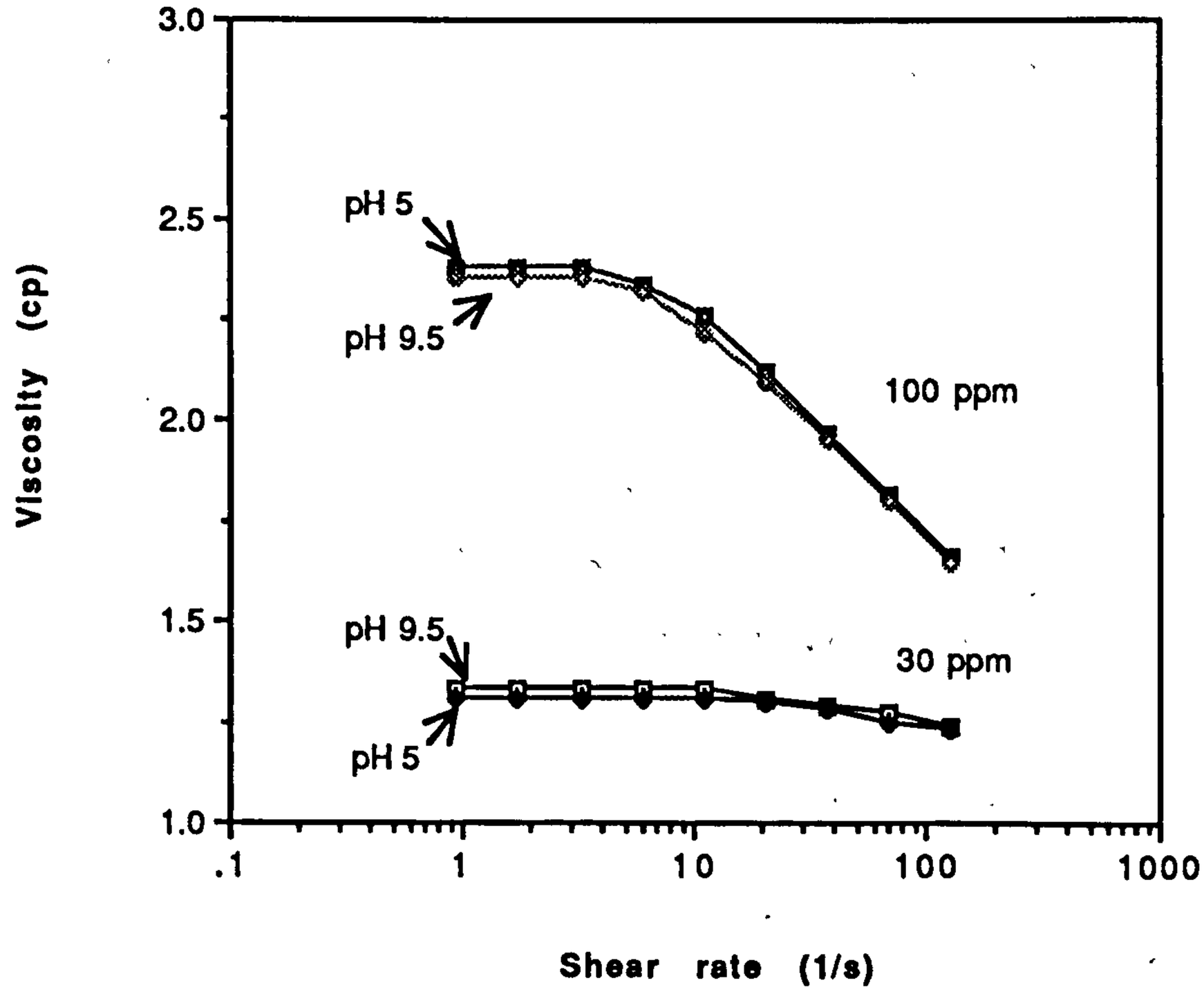

Figure 4.16 The effect of pH on the bulk viscosity of 30 and 100 ppm xanthan solutions over the pH range of the experiments

expected from conventional analysis of core flood data due to the difficulty of extracting a reliable evaluation of the in situ polymer flow behaviour.

The results presented here show that, at ambient conditions in fairly high permeability packs (k ≈ 1 Darcy), xanthan shows quite significantly apparent slip effects in its rheology within the porous medium. This may cause a significant drop in apparent viscosity; for example, the drop from the bulk viscosity to apparent viscosity for 100-200 ppm solutions in 35 g/l NaCl brine is ~ 17% and this rises to ~ 40% for the higher concentration (400 ppm) solutions (see Table 4.5). This reduction may be even larger for higher viscosity xanthan solutions although, when the temperature of the system is higher, the solution relative viscosity is more comparable with those used in this work. This in situ apparent viscosity is clearly a function of parameters that pertain to the polymer solution, the porous medium and to the interactions between the polymer and pore wall (adsorption and exclusion). In order to have the correct apparent viscosity in a polymer flood simulation, experimental data for a range of concentrations and permeabilities should be collected. It may also be possible to derive simple correlations based on the theoretical models proposed in the literature to describe the in situ rheology of xanthan. Given the magnitude of the effects that have been demonstrated in this chapter, we suggest that this may be an important area for further study in the context of its effect on oil recovery.

4.8 Comments on pH Effects

Finally, we comment briefly on the results of measuring the effluent pH in the ballotini pack floods. Although solutions of both brine and polymer were injected at pH = 5-6, the value of pH = ~ 9.5 was found for the collected effluent. This implies that ion exchange or dissolution of impure species on ballotini surface has occurred while the solution was passing through the glass bead packed column. It is well known that the pH has an effect on the surface charge of the silica in the porous medium. This introduces the possibility of electrostatic interaction between the xanthan, which is a polyelectrolyte,

and the surface although we would expect this to be quite strongly screened in the 35 g/l NaCl used here. Whatever the nature of the polymer-surface interation, it is very important that the viscosity of the bulk xanthan rheology be insensitive to pH over the range found in this study. Otherwise, the observed in situ rheology could simply be due to pH and the in situ rheology would not be interpretable in terms of an apparent slip effect. The effect of pH on the bulk viscosity of xanthan solution over the pH range of our experiments has been examined and is shown in Figure 4.16. This figure indicates that the effect of pH on xanthan rheology is negligible over the range encountered in our experiments. The effect of a wider range of solution pH on the bulk viscosity of xanthan, the surface charge of the ballotini and the resulting in situ rheology, will be discussed in detail in next chapter.

4.9 Summary and Conclusions

In this chapter, experimental results on both the transport and in situ rheological behaviour of xanthan biopolymer within unconsolidated porous media have been presented. Frontal advancement of the macromolecules was observed compared with tracer species in transport through the porous media and apparent slip effects were observed on the polymer in situ rheology. Both of these observations arise due to the same surface exclusion/depleted layer effect and, in this respect, these results confirm previous findings. The rheological results have been analysed using two simple analytical models, the two fluid model of Chauveteau and coworker and a linear layer model by Sorbie.

The main conclusions arising from the theoretical analysis of the experimental results reported above on the flow of xanthan solution in porous media are summarized as follows:

(1) Using very carefully prepared, microgel-free xanthan solution in well packed non-adsorbing ballotini packed columns, accurate and consistent results for *both* xanthan in situ rheology and transport have been obtained.

(2) Early breakthrough of the polymer relative to the tracer is clearly visible in a concentration range of 30 ppm to 400 ppm mainly due to the presence of a surface-exclusion effect where the polymer molecules are more likely to pass through the faster streamlines close to the centre of the pore.

(3) The apparent viscosity in the low flow rate Newtonian regime during flow through porous media is always less than the bulk viscosity even at very low xanthan concentrations down to 30 ppm. The origin of this apparent slip effect is also due to the same surface exclusion / depleted layer effect near the wall of the porous medium, which is consistent with the results on polymer transport mentioned above.

(4) Two analytical models have been used to analyse the rheological data in terms of a surface exclusion / depleted layer phenomenon. The simpler of these, the two fluid model, has some approximations and assumptions which the more complex linear layer model does not have. However, both of these models show essentially the same analysis when applied to the experimental results.

(5) The magnitude of the observed slip effect is a function of the polymer concentration. Using the different theoretical models referred to above, it appears that the *apparent* depleted layer thickness, (δ/r), decreases with increasing xanthan concentration over the low concentration range of 30 to 200 ppm, and tends to a constant value at higher concentrations (400 ppm). This observation may be interpreted as the increased polymer-polymer interaction at higher concentration causing hindered molecular rotation leading to a compression of the depleted layer. However, further work is required in order to really understand this mechanism and an alternative view is tentatively proposed in Appendix B.

(6) The in situ power law index, n, is higher in the porous medium than in the bulk solution (η_{app} vs $\dot{\gamma}_{pm}$ curve is less steep in the shear thinning region) and decreases with increasing polymer concentration. This is consistent with the interpretation that the depleted layer thickness decreases at higher flow rates within the porous medium possibly due to molecular orientation effects. However, even without the assumption of this decrease, previous theoretical work has predicted this effect using direct network calculations.

CHAPTER 5

THE EFFECTS OF PH AND SALINITY ON XANTHAN FLOW BEHAVIOR IN POROUS MEDIA

5.1 Introduction

The flow behaviour of xanthan within porous media depends on both the molecular structure of xanthan as well as the microscopic structure and geometry of the porous medium itself. Both the polymer structure and the properties of the porous medium may, to some extent, be affected by factors such as the in situ pH value, salinity and temperature. Xanthan is a polyelectrolyte with many COO^- groups along the backbone of the molecular chain. Holzworth (1976) showed that the uptake of acid by xanthan dramatically increased with hydrogen ion titration, indicating that native xanthan behaves as a typical polyelectrolyte with moderate interaction between the COO^- groups. Virtually all of the work on the flow of xanthan in porous media has been carried out at near neutral pH and higher salinity and hence the xanthan molecule has been in a more rigid conformation sometimes described as a worm-like chain (Sato et al, 1984; Lecourtier et al, 1986). A simplified model of the xanthan molecule that has been employed to analyse its flow behaviour in porous media is to view it as a rigid rod (Rinaudo and Milas, 1978; Chauveteau and Zaitoun, 1981; Chauveteau, 1982). Although this is an approximation, expressions exist to calculate the effective hydrodynamic rod length, l, from viscometric data (Layec and Wolff, 1974; Richards, 1980; Chauveteau, 1982) as shown in Section 3.5. For this simple model, the thickness of the depleted layer should be of order the molecular size; that is, $l \approx \delta$. In this chapter, the particular focus will be on the effect of pH and salinity which may affect both the charge on the xanthan polyelectrolyte (and hence its conformation) as well as the charge on the surface of the porous media. We are interested in the effect of pH and salinity mainly on the in situ rheological behaviour of

xanthan, particularly as it relates to the surface exclusion of polymer molecules close to the pore wall as discussed above. The extension of the xanthan molecule depends both on the intrinsic stiffness of the polymer backbone and on the electrostatic repulsion between the COO^- groups along the chain although the latter effect is thought by some workers (Zhang, et al, 1987; Tinland and Rinaudo, 1989) to be less important. Thus, if the depleted layer thickness depends on the size of the molecule and this, in turn, is affected by the pH or salinity, we would expect a larger effect at pH or salinity values where the xanthan molecule is more extended.

The xanthan concentration used in this chapter, unless otherwise stated, is a 100 ppm solution and pH effect was studied at salinity 35 g/l NaCl. Also in this chapter, both the simple two fluid and linear layer models for the depleted layer have again been used to interpret the experimental in situ rheological results and the same general conclusions have been obtained from each model. The main finding is that, in flow through the ballotini pack, the relative depleted layer thickness, (δ/r), increases with pH over the range, pH ≈ 1 to ≈ 10. Also, δ/r decreases with increasing salinity in a salinity range of 0.1 to 35 g/l NaCl. This is interpreted in terms of both the *effective hydrodynamic size* of the xanthan molecule, which is mainly related to the intrinsic viscosity of xanthan or the stiffness of the molecule, and the *surface charge* on the ballotini beads making up the porous medium. The importance of the pH or salinity / (δ/r) effect described in this chapter is related to the potential application of polymers in oil recovery processes where pH may vary very considerably as in alkali-polymer flooding or in polymer flooding processes after acidisation, as well at higher total disolved solid (TDS) situation. To the author's knowledge, no detailed results have appeared in the literature to date on this specific topic.

5.2 Reversible Transition of Xanthan Molecules with pH

Most previous investigations of pH effects on xanthan viscosity or stability has focussed on the long term stability of xanthan solutions (Wellington, 1983; Ash et al, 1983; Seright

and Henrici, 1986). In particular, the work of Seright and Henrici (1986) has established that the xanthan backbone is degraded via acid (low pH) or alkali (high pH) hydrolysis over an extended period of time especially at elevated temperatures ($> 90^0$C). Our experiments were completed within a few hours with freshly acidified or alkaline xanthan solutions at room temperature under conditions unlikely to cause irreversible degradation. Figure 5.1 shows a comparison of the bulk rheological behavior of xanthan solution at normal pH (pH = 5.0) and very low pH (pH = 1.2), which clearly demonstrates the pH effect. Bulk Newtonian viscosity as a function of solution pH for 100 ppm xanthan solution is shown in Figure 5.2. The viscosity of the xanthan solution shows little change over the range of pH 3 to pH 10, but decrease dramatically for pH values less than 3. Using different concentration solution (30, 100, 150 ppm), as shown in Figure 5.3, indicates that, under alkaline conditions (high pH value), there is little effect on xanthan rheological behavior at least in the low concentration region. This sharp reduction in viscosity at pH < 3 may be due either to chemical degradation or to acid catalysed hydrolysis (Seright and Henrici, 1986) which would be irreversible, or to a change in molecular conformation or some loosening of the inner structure of the helix (Zhang et al, 1987) which may or may not be reversible.

In order to investigate the viscosity/pH behaviour of the bulk xanthan solution in more detail, a cycle of titration experiments was performed in which the bulk solution was titrated with acid (HCl) to pH ≈ 1, and was then titrated back with alkali (NaOH) to pH ≈ 10 which was well above the original bulk solution pH (~ 5). The corresponding viscosity was measured for each pH value and was compared with that of a similar blank sample of the original bulk solution which was also titrated with the same volume of brine. Using this procedure, a very good recovery of viscosity is found as the pH is cycled back to its original value as shown in Table 5.1 indicating that the viscosity drop observed at low pH is reversible. Thus, no acid-catalyzed hydrolysis of xanthan occurred during acidation under the conditions of this experiment (i.e. over a few hours at 21°C).

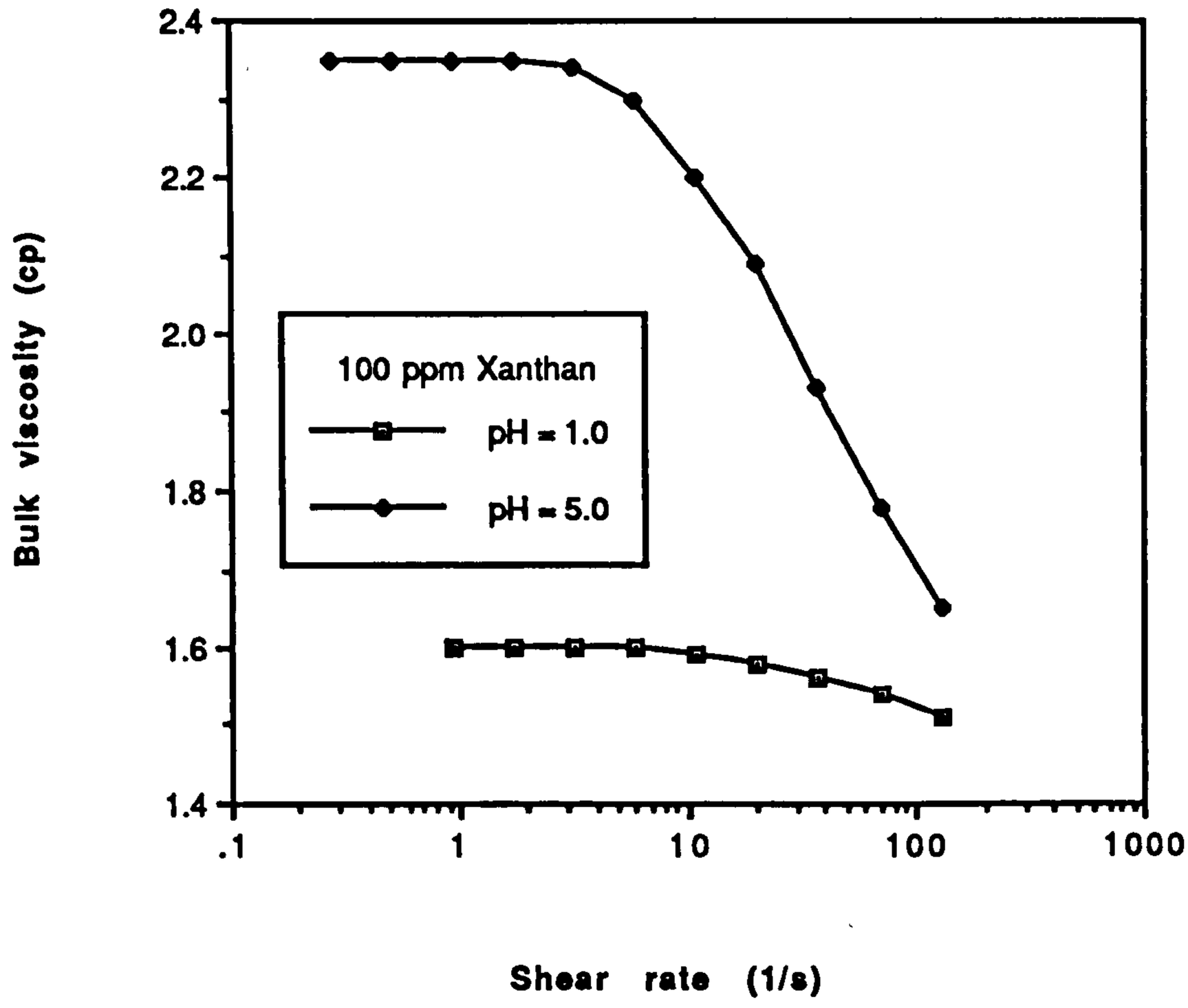

Figure 5.1 pH effect on xanthan bulk rheological behavior

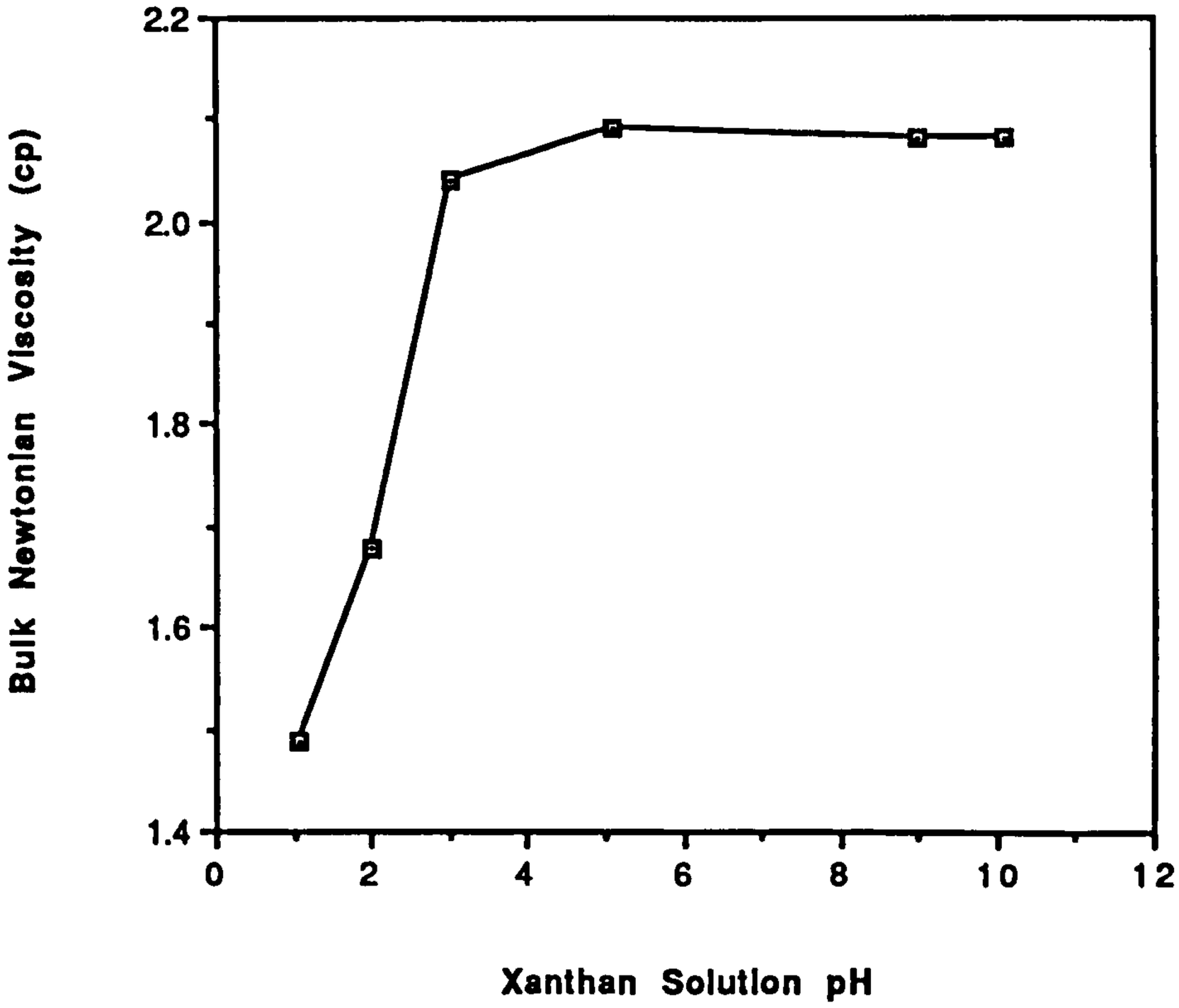

Figure 5.2 Bulk Newtonian viscosity of 100 ppm xanthan solution as a function of pH

Table 5.1

Reversibility of Viscosity Change with pH in Xanthan Solution

pH	η_{pH} (cp)	η_b (cp)	η_{pH}/η_b	Condition
4.90	2.14	2.14	1.00	Initial bulk solution
2.30	1.88	2.14	0.88	pH change by titrating the sample with acid (HCl) or Alkali (NaOH)
1.70	1.63	2.10	0.78	
1.30	1.56	2.08	0.75	
1.40	1.58	2.08	0.76	
1.61	1.61	2.06	0.78	
5.60	2.05	2.05	1.00	

Another interesting result is shown in Figure 5.4. For 200 ppm xanthan samples, the viscosity of pH 1.1 solution is much lower than that at pH 5.0. However, the low viscosity value of that low pH solution is recoveried back to normal value when the solution pH is adjusted to pH 10.5 by adding solid NaOH into the sol. The reason for the (reversible) decrease in the xanthan viscosity at low pH must therefore be due to a change in conformation of the macromolecule. The carboxyl groups along the molecule will be neutralised to -COOH by the addition of HCl , which reduces the repulsion between adjacent groups (Holzwarth, 1976). This may allow the molecule to change its conformation both due to the reduced electrostatic repulsion and possibly also due to disruption of the chain-chain interactions in the two-stranded structure of the xanthan molecule. This latter change is sometimes referred to as the helix-coil (or order-disorder) transition (Seright and Henrici, 1986) and it is known to affect a number of the physical properties of the macromolecular solution such as viscosity, optical properties, etc. (Ash et al, 1983; Seright and Henrici, 1986). Muller thought (private communcation, Sept. 1991) that, as a perfect reversibility holds, this means that the viscosity change results from an intramolecular process from an extended double helix (pH > 3) to a more compact one (pH < 3). Clearly, the situation is a complex one, in which pH may also

affect the solubility of xanthan (depending on the solute employed) as suggested by Sutherland (private communcation, Feb. 1991). Highly charged xanthans carrying high pyruvate, in which the charge/repeat unit mass ratio is close to 2:1 are very poorly soluble in the protonated form although relatively soluble as salt form polymer. Thus the decrease in solubility could affect viscosity through yielding an effectively low xanthan concentration in solution. Reversal of pH towards neutrality would bring more molecules back into true solution and consequently increase viscosity.

The sensitivity of this transition to pH depends on the salinity of the solution which can be judged by the uptake of acid added in solution. Holzwarth (1976) showed that the most rapid acid uptake occurred at a pH less than 3 at higher salinity (0.2 M NaCl). Thus our experimental results (~ 0.6 M NaCl) are consistent with Holzwarth's work in that the viscosity of the polymer solution decreases very rapidly at pH less than 3 corresponding to a rapid H^+ ion uptake of the xanthan molecules. After back-titration with alkaline solution (NaOH), the COOH groups lose H^+ to form COO^- and the reverse semiflexible-helix transition occurs leading to an increase in molecular size, a stiffening of the xanthan backbone and an increase in solution viscosity.

5.3 Surface Charge on Ballotini Glass Beads

The ballotini glass beads are made mainly from quartz (SiO_2) and it is well known that the surface characteristics of silica depend strongly on the pH. It is generally considered (Iler, 1979) that the hydroxylated surface of silica has a point of zero charge (pzc) at a pH value of ~ 2, and it is only above a pH of about 7 that a sufficient concentration of negative charge is developed on the surface of the particles. The concentration of charges on the hydroxylated silica surface at different pH values and concentrations of NaCl electrolyte was determined by Bolt (1957). In the pH range from 3.5 to 10.5 hydroxyl ions are adsorbed by the silica surface in amounts increasing with pH. Bryant (1952) studied the effect of particle size and electrolyte concentration on the pH titration curve of silica solutions and interpreted results in terms of the theory of polymeric electrolytes,

taking into account the preferential adsorption of cations and also that, at high pH, the particles dissolve as silicate. Heston et al (1960) showed that, at a given pH, the number of charges per unit area of silica surface is independent of particle size.

The surface charge density on the particles was determined as a function of the pH using a modified Bolt's method (1957) described in Section 3.4. The experimental results are presented in Figure 5.5. The zero point charge (zpc) occurs at pH ≈ 4.5 and the uncertainty in the determination of zpc is limited to 2.0×10^{-4} m.e./g(ballotini). Our zpc value is a little higher than previous results (pH 2 - 3) reported (Iler, 1979), which may be due to the particular surface properties of the ballotini particles used in this work. Figure 5.5 shows that increasing amounts of hydroxyl ions are adsorbed by the silica surface as the pH is increased from 4.5 to 10. From pH 4.5 up to about pH 8, the concentration of negative charges increases but remains fairly low and above pH ≈ 8 the surface charge increases very rapidly with pH which is consistent with previous work (Bryant, 1952; Bolt, 1957; Heston et al, 1960; Iler, 1979;). The surface structure and chemical properties of silica have been studied in detail for a considerable time although, in this work, we are interested only in the relative change in the charge density on the surface of the ballotini porous medium with increasing pH.

5.4 Xanthan Intrinsic Viscosity

The effect of pH or salinity on the in situ rheological behavior of xanthan biopolymer is related to the intrinsic viscosity [η] of xanthan or the stiffness of the molecules. Figure 5.6 demonstrates the pH effect on xanthan intrinsic viscosity. It is clear that [η] is reduced to 3,600 cm^3/g at pH 1.1 from normal 6,300 cm^3/g at pH 5.0. This is consistent with Zhang et al's results (1987). In Zhang et al's work, they found that [η] of xanthan in 0.01M aqueous NaCl fairly sharply decreased and showed a dimer behaving as a semiflexible chain when the pH of the solvent was lowered from about 6 to 2. From the light scattering and viscosity data, they concluded that the xanthan dimer at pH = 2 assumes a double-helical structure, which is geometrically the same as, but is more

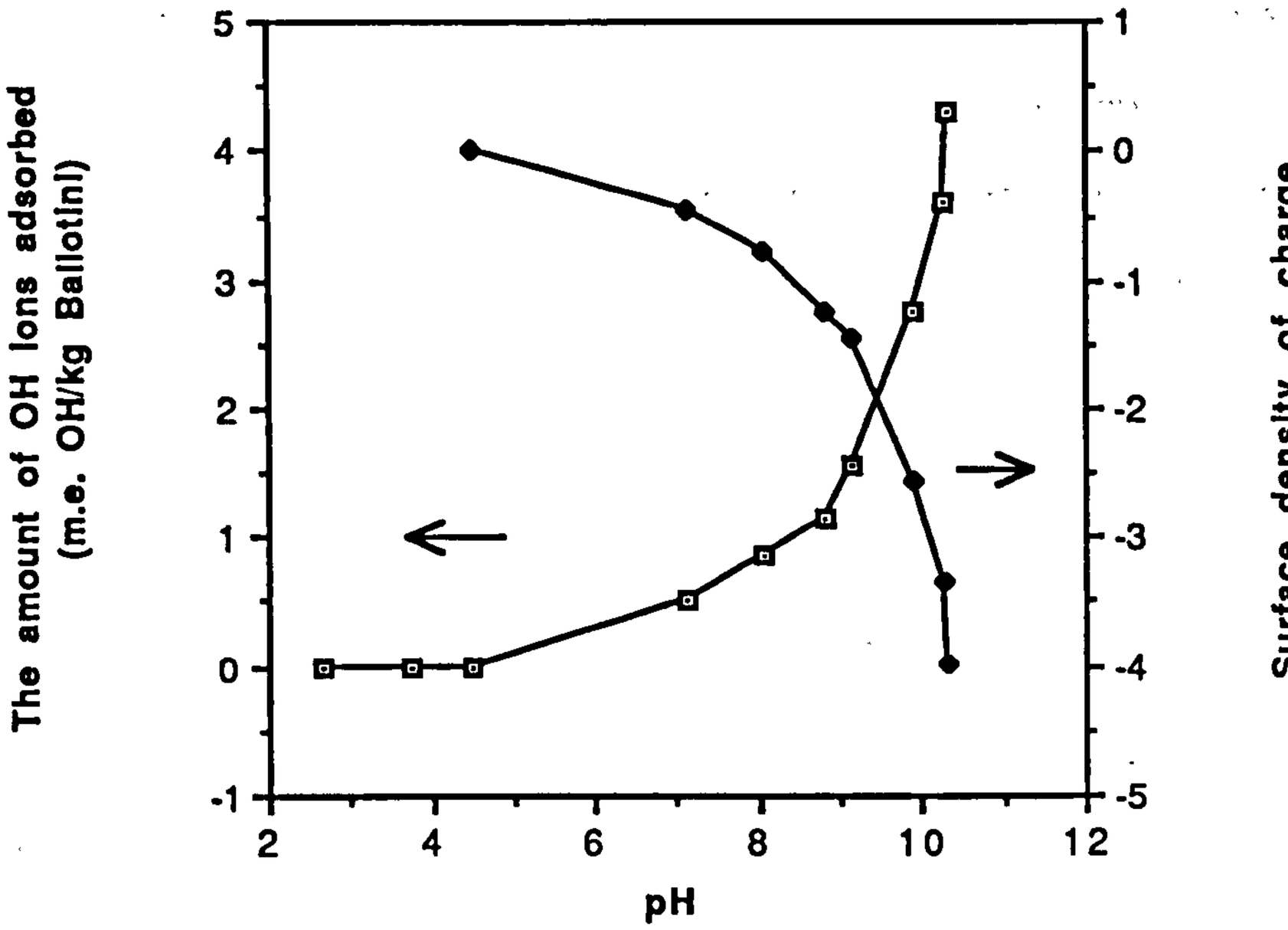

Figure 5.5 Surface charge on the ballotini glass beads

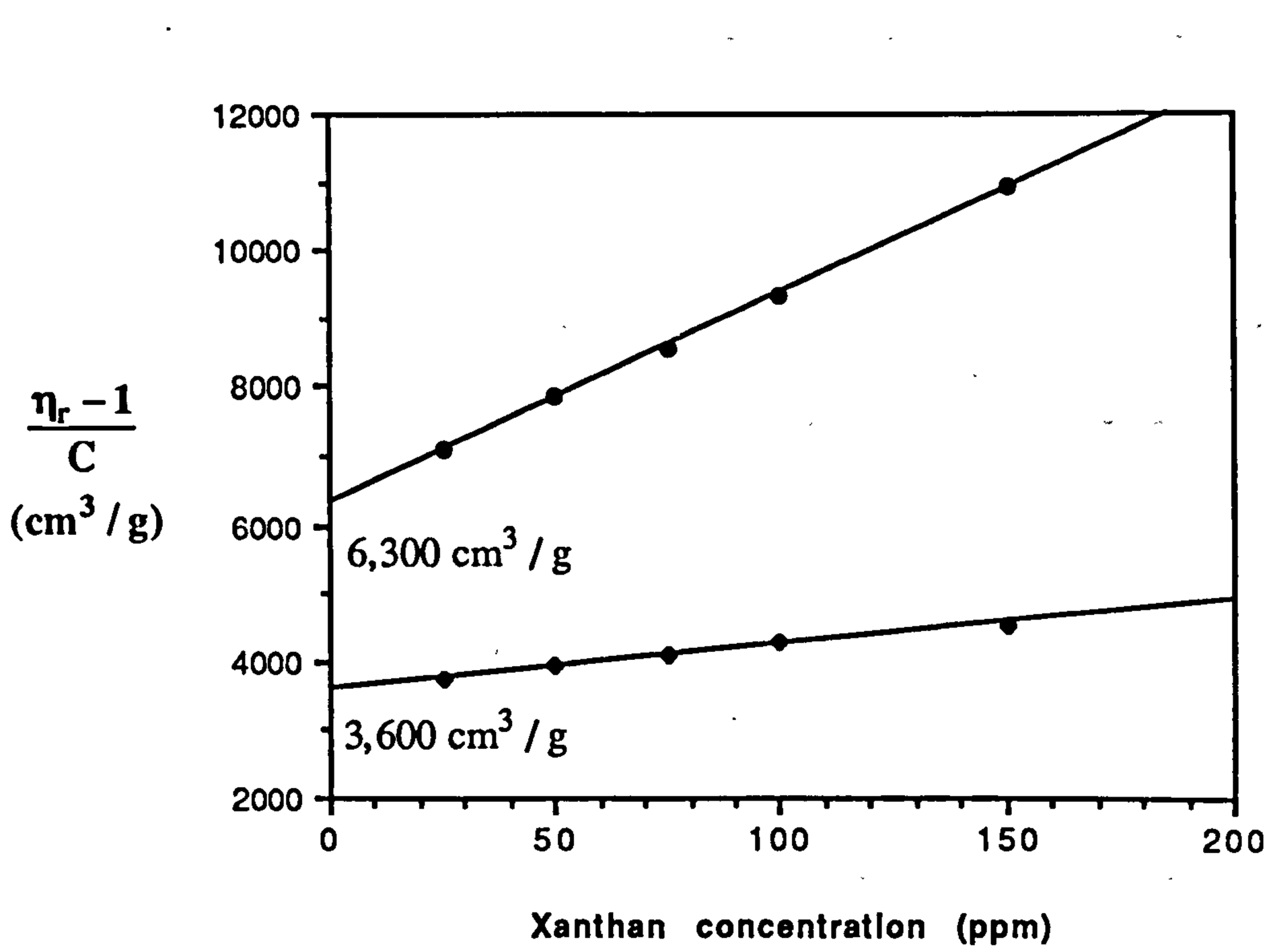

Figure 5.6 Intrinsic viscosity of xanthan solution at different pH:
● pH 5.0 and ◆ pH 1.2

flexible than, that at neutral pH. Morris (private communcation, Mar. 1991) also thought that the reduction in intrinsic viscosity at low pH is certainly a large effect, but was not likely to be conversion to a coil form because the final intrinsic viscosity under acidic conditions is still rather higher than the values measured for know 'random coil' polysaccharides with the same backbone geometry. It is possible that steric clashes between xanthan sidechains might be enough to increase the coil dimensions into this range.

Table 5.2

Intrinsic Viscosities of Xanthan Solution at Different Ionic Strengths and pHs

Salinity (NaCl g/l)	Ionic strength	pH	Intrinsic viscosity (cm^3/g)	Huggins constant
35	$5.99x10^{-1}$	5.0	6300	1.28
35	$5.99x10^{-1}$	1.1	3600	0.59
5.0	$8.56x10^{-2}$	5.0	6400	1.10
0.5	$8.56x10^{-3}$	5.0	7400	0.94
0.1	$1.71x10^{-3}$	5.0	8300	0.71
0.1	$1.71x10^{-3}$	1.1	3700	0.60

Intrinsic viscosity [η] and Huggins constant k′ of xanthan solution at different ionic strengths and pH values are shown in Table 5.2. Both [η] and k′ increase with the decrease of ionic strengths and obviously reduce at low pH. As discussed earlier in Section 3.3, the value of the Huggins constant was very sensitive to the method of fitting the rheological data, so here only the intrinsic viscosity is considered in some detail. The results shown in Table 5.2 indicate a certain sensitivity of the viscosity of dilute xanthan solutions in the presence of external monovalent salt; for example, [η] decrease 24.1 % when the salinity increases from 0.1 to 35 g/l NaCl. And a high sensitivity of [η] is

demonstrated with pH change; for example, [η] decrease about 55.4 % when pH of solution decrease from 5.0 to 1.1 in 0.1 g/l NaCl solution. In addition, at low pH (pH 1.1), the effect of ionic strength is weakened. For the case of salinity decrease from 0.1 to 35 g/l NaCl, at low pH (pH 1.1), [η] decrease only 2.7 %, compared with the 24.1 % decrease of [η] at high pH (pH 5.0).

On the other hand, it seems that the pH effect on xanthan intrinsic viscosity is much stronger at low salinity (0.1 g/l NaCl) than at high salinity (35 g/l NaCl). This conclusion is also consistent with Zhang et al's (1987) results. In Muller's opinion (private communcation, Sept. 1991), this relates to the pK and the autodissociation of xanthan. Like Holzwarth's work (1976), Muller (private communcation, Sept. 1991) found that xanthan behaves as a stronger acid when the salinity increases and at high salinity it needs a large amount of HCl to totally suppress the autodissociation of the COOH groups. In fact, the viscosity drop (and thus the collapse of the molecule) only occurs when the autodissociation is totally suppressed by adding HCl.

To further investigate the confomation of xanthan molecules in different salinities and pH values, we assume that the molecular weight of xanthan polymer, M, is a constant value of $M = 4 \times 10^6$ (see section 3.5). A constant M is supported by early experimental results. Applying Eqs. [3.5] and [3.7], the xanthan molecular length, *l*, at different salinities and pH values is estimated and is shown in Table 5.3. From Table 5.3, the length-to-diameter ratio of the molecule, p, is increased with the decrease of salinity, and is distinctly decreased with the decrease of pH. The results show that the molecular conformation trend toward prolate ellipsoids at very low pH (pH 1.1) from rods at normal pH (pH 5.0), although it still keeps a helical structure.

The salinity, or more precisely the ionic strength, I, of the solution has some effects on the rheological behaviour of xanthan biopolymer. It is well known that the viscosity decreases for polyelectrolytes with increasing salinity of the solution (Tinland and Rinaudo, 1989). Figure 5.7 shows that [η] is nearly a linear function of the reciprocal

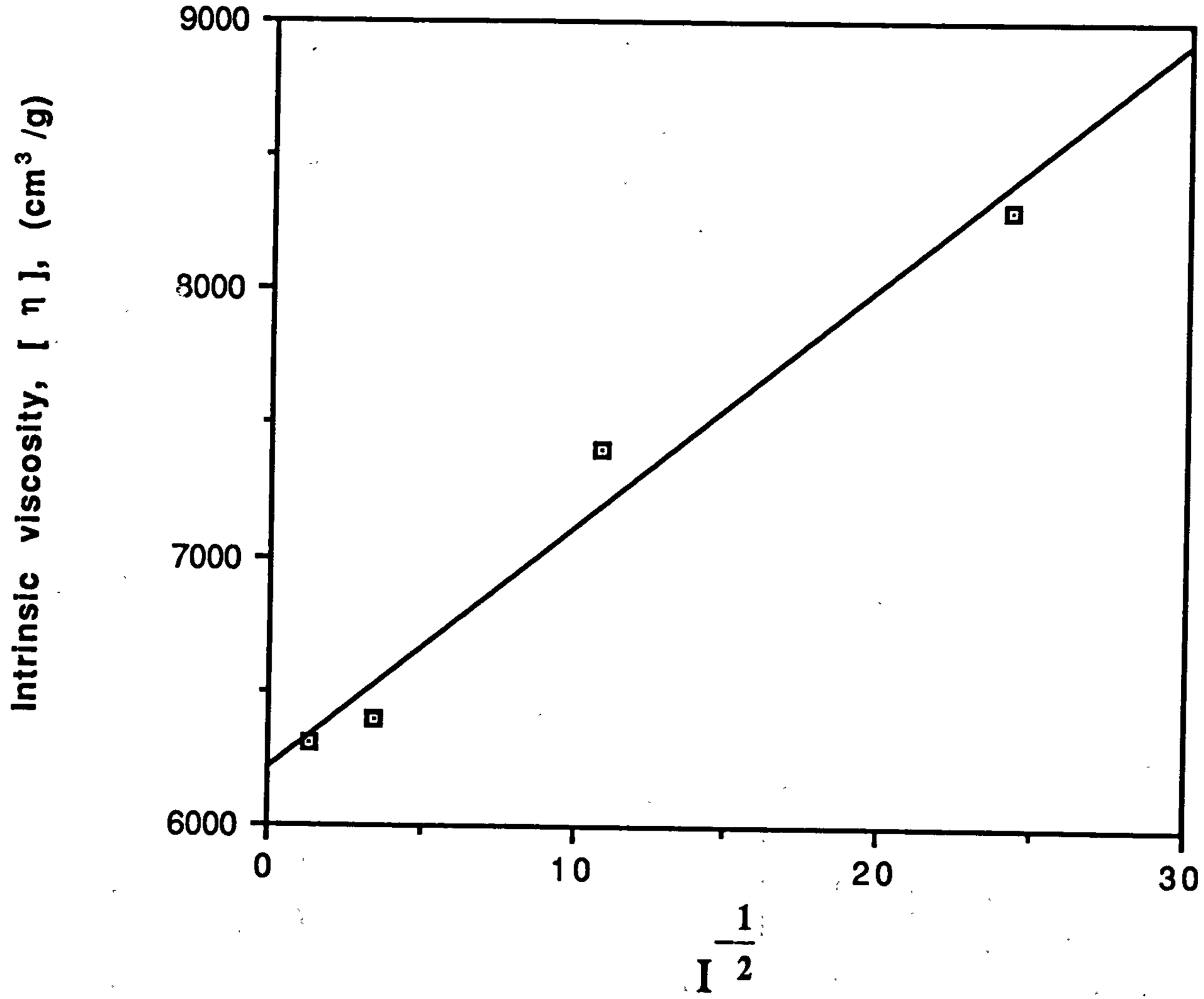

Figure 5.7 Intrinsic viscosity as a function of the reciprocal square root of the ionic strength

square root of the ionic strength, $I^{-1/2}$. This result is consistent with the findings of Tinland and Rinaudo (1989) and to some of the theoretical work that is referred to in their paper. The data were extrapolated to infinite ionic strength, giving a value of $[\eta]_\infty$ = 6200 cm^3/g.

Table 5.3

Xanthan Molecular Conformation at Different Salinities and pH Values

Salinity (NaCl g/l)	pH	Length-to-diameter ratio p	Molecular length *l* (μm)	Molecular diameter (L/p) D (10^{-8}cm)
35	5.0	465.8	1.19	25.5
35	1.1	341.4	0.97	28.4
5.0	5.0	469.9	1.20	25.5
0.5	5.0	509.3	1.26	24.7
0.1	5.0	542.8	1.32	24.3
0.1	1.1	346.6	0.98	28.3

5.5 Polymer Transport

Both the advancement of the polymer molecules relative to the tracer during transport and the corresponding rheological behaviour for the same system are studied in this chapter. Polymer transport experiments were performed at an injection rate of 10 ml/hour, corresponding to a frontal velocity of u = 1.0 x 10^{-2} cm/s. No xanthan adsorption on the ballotini packs was observed during these experiments.

Typical examples of the frontal breakthrough effluent profiles of both xanthan and Li^+ tracer for low pH (~ 1.2) and moderate pH (~ 5.0) are shown in Figures 5.8 and 5.9 respectively. All of the experimental results clearly show the polymer advancement

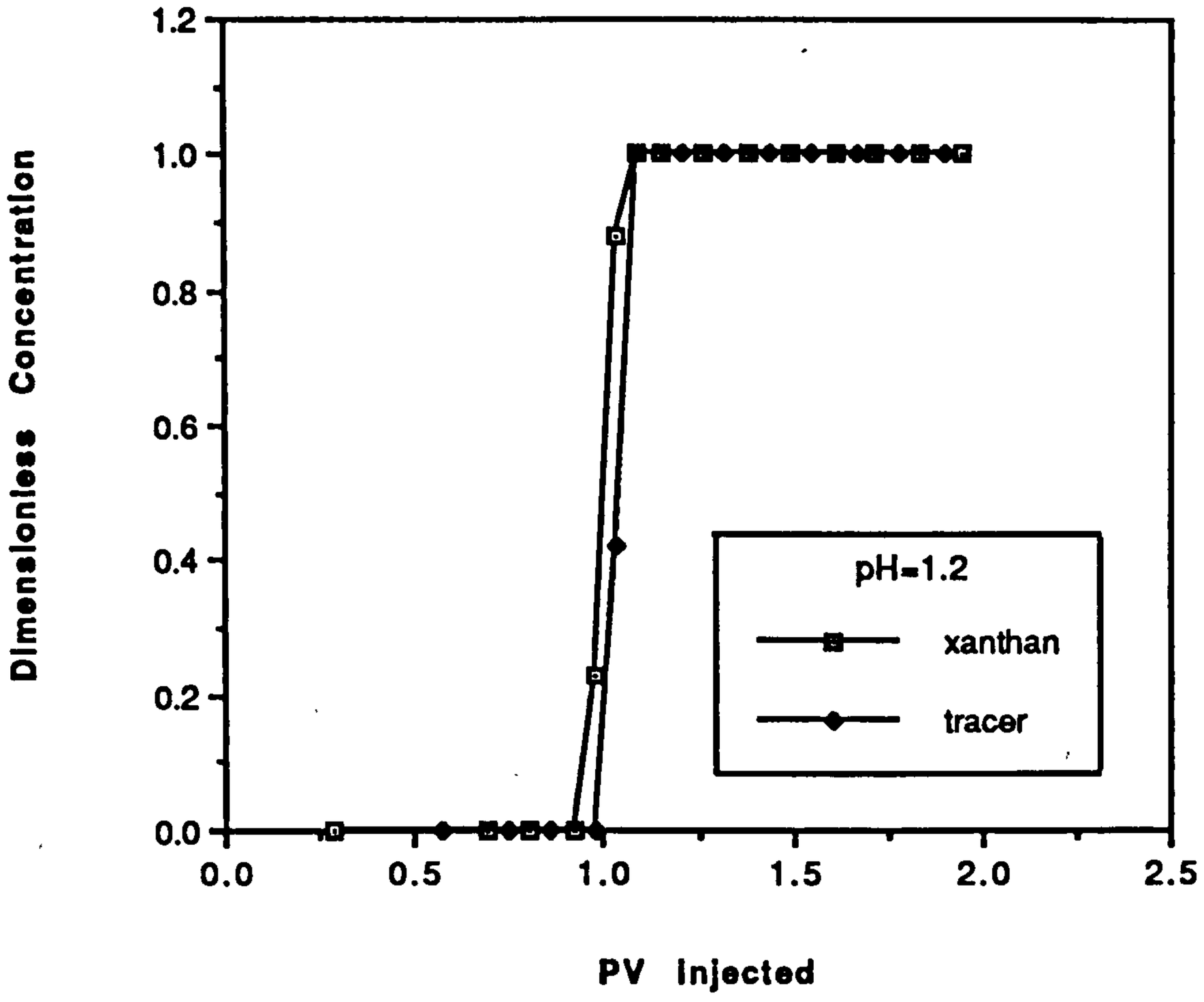

Figure 5.8 Frontal effluent profiles (dimensionless concentration vs PV injected) for 100 ppm pH 1.2 xanthan solution and lithium tracer

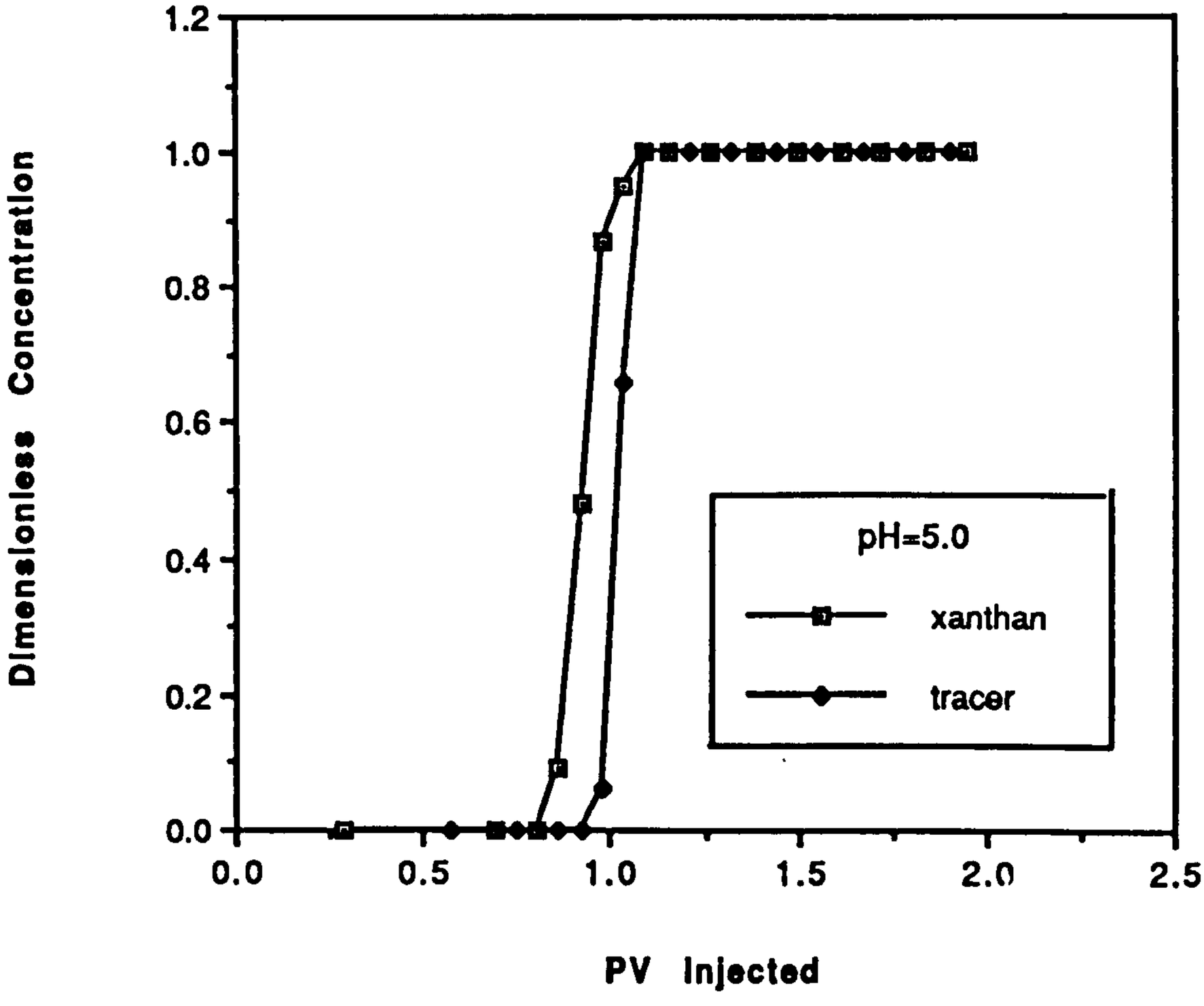

Figure 5.9 Frontal effluent profiles (dimensionless concentration vs PV injected) for 100 ppm pH 5.0 xanthan solution and lithium tracer

relative to the lithium tracer. The main difference with pH appears to be that the polymer advancement for pH ~ 1.2 is much lower than that for pH ~ 5.0. Indeed, there is a trend for the polymer advancement to increase with pH as shown in the results presented in Table 5.4.

Table 5.4

Frontal Analysis of Effluent Profiles[1]

Expt. No.	pH	$D_{polymer}$ (x 10^{-4})	D_{tracer} (x 10^{-4})	D_r	F_ϕ
1	1.0	3.0	1.3	2.31	0.962
	3.0	7.3	3.2	2.28	0.917
	9.5	5.4	2.1	2.57	0.918
2	1.2	3.2	1.3	2.46	0.966
	3.0	3.7	1.8	2.06	0.910
	5.0	6.0	2.1	2.86	0.907
	9.0	8.8	3.8	2.32	0.913

1. Flow rate is 10 cm^3/hour and the corresponding frontal velocity is 1.0×10^{-2} cm/s.

In order to estimate the magnitude of the polymer exclusion in the pack, we calculate the relative exclusion volume (PV_ϕ) as follows:

$$PV_\phi = \frac{PV - PV_p}{PV} = 1 - F_\phi \qquad [5.1]$$

and F_ϕ is known as the exclusion factor (Eq. [4.1]). A plot of the relative exclusion volume as a function of pH is shown in Figure 5.10 where it is compared with the corresponding bulk xanthan viscosity (note different scales). It is clear from this figure that the overall trend in the change of both quantities, PV_ϕ and viscosity, with pH is very similar. The exclusion volume ranges from 0.035 to 0.1 pv of the pack as the pH

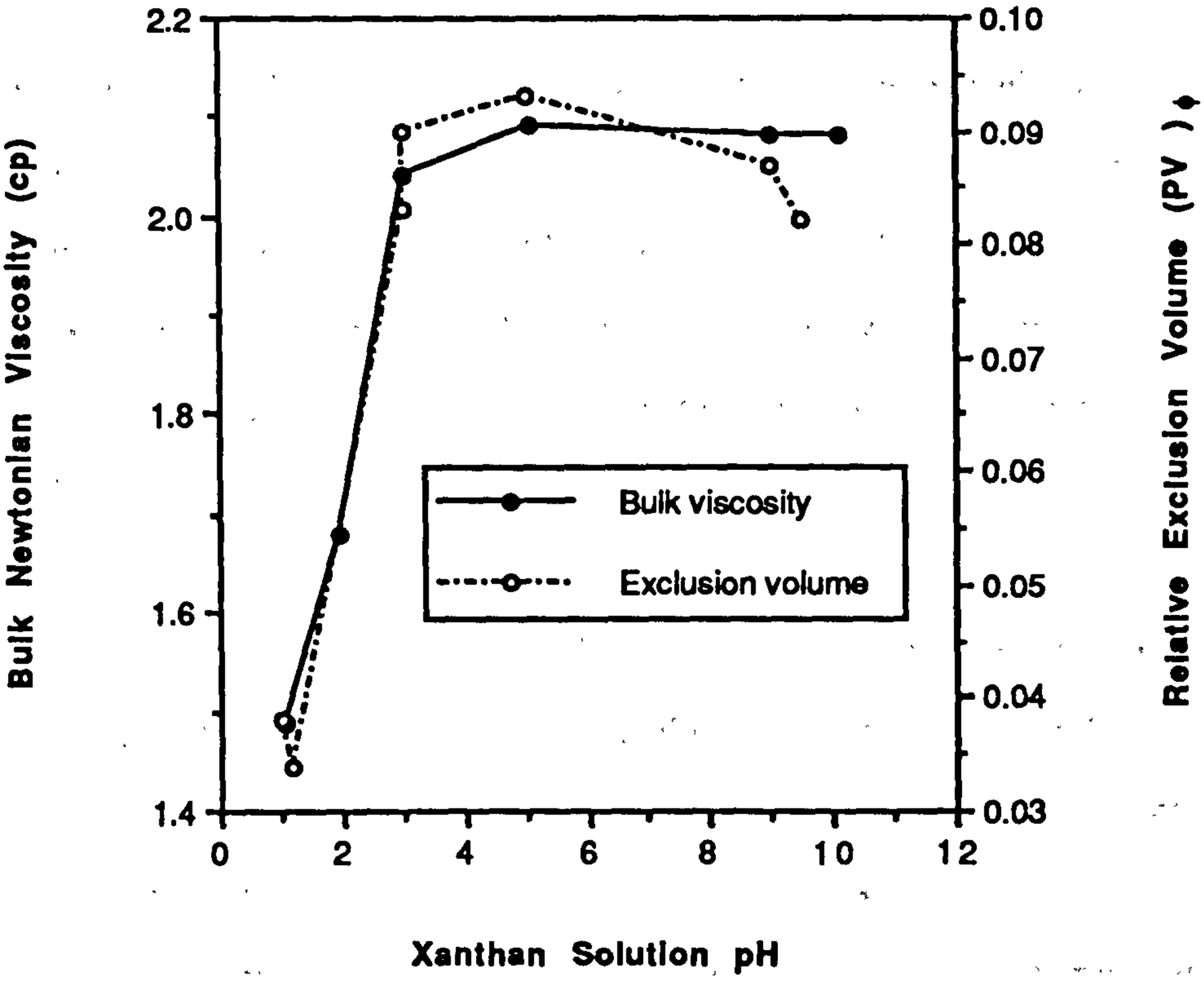

Figure 5.10 Comparison of the relative exclusion volume of polymer in the porous medium with the corresponding bulk xanthan viscosity as a function of pH

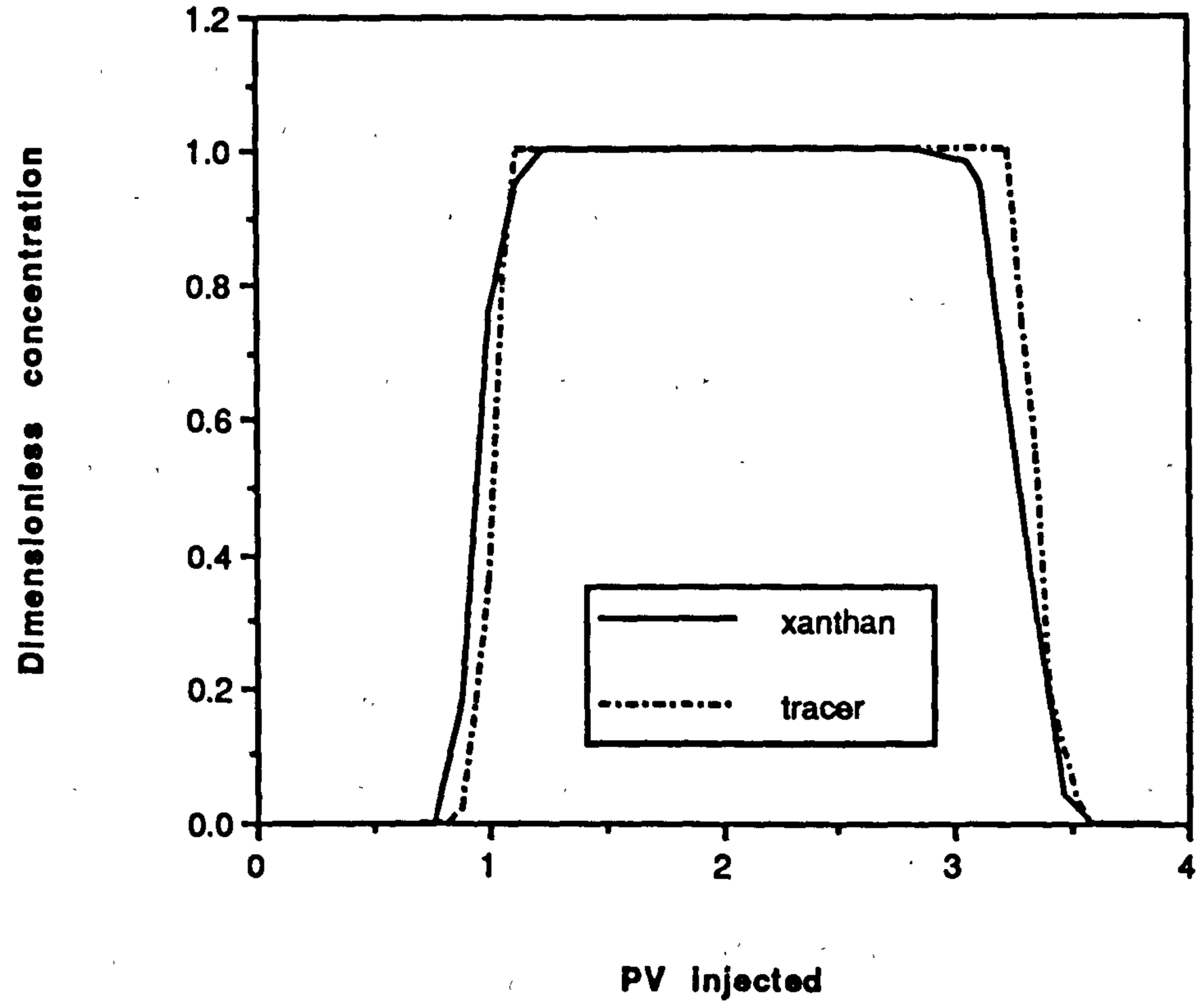

Figure 5.11 The effluent profiles for 100 ppm xanthan solution in 0.1 g/l NaCl and lithium tracer

increases from ~ 1 to 10 indicating that, even at the relatively high injection rate (10 ml/hour) used in the transport experiments, the effect of xanthan molecular structure on the relative pack exclusion volume is still quite significant. It also appears that the effect of the ballotini surface charge on pack exclusion is not very significant at such flow rate since the relative exclusion volume is approximately constant between pH ~ 4 and ~ 10 as shown in Figure 5.10.

The same method as shown in section 4.2 is used to analyse the experimental transport results by fitting the effluent profiles to analytical solutions of the 1D convection-dispersion equation. Calculations based on the effluent polymer and tracer profiles for all of the floods are presented in Table 5.4, where the exclusion factor, F_ϕ, and the dispersion coefficient, D, are presented. The ratio of polymer to tracer dispersion coefficient, D_r, is defined as follows:

$$D_r = \frac{D_{polymer}}{D_{tracer}} \qquad [5.2]$$

where $D_{polymer}$ and D_{tracer} are polymer and tracer dispersion coefficients respectively. It can be seen in Table 5.4 that the the quantity $D_{polymer}$ is greater than D_{tracer} by a factor of around 2 to 3 as has been metioned in the last chapter. It is simply noted that, considering the consistency of these results with earlier experimental findings (see Section 4.2), we observe that the relative dispersion coefficient (D_r) is independent of polymer concentration and pH at least under the condition of higher frontal velocity used in these experiments.

The effluent profiles for 100 ppm xanthan solution at 0.1 to 35 g/l NaCl and lithium tracer are shown in Figure 5.11 to 5.14 respectively. For all floods, xanthan molecules are transported through the porous medium faster than those of inert tracer species. Also a long trailing edge was not observed from each effluent profile, which means that viscous fingering is probably not occurring. These results also tend to indicate that level of adsorption/retention within the porous medium is very low. Using material balance,

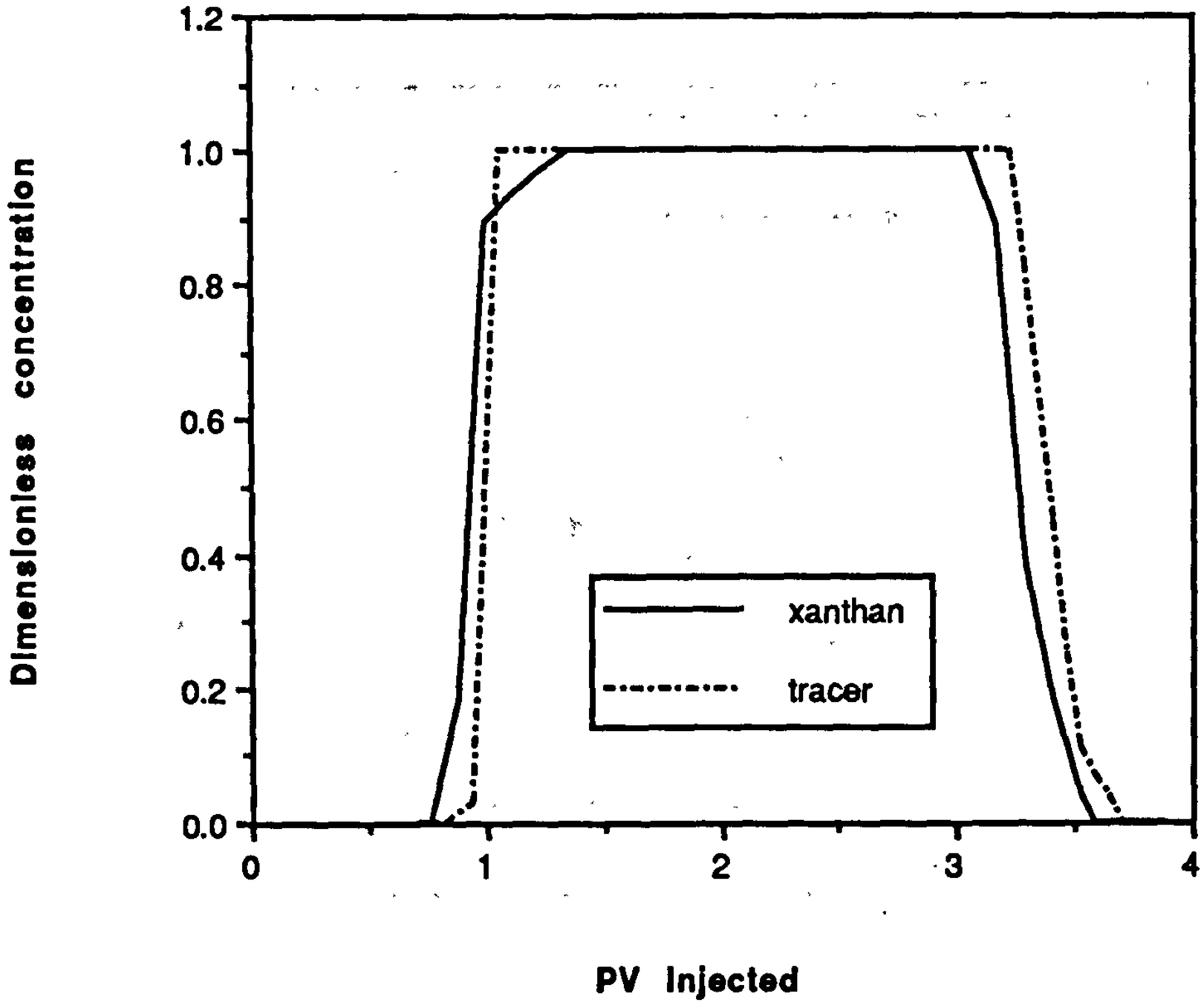

Figure 5.12 The effluent profiles for 100 ppm xanthan solution in 0.5 g/l NaCl and lithium tracer

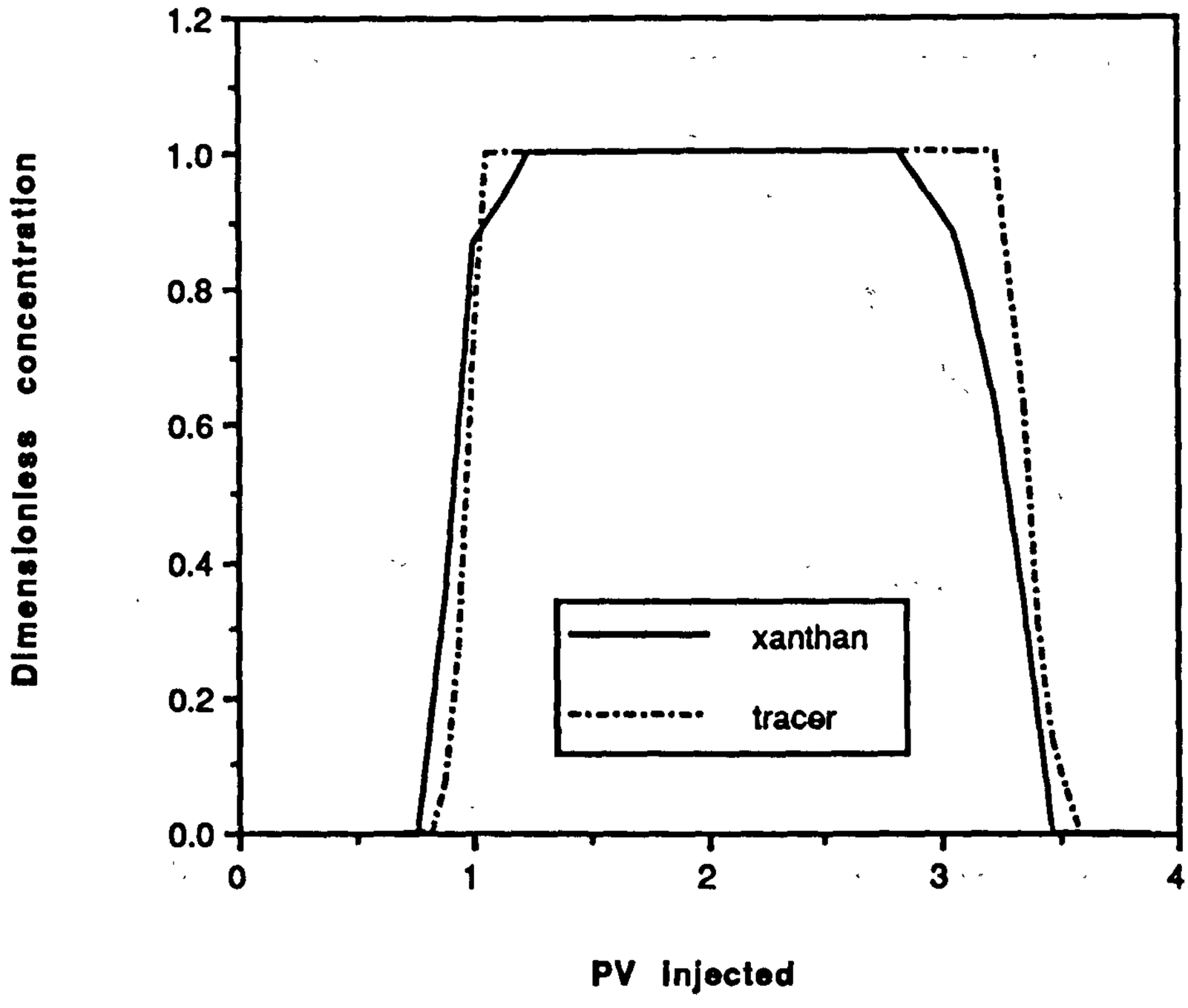

Figure 5.13 The effluent profiles for 100 ppm xanthan solution in 5.0 g/l NaCl and lithium tracer

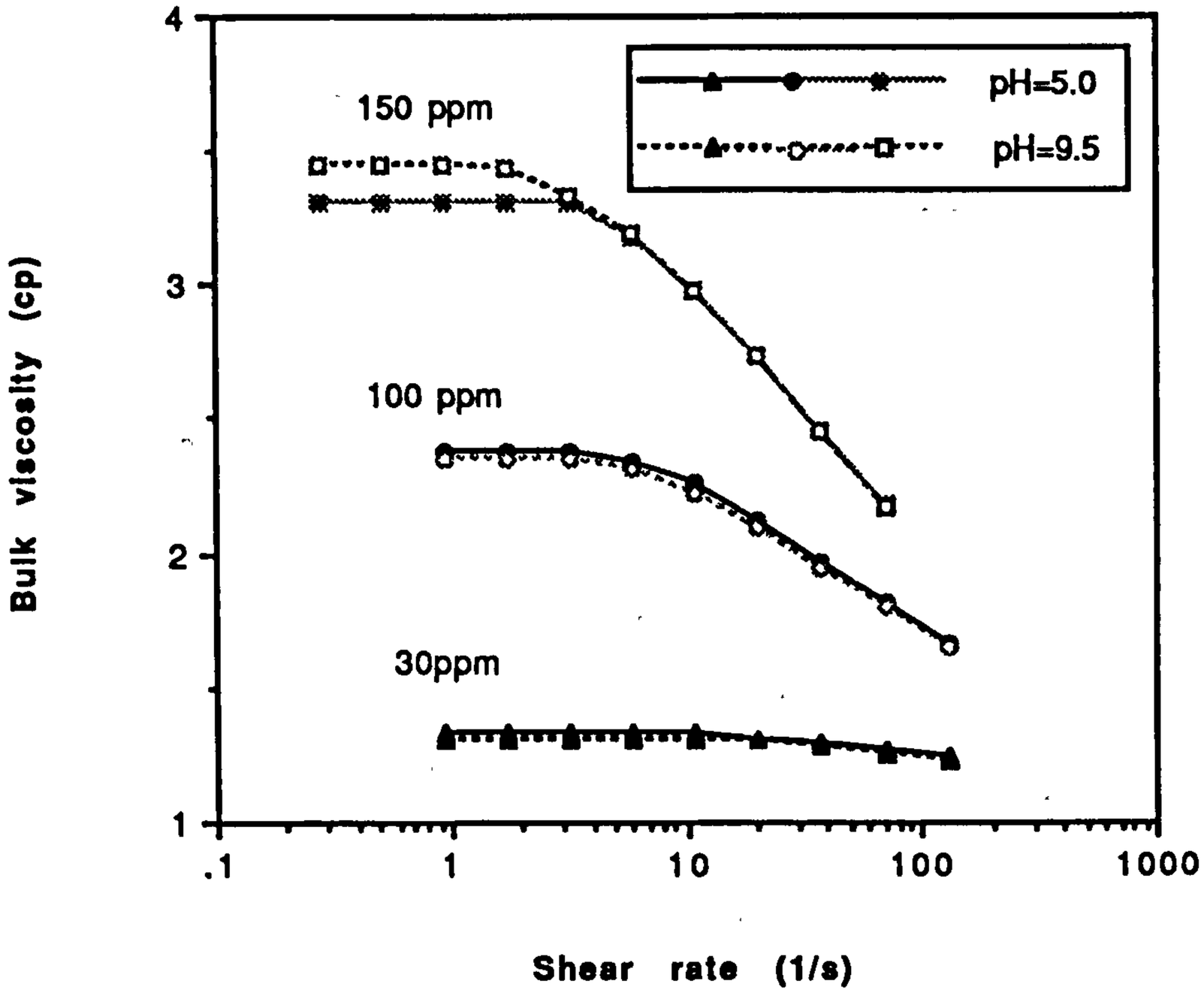

Figure 5.3 Bulk viscosities of xanthan solution measured in viscometer at different concentrations and pHs

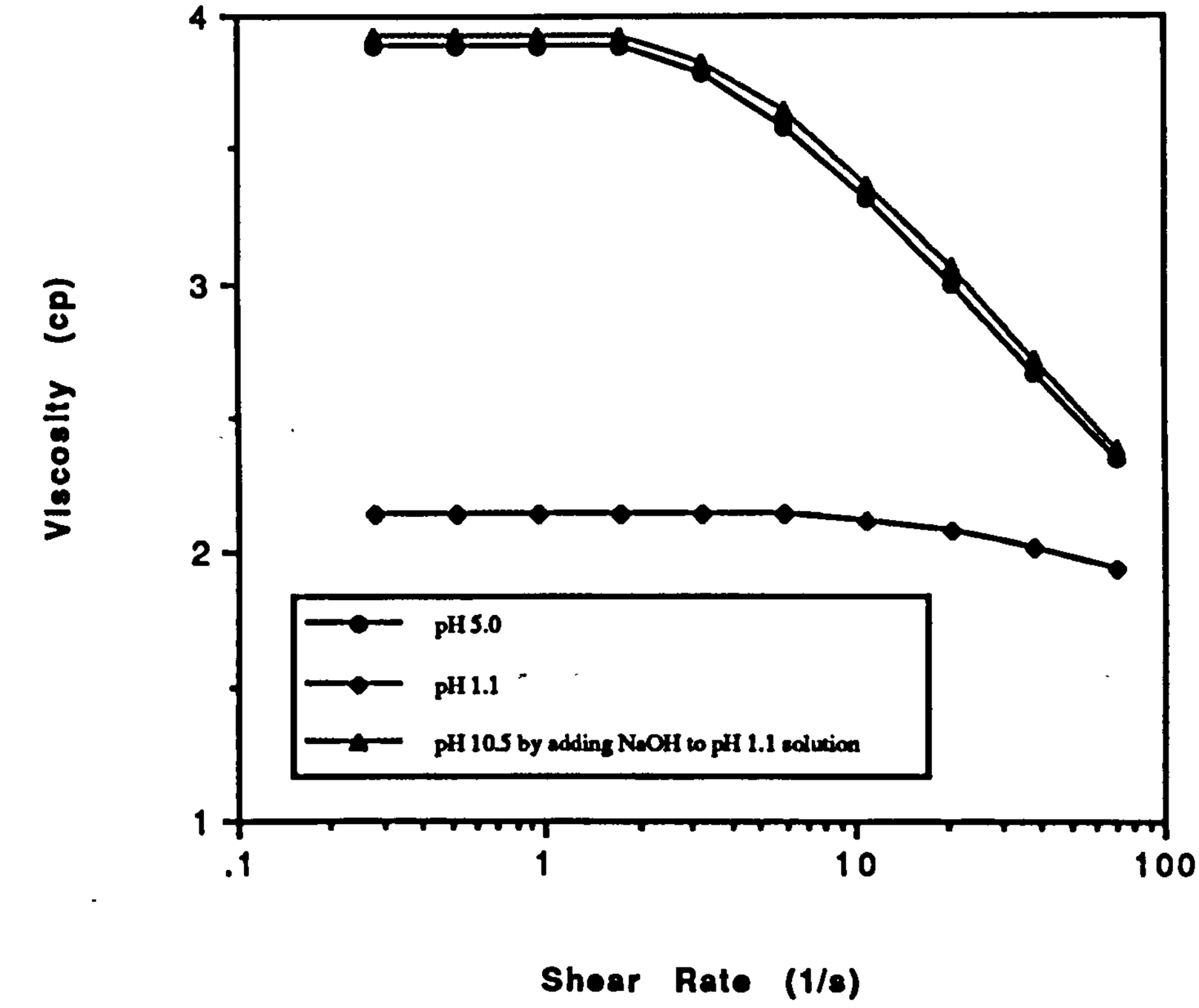

Figure 5.4 Reversible viscosity change with pH for 200 ppm xanthan solution

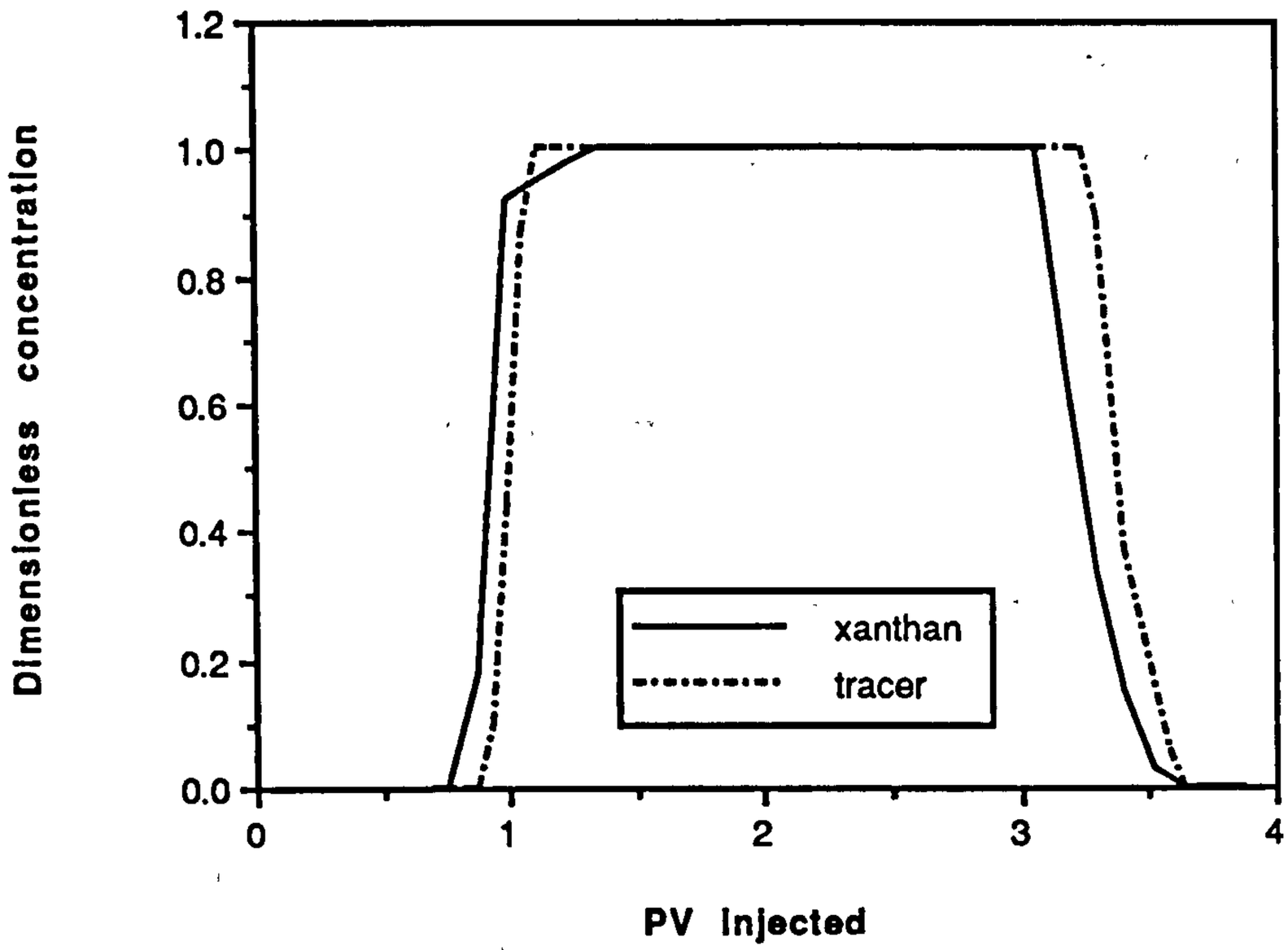

Figure 5.14 The effluent profiles for 100 ppm xanthan solution in 35 g/l NaCl and lithium tracer

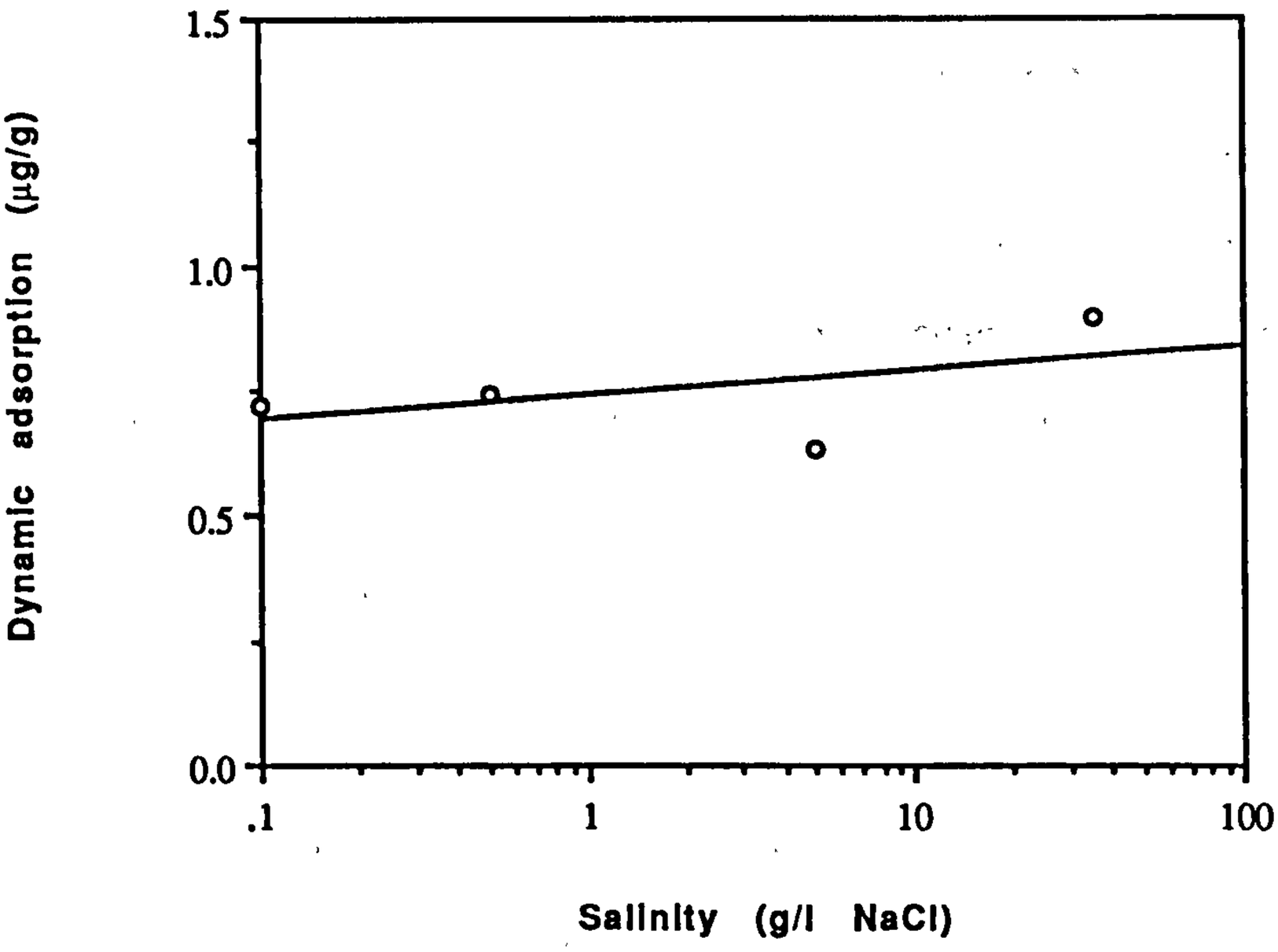

Figure 5.15 Xanthan dynamic adsorption in porous media during each fast polymer flooding

the amount of xanthan adsorption has been calculated in the pack floods and this is shown in Figure 5.15. Very low adsorption levels of about 1 μg/g have been found for all values of salinity used in the original floods where the flow rate is 160 μl/min (9.7×10^{-3} cm/s) and the total flooding time is within one day. The adsorption of xanthan solution will be fully discussed in Chapter 6.

5.6 pH Effect on In Situ Rheology

In last chapter, we studied mainly the in situ rheological behaviour in the flow of low-concentration xanthan solutions (30 - 200 ppm) through porous media as a function of the polymer concentration. In this chapter, low concentration xanthan solutions are still used (100 ppm), but over a range of pH values (pH ~ 1, 3, 5, and 9). As previously, we compare the in situ rheological behaviour (η_{app} vs. $\dot{\gamma}_{pm}$) with the viscometric behaviour (η vs. $\dot{\gamma}$) and the most detailed analysis is made of the low flow rate (Newtonian) data. Figure 5.16 to 5.19 shown some typical experimental examples of the comparison of in situ and viscometer rheologies for pH ≈ 9.0 to pH ≈ 1.0 xanthan solutions. All of the experimental results on the Newtonian viscosities are also summarised in Table 5.5 where they are analysed using both the simple two fluid and linear layer models for the depleted layer, as described previously. Note that in all cases presented in Table 5.5, the in situ viscosities are below the bulk fluid viscosities in the low shear rate Newtonian regime. This is due to the depleted layer effect where macromolecules are excluded from the pore wall as discussed in some detail above and elsewhere. The important finding in this work is that the decrease of in situ Newtonian viscosities is significantly affected by the pH values in solution as shown in Figure 5.20.

We mainly consider the linear depleted layer model to analyse the results in Table 5.5, so that the relative depleted layer thickness, (δ/r), may be calculated in each case. A very clear and interesting finding is shown in Figure 5.21 and the corresponding numerical results are presented in Table 5.5. The depleted layer thickness increases markedly with increasing bulk pH over the pH range used in this work (pH 1.0 - 9.5). Although the

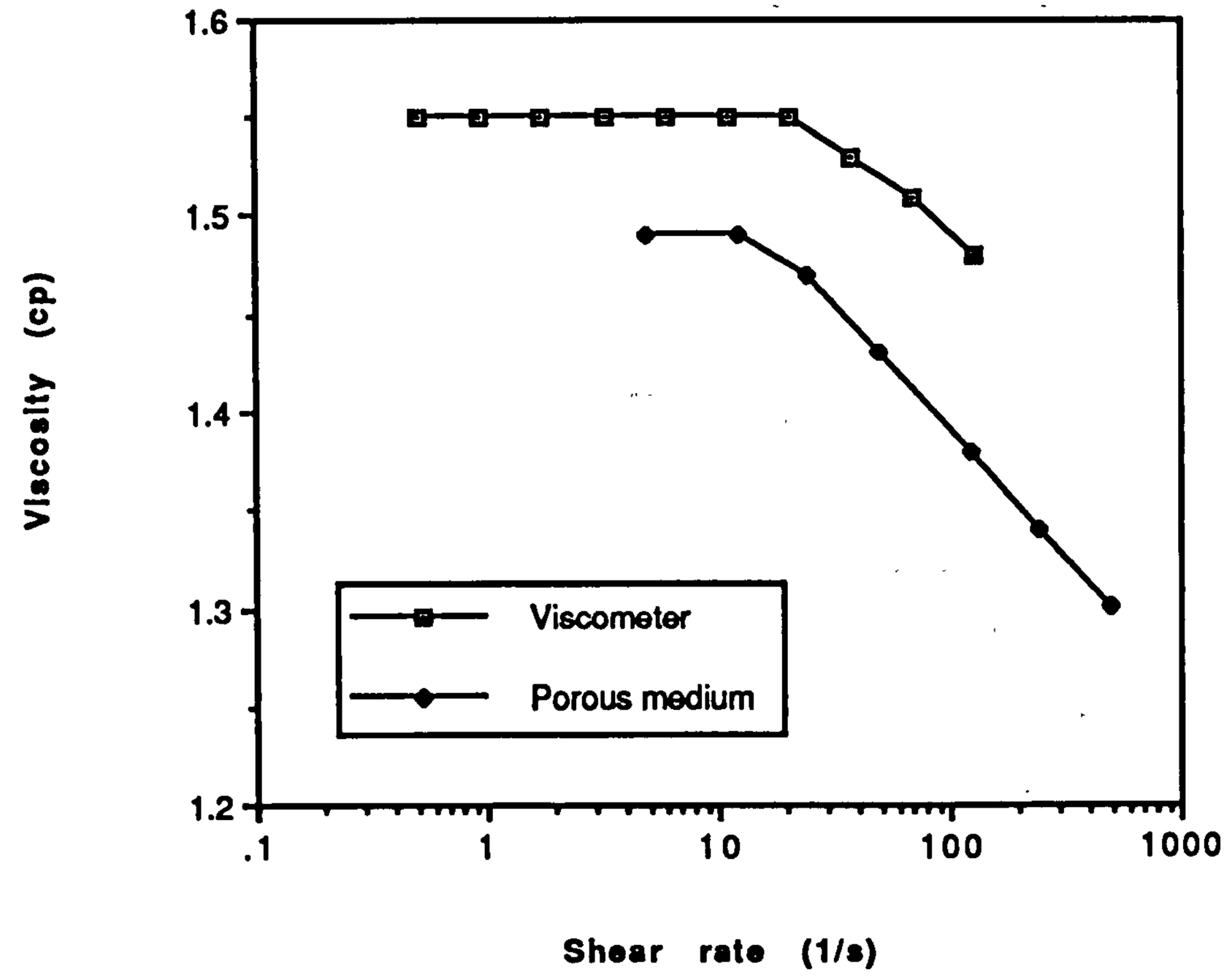

Figure 5.16 Comparison of in situ apparent viscosity and bulk viscosity for pH 1.2 xanthan solution (100 ppm)

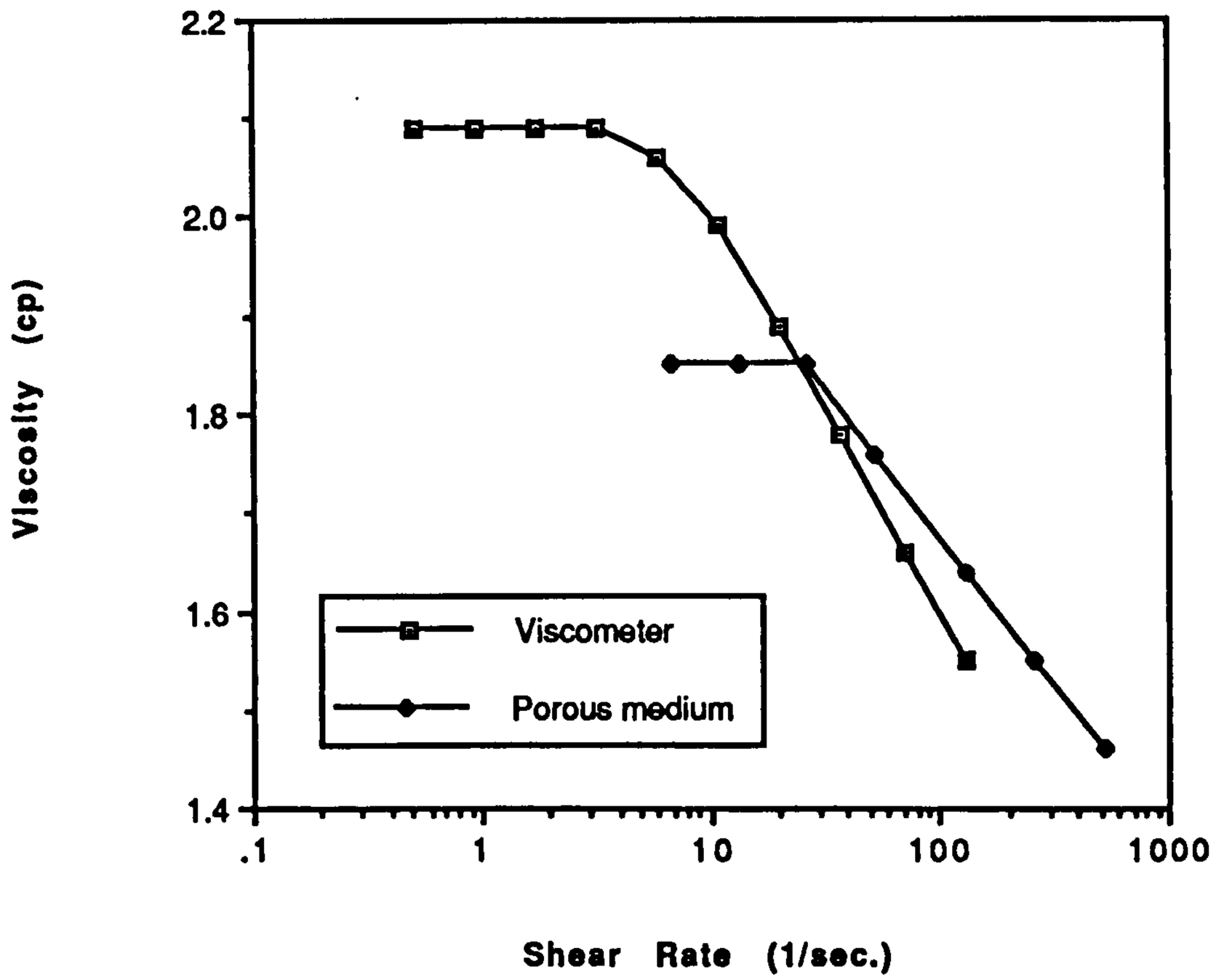

Figure 5.17 Comparison of in situ apparent viscosity and bulk viscosity for pH 3.0 xanthan solution (100 ppm)

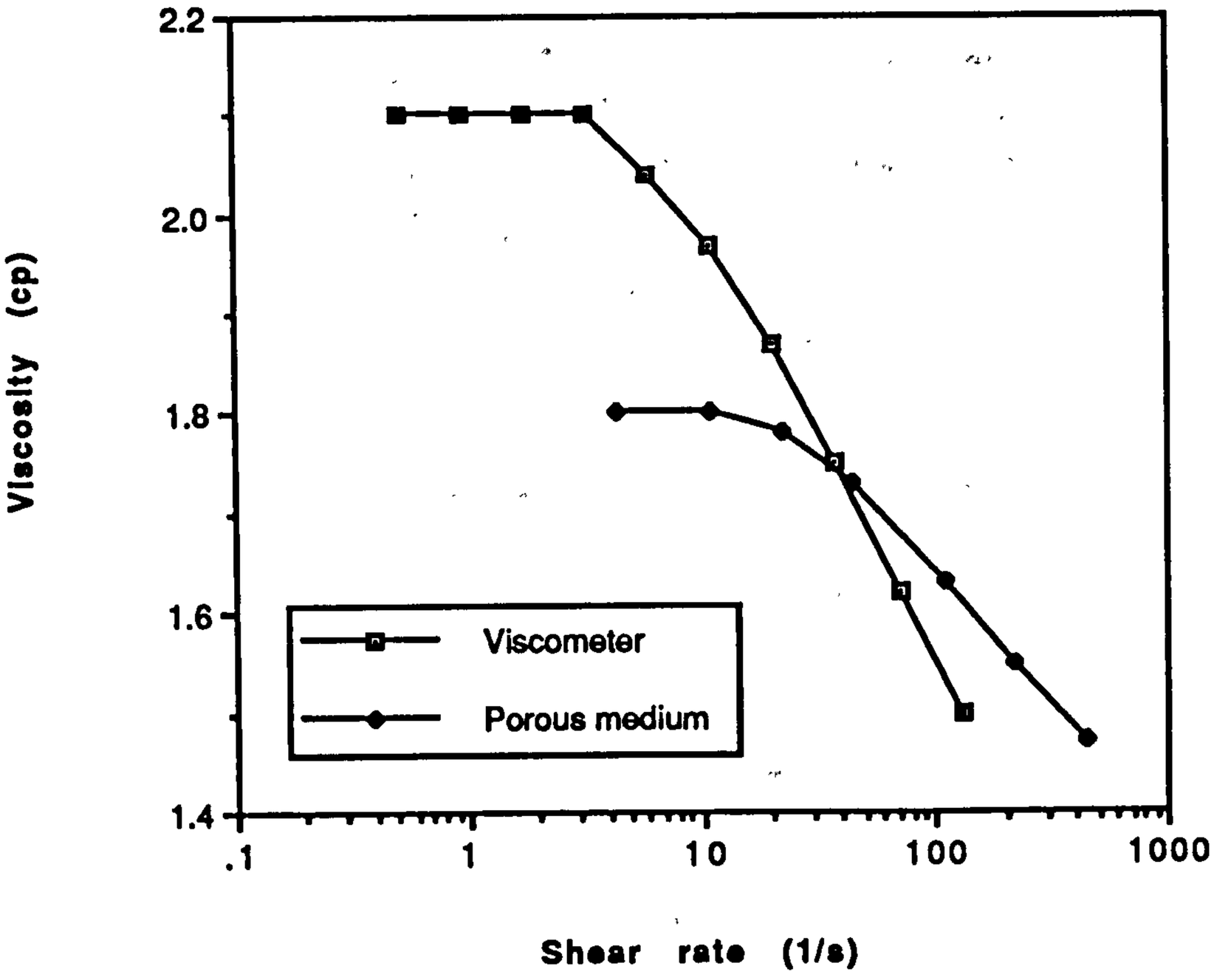

Figure 5.18 Comparison of in situ apparent viscosity and bulk viscosity for pH 5.0 xanthan solution (100 ppm)

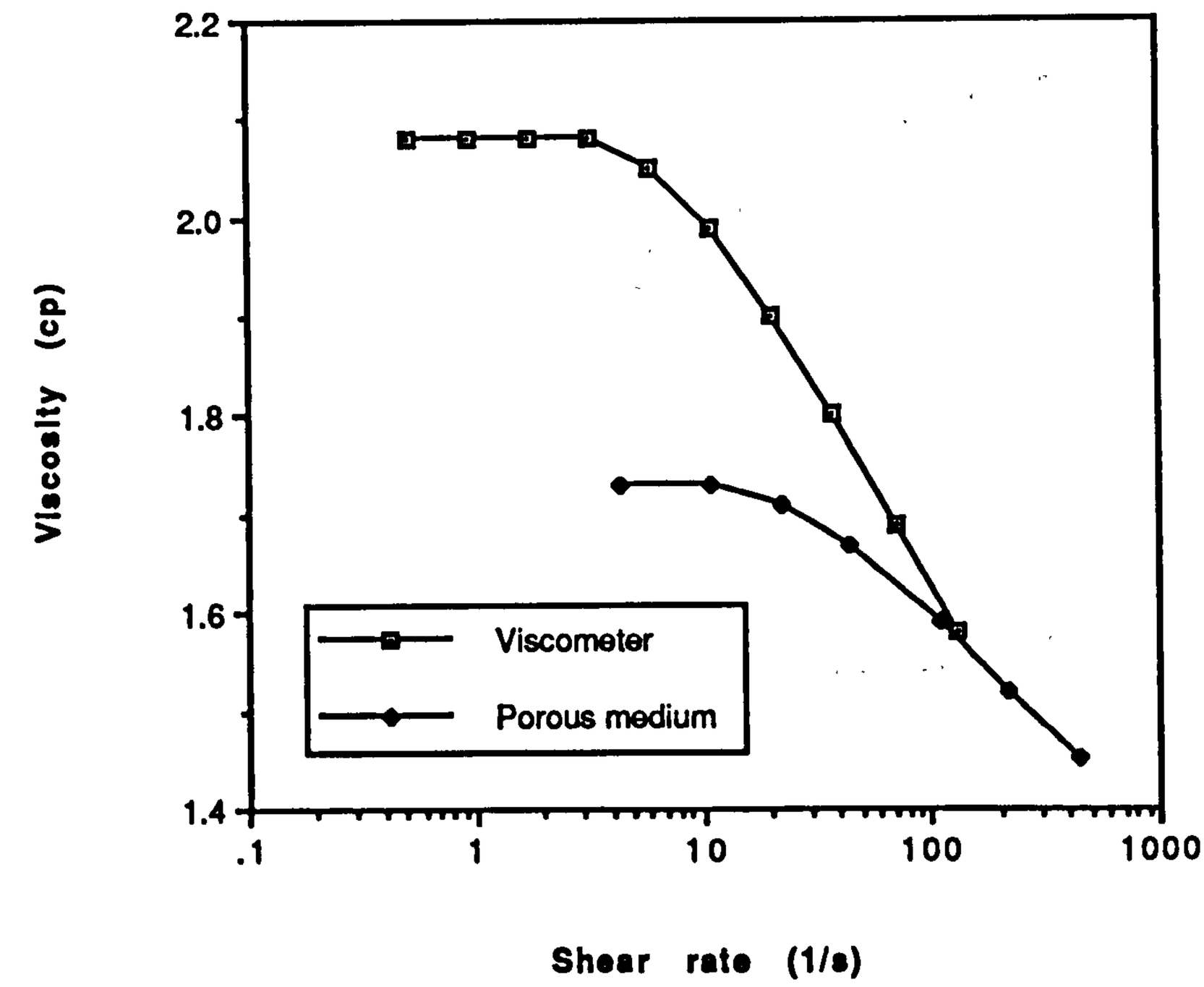

Figure 5.19 Comparison of in situ apparent viscosity and bulk viscosity for pH 9.0 xanthan solution (100 ppm)

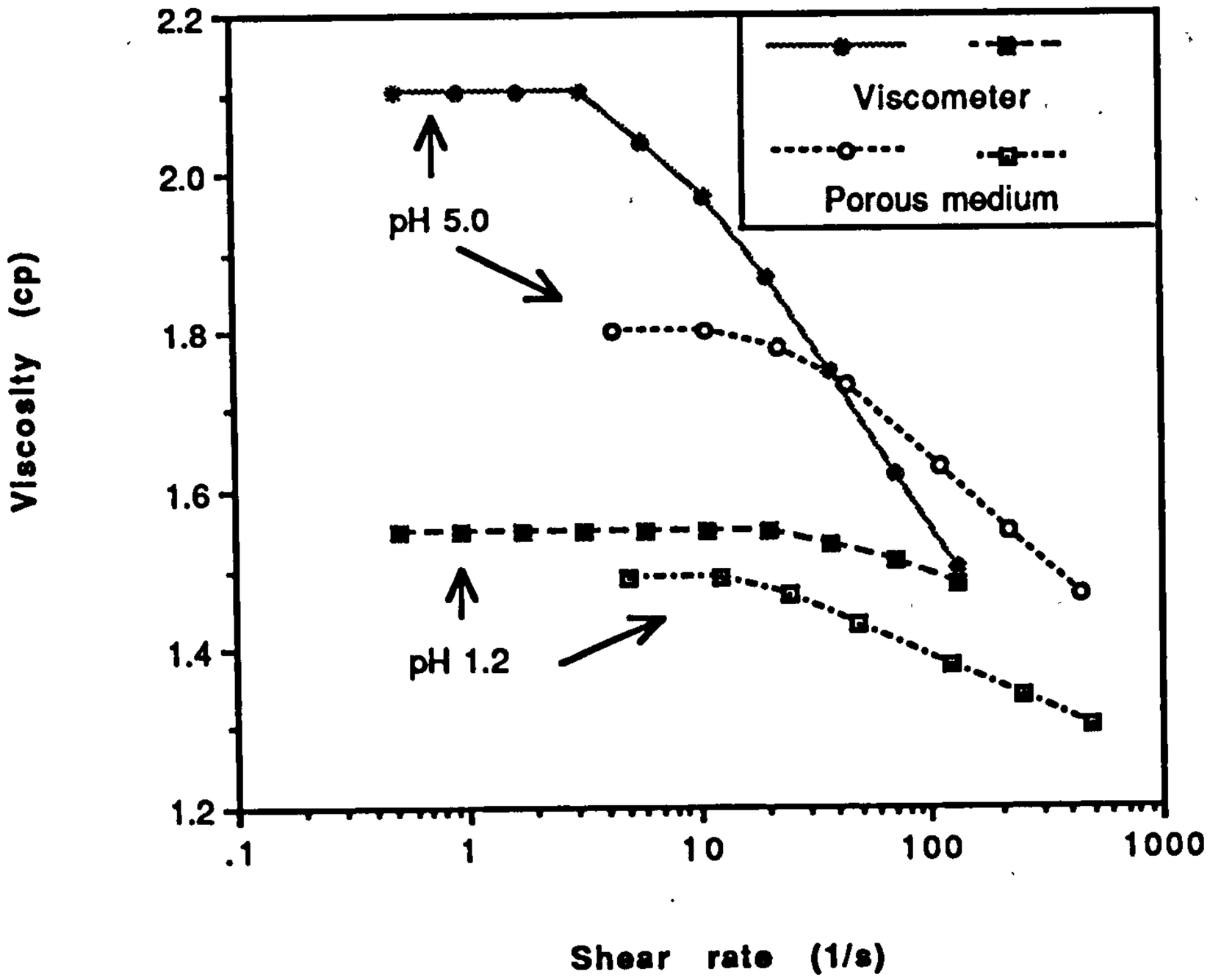

Figure 5.20 The comparison of porous medium and viscometer rheologies for pH 1.2 and 5.0 xanthan solutions

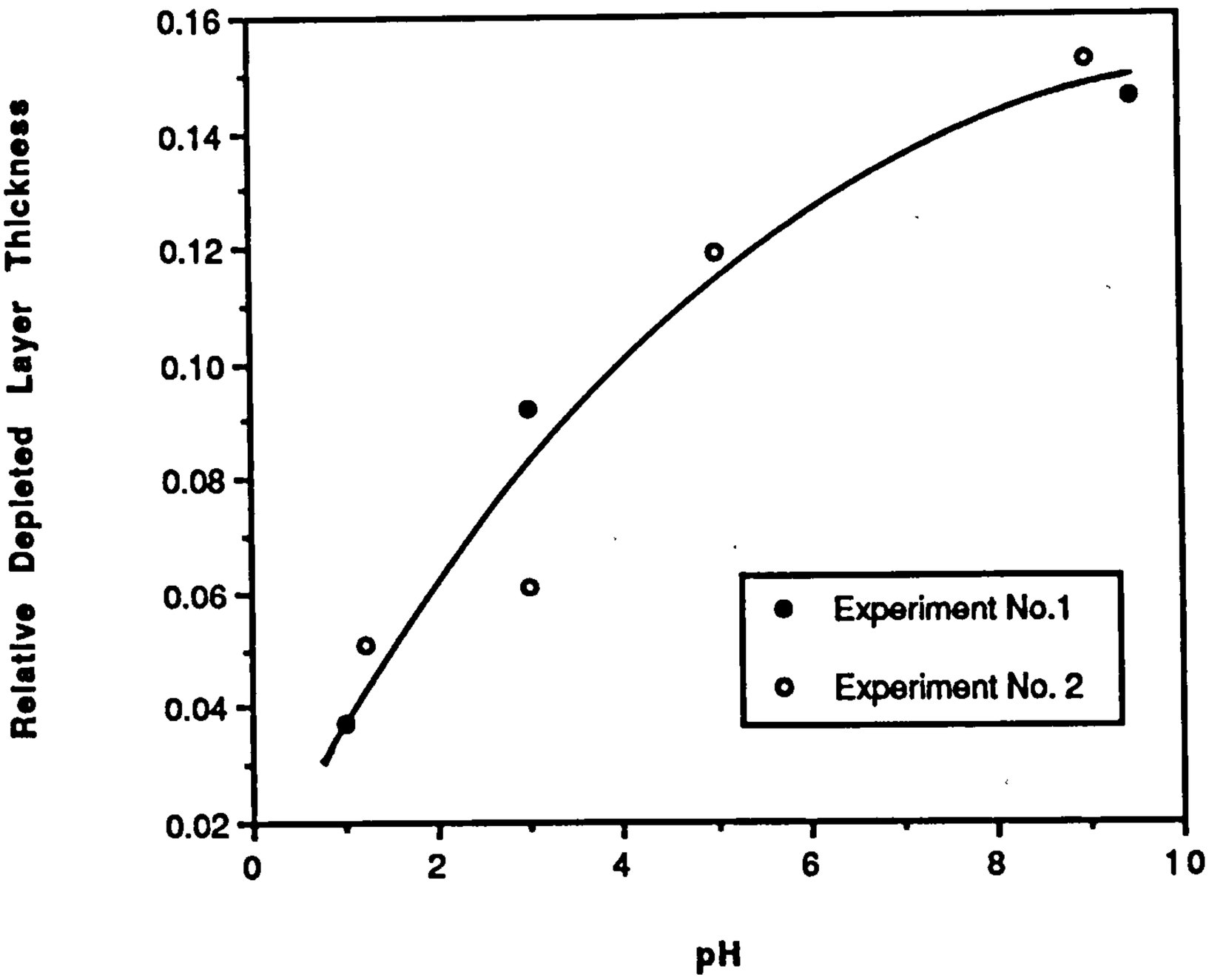

Figure 5.21 Dependence of the relative depleted layer thickness in the porous medium for xanthan solution as a function of pH as calculated using the linear layer model

results in Figure 5.21 are derived from the linear layer model, the two fluid model leads to the same conclusion as shown in Table 5.5. Both of these models for the rheological effect of the depleted layer phenomenon have been compared and discussed in some detail in Section 2.5.

Table 5.5

The pH Effect on Depleted Layer Thickness

Experiment	pH	$[\eta]_0$ (cm^3/g)	η_b (cp)	η_{app} (cp)	% viscosity decrease	δ/r (Two fluid model A1)	δ/r (Linear layer model A3)
No. 1	1.0	3600	1.60	1.55	3.13	0.041	0.037
	3.0		2.09	1.85	11.5	0.117	0.092
	9.5	6300	2.08	1.74	16.4	0.202	0.146
No. 2	1.2	3600	1.55	1.49	3.87	0.057	0.051
	3.0		2.04	1.88	7.84	0.074	0.061
	5.0	6300	2.10	1.80	14.3	0.159	0.119
	9.0	6300	2.08	1.73	16.8	0.212	0.152

The dependence of the apparent depleted layer thickness on the bulk pH of the xanthan solution shown in Figure 5.21 can be explained by considering the pH effect on both the molecular conformation of the xanthan molecule and the surface charge on the porous medium. From our experimental results, (Figures 5.2 and 5.5), three significant pH regimes can be established as follows (see Figure 5.22):

(i) pH 1 - 3: where the xanthan molecule is almost neutral and demonstrates a smaller semiflexible conformation and there is no surface charge on the pore walls

(ii) pH 3 - 5: the xanthan molecule is a polyanion and is in its more extended worm-like chain conformation but there is weak surface charge and probably now negligible potential, z, on the pore walls

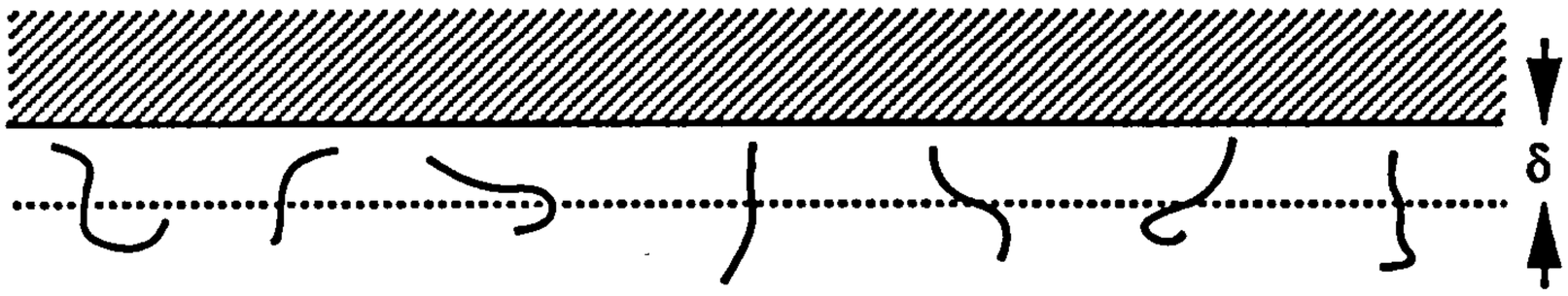

(a) pH (1-3): semiflexible neutral xanthan / no surface charge

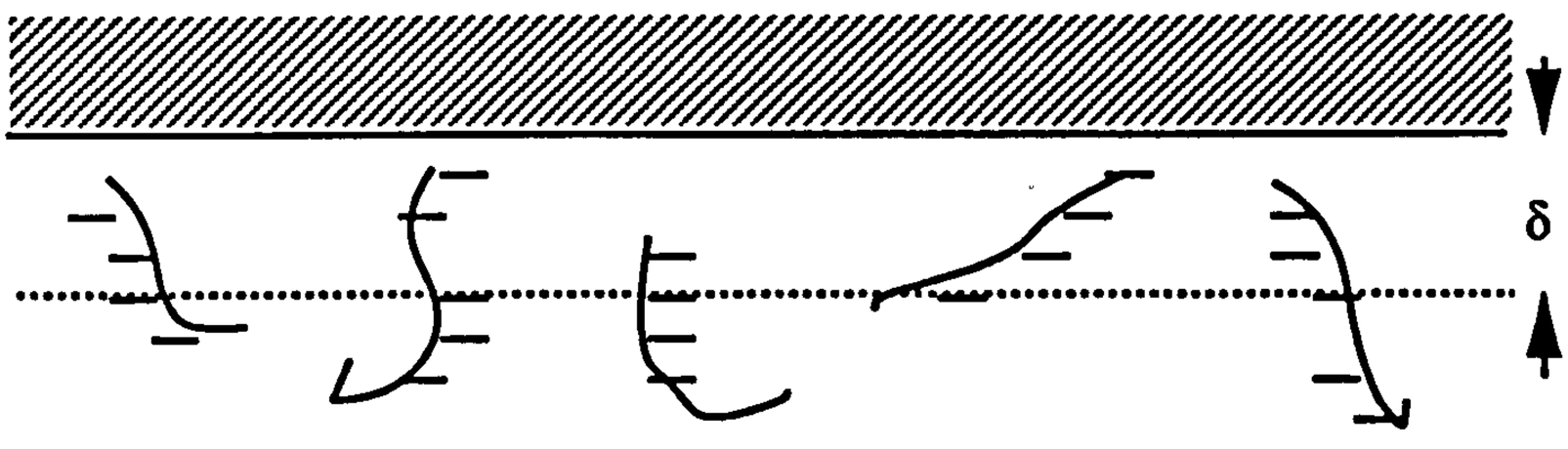

(b) pH (3-5): extended polyanionic xanthan / weak charged surface

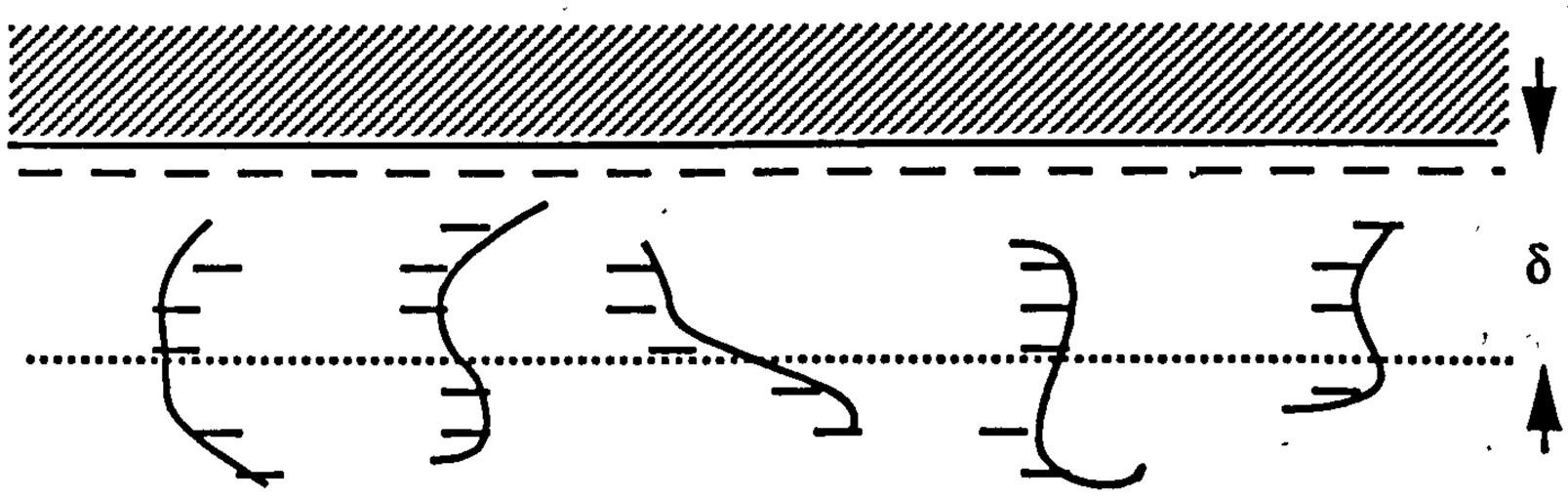

(c) pH (5-10): extended polyanionic xanthan / negatively charged surface

Figure 5.22 Schematic diagram interpreting the dependence of the apparent depleted layer thickness on the in situ xanthan solution pH

(iii) pH 5 - 10: the xanthan is in the same polyanionic rigid conformation but there is an increasing surface charge (with increasing pH) on the pore walls

In pH range (i) above, the smaller molecular dimensions and lower electrostatic repulsion result in a lower exclusion of polymer molecules from the walls of the porous medium resulting in a small depleted layer as shown schematically in Figure 5.22(a). In range (ii), where the xanthan has a more extended molecular size but there is zero surface charge on the porous medium, the steric exclusion of polymer molecules from the pore wall is greatly increased mainly due to the increase in molecular size of the xanthan as shown schematically in Figure 5.22(b). In the higher pH range (iii), where the polyanionic xanthan molecule is more extended and the porous medium has a negative surface charge, the depleted layer thickness (δ) is increased even further due to both the large steric exclusion due to the larger xanthan molecule and also due to electrostatic repulsion between the xanthan molecule and the surface [see Figure 5.22(c)]. However, since the largest increase occurs over the lower pH range (pH ~ 1 to 6), this indicates that the extension of the molecular structure has a much more significant effect on the depleted layer thickness than does the additional surface charge on the porous medium. Only at very low salinity should we expect a larger pH dependence due to the electrostatic contribution (q_e) to the total persistence length ($q_0 + q_e$). In our salinity condition (0.6 M NaCl) the xanthan molecule is always in a double helix ordered conformation whatever the pH is. From δ/r and η versus pH (Figure 5.21 and 5.2), it is clear that a more compact conformation is initiated in acidic condition, i.e. the xanthan dimer is more flexible at acidic pH (lower persistence length and lower hydrodynamic volume) as a consequence of an intramolecular reorganization of the double helical structure.

Finally, in this section, an important point is illustrated concerning the thickness of the depleted layer. The bulk viscosity of the 50 ppm xanthan solution at pH ≈ 5 is η_b = 1.57 cp and is very close to the viscosity of one of the 100 ppm xanthan samples used in this work (η_b = 1.55 cp) but where the pH = 1.2. The bulk and in situ viscosities as functions of shear rate (bulk or porous medium) are shown in Figure 5.23 for each of

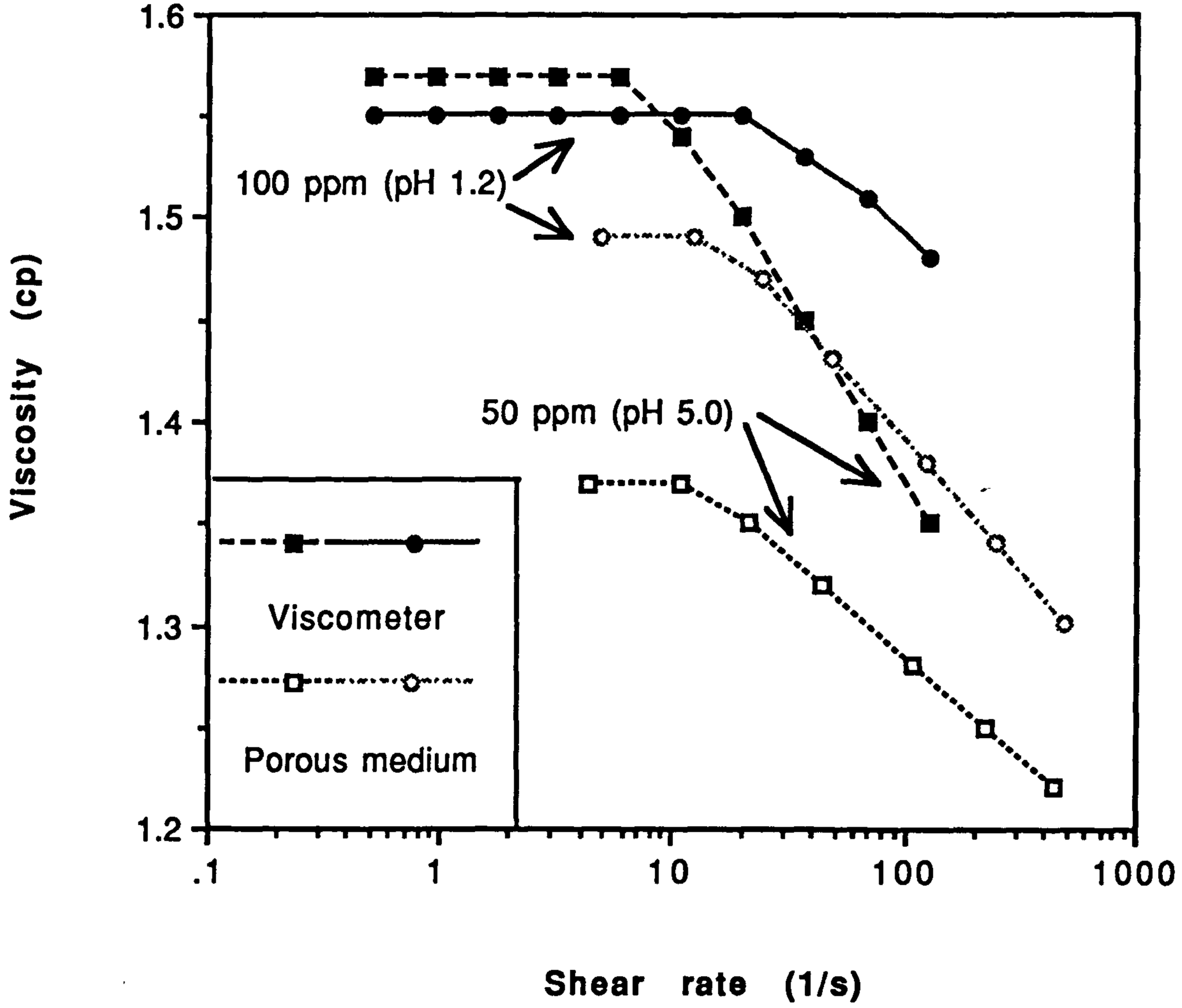

Figure 5.23 Comparison showing different in situ rheological behavior for solutions having very similar Newtonian viscosities in bulk solution but different pH values

these solutions. This figure shows that very different in situ rheological behaviour is observed for these two solutions even though their bulk viscosities are almost the same at low shear rate. Using the linear layer model to calculate the relative depleted layer thickness, the 50 ppm (pH ≈ 5) solution has a value of 0.206 which is approximately four times that of the 100 ppm (pH = 1.2) value of 0.051. This indicates that considering only the solution viscosity is not sufficient to determine the polymer in situ rheology which depend strongly on the polymer structure and, to a lesser extent, on the surface properties of the porous medium.

5.7 Salinity Effect on In Situ Rheology

Low fixed-concentration xanthan solutions of concentration 100 ppm were used to carry out the in situ rheological experiments and typical examples are shown in Figure 5.24 to 5.27 at salinity 0.1, 0.5, 5.0 and 35 g/l NaCl respectively. A comparison of the measured η_{app} vs $\dot{\gamma}_{pm}$ and corresponding bulk fluid η vs $\dot{\gamma}$ data for various values of salinity is shown in Figure 5.28. The relative viscosity, η_r, in Figure 5.28 is defined as the ratio of polymer viscosity to that of the solvent. The relative depleted layer thickness, (δ/r), calculated using the linear layer model is shown as a function of salinity in Figure 5.29 and this is compared with the two fluid model in Table 5.6. Our results indicate that (δ/r) decreases with increasing salinity over the range studied from 0.1 to 35 g/l (1.7×10^{-3} to 6×10^{-1} M) NaCl. It is also clear from Figure 5.29 that the overall trend in the change of (δ/r) and $[\eta]$ with salinity is very similar which is as we would expect.

The behavior exhibited by xanthan solutions in response to increasing ionic strength is typical for polyelectrolytes. Normally, polyelectrolyte chains contract in the presence of a salt, resulting in significantly smaller hydrodynamic radii, and lower viscosities, than at low ionic strength. Southwick et al (1982) summarized the effect of salinity on xanthan as follows: at low ionic strength, the xanthan molecule is a highly extended chain in solution, as a result of intra-chain, electrostatic repulsion; and at higher ionic strengths, self-association of these worm-like coils occurs. But the measured $[\eta]$ by Sho et al

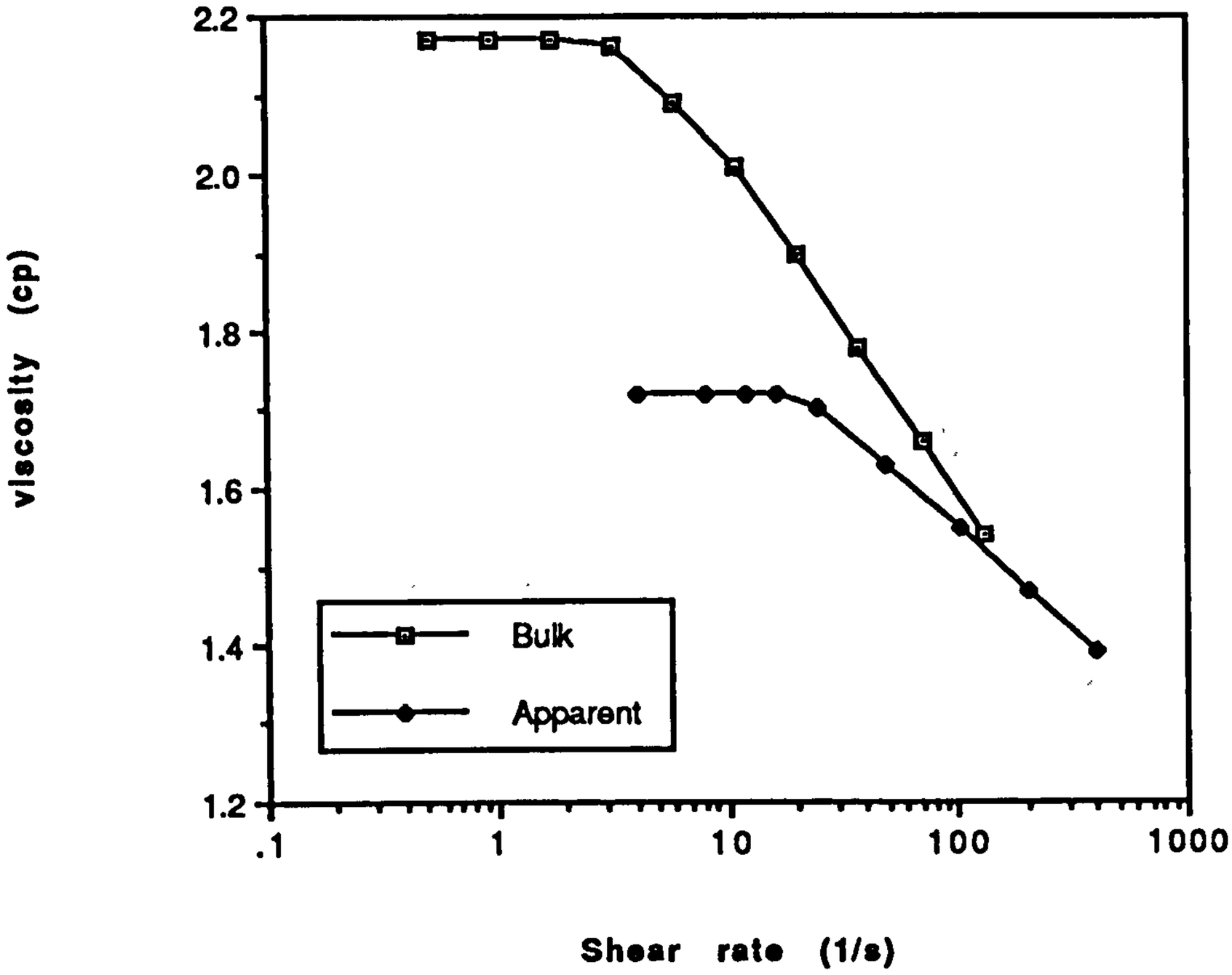

Figure 5.24 Comparison of in situ apparent viscosity and bulk viscosity for 100 ppm xanthan solution in 0.1 g/l NaCl

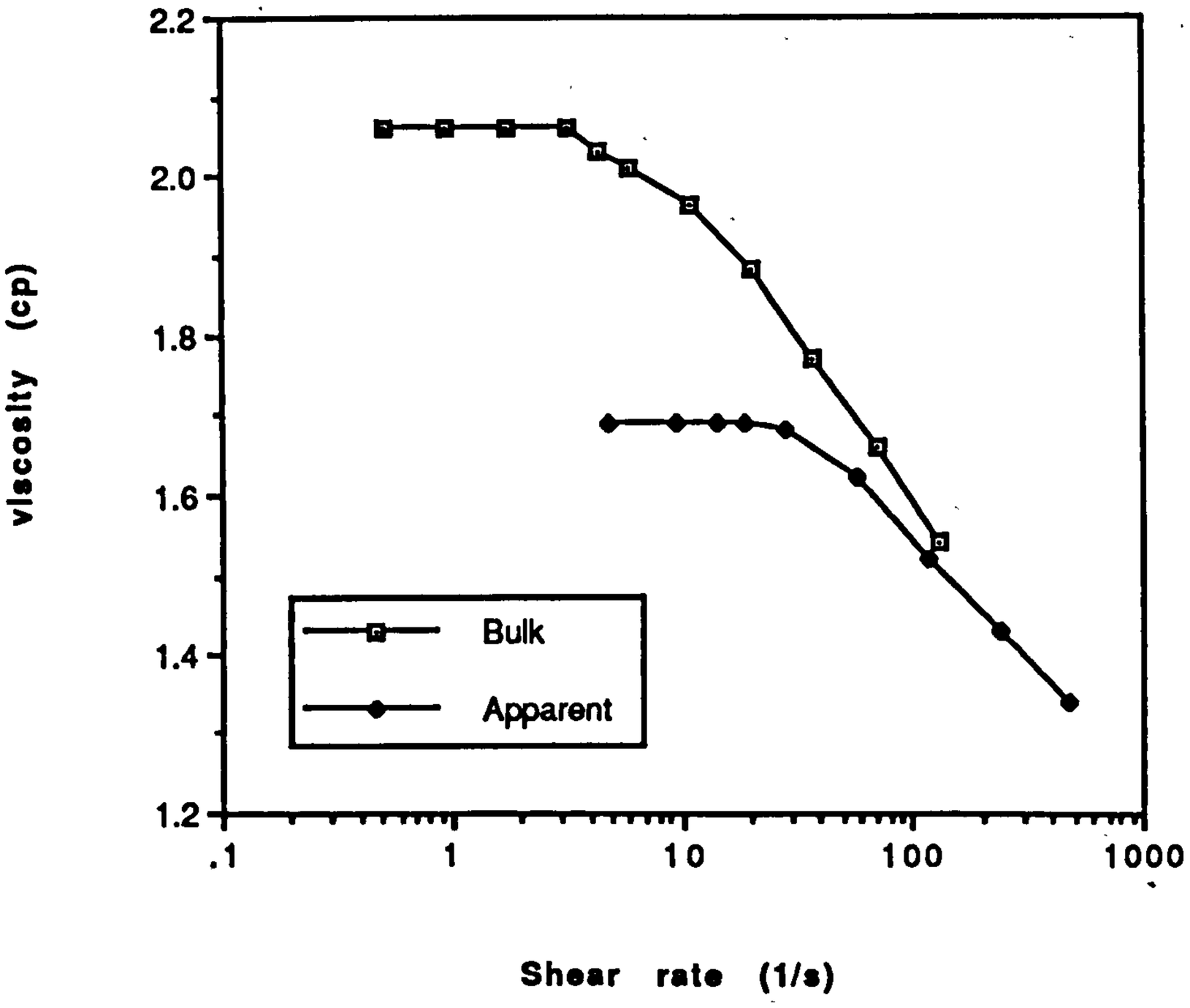

Figure 5.25 Comparison of in situ apparent viscosity and bulk viscosity for 100 ppm xanthan solution in 0.5 g/l NaCl

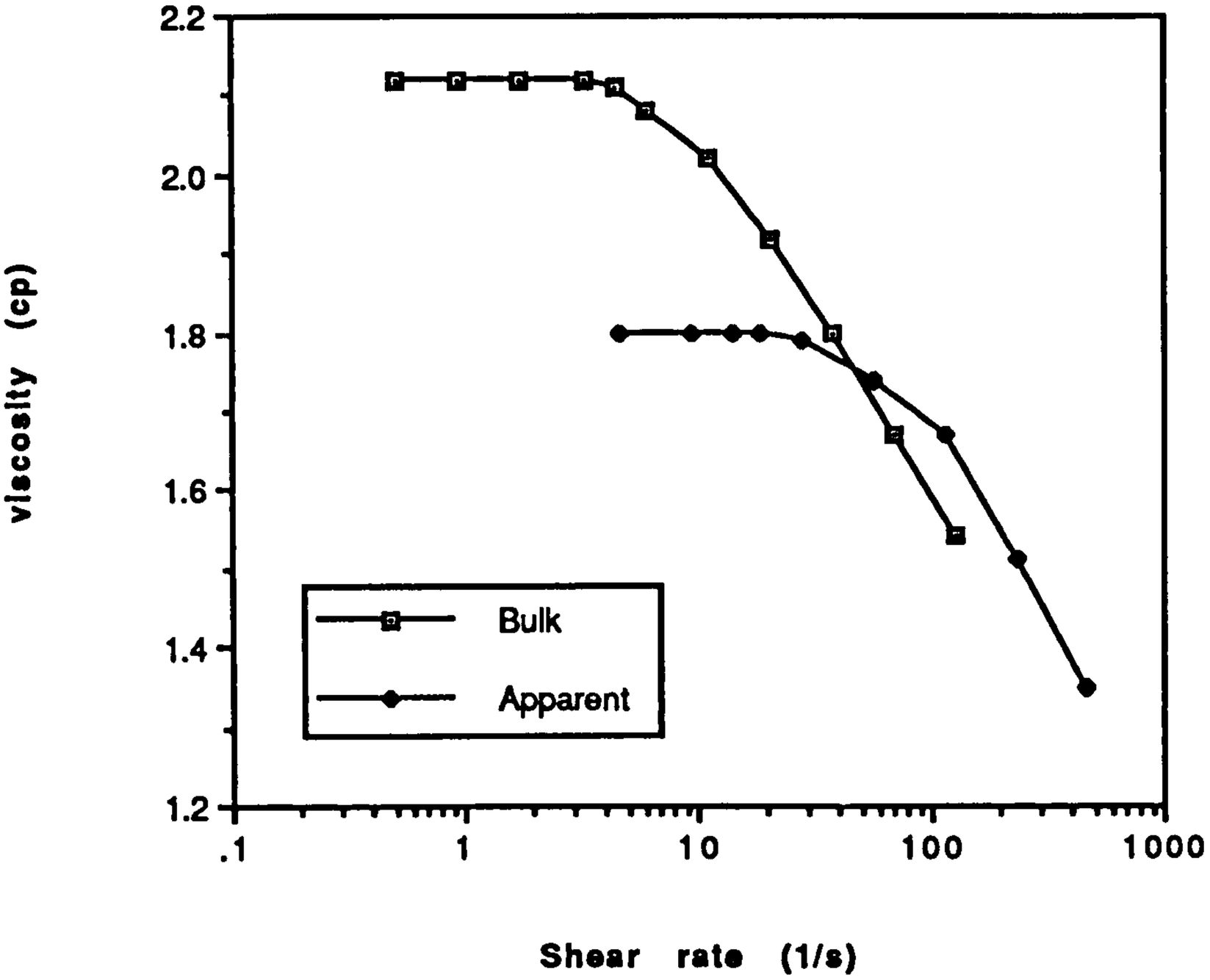

Figure 5.26 Comparison of in situ apparent viscosity and bulk viscosity for 100 ppm in 5.0 g/l NaCl

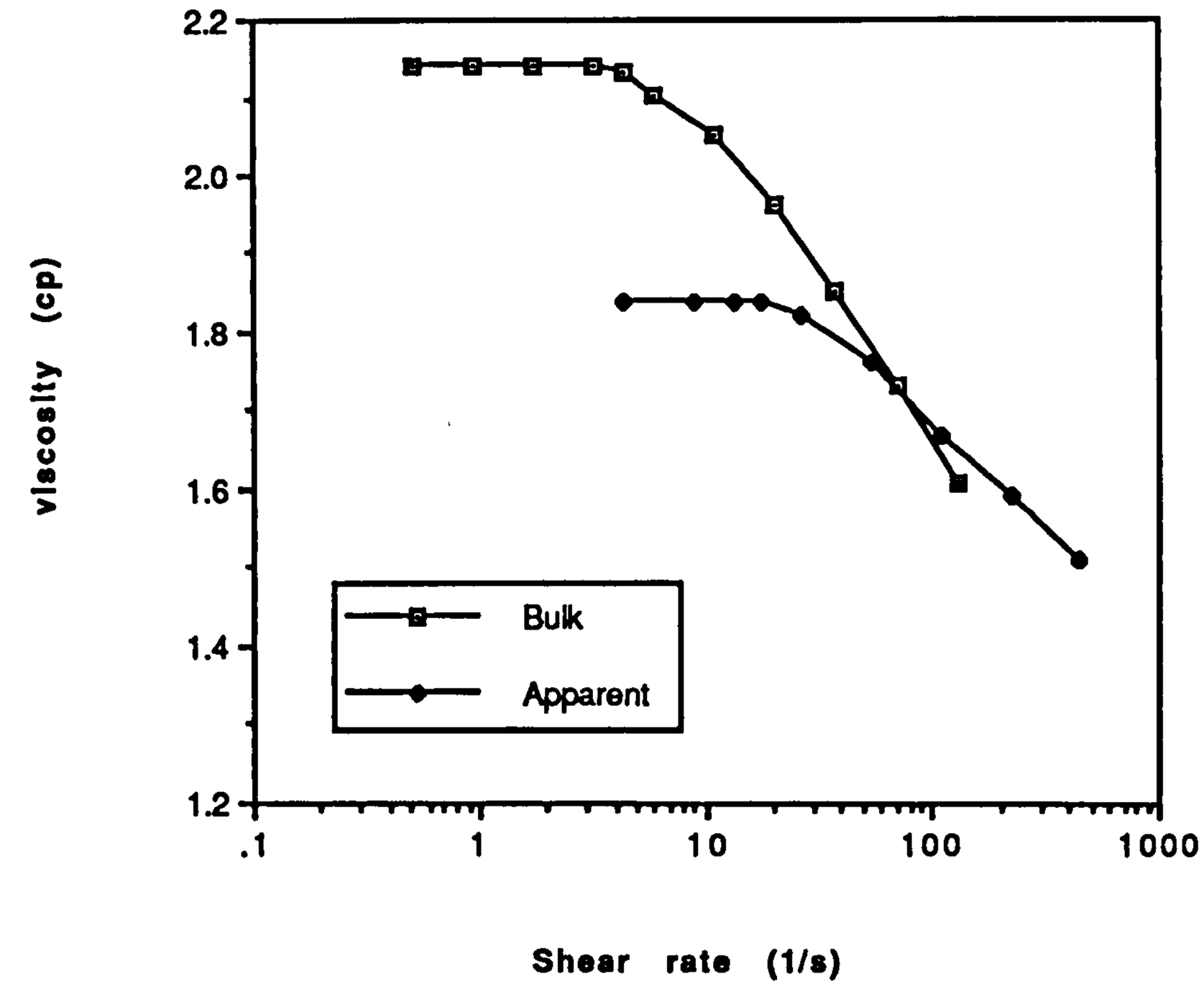

Figure 5.27 Comparison of in situ apparent viscosity and bulk viscosity for 100 ppm xanthan solution in 35 g/l NaCl

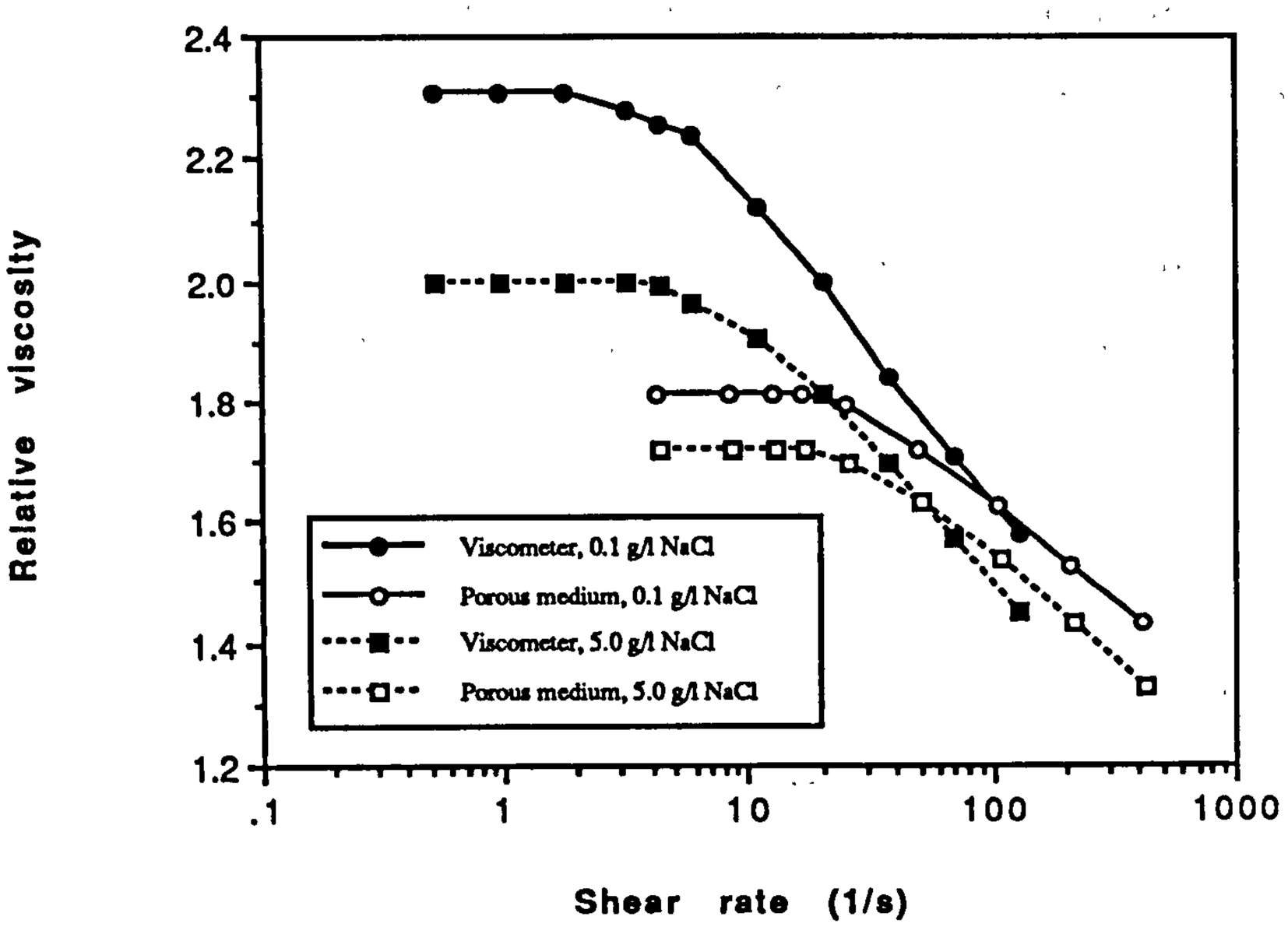

Figure 5.28 An example of the comparison of porous medium and viscometer rheologies for 100 ppm xanthan solution at 0.1 and 5.0 g/l NaCL salinity

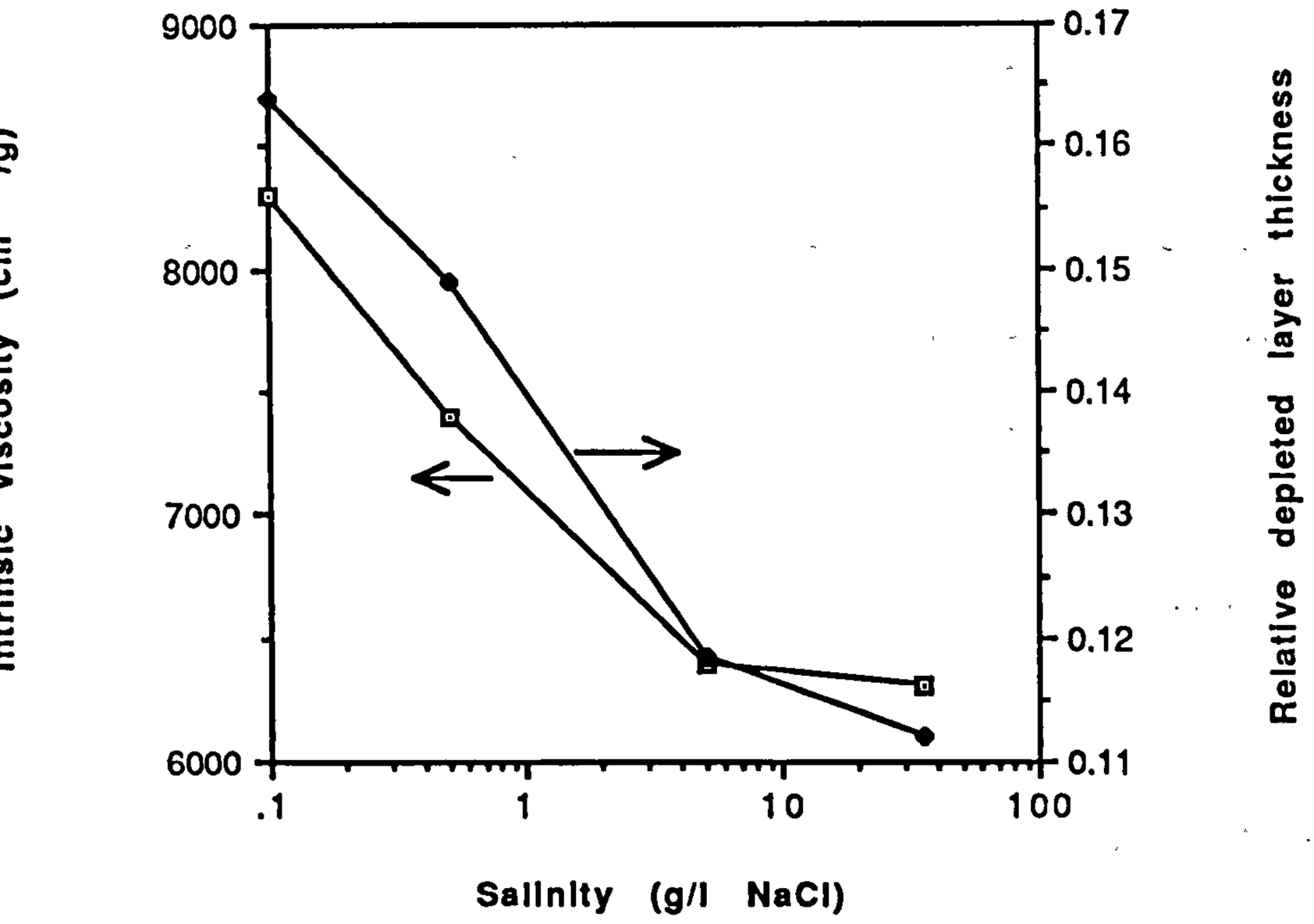

Figure 5.29 Dependence of xanthan intrinsic viscosity and depleted layer thickness on salinity

(1986) for xanthan samples was almost independent of salt concentration between 0.005 and 1 M NaCl which showed that the electrostatic persistence length, q_{el}, << the structural persistence length, q_0. The findings of Muller et al (1986) indicate that, for a single-stranded xanthan, the persistence length at higher salinities (above 10^{-2}M NaCl) can be regarded as the structural persistence length and the electrostatic persistence length is negligible. However, at low salinity (below 10^{-3}M NaCl), a high value of persistence length was found due to electrostatic repulsions between charged groups.

Table 5.6

The Effect of Salinity on the Relative Depleted Layer Thickness, (δ/r)

Experiment No.	Salinity (g/l NaCl)	Solvent Viscosity η_s (cp)	Inlet (Bulk) Viscosity η_{in} (cp)	Apparent Viscosity η_{app} (cp)	Relative Depleted Layer Thickness (δ/r)	
					TF Model [A1]	LL Model [A3]
1	0.1	1.02	2.17	1.72	0.276	0.180
	0.5	1.03	2.06	1.69	0.235	0.164
	5.0	1.06	2.12	1.80	0.173	0.129
	35	1.07	2.14	1.84	0.155	0.117
2	0.1	1.02	2.35	1.85	0.251	0.164
	0.5	1.03	2.27	1.84	0.216	0.149
	5.0	1.06	2.12	1.82	0.157	0.118
	35	1.07	2.11	1.83	0.146	0.119

The effect of xanthan molecular structure on the magnitude of the apparent surface exclusion is quite significant. Since (δ/r) depends on the size of the molecule and this, in turn, is affected by the salinity, we expect a larger depletion zone at lower salinity where the xanthan molecule is more extended. Compared with pH effect, the salinity effect is somewhat smaller due to the weak effect of salinity on the intrinsic stiffness of

the xanthan backbone. Our experimental findings are in agreement with the conclusion of Tinland and Rinaudo (1989) that the degree of extension of the xanthan molecule is mainly caused by the intrinsic stiffness of the polymer backbone and is affected to a lesser extent by electrostatic repulsion caused by the charged groups.

It is clear that the solution behavior of xanthan is well understood by considering the intrinsic rigidity of the backbone as evidenced by the value of the intrinsic persistence length. This explains the slight viscosity change in a rather large range of both pH and salinity. The conformation of xanthan may become more compact or flexible at some extreme cases such as very low pH or high salinity, which may lead to a effect on xanthan rheological behavior more or less.

5.8 Summary and Conclusions

In summary, we find that both the transport and in situ rheological behaviour of xanthan biopolymer are strongly affected by the value of the in situ pH as well as by salinity. Experimental results clearly indicate the existence of a layer depleted in polymer close to the pore wall. these results in the more rapid transport of polymer molecules compared with tracer species and also causes an apparent slip effect in the polymer in situ rheology. The magnitude of this depleted layer effect is a function of both the molecular conformation and the surface charge on the porous medium both of which depend on the local solution pH and salinity. Using a linear layer model to analyse the experimental in situ rheological results, it has been found that the relative depleted layer thickness, (δ/r), increases with increasing pH over the range 1 to 10 and with decreasing salinity in a range of 35 to 0.1 g/l NaCl. This has been interpreted in terms of the effect of pH or salinity on the molecular conformation of xanthan and the surface charge on the porous medium.

The specific conclusions from this work are summarised as follows:

(1) The viscosity of low-concentration xanthan solution is changed reversibly as the solution pH value drops below 3 and is then returned to higher pH due to a conformational transition of the xanthan molecules similar to the order/disorder transition. In the disordered state at pH < 3, the xanthan has a low viscosity and the molecule is probably near neutral and is hydrodynamically smaller than at higher pH (in the range ~ 4 - 10).

(2) The point of zero charge is reached for ballotini glass beads in 3.5% NaCl brine at pH ≈ 4.5 and, at higher pH, the surface charge on ballotini increases with pH, especially above pH ≈ 8.

(3) The intrinsic viscosity of xanthan solution related to the structural persistence length of xanthan molecules depends on the solution pH and salinity, which more or less affects the xanthan rheological behaviour.

(4) In transport through the porous medium in a series of fixed pH (between 1 and 10) or salinity (between 0.1 and 35 g/l NaCl) polymer/tracer breakthough experiments, the polymer clearly travels through the porous medium faster than the tracer. The advancement of the polymer, as measured by the relative exclusion volume (PV_ϕ), is lower at low pH (< 3) and increases up to a constant value between pH ≈ 4 and 10 which corresponds very closely with the pH behaviour of the solution viscosity.

(5) The in situ polymer viscosity is always below the bulk fluid viscosity in the low shear rate Newtonian regime for all cases in our experiments due to a surface-exclusion effect between polymer and pore wall although the magnitude of the effect depends on the solution pH or salinity.

(6) The relative depleted layer thickness (δ/r), which may be estimated by analytical models, apparently increase with increasing bulk pH. The increase of the relative depleted layer thickness, (δ/r), with pH may be interpreted in terms of the pH

dependence of the xanthan conformation (charge and molecular size) and the surface charge on the porous medium. Three combinations of the molecule/surface states with increasing pH can be identified as follows:

(a) pH (1 - 3) small neutral xanthan molecule/neutral surface leading to a low (δ/r)

(b) pH (3 - 5) extended polyanionic xanthan/weak charged surface giving a higher (δ/r)

(c) pH (5 - 10) extended polyanionic xanthan / negatively charged surface leading to an increased value of (δ/r) due to the extended xanthan and the additional electrostatic repulsion

It also appears that the extension of the xanthan molecule over the lower pH range (1 - 5) contributes more significantly to the thickness of the depleted layer than does the additional electrostatic repulsion at higher pH values.

(7) The magnitude of the observed slip effect is also a function of solvent salinity and (δ/r) is found to decrease with increasing salinity. This decrease is in accord with the decreasing intrinsic viscosity. This indicates that the degree of xanthan molecular extension is caused mainly by the intrinsic stiffness of the polymer backbone. The salinity effect is smaller than pH effect on the in situ rheological behaviour.

CHAPTER 6

XANTHAN ADSORPTION AT THE SOLID-LIQUID INTERFACE AND ADSORPTION EFFECT ON IN SITU RHEOLOGICAL BEHAVIOUR

6.1 Introduction

The adsorption and the in situ (porous medium) rheology of xanthan have been studied by a number of workers due to the importance of this biopolymer in enhanced oil recovery processes. The level of xanthan adsorption (or retention) is one of the key factors in determining the economic viability of a polymer flood using this biopolymer. In this chapter, many results are presented on xanthan static and dynamic adsorption and especially, the effect of solid / liquid ratio on xanthan static adsorption. An adsorption isotherm model is proposed to take accunt of the depleted layer effect, which indicates that the actual adsorption level seems somewhat higher than the the apparent measured one if a depleted layer is presented. It seems that the static adsorption level strongly depends on the solid / liquid (ballotini / polymer solution) ratio. A lot of work has been done to try to explain this unexpected phenomenon. Discussions with Chauveteau (private communication, 1991; 1992) have lead to a number of models. These models which have been proposed for describing the solid/liquid ratio effect are known as: the aggregation limited adsorption model (ALA) and the collision limited adsorption model (CLA) by Chaveteau; and the dissolved species model (DSM).

In previous chapters, some specific sensitivities of the in situ xanthan flow behaviour have been studied experimentally and theoretically. For example, in situ rheological behaviour in various polymer concentration regimes and the effects of pH and salinity (i.e. surface charge and molecular conformation) have been investigated. But those

previous studies have not considered the effect of xanthan adsorption due to the low dynamic adsorption levels. In this chapter, however, we focus more on xanthan static and dynamic adsorption, and the effect of this adsorption on the in situ rheological behaviour. In particular, we wish to examine whether the presence of an adsorbed layer on the surface of the pore walls affects the depleted layer thickness (δ/r) and hence the in situ rheology of xanthan. Some results have been reported in the literature on the behaviour of the depleted layer in the presence of adsorption of the synthetic polymer, partially hydrolysed polyacrylamide (HPAM) (Chauveteau et al, 1984) and here we present results for xanthan. The depleted layer effect is measurable both before and after dynamic adsorption has reached equilibrium. However, the additional effect of the adsorbed layer close to the pore wall is small indicating that xanthan molecules are adsorbed very flat against the pore wall. Most of above findings have not previously appeared in the literature.

6.2 Xanthan Static Adsorption

Ballotini glass beads were supplied by The English Glass Co. Ltd, and the sand is a commercial sample from BDH Laboratory Supplies, England. The particle sizes and distributions of ballotini and sand were determined using a Malvern MS20 Master Sizer or a BET method. Ballotini has an average Specific Surface Area (SSA) 0.123 m^2/g with an average size 52 μm and sand has an average SSA 0.022 m^2/g with an average size 300 μm. See Section 3.4 for detail. Solid samples were treated with dilute hydrochloric acid and were postwashed by distilled water. The samples were then dryed in an oven at 100°C. Unless otherwise stated, the ballotini samples were used in the experiments. Xanthan static adsorption was carried out with shaking of the samples. All the experiments were completed at room temperatures.

The adsorption amount (Γ) of xanthan solution was determined from the following equation:

$$\Gamma = \frac{(C_0 - C_e)v}{m} = \frac{(C_0 - C_e)}{R} \qquad [6.1]$$

where C_0 and C_e are initial and equilibrium polymer concentrations before and after adsorption respectively, v and m are the total volume of xanthan solution and total mass of solid respectively. R is solid/liquid ratio in mass/volume. Polymer concentration was determined from viscosity data using the calibration plot of viscosity vs xanthan concentration at Newtonian shear rate region as shown in Section 3.2.

Figure 6.1 shows a typical example of adsorption as a function of time for a 100 ppm xanthan solution in 35 g/l NaCl brine. Equilibrium adsorption is reached after about 50 hours which indicates a slow adsorption process. A series of experiments have been performed to investigate some effective factors on xanthan static adsorption. The effect of bulk concentration at 35 g/l NaCl on xanthan equilibrium adsorption is shown in Figure 6.2. The adsorption amount (Γ) linearly increases with bulk concentration at constant solidliquid ratio (1:1) in the region from 10 ppm to 400 ppm. The adsorption equilibrium process is very slow with concentration and no maximum equilibrium adsorption, Γ_m, (i.e. a pseudoplateau) is reached even at high polymer concentration (400 ppm). A simple empirical equation is obtained as follows:

$$\Gamma = a + bC_e \text{ (or } C_0) \qquad [6.2]$$

where a and b are empirical constants, equal to 5.8055 in μg/g and 0.2053 in ml/g respectively in this experiment. More results also are shown in Table 6.1. The static adsorption level of higher concentration solution is really very high, for example, 577 $\mu g/m^2$ at 400 ppm. Chauveteau et al (1988) thought that the adsorption density at the plateau, Γ_m, depends strongly on polymer flexibility. For xanthan, Γ_m increases when polymer-polymer electrostatic repulsions decrease, from low values (100 $\mu g/m^2$) up to reach a maximum (600-800 $\mu g/m^2$) corresponding to a monolayer at low pH or high salinities. The pHs from Table 6.1 do not show a large change with adsorption levels

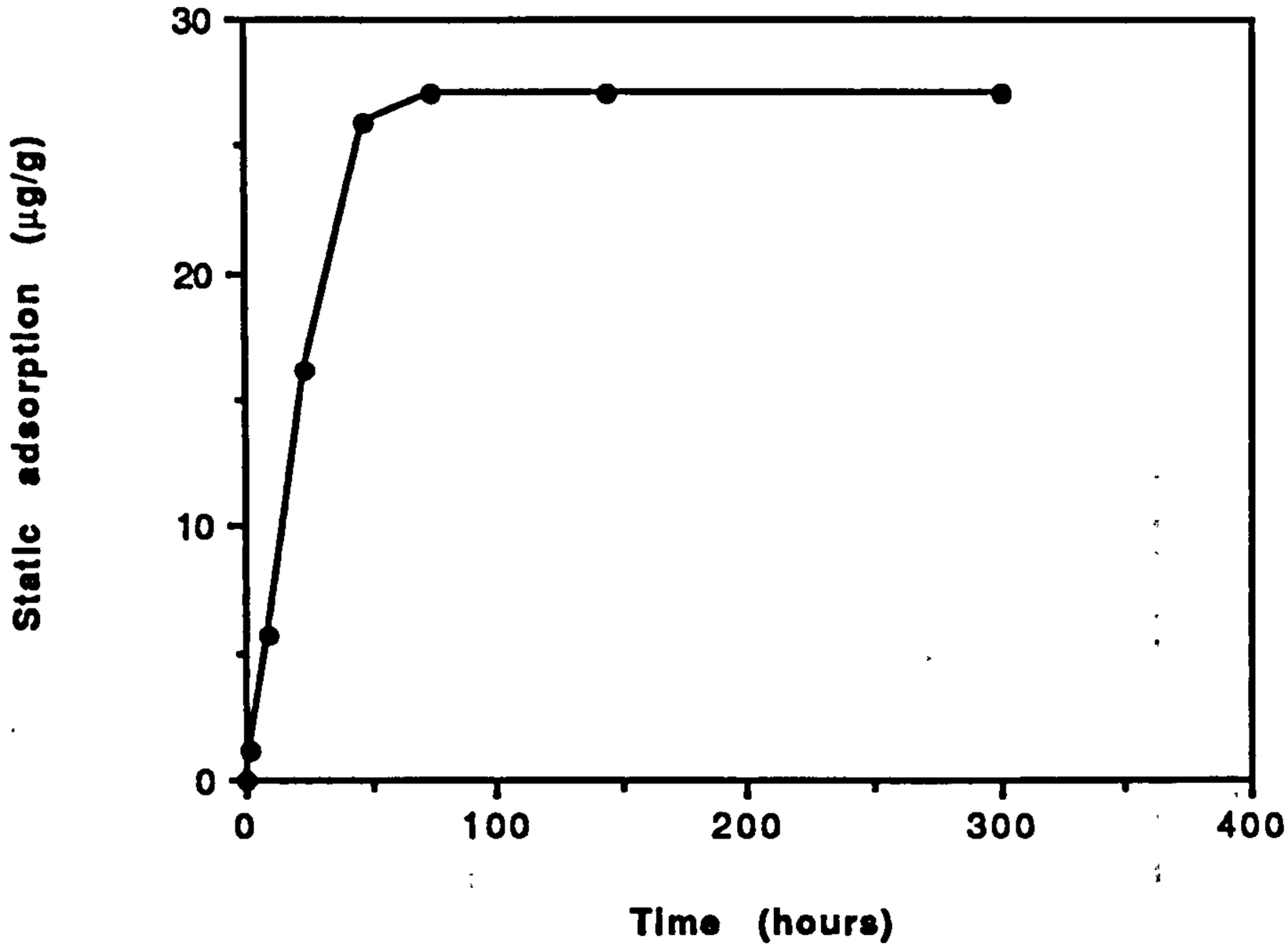

Figure 6.1 Adsorption isotherm of 100 ppm xanthan solution in 35 g/l NaCl and solid/liquid ratio 1/2

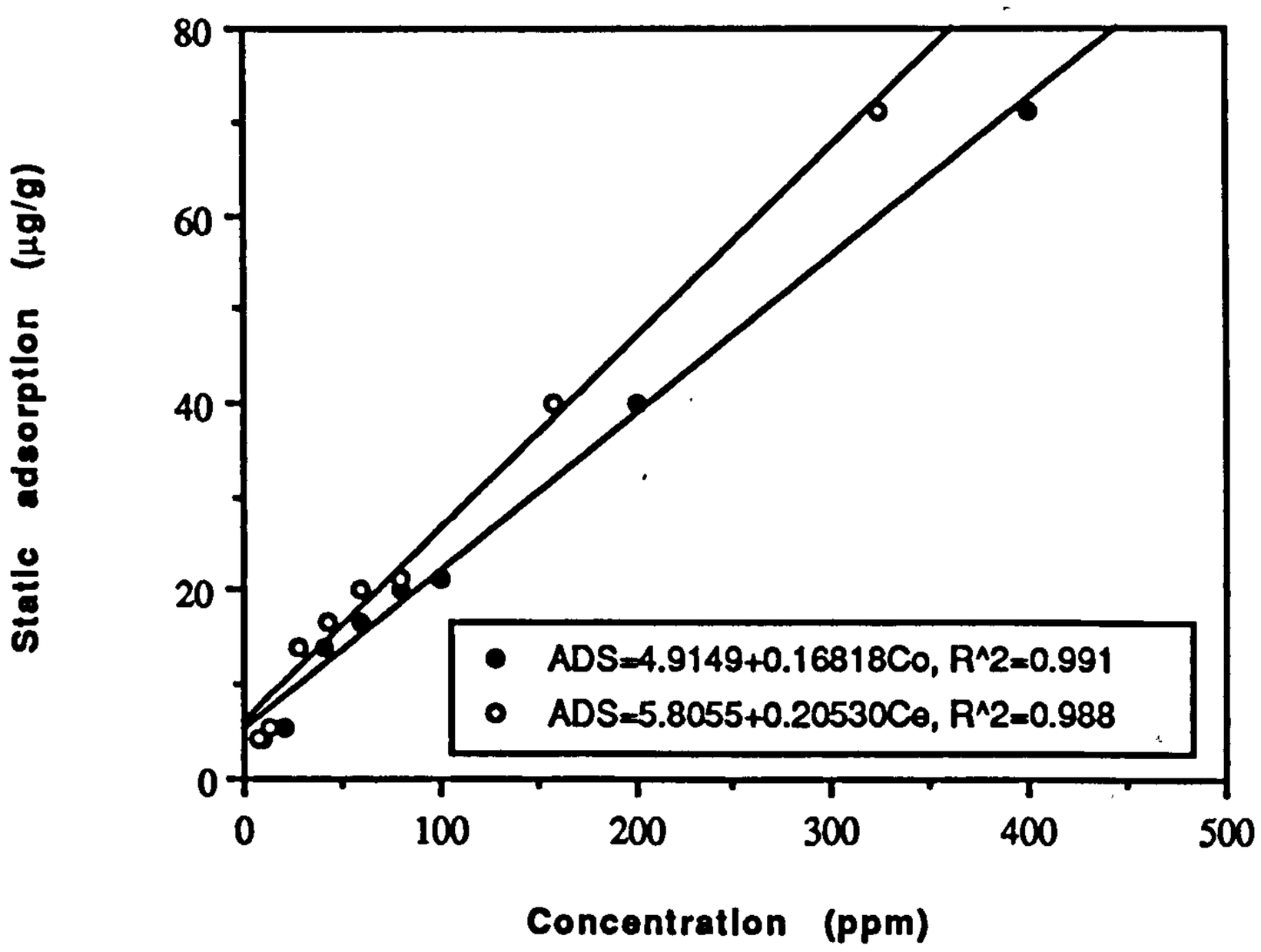

Figure 6.2 The effect of bulk concentration on xanthan static adsorption at 35 g/l NaCl and solid/liquid ratio 1/1

(pH 9.6 to 9.8), although the initially experimental pH of the polymer solution is about pH 6. This large change will be discussed later.

Table 6.1

The Effect of Bulk Concentration on Xanthan Static Adsorption *

Concentration		Viscosity		Adsorption		pH
Bulk (ppm)	After ADS (ppm)	Bulk (cp)	After ADS (cp)	(μg/g)	(μg/m^2)	
10	6.65	1.08	1.05	4.14	33.7	9.79
20	13.50	1.14	1.10	5.25	42.7	9.86
40	27.51	1.33	1.21	13.91	113	9.72
60	42.52	1.50	1.34	16.59	135	9.52
80	59.11	1.72	1.50	20.13	164	9.72
100	79.24	1.99	1.72	21.44	174	9.55
200	158.5	3.73	2.87	39.94	325	9.79
400	323.7	11.85	7.65	70.96	577	9.62

* The Solid/Liquid Ratio is 1/1 in g/ml and the experimental temperature is about 23°C.

Table 6.2 and 6.3 collect all of the xanthan static adsorption results from experiment numbers 6.1 to 6.7 at 0.1 and 35 g/l NaCl respectively. The Corresponding plot of Γ vs C_e is shown in Figure 6.3 which indicates a rather irregular change of Γ as a function of C_e. The relation, $\Gamma = kC$, clearly does not apply. This result is unexpected, and should probably have followed Langmuir-type behaviour. From Table 6.2 and 6.3, it can be seen that the adsorption level is strongly dependent on the solid/liquid ratio. Although the equilibrium concentration, C_e, decreases with increasing solid/liquid ratio, the adsorption level still markedly decreases with the increase in solid/liquid ratio. In addition, if the ballotini glass beads were not pretreated by HCl, the adsorption level and bulk pH is

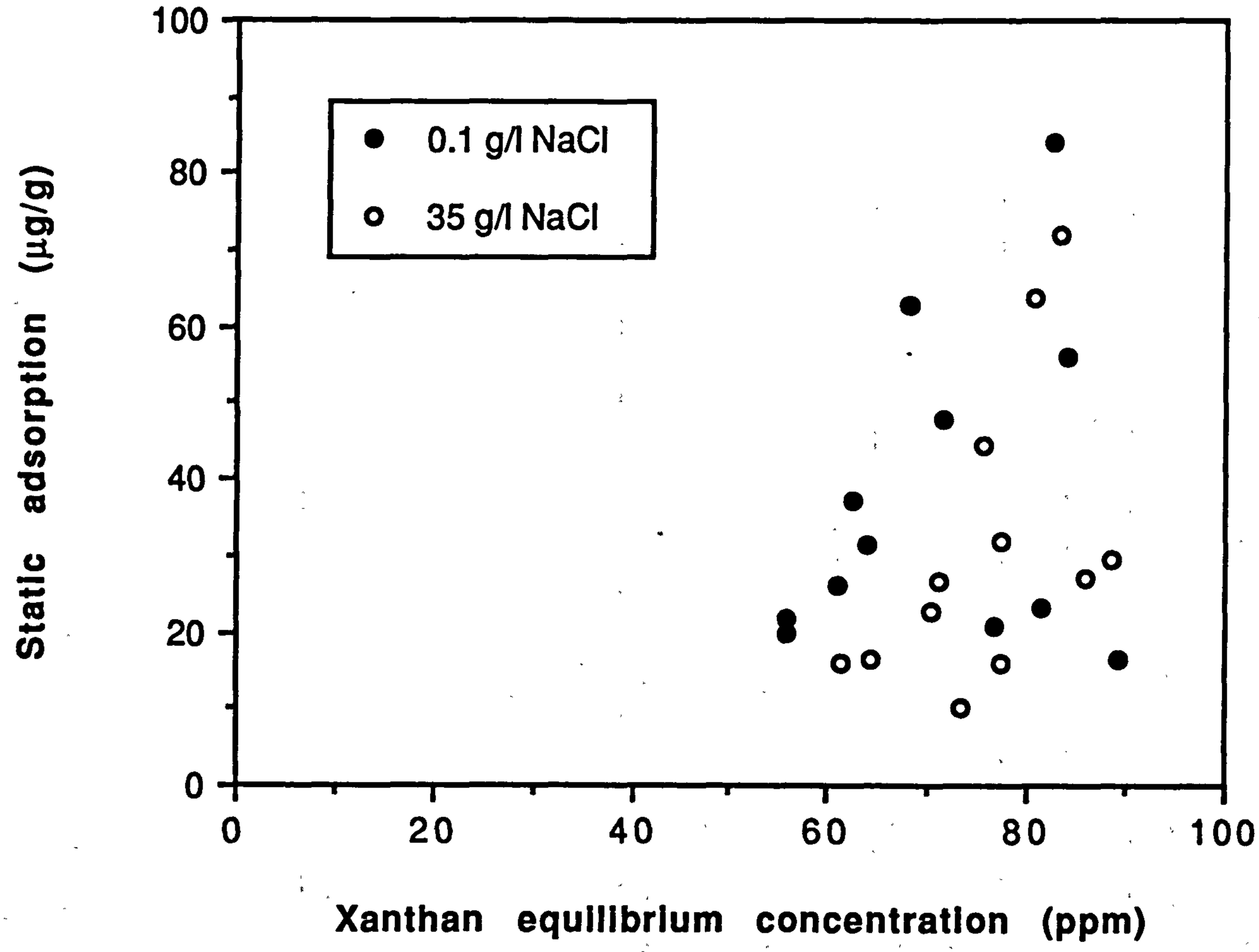

Figure 6.3 Adsorption as a function of equilibrium concentration in initial xanthan concentration about 100 ppm

somewhat higher than the HCl pretreated cases. These observations will be considered in more detail in next two sections.

Table 6.2

Xanthan Static Adsorption in 0.1 g/l NaCl Solution

Exp. No.	Time (hours)	Solid/ Liquid (ml/g)	Temp. (°C)	pH	Concentration (ppm)		Adsorption	
					C_e	C_o	µg/g	µg/m^2
6.1*	330	0.5	20.5		81.45	93.01	23.20	189
6.3*	118	0.5	20.7		89.09	97.35	16.54	134
6.5*	195	1	22.5	9.82	76.50	102.55	26.05	212
		2		10.97	61.03	102.55	20.76	169
6.6**	144	0.2	24.0	10.51	82.65	99.46	84.05	683
		0.5		10.77	68.00	99.46	62.92	512
		1		11.10	62.45	99.46	37.01	301
		2		11.27	55.89	99.46	21.79	177
6.7*	144	0.1	20.0	7.27	88.52	95.20	66.78	543
		0.2		7.58	83.96	95.20	56.19	457
		0.5		9.47	71.34	95.20	47.72	388
		1		9.86	63.86	95.20	31.34	255
		2		9.85	55.89	95.20	19.65	160

* HCl pretreated ballotini

** not pretreated ballotini

Table 6.4 shows effect of the salinity on xanthan adsorption. The two cases (0.1 g/l NaCl and 35 g/l NaCl) have very similar tendency, and it appears that the 0.1 g/l NaCl brine case has a little higher adsorption level than the corresponding 35 g/l NaCl system. This result seems somewhat in disagreement with the expectation of increasing Γ with decreasing polymer-polymer electrostatic repulsion. Since this difference is not very large and may be due to the effect of some other factors mentioned later.

Table 6.3

Xanthan Static Adsorption in 35 g/l NaCl Solution

Exp. No.	Time (hours)	Solid/ Liquid (ml/g)	Temp. (°C)	pH	Concentration (ppm)		Adsorption	
					C_e	C_0	µg/g	µg/m^2
6.1*	330	0.5	20.5		88.53	103.27	29.48	240
6.2*	144	0.5	20.3		85.87	99.73	27.12	220
6.4*	195	2	21.7	9.61	73.20	93.89	10.35	84
6.5*	334	1	22.5	9.41	77.34	93.29	15.95	130
6.6**	144	0.2	24.0	10.26	83.23	97.63	72.00	585
		0.5		10.41	75.34	97.63	44.58	362
		1		10.61	70.84	97.63	26.79	218
		2		10.81	64.31	97.63	16.66	135
6.7*	144	0.1	20.0	8.89	86.71	93.29	65.83	535
		0.2		9.46	80.50	93.29	63.94	520
		0.5		9.39	77.34	93.29	31.91	259
		1		9.58	70.36	93.29	22.93	186
		2		9.53	61.47	93.29	15.91	129

* HCl pretreated ballotini

** not pretreated ballotini

To investigates the effect of ballotini surface properties on xanthan static adsorption, a new experiment was performed using a 100 ppm polymer solution in a 35 g/l NaCl - HCl pretreated ballotini system. One problem may be the ageing of the glass beads in the presence of water over long periods of time. It is possible that a hydration layer forms which decreases polymer adsorption. This is related to the obseravation of very low dynamic adsorption during polymer flow through the balloniti as shown in Section 5.5. The experimental results are shown in Table 6.5, which indicate that brine ageing of ballotini has a small effect on xanthan adsorption.

Table 6.4

The Effect of Salinity on Xanthan Static Adsorption*

Solid/Liquid Ratio (g/ml)	35 g/l NaCl			0.1 g/l NaCl		
	$\overline{C}_0$ ** (ppm)	Γ_a*** (μg/g)	Γ_a*** (μg/m^2)	$\overline{C}_0$ ** (ppm)	Γ_a*** (μg/g)	Γ_a*** (μg/m^2)
2/1	94.94	14.31	116	99.07	20.73	169
1/1	94.74	21.78	177	99.07	31.47	256
1/2	98.48	33.27	270	96.26	37.60	306
1/5	95.46	67.97	553	97.33	70.12	570

* Data are based on Table 6.2 and 6.3.

** $\overline{C}_0$ is the average bulk concentration around 100 ppm from various experiments (No. 6.1-6.7).

*** Γ_a is average adsorption level.

Table 6.5

The Effect of Ballotini Surface Properties on Xanthan Static Adsorption

Condition*	C_0 (ppm)	C_e (ppm)	Γ (μg/g)	Γ (μg/m^2)
100 g ballotini+50 ml brine for pre-age 6 days, then + 50 ml 200 ppm xanthan solution	99.20	78.38	20.82	169
100 g ballotini+100 ml 100 ppm xanthan solution	99.20	76.65	22.55	183

* The experimental time of static adsorption is 144 hours (6 days) and the experimental temperature is 23°C.

The results in this section demonstrate some factors which to some degree affect the xanthan adsorption level. It is clear that, at a given xanthan concentration, the most significant factor is the solid/liquid ratio. The following factors also have a small effect on xanthan adsorption onto ballotini: (i) the experimental pH change in a region of pH 7-11; (ii) the effect of salinity (0.1 g/l and 35 g/l NaCl); (iii) the small change of ballotini surface properties, such as pretreatment with diluted HCl and brine ageing; and (iv) the experimental temperature.

6.3 Adsorption Isotherm with Depleted Layer Effect

In this section, the adsorption isotherm in the presence of a depleted layer effect will be discussed. From the apparent decrease in relative depleted layer thickness, (δ/r), with C_p shown in Chapter 4, it seems that adsorption is reversible. Adsorption energy is thus expected to be low for this system: negatively charged xanthan on glass beads (negative and hydrated).

From this quasi-linear isotherm, we expect that the frontal velocity does not change with polymer concentration. More interestingly, reversible quasi-linear adsorption means that the concentration in the depleted layer is *higher* than that predicted from the purely repulsive case assumed by Chaveteau's two fluid flow model. Due to osmotic pressure effects, polymer concentration in depleted layer increases more than linearly with bulk concentration causing an increase of η_{rw} with C_p higher than predicted and this gives apparently a decrease in depleted layer thickness if the correct depleted layer model is taken. Chaveteau (private communication, 1992) simulated this behaviour by putting into the model a concentration in the depleted layer taking into account this reversible adsorption, but the thickness of this deplted layer should be different and smaller than δ. Note that, even in the case of adsorption, there is always a depletion layer above adsorbed layer so that the material balance must be written as:

$$LC_0 = (L - \delta S\sigma)C + \Gamma C\sigma \qquad [6.3]$$

where L is liquid volume; C_0 and C are the original and equilibrium (after adsorption) polymer concentrations respectively; δ, S, σ, and Γ have the meaning explained below Eq. [6.4]. We have extended Chaveteau's idea by taking account of the depleted layer polymer concentration, C_w. Fig. 6.4 illustrates schematically the molecular origin of polymer adsorption and surface exclusion effects. Using material balance,

$$\begin{aligned} LC_0 &= L_bC_e + L_{dl}C_w + \sigma S\Gamma \\ &= (L - \sigma S\delta)C_e + \sigma S\delta C_w + \sigma S\Gamma \end{aligned} \qquad [6.4]$$

where L, L_b, and L_{dl} are original, bulk (after adsorption), and depleted layer liquid volumes in vol. respectively, $L=L_b+L_{dl}$; C_0, C_e, and C_w are original, equilibrium (after adsorption), and depleted layer polymer concentrations in mass/vol. respectively; σ is specific surface area of solid (SSA) in area/mass; S is the solid mass; Γ is adsorption level in mass/area; and δ is the depleted layer thickness.

From Eq.[6.4], let $C_w = \alpha C_e$ (approximate linear relation):

$$LC_0 = \left[(L - \sigma S\delta) + \sigma S\delta\alpha\right]C_e + \sigma S\Gamma \qquad [6.5]$$

$$\therefore \quad \Gamma = \frac{LC_0 - [(L - \sigma S\delta) + \sigma S\delta\alpha]C_e}{\sigma S}$$

$$\begin{aligned} &= \frac{L}{\sigma S}(C_0 - C_e) + \delta(1-\alpha)C_e \\ &= \Gamma_a + \delta(1-\alpha)C_e \end{aligned} \qquad [6.6]$$

where Γ_a is apparent adsorption level or surface excess, and α is a constant.

Note that if no adsorption occurs, $\Gamma = 0$, the situation is back to two fluid flow model (need relation between C_w and C_e); If $\delta = 0$, $\Gamma = \Gamma_a = L(C_0 - C_e)/\sigma S$, which is the "normal" adsorption (surface excess) expression. This is similar to Chauveteau's suggestion (private communication, 1992) except that, there he assumed C_w=0 which

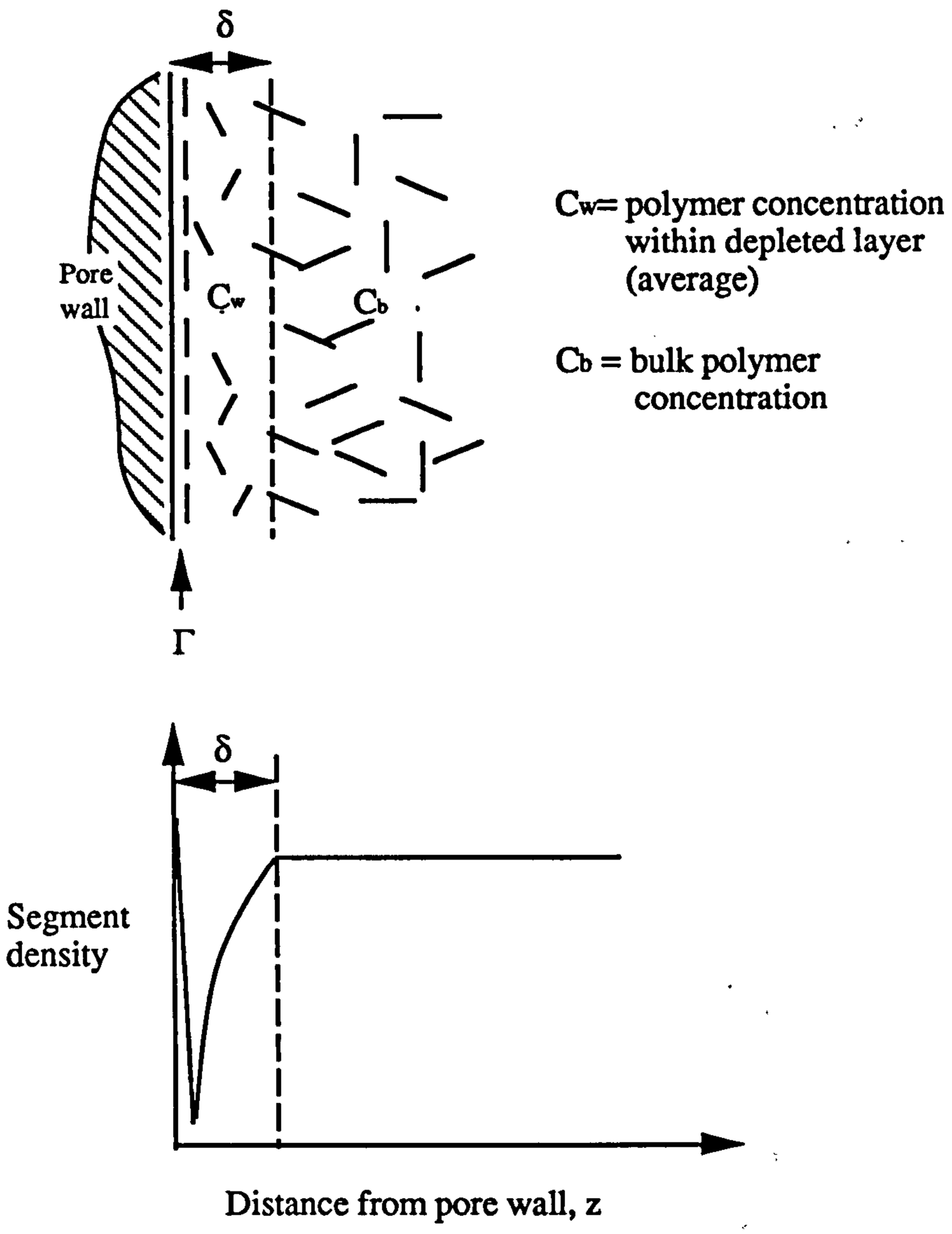

Figure 6.4 A schematical diagram of the molecular origin of polymer adsorption and surface exclusion effect

would mean $\alpha = 0$ in Eq. [6.6]. This model tells us that the "real" adsorbed amount Γ is greater than the "apparent" adsorbed amount, Γ_a. It is the latter quantity which we actually measure experimentally.

Fig 6.5 show some results of Γ calculated by using Eq.[6.6] assuming $\delta = 0.5\ \mu m = 5x10^{-5}$ cm and $\alpha = 0.64$ for which if we adopt $\delta = 0.95$ L (with L = end-to-end distance), then $C_w/C_e = \alpha = 0.64$ (Chauveteau et al., 1984), and compared to corresponding experimental Γ_a. The basic data come from Table 6.2 experimental No. 6.7. These results indicate that the effect of the depleted layer on the real adsorption level is not very important in which the total adsorption level increase about 3 to 6 %. But this difference is not negligible especially for very low apparent adsorption case in porous media (for example, at $\delta = 0.5\ \mu m$, $\alpha = 0.64$ and C = 100 ppm, $\Gamma - \Gamma_a = 18\ \mu g/m^2$ compared with 8 $\mu g/m^2$ at fast dynamic adsorption case shown in section 5.6 and Figure 5.15)

So far, the above discussion gives us no idea why the Γ_a depends on the solid/liquid ratio, S/L. Eq.[6.6], either with $\alpha = 0$ or $\alpha \neq 0$, gives a dependence of Γ_a on C_e, but no clear relation between Γ_a and S/L.

6.4 The Effect of Solid/Liquid Ratio on Xanthan Adsorption

Figure 6.6 shows examples of adsorption level with time for two solid/liquid ratios. The lower solid/liquid ratio case shows a clear higher adsorption level than the higher ratio. Rearranging the experimental data in Table 6.2 and 6.3, the plots of adsorption level vs 1/R (liquid/solid ratio) at 0.1 and 35 g/l NaCl are shown in Figures 6.7 and 6.8 respectively. The data of average adsorption level from Table 6.4 is plotted in Figure 6.9. It appears that there is a more linear relationship between Γ and 1/R in the relative high solid/liquid ratio regime (S/L > 0.2) for the given ~ 100 ppm xanthan solution. To explain the experimental results, we define a new quantity, the equivalent equilibrium concentration, C_{ee}, which represents the equilibrium polymer amount per unit solid weight (or surface area in fact) in $\mu g/g$ (ppm),

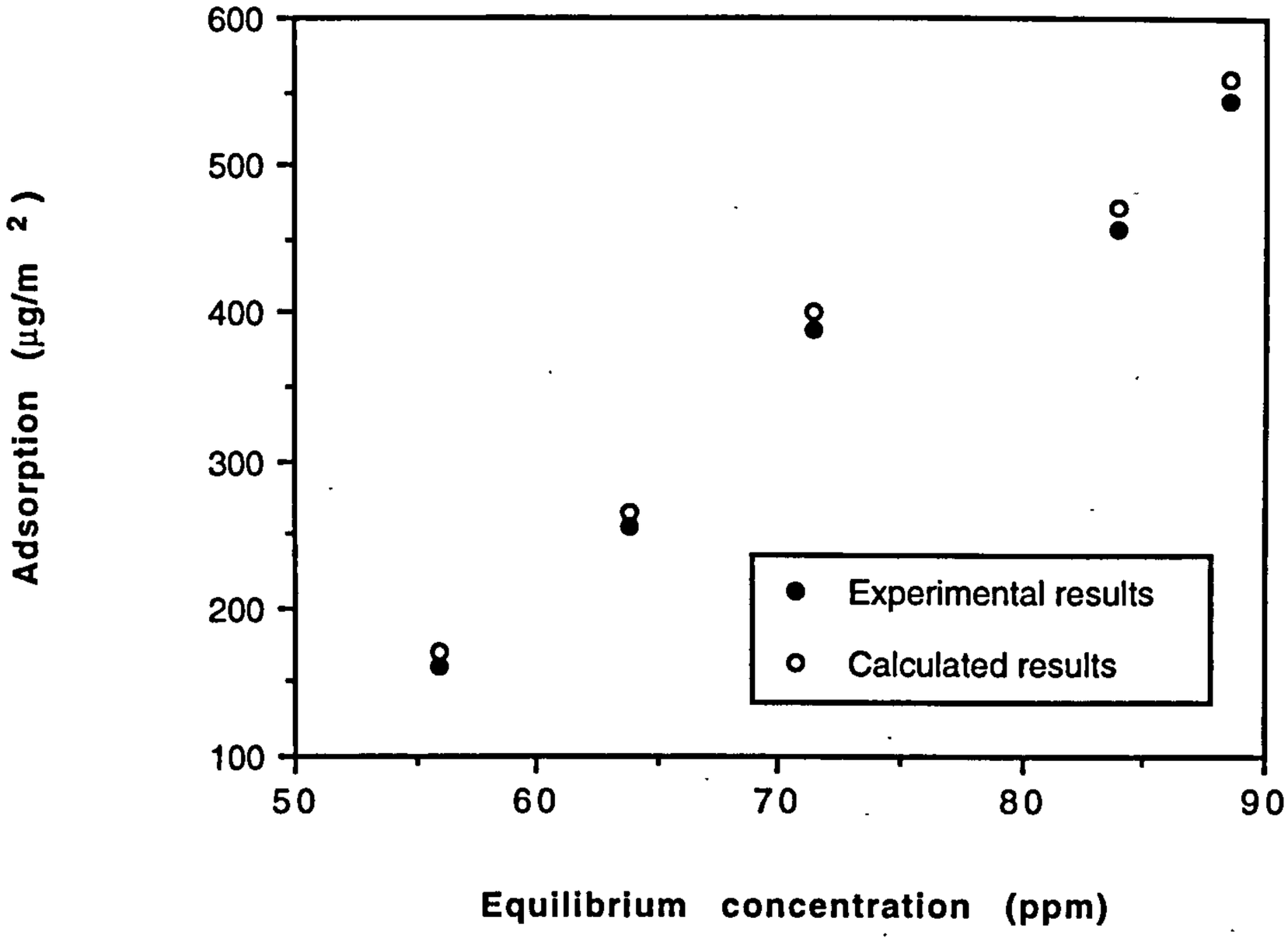

Figure 6.5 Depleted layer effect on adsorption - a comparison of experimental (No. 6.7, Table 6.2) and calculated (Eq.[6.6]) results

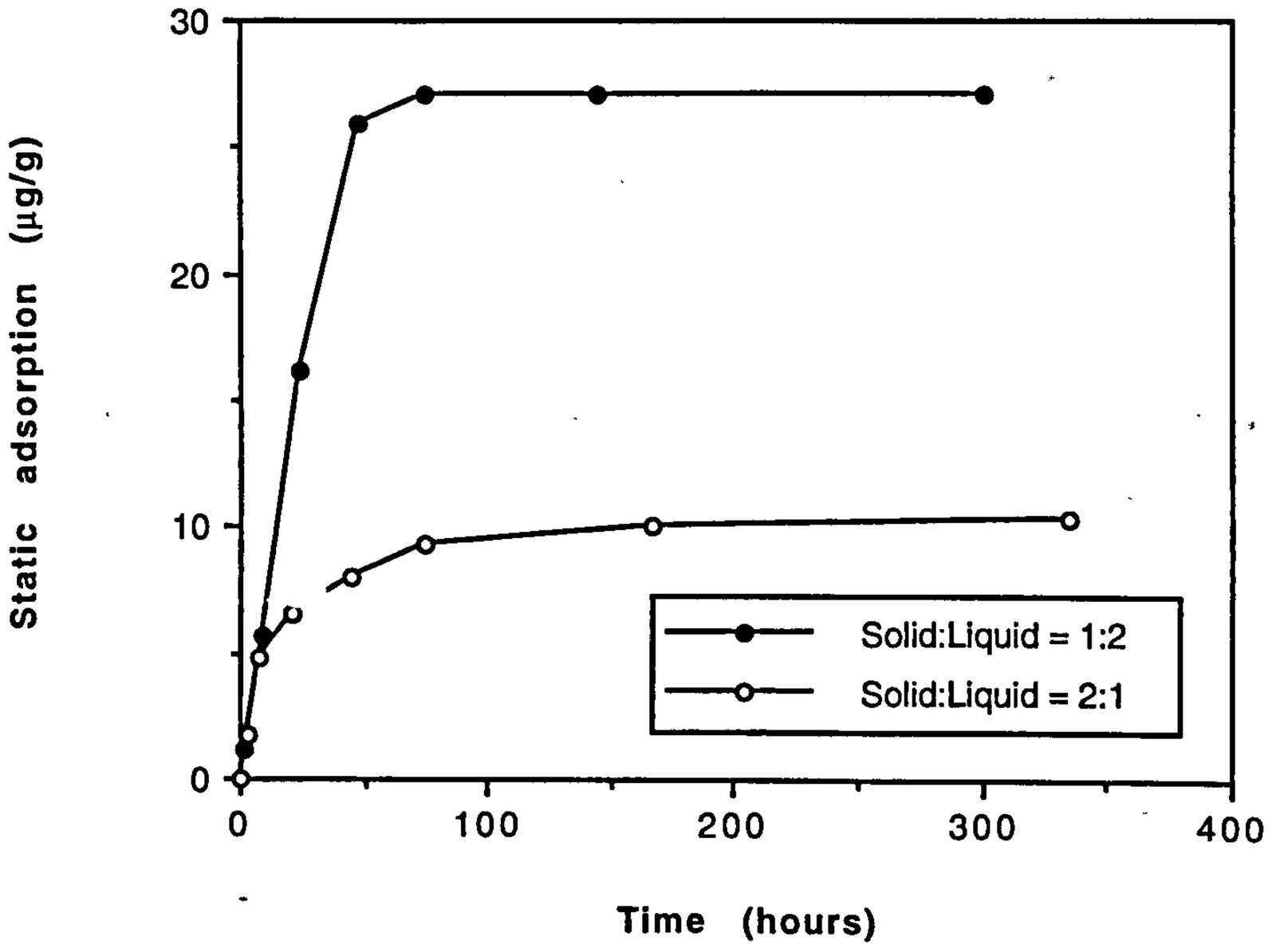

Figure 6.6 Adsorption isotherm of 100 ppm xanthan solution in 35 g/l NaCl with solid/liquid ratio 1/2 (Exp. 6.2) and 2/1 (Exp. 6.4) of Table 6.3

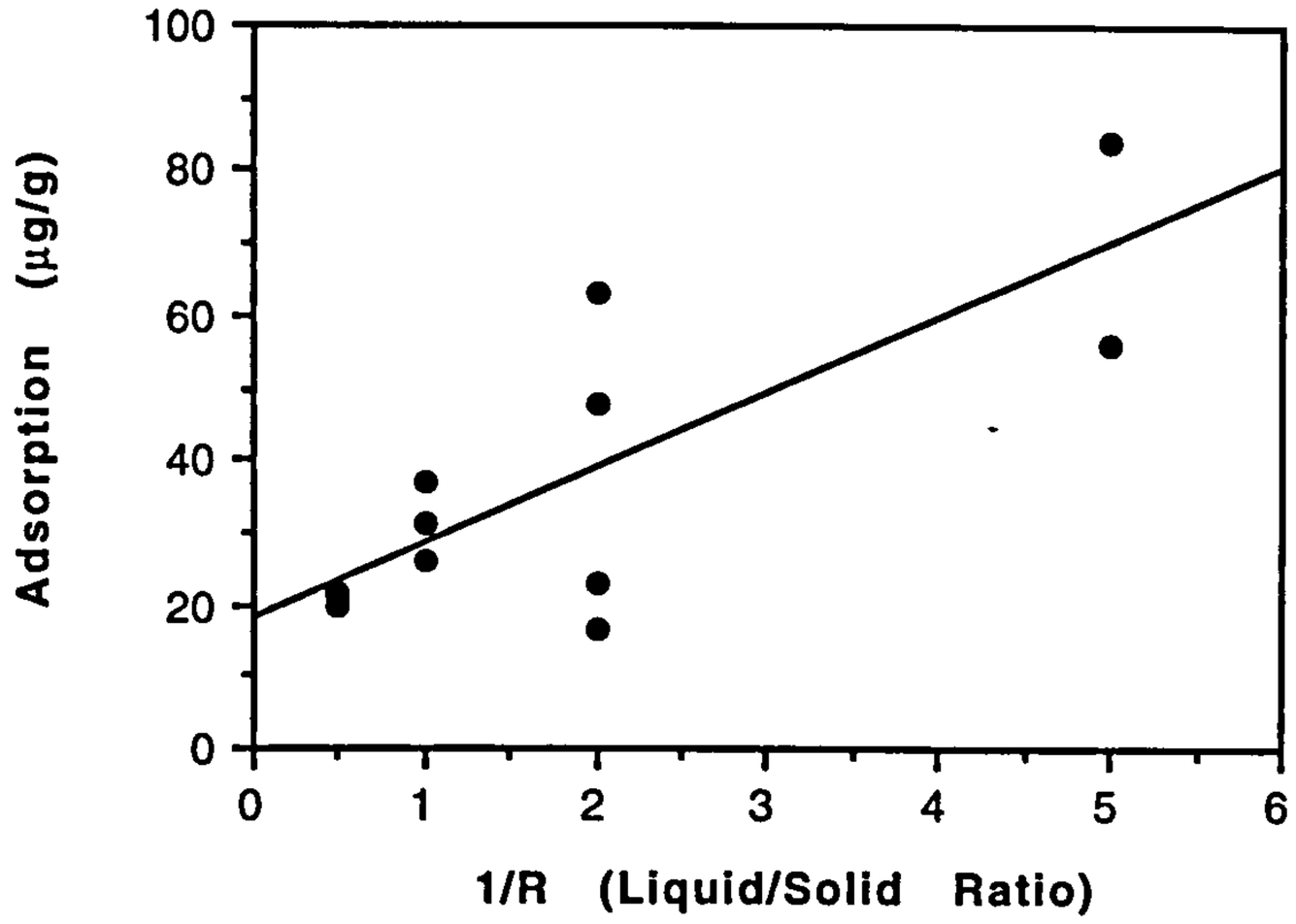

Figure 6.7 The static adsorption of 100 ppm xanthan in 0.1 g/l NaCl as a function of the reciprocal solid/liquid ratio, 1/R

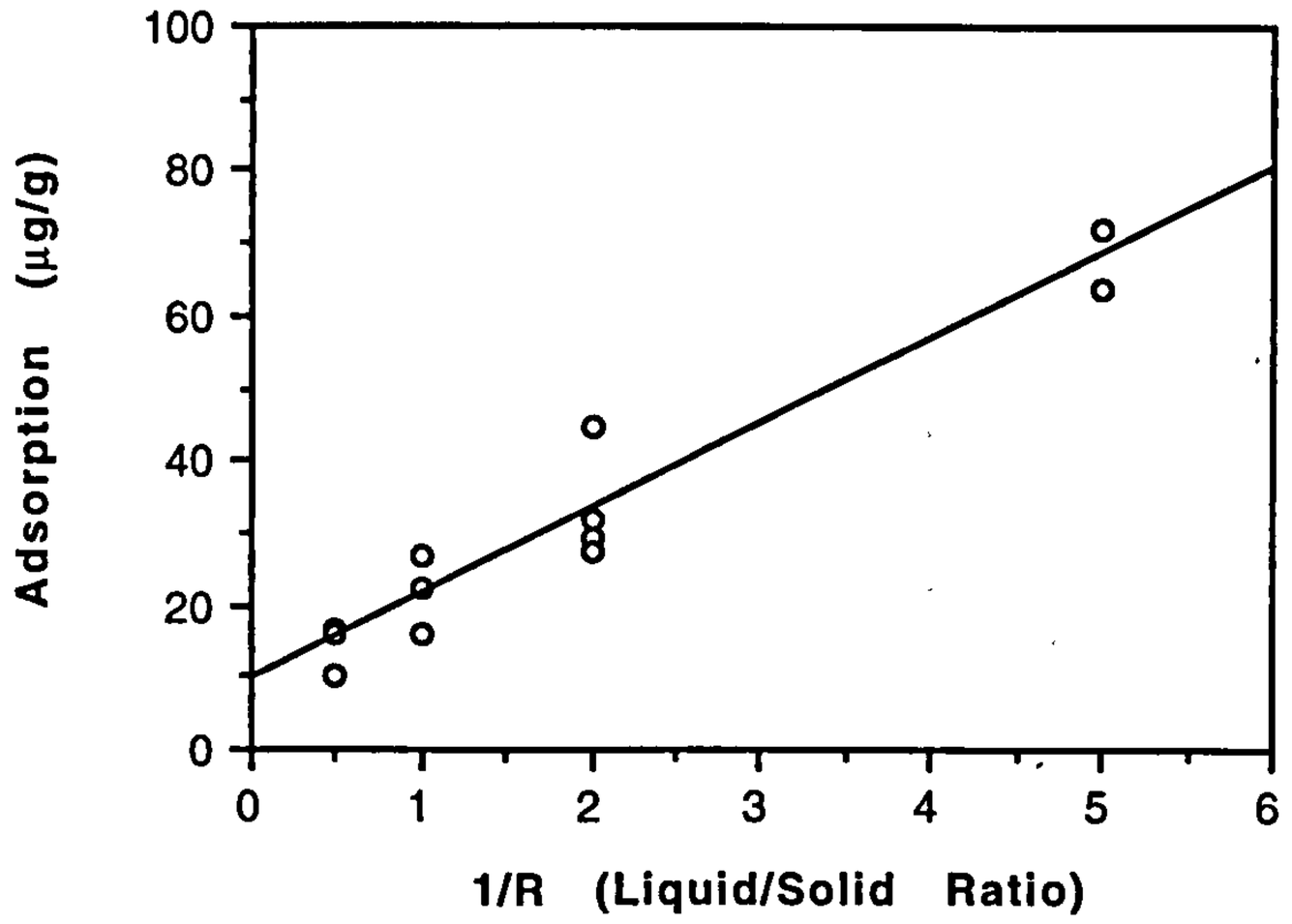

Figure 6.8 The static adsorption of 100 ppm xanthan in 35 g/l NaCl as a function of the reciprocal solid/liquid ratio, 1/R

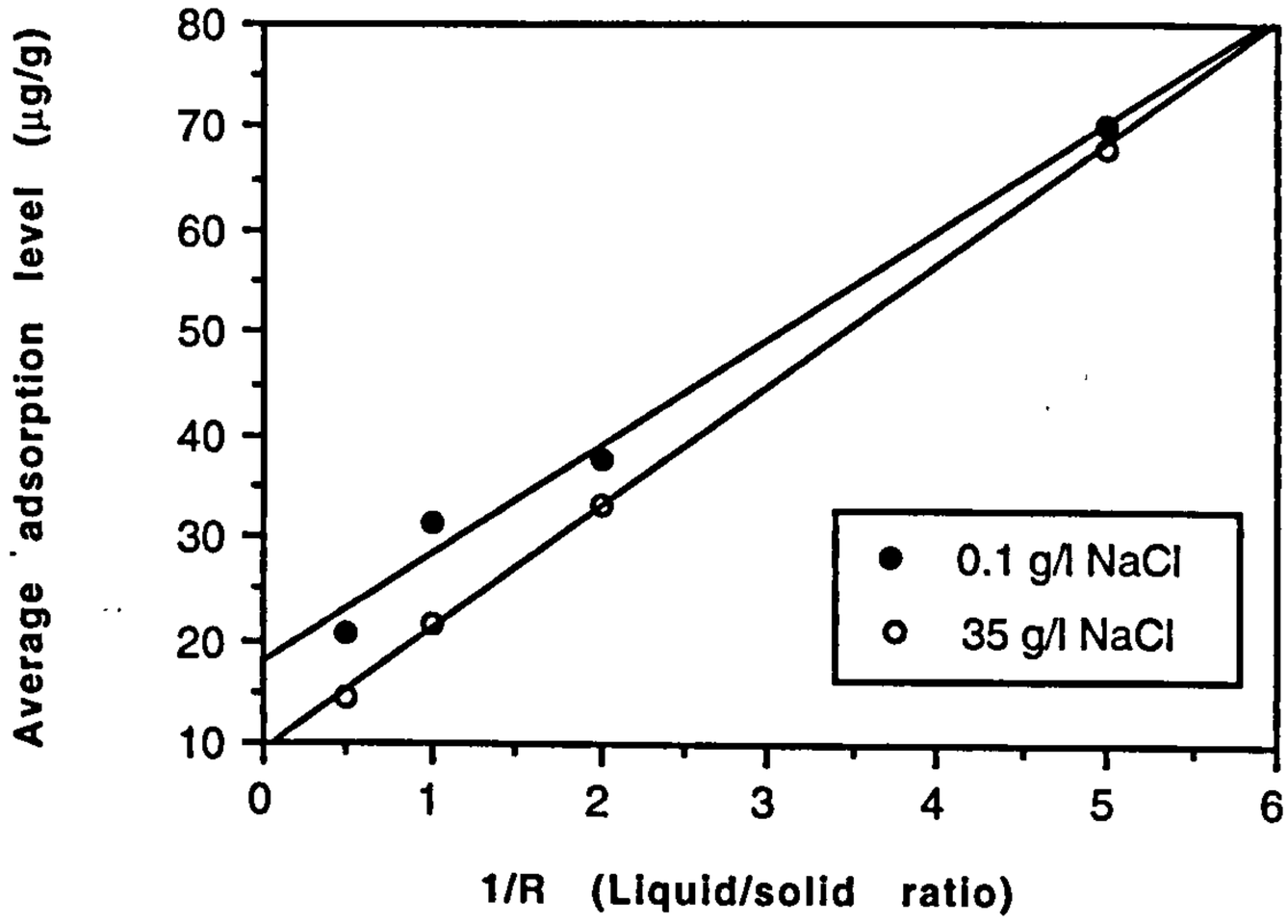

Figure 6.9 Average adsorption level of 100 ppm xanthan from Table 6.4 based on Experiment 6.1-6.7 as a function of liquid/solid ratio (1/R)

$$C_{ee} = C_e/R \qquad [6.7]$$

where C_e and R are equilibrium polymer concentration and Solid/liquid ratio respectively. Using the data of experiment No. 7 (Tables 6.2 and 6.3), a plot of Γ vs C_{ee} is shown in Figure 6.10. Fairly good Langmuir-type behaviour is displayed for both high and low salinity solutions. To confirm the effect of solid/liquid ratio, new results are shown in Table 6.6 which indicate further that with defferent initial concentration C_0 (50, 100, 200 ppm) but the same C_{ee} the total adsorption is almost the same.

Table 6.6

The Equivalence Equilibrium Concentration and Xanthan Adsorption

Solid/Liquid Ratio (g/ml)	C_0 (ppm)	C_e (ppm)	C_{ee} (ppm)	Γ ($\mu g/g$)	Γ ($\mu g/m^2$)
0.5	50.01	39.19	78.38	21.64	176
1	99.20	76.65	76.65	22.55	183
2	199.26	153.11	76.56	23.08	188

* The salinity of xanthan solution is 35 g/l NaCl and the experimental temperature is 23°C.

Table 6.7 and Figure 6.11 are sand-experiment results. A saturated adsorption is observed even at low concentration (50 ppm or 5 ppm at equilibrium concentration). Using sand, a fast adsorption equilibrium with concentration can be obtained. So the effects of concentration and liquid/solid ratio on xanthan adsorption are not very significant within experimental regime. The pH of final samples are much lower (the same original bulk pH about pH 5-6) than ballotini samples (about pH 9-11). The adsorption level is nearly the same in $\mu g/g$, but much higher in $\mu g/m^2$ than those of ballotini samples due to a low Specific Surface Area (SSA), 0.022 m^2/g, of sand, compared with 0.123 m^2/g of ballotini.

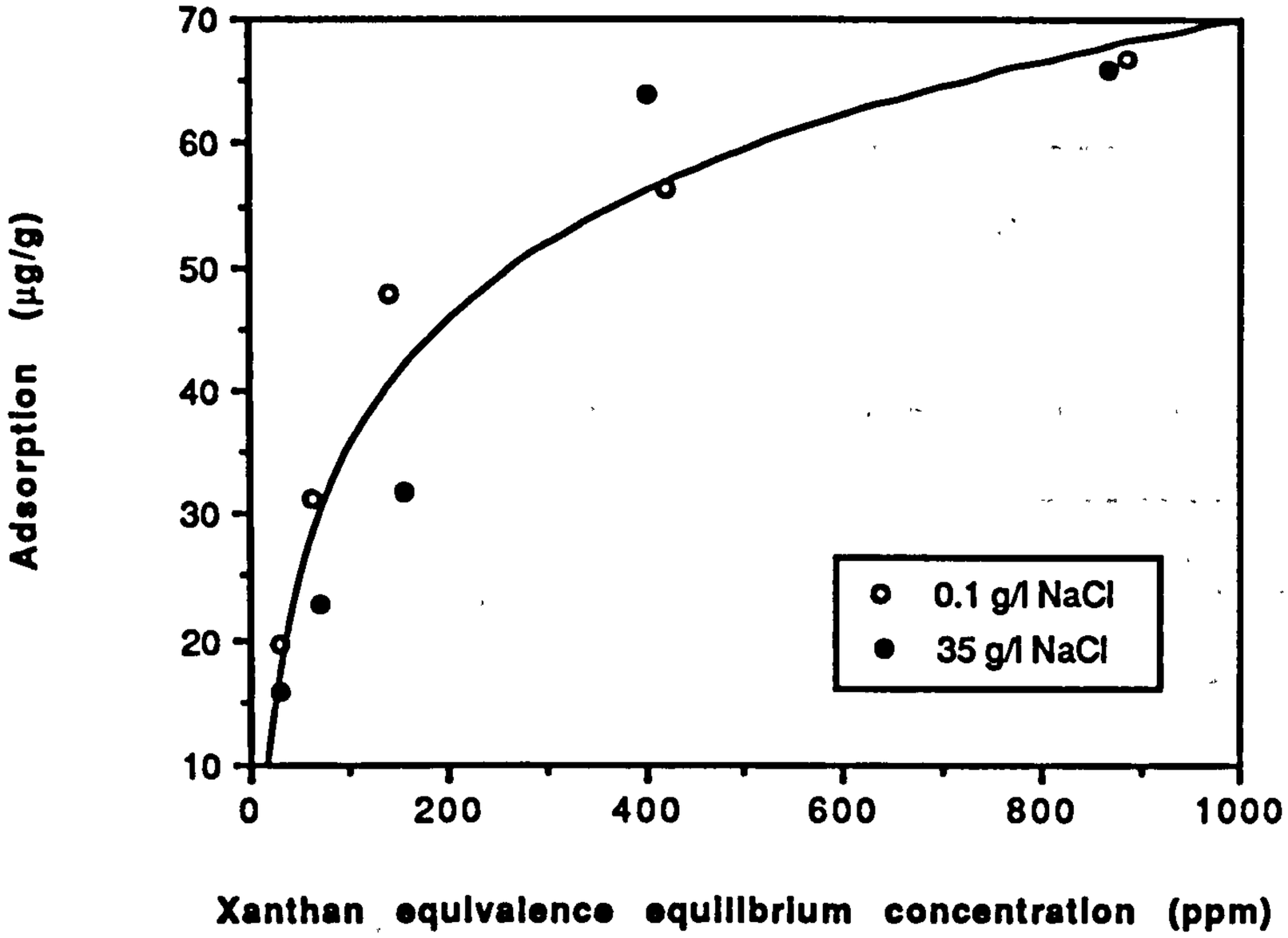

Figure 6.10 Xanthan static adsorption as a function of equivalence equilibrium concentration defined as Cee = Ce/R

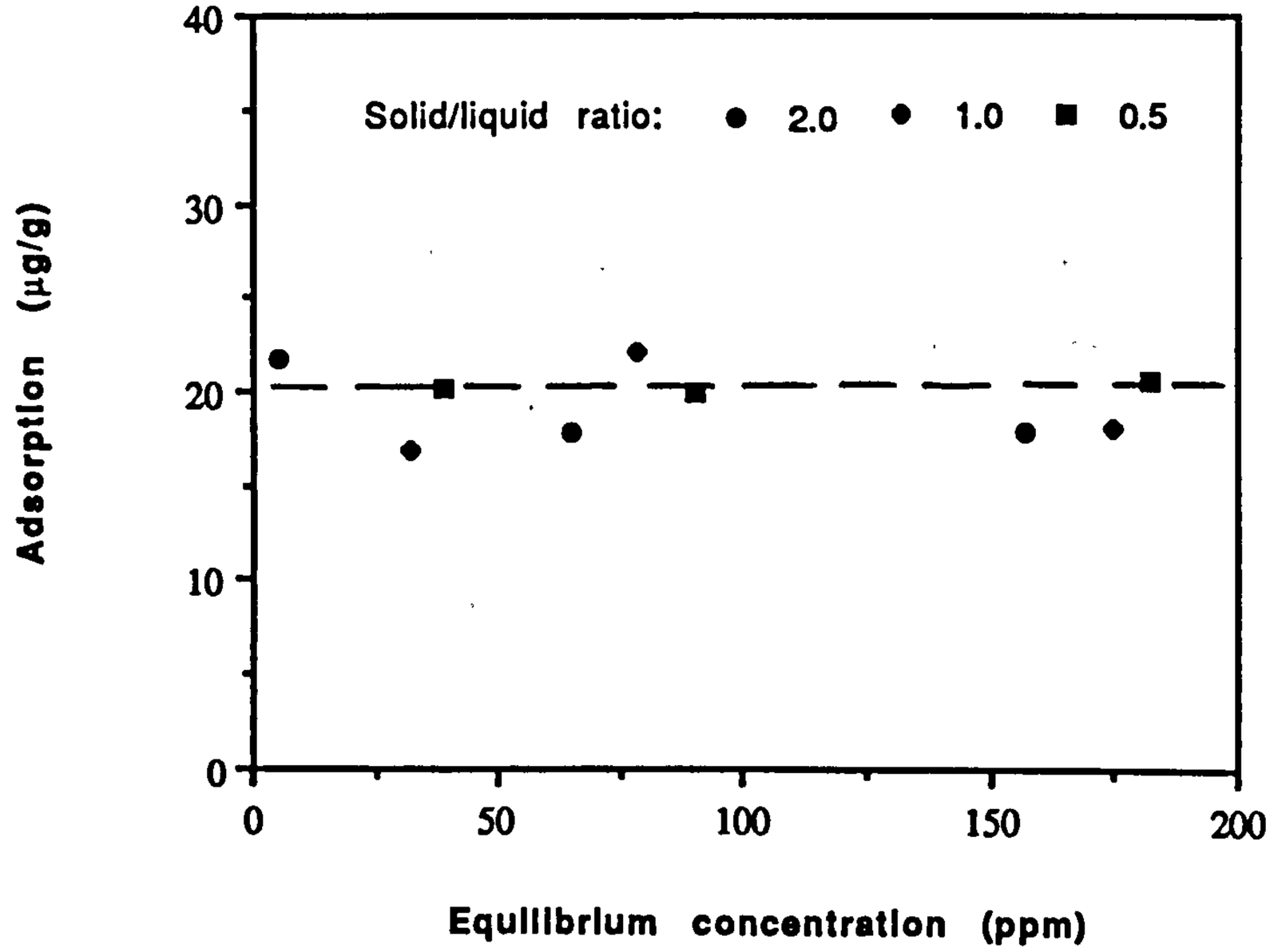

Figure 6.11 Xanthan adsorption as a function of equilibrium concentration in sand-0.1 g/l NaCl system

Table 6.7

Xanthan Static Adsorption onto the Surface of Sand*

R (solid/liquid) (g/ml)	C_0 (ppm)	C_e (ppm)	η_0 (cp)	η_e (cp)	Adsorption ($\mu g/g$)	($\mu g/m^2$)	pH
2	48.73	5.22	1.51	1.09	21.76	989	6.07
1	48.73	31.78	1.51	1.33	16.95	770	5.85
0.5	48.73	38.63	1.51	1.40	20.20	918	5.54
2	100.18	64.55	2.22	1.70	17.82	810	6.18
1	100.18	77.99	2.22	1.88	22.19	1009	4.97
0.5	100.18	90.20	2.22	2.06	19.97	908	5.45
2	192.42	156.70	4.43	3.39	17.86	812	5.78
1	192.42	174.38	4.43	3.87	18.04	820	5.23
0.5	192.42	182.09	4.43	4.10	20.67	940	5.23

* The salinity of xanthan solution is 0.1 g/l NaCl and the experimental temperature is 21°C.

These results of solid/liquid ratio are interesing, but remains to be explained. Chaveteau (private communication, 1992) proposed two models to interpret observed results on the effect of solid/liquid ratio and there are developed below:

A) Model A: Aggregation Limited Adsorption (ALA)

Since solid/liquid ratio values are high (the system is not dilute), there is considerable aggregation of beads in the adsorption batch, the size of which increases with S/L ratio. It is assumed that polymer adsorption occurs only at the periphery of aggregates as a first step, so that the amount of adsorption is proportional to the external surface of the

aggregates. In a second step, adsorption may occur progressively inside the aggregates with a very slow rate limited by diffusion inside the pores.

Such a model may be applied when polymer radius of gyration, R_G, is close or less than the pores inside the aggregates. Note that this interpretation of adsorption around aggregates is consistent not only with the S/L dependence, but also with the very slow kinetics, explainable by low diffusion through aggregates and with the fact that with large particles like sand, no S/L dependence is found since adsorption occurs inside aggregates. The problem is the particle size. They are really far too big (the mean size ~ 52 μm). It is very unlikely that exclusion could occur for the fractal structures formed by aggregating beads. Pefferkorn and Elaissari (1989; 1990) in their series of papers referred to very small particles of colloidal dimension which show this effect. However, if our ballotini samples are polydispersed, even a few of small size beads would probably change this conclusion. Figure 3.4 shows that small particles (such as less than 5 μm) is about 3.2% of total mass in which 66 % of them has a size < 1.0 μm.

Applying this idea, a correct value of adsorption might be obtained by extrapolation at S/L→0 at value around 66 μg/g (540 μg/m^2) for experiment 6.7, which is a large but acceptable value at 100 ppm. That experiment has been conducted at relative neutral pH (pH≈7 to 9). For experiment 6.6, the absence of an experimental point at S/L=0.1 prevents a reliable extrapolation. Chaveteau suggested that the higher adsorption level in experiment 6.6 could be related to dissolved species like Ca for the glass beads; sodacalcic glass is soluble at high pH≈10 to 11 which will be discussed in next section.

B) Model B: Collision Limited Adsorption (CLA)

When the particle diameter, a, is large compared with the polymer size, $2R_G$, so that aggregate pores remain larger than $2R_G$ and when adsorption is reversible (this is the case of our experiments with xanthan adsorbed on glass beads $2R_G \approx 1$ μm, a ≈ 50 μm),

adsorption can occur onto each bead. However a fraction, f, of the particle surface is not accessible during time of contact as shown schematically in Figure 6.12

For a given $2R_G$ and a, there is an inaccessible particle surface area (analogous to the concept of inaccessible volume), which is a function of $2R_G/a$ for close contact, i.e. in porous medium. While particles are mixed in the batch, it can approximate for instance in a cubic lattice:

$$\frac{S}{\rho L} = \frac{a^3}{(a+x)^3 - a^3}$$

$$= \frac{a^2}{3a^2x + 3ax^2 + x^3} \qquad [6.8]$$

Thus

$$x \propto \left(\frac{S}{L}\right)^{-1}, \text{ for } x << a$$

Since there is no adsorption during the time of collision (i. e. when $x < 2R_G$) and assuming pure repulsion between particles, no lubrication, etc, at high S/L, Γ/Γ_0 tends to

$$\frac{\Gamma}{\Gamma_0} \propto \frac{\alpha a}{2R_G}\left(\frac{S}{L}\right)^{-1} \qquad [6.9]$$

Γ_0 is the full adsorption value and α is a geometric factor which can be calculated for simple geometries and can be determined experimentally.

The model B seems more suitable for our experiments on xanthan adsorption onto ballotini, but model A could be used for smaller particles. Note that, for spheres, the excluded surface for adsorption due to collision is much higher than that for sharp-edged particles like sand. In addition, the sand particle size is larger. Thus the collision limited surface could be at least 10 times higher for the ballotini glass beads than for sand, and

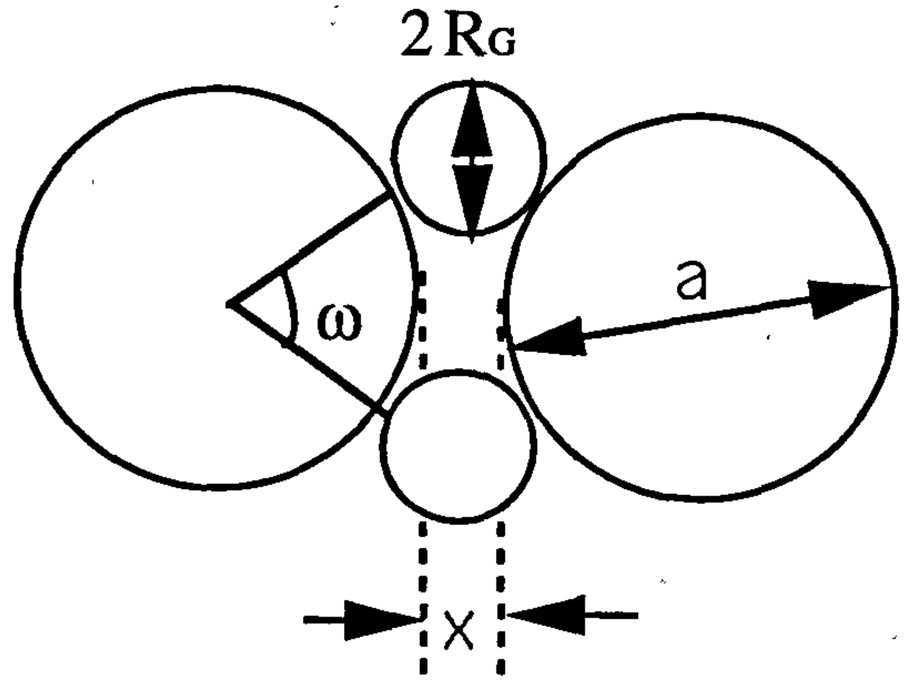

$$\begin{cases} f \propto \omega^2 \\ \omega = f(R_G / a,\ x) \\ x = 0 \end{cases}$$

Figure 6.12 Schematical diagram of collision limited adsorption model, for $2R_G / a << 1$, $\omega^2 \propto 2R_G / a$, and $x = 0$, at close packing or porous medium case: $S / L \approx 4.5$

thus the adsence of visible solid/liquid ratio effect in the adsorption tests using sand is not a fully convincing argument for ruling out the relevance of the CLA model for explaining our results. Also, extrapolation from the batch to the porous medium case is possible with this model and the value of α expected from calculation can be compared to experimental results. However, a doubtful point still remains for the CLA model. The accumulation of ballotini particles (which have a high density of 2.65 g/cm^3) is more independent of the solid/liquid ratio than that of a colloid system. Therefore, the bead particle collision should tend to a constant even if we do not consider the effect of regularly shaking the samples. The CLA model should better explain the reason for the very low adsorption level in packed system (i.e. porous medium) in which there is a high solid/liquid ratio (4.5:1) and a fixed closed pack.

6.5 The Effect of the Dissolved Species on Xanthan Adsorption

Chaveteau's ALA and CLA models are useful for explaining the effect of solid/liquid ratio on xanthan adsorption. But some questions still remain. The main doubtful points are (i) the very slow adsorption kinetics as shown in Figure 6.1, (ii) the relative high adsorption level of unpretreatedballotini, and (iii) the adsorption increases with pH, while adsorption is expected to decrease with pH increasing. We here considered the effect of potential dissolved species from the bead surface.

Reviewing the experimental results in Sections 6.2 and 6.4, ballotini glass beads with and without pretreatment by diluted HCl were used in xanthan static adsorption experiments (see Tables 6.2 and 6.3: Exp. No. 6.6 and 6.7 respectively). The pH values of the supernatant fluids markedly increase to pH 8-10 for ballotini with pretreatment, and pH 10-11 for cases without pretreatment, compared with the pH values of 5-6 for the original xanthan solution. We find that xanthan shows a lower adsorption level onto the pretreated ballotini than onto the natural untreated ballotini. Also, it indicates a small effect of S/L by using pretreated ballotini compared to using natural ballotini shown in

Figure 6.13. The result found by using pretreated sand clearly indicates no pH change and no S/L effect as shown in Table 6.7.

This behaviour could possibly be related to the effect of dissolved species like silica or calcium from the surface of the ballotini. Figure 6.14 is a schematic diagram showing the origin of the polymer adsorption due to the dissolved species effect. Those dissolved species form new nucleating centres for adsorbed polymer molecules. To prove this idea, an experiment was performed, which was also suggested by Chauveteau (private communication, 1992) at almost the same time. Firstly, the natural ballotini was soaked in 0.1 g/l NaCl brine with S/L ratio 1:1, then the supernatant fluid was withdrawn and filtrated using filter paper. Secondly, 200 ppm xanthan solution was mixed with equivolume supernatant and brine respectively. Viscosities of both samples were measured later. Figure 6.15 shows the results of this esperiment. It appears that some xanthan has been lost from solution. We propose that it has been adsorbed onto the small dissolved particles now in solution. Note that these particles show adsorption and exclusion effects as shown schematically in Figure 6.16.

A dissolved species model (DSM) is proposed to explain the results. The same treament as mentioned in Section 6.3 is used in this section. From material balance, the DSM gives the following (see Figure 6.16):

$$LC_0 = (L - \sigma S\delta)C_e + \sigma S\delta C_w + \sigma S\Gamma + \sigma' S'\delta' C_w' + \sigma' S'\Gamma' \qquad [6.10]$$

where superscript ′ means corresponding dissolved colloidal species, and all of the symbols have the same meanings as in Eq. [6.4].

First we simplify by making $C_w = 0$ (largest effect of depleted layer possible), then

$$LC_0 = (L - \sigma S\delta)C_e + \sigma S\Gamma + \sigma' S'\Gamma' \qquad [6.11]$$

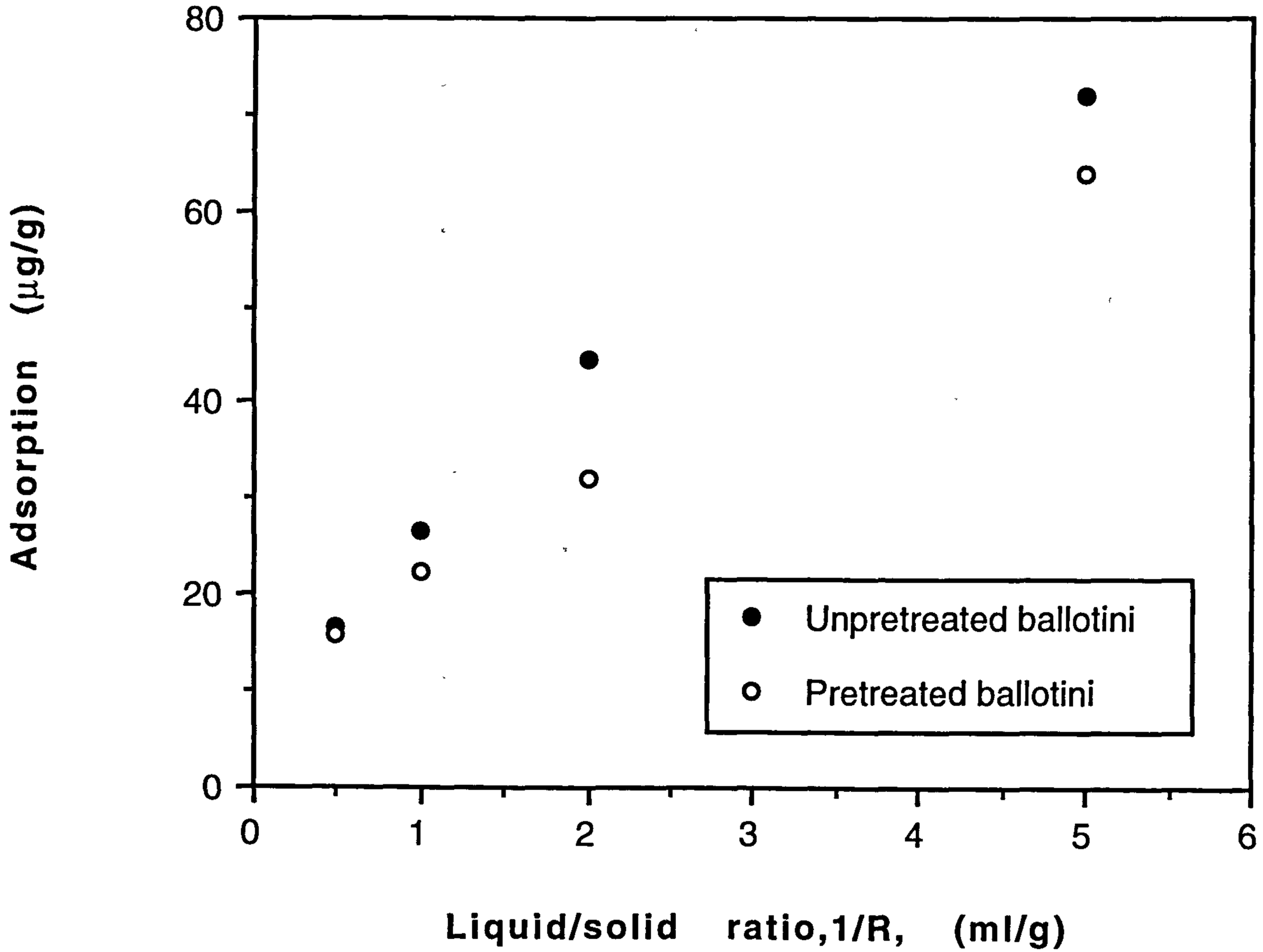

Figure 6.13 A comparison of solid/liquid ratio effect on adsorption using unpretreated or pretreated ballotini

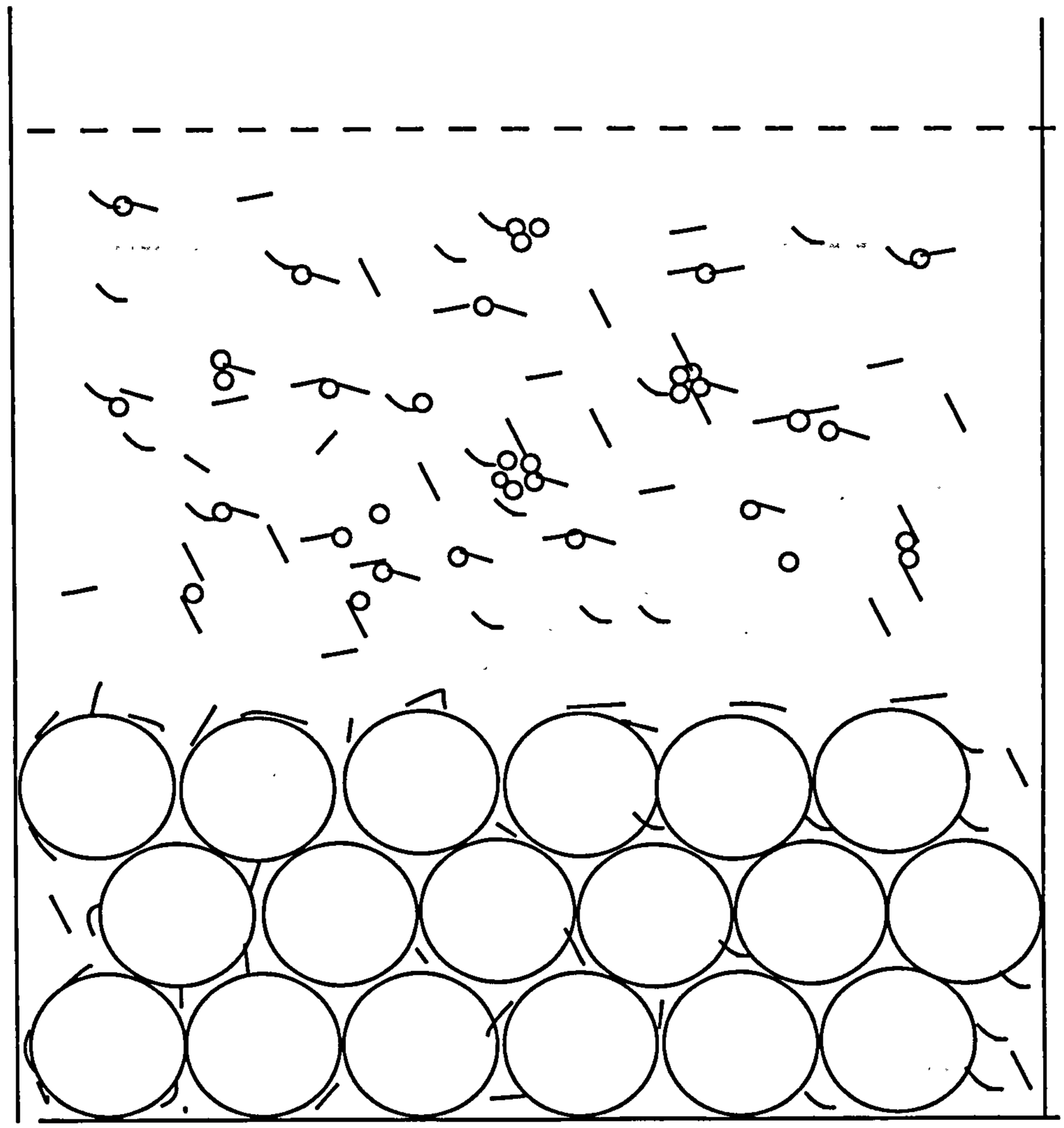

Ballotini glass beads

Dissolved species of balloniti

Xanthan biopolymer molecules

Figure 6.14 A schematic diagram of the polymer adsorption origin due to the dissolved species effect

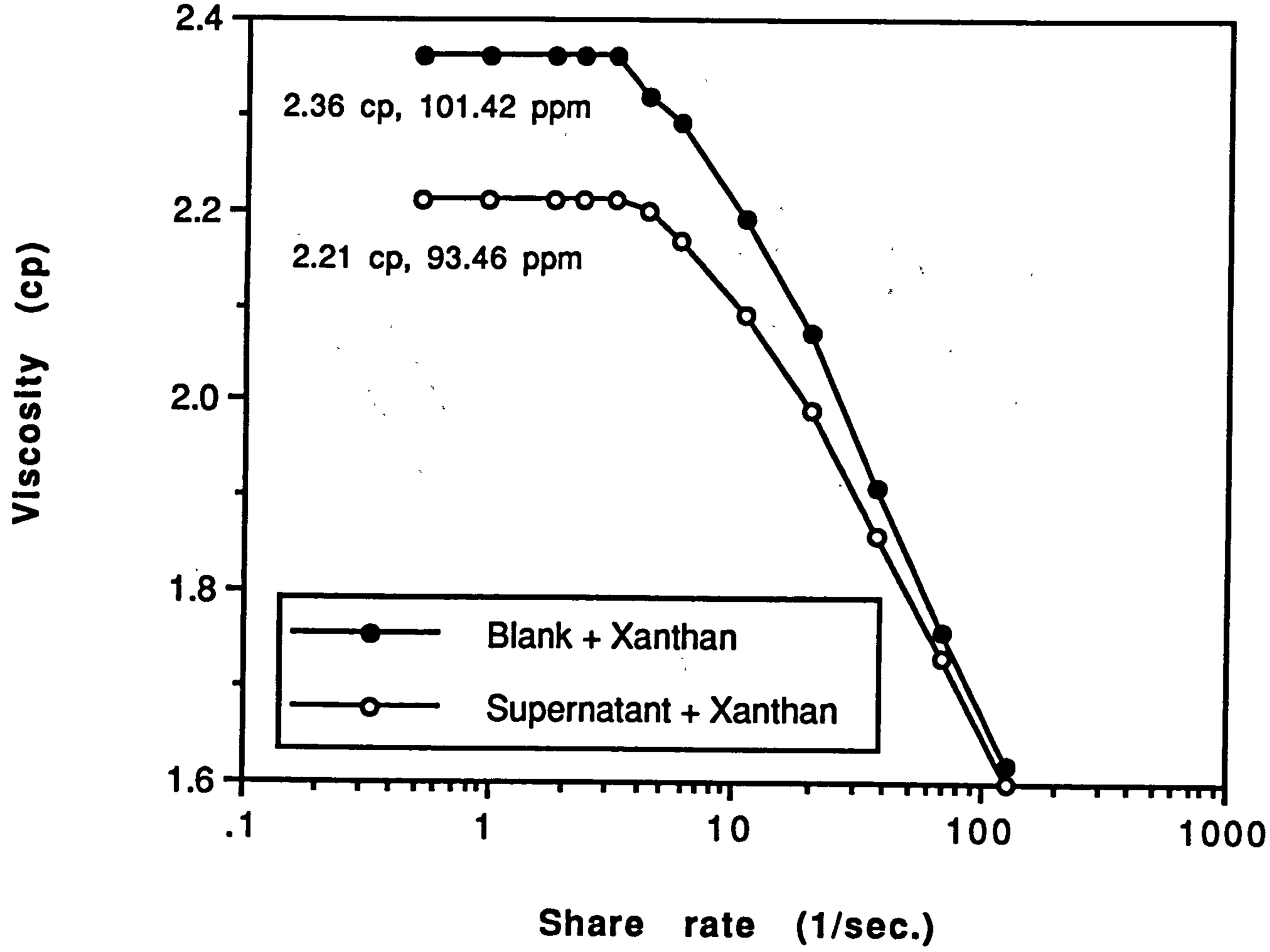

Figure 6.15 Dissolved species effect on viscosity reduction of 100 ppm xanthan in 0.1 g/l NaCl solution

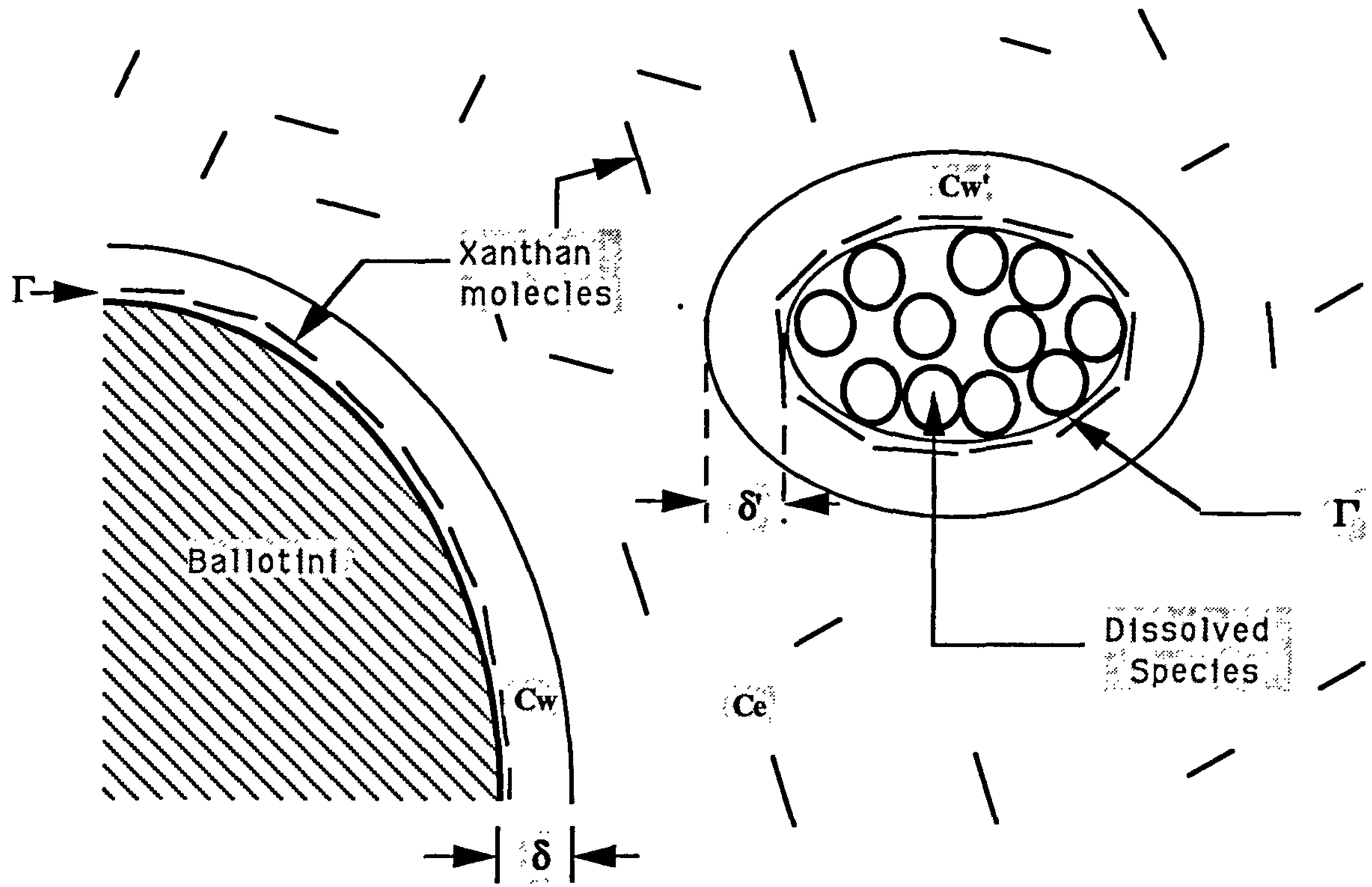

Figure 6.16 Schematical diagram of xanthan adsorption an surface exclusion effects at the presence of dissolved species

and therefore

$$LC_0 = (L - \sigma S\delta)CLC_0 = \Gamma = \frac{L}{\sigma S}(C_0 - C_e) + \delta C_e - \frac{\sigma' S' \Gamma'}{\sigma S} \qquad [6.12]$$

Suppose S' = $C_{cs}L$, where C_{cs} is concentration or solubility of dissolved colloidal species in mass/vol. and fixed i. e. independent on solid/liquid ratio (which is possible; from Table 6.2 and 6.3, the pHs have only small changes with S/L for each experiment generally). This gives:

$$\Gamma = \frac{L}{\sigma S}(C_0 - C_e) + \delta C_e - \left(\frac{L}{S}\right)\left(\frac{\sigma' C_{cs}}{\sigma}\right)\Gamma' \qquad [6.13]$$

Assuming that $\Gamma' = \Gamma$, we obtain:

$$\Gamma = \Gamma_a + \delta C_e - \frac{L}{S}\left(\frac{\sigma' C_{cs}}{\sigma}\right)\Gamma \qquad [6.14a]$$

$$\therefore \quad \Gamma_a = \left[1 + \left(\frac{L}{S}\right)\xi\right]\Gamma - \delta C_e \qquad [6.14b]$$

where $\xi = \frac{\sigma' C_{cs}}{\sigma} =$ constant.

But we might expect: $\Gamma = \beta C_e$, which leads to:

$$\Gamma_a = \left(1 + \frac{L}{S}\xi\right)\beta C_e - \delta C_e$$

$$= \left[\beta - \delta + \xi\beta\left(\frac{L}{S}\right)\right]C_e \qquad [6.15]$$

which we can write as:

$$\Gamma_a = \kappa_1\left[1 + \kappa_2\left(\frac{L}{S}\right)\right]C_e \qquad [6.16]$$

where $\kappa_1 = \beta - \delta$, and $\kappa_2 = \frac{\xi\beta}{\beta - \delta}$ are constants.

Assuming the form of Eq. [6.16], the data from Experiments 6.6 and 6.7 (Table 6.2 and 6.3) are plotted in Figures 6.17 and 6.18. There is a reasonably good straight line fit for the relative high S/L ratio (i.e. L/S<2) cases. At low S/L ratio (L/S>2), Γ_a/C_e tends to reach a maximum amount and the curves of Γ_a/C_e vs L/S displays a plateau which implies that Γ_a is independent of solid/liquid ratio. Clearly, as we can see from the raw data, the effect of S/L is larger in unpretreated ballotini than for pretreated ballotini. This is as we would expect for our DS Model where more particulates may be present. A small effect of salinity can also be see in Figure 6.18.

The result is fairly clear. Dissolved species decrease viscosity, thus leading to underestimation of polymer concentration. This explains why the adsorption seemed to increase as pH increases, a result clearly opposite to that expected and why the adsorption kinetics also seemed to be so slow. We are not full convinced about the dissolved species model (DSM), but it is the only one which is both plausible and gives a reasonable S/L dependence for Γ_a.

A possible empirical generalisation of Eq. [6.16] might be

$$\Gamma_a = \kappa_1\left[1 + \kappa_2\left(\frac{L}{S}\right)^{\kappa_3}\right]C_e \qquad [6.17]$$

where κ_3 might be related to the aggregates of dissolved species. But there is no rigourous justification of Eq.[6.17] at this moment. Also when we fit such a case, the results do not look significantly better.

In order to get more information from the effect of dissolved species on viscosity, a series new experiments were carried out in exactly the same way mentioned above. The particles were mixed with brine at a given solid/liquid ratio and then the supernatant was mixed

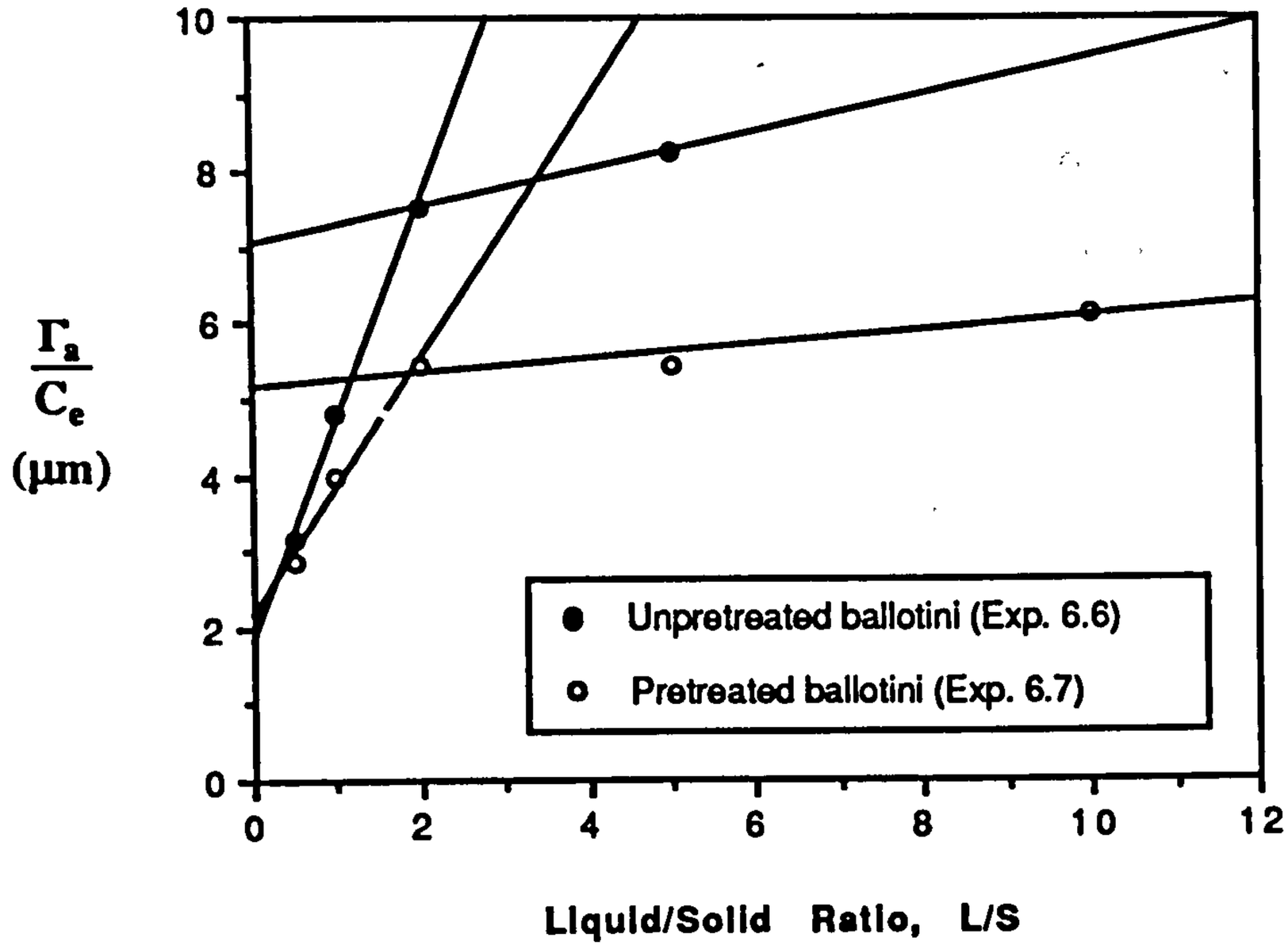

Figure 6.17 Γ_a / C_e as a function of liquid / solid ratio, 1 / R, defined in Eq. [6.16] in 100 ppm xanthan - 0.1 g / l NaCl system based on data of No.6.6 and 6.7 in Table 6.2

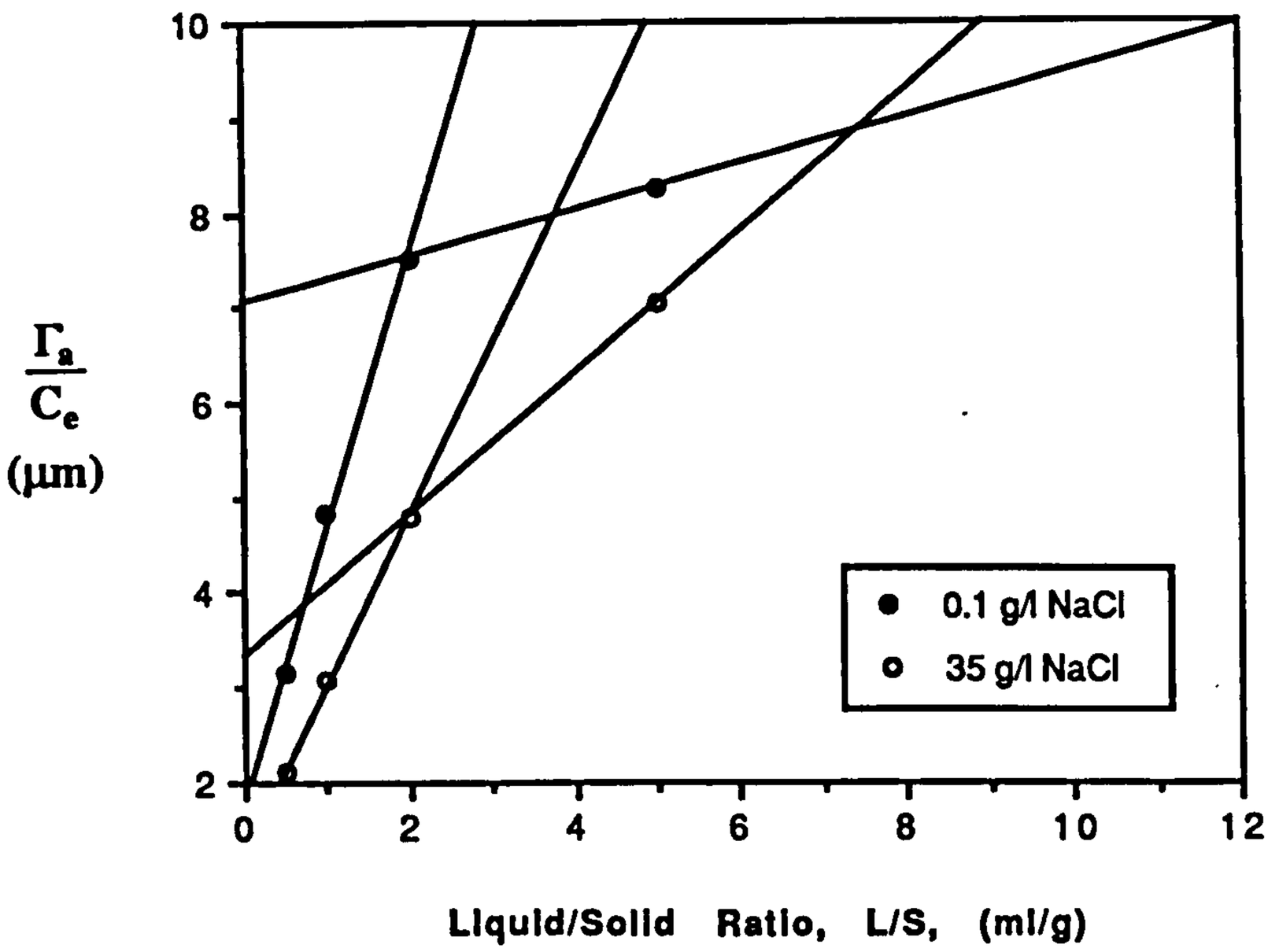

Figure 6.18 Γ_a / C_e as a function of L / S (liquid / solid ratio) in 100 ppm xanthan - unpretreated ballotini system

with polymer solution in the ratio 1:1 in volume. The results are shown in Figure 6.19 and Table 6.8. Some conclusions are clearly obtained. The apparent solid/liquid ratio is obtained by a simple calculation. For example, ballotini/brine ratio is 1/1 in g/ml, and then the withdrawn supernatant is mixed with polymer solution in an equivalent volume. Thus, the final solid/liquid ratio is referred to as 1/2 in g/ml. Comparing samples with each other in Table 6.8, demonstrates that (1) the dissolved species reduce the bulk viscosity for more or less all of the experimental systems; (2) the supernatant from unpretreated ballotini displays a more significant effect than that from pretreated ballotini because unpretreated ballotini may produce more dissolved species; (3) solid/liquid ratio has less (in proportion to) effect on viscosity reduction. Thus, converserly, it demonstrates a significant influence on the estimated adsorption level; (4) the effect of dissolved species for sand is less important than is shown in ballotini.

Table 6.8

The Effect of Dissolved Species on Xanthan Adsorption

Samp. No.	Supernatant	η_0 (cp)	η_e (cp)	C_0-C_e (ppm)	Γ_{app}* (μg/g)	S/L (app)
1	pretreatedballotini: brine, 1:1 (pH 8.55)	2.28	2.14	7.68	15.36	1:2
2	unpretreatedballotini: brine, 1:1 (pH 10.57)	2.28	2.06	12.29	24.58	1:2
3	unpretreatedballotini: brine, 1:5 (pH 9.41)	2.28	2.17	6.00	60.0	1:10
4	pretreated sand: brine, 1:1 (pH 6.02)	2.28	2.24	2.06	4.12	1:2
5	Blank brine (pH 6.50)	2.28	2.28	0.00	-	-

* $\Gamma_{app} = (C_0\text{-}C_e)/(S/L)_{app}$

The last issue is to determine, after correction due to the effect of dissolved species on viscosity, if there is any adsorption on glass beads. The answer might be obtained from a comparison of old and new experimental results as shown in Table 6.9. It seems that the contribution of dissolved species on total apparent adsorption level is 30-40 % for ballotini glass beads, and 20 % for sand. Chaveteau (private communication, 1992)

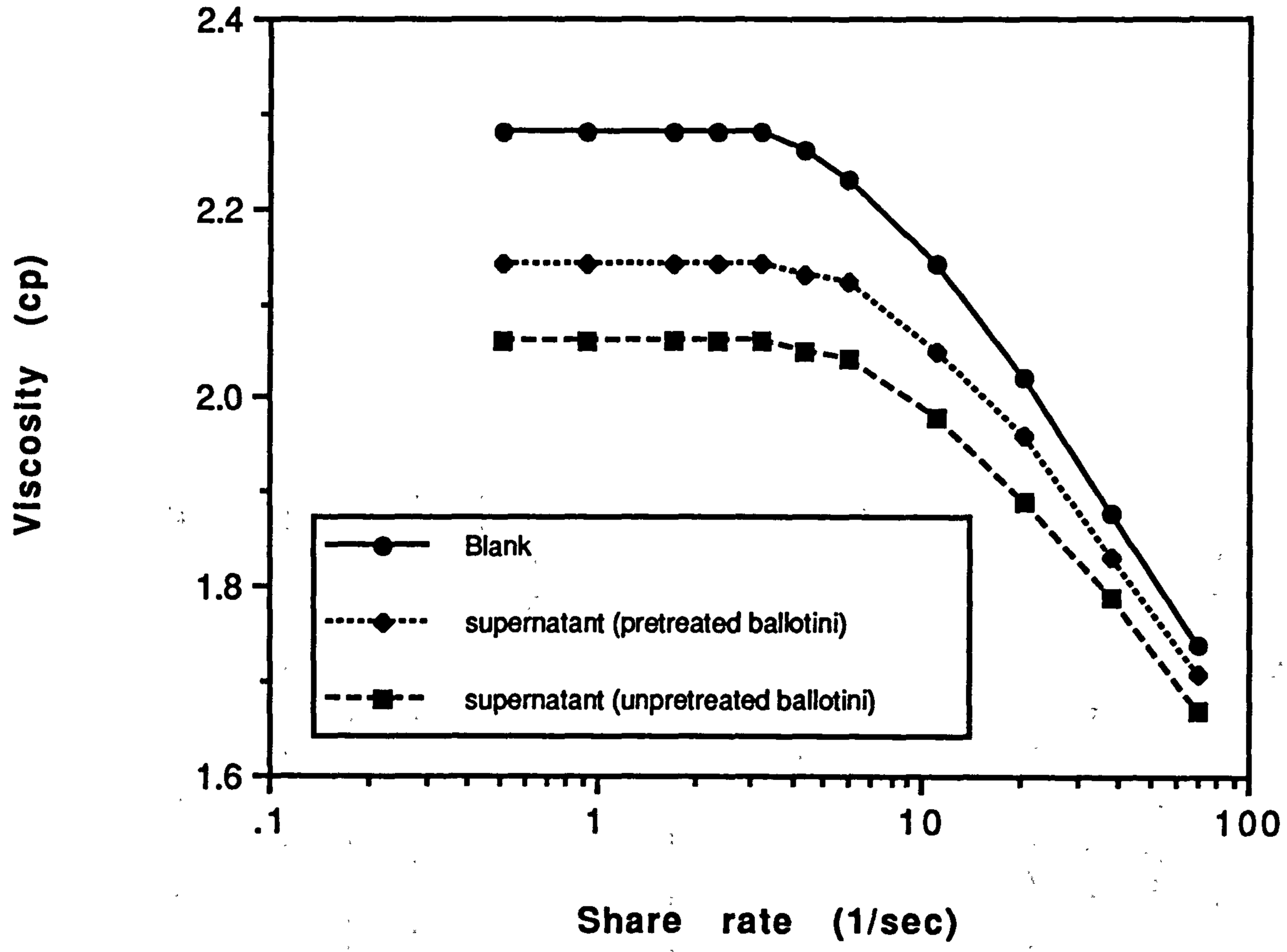

Figure 6.19 Viscosity reduction of 100 ppm xanthan solution (35 g/l NaCl) in supernatant of unpre- and pre-treated ballotini

thought that there is no xanthan loss but only a decrease in viscosity in this process because any dissolved species has no chance to reprecipitate, if pH is not decreased. If there were any substantial precipitate, the solution would be turbid which is not observed in our experiments. In Chaveteau's opinion, the dissolved species are more likely to be calcium (which reduces viscosity) than pure silica. Otherwise, the same effect should be found on sand; in addition, silica dissolution does not affect pH substantially. However, from the new experimental results shown in Tables 6.8 and 6.9, the dissolved species effect has really been observed without a pH effect on the sand. Also, we added CO_2 (by blowing) into the supernatant and observed no any turbidity ($CaCO_3$). It seems that at least part of the dissolved species results from the colloidal silica or more possible from the fine quartz.

Table 6.9
A Comparison of Adsorption Level due to Dissolved Species Effect and Total Adsorption Level

Particles	S/L Ratio	Γ' (dissolved species)	Γ (Total)	Γ'/Γ (%)
Pretreated ballotini	1/2	15.36	47.72	32
Unpretreated ballotini	1/2	24.58	62.92	39
Pretreated sand	1/2	4.12	19.97	21

Finally, we would like to mention potential chemical aspects of solid/liquid ratio effect on static adsorption levels. It is possible that some kind of chemical adsorption happens, especially considering the slow changes of the adsorption level with time. The potential ionic exchange between polymer molecules and the surface of the glass beads also depends on the solid/liquid ratio (which at least has been proved by author¢s earlier work in China on the effect of solid/liquid ratio on alkaline consumption level). Other possibilies include the existence of any kind of polymer aggregates or complexes although we are not sure about this at the moment. These posibilies make this work much more

complex and more difficult to interpret unambiguously. We suggest that future work should tackle this difficult issue of the chemical characterisation of this system.

6.6 Xanthan Dynamic Adsorption in Porous Media

Generally, there are three main retention mechanisms when polymer solutions flow through porous media including polymer adsorption, mechanical entrapment, and hydrodynamic retention. In these experiments, xanthan adsorption is the only important cause of polymer retention because of the higher permeability (1.1-1.2 Darcy) and relative homogeneity of the ballotini glass packed column. Here the total viscosity loss is still considered as adsorption (or apparent adsorption) for easy of discussion even the presence of potential dissolved species effect since the interest of oilfield operations mainly focuses on fluid viscosity (or mobility).

For the high flow case, the effluent profiles for 100 ppm xanthan solution and lithium tracer have already been shown in Figure 5.11 to 5.14 in Chapter 5. These results tend to indicate that the level of adsorption within the porous medium is very low. Using material balance as shown in Figure 6.20, the amount of xanthan adsorption has been calculated in the pack floods and this is shown in Figure 6.21 (also see Figure 5.15). Very low adsorption levels of about 1 $\mu g/g$ (8 $\mu g/m^2$) have been found for all the values of salinity used in the original floods where the flow rate is 160 $\mu l/min$ (9.7×10^{-3} cm/s) and the total flooding time is within one day.

To examine the full adsorption of xanthan (or full viscosity loss) in porous media, a series of new experiments were performed in which, after full breakthrough of polymer, the flood column was shut in for 5 days. The pack was then reopened to continued polymer flooding followed, after a few PV of polymer solution, by a water postflush. Some typical polymer effluent profiles of 100 ppm xanthan in 0.1 to 35 g/l NaCl solutions are presented in Figures 6.22 to 6.24 and additional polymer adsorption results are shown in Table 6.10.

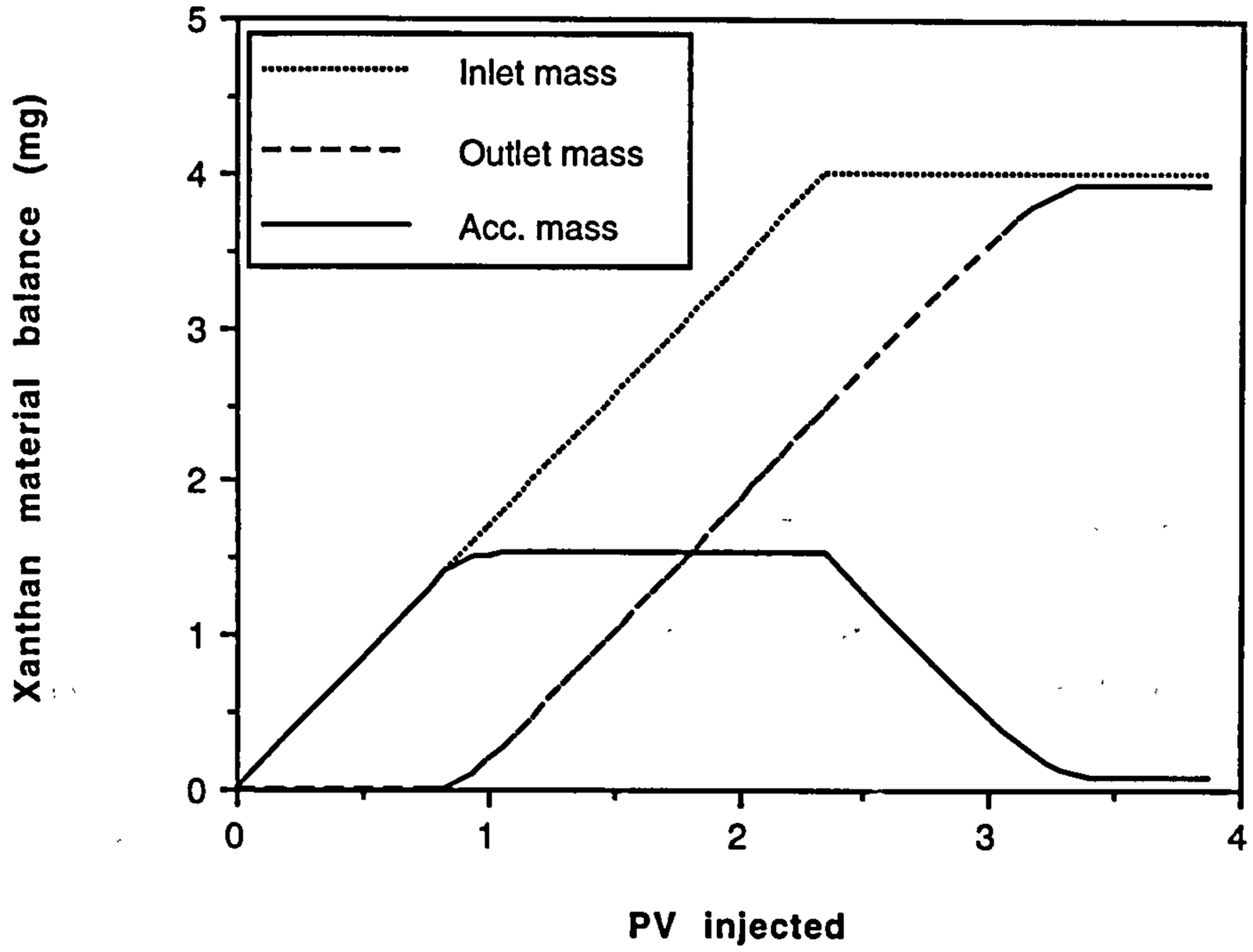

Figure 6.20 The material balance of xanthan in 35 g/l NaCl brine flowing through porous medium (reference Fig. 5.14)

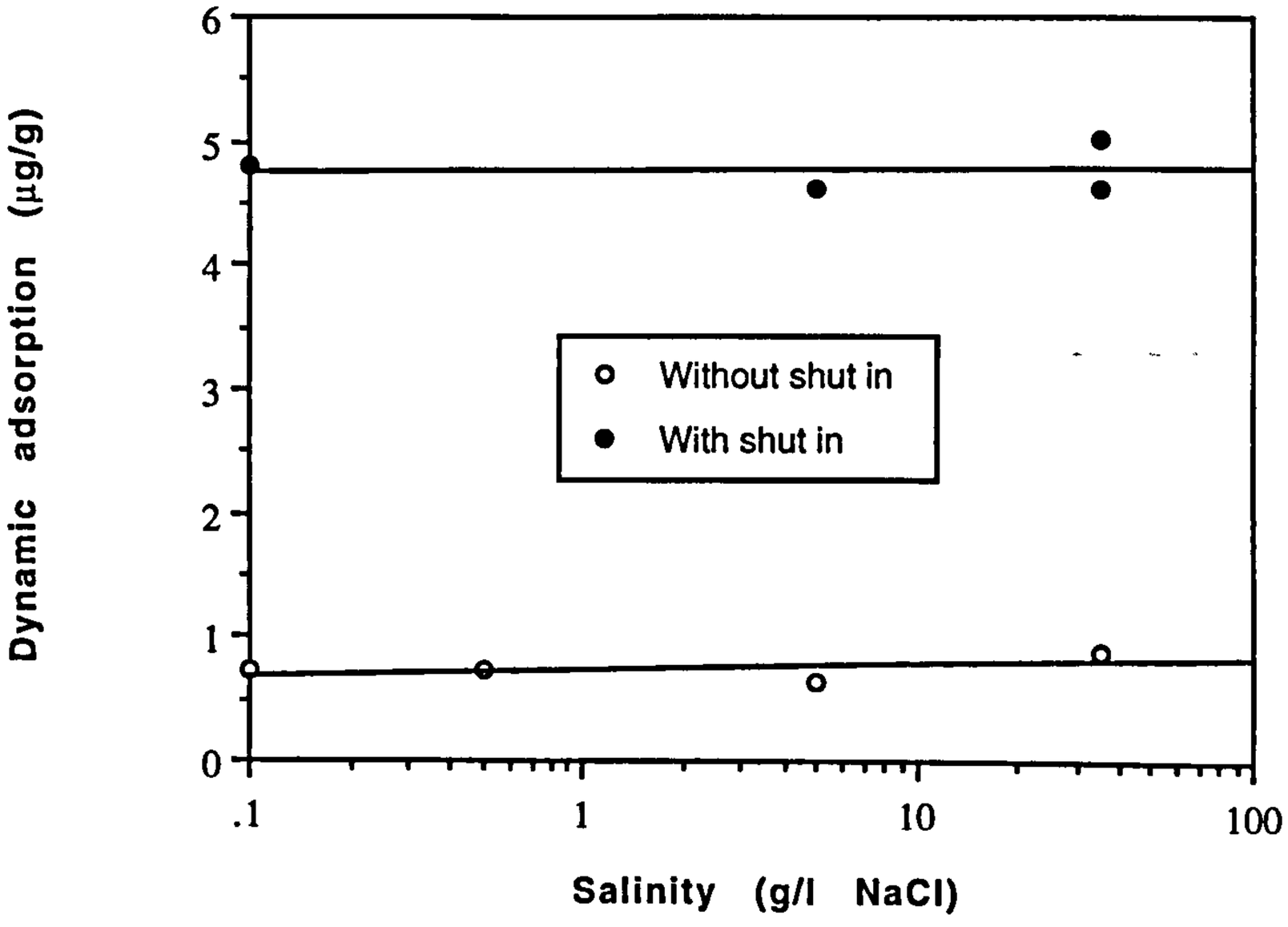

Figure 6.21 A comparison of 100 ppm xanthan dynamic adsorption in porous media with and without a core shut-in

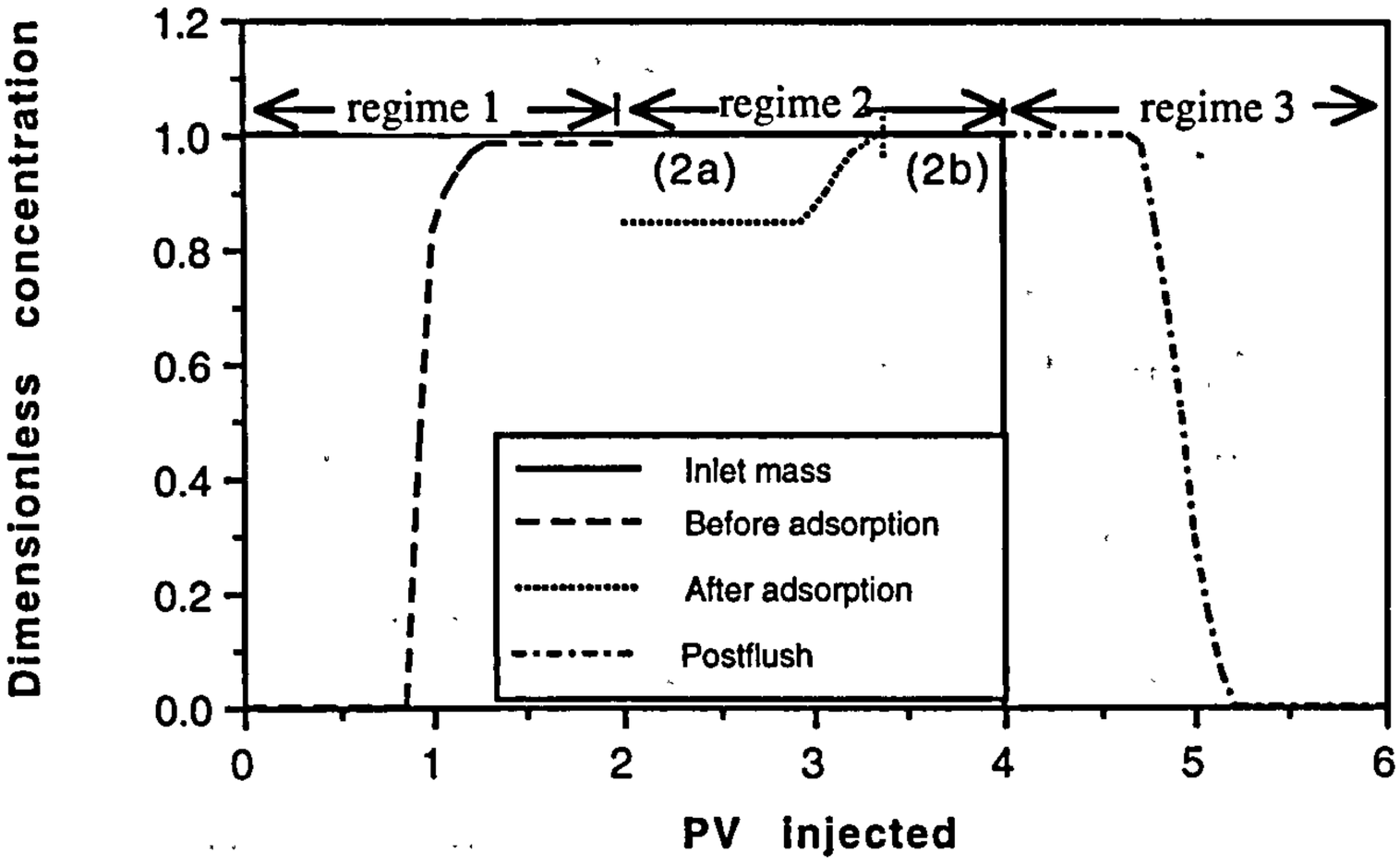

Figure 6.22 Plot of effluent concentration vs PV injected for 100 ppm xanthan solution at o.1 g/l NaCl salinity with a shut-in

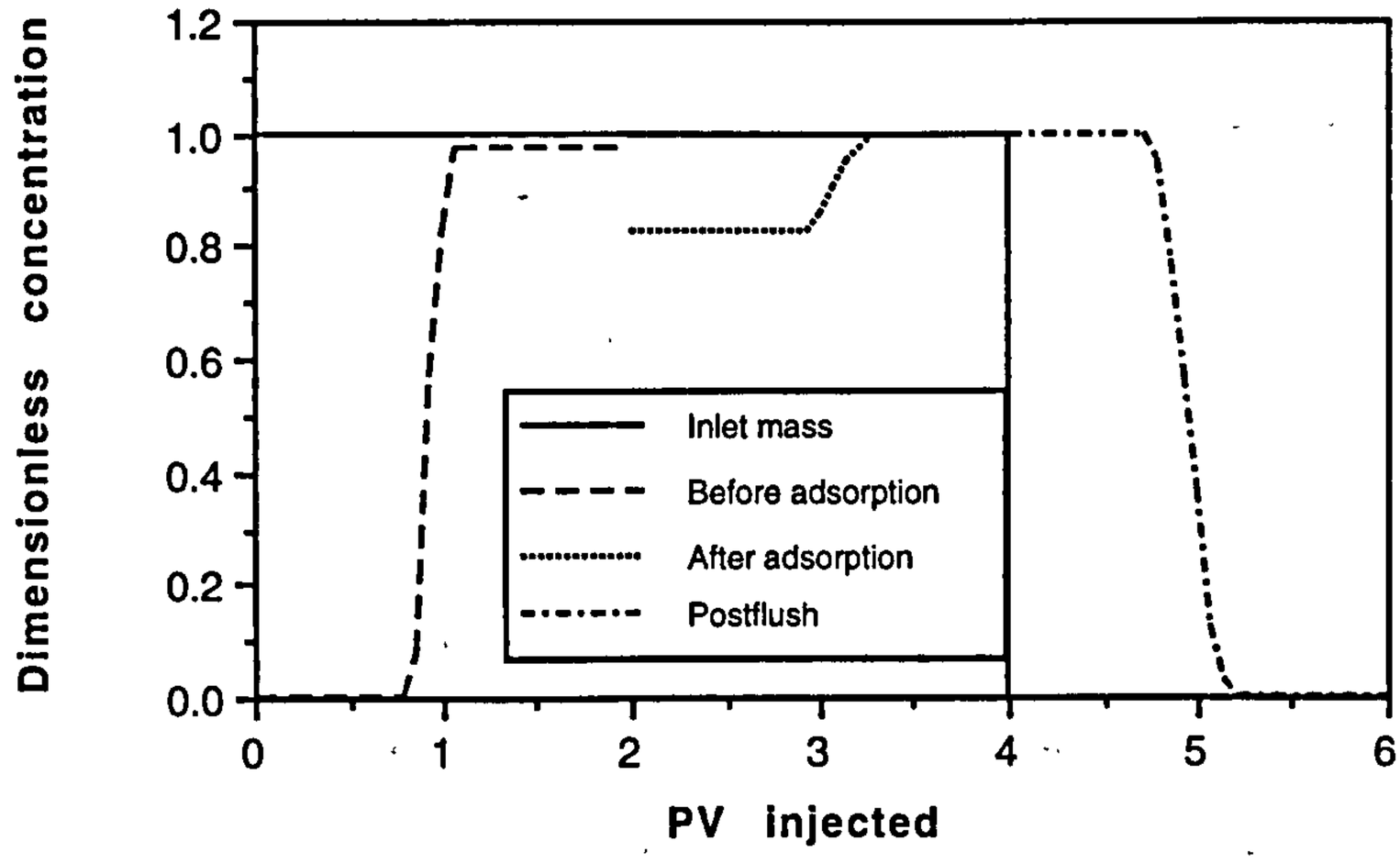

Figure 6.23 Plot of effluent concentration vs PV injected for 100 ppm xanthan solution at 5.0 g/l NaCl salinity with a shut-in

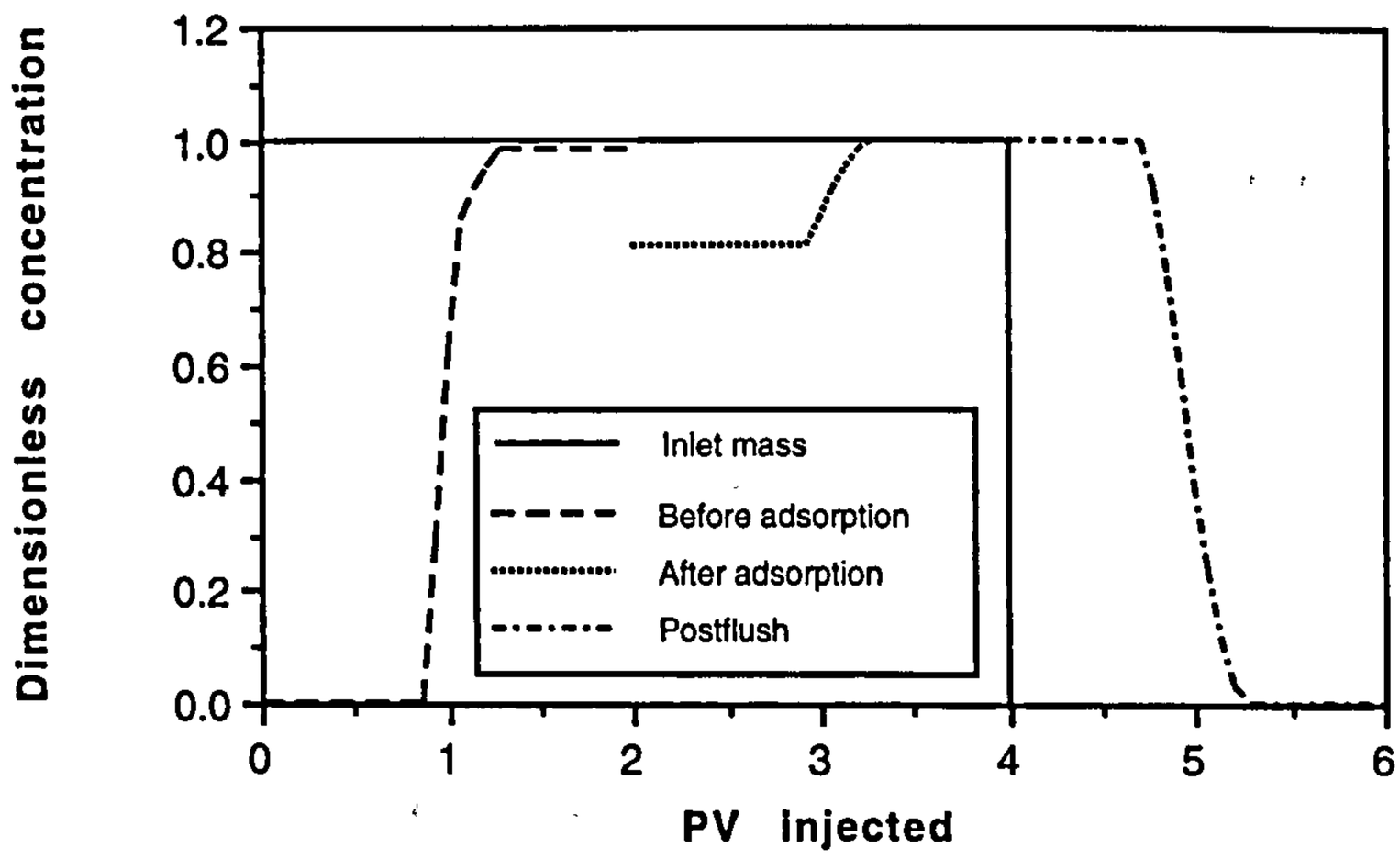

Figure 6.24 Plot of effluent concentration vs PV injected for 100 ppm xanthan solution at 35 g/l NaCl salinity with a shut-in

Table 6.10

The Dynamic Adsorption of Xanthan Solution in Ballotini Packed Columns

Salinity (g/l NaCl)	Shut in			Total Adsorption*		PRF**
	Time (hours)	Bulk Conc. (ppm)	Conc. after Shut in (ppm)	(μg/g)	($\mu g/m^2$)	k/k_0
0.1	120	102.20	85.25	4.797	39.0	0.974
5.0	139	107.64	89.21	4.613	37.5	0.974
35	115	95.08	74.52	4.612	37.5	0.974
35	140	97.49	78.82	5.007	40.7	0.966
35	138	407.21	323.74	20.95	170	0.945

* The solid/liquid ratio in the pack flood experiments is 4.5/1 in g/ml.

** PRF is the permeability reduction factor

Three significant flooding regimes can be established as follows: (i) polymer injection and breakthrough from 0 to 2 PV, (ii) after shut in for 5 days, polymer injection again from 2 to 4 PV, and (iii) brine postflush from 4 to 6 PV. The xanthan adsorption in the porous medium is clearly visible immediately after the shut in in the second regime for all floods (e.g. see Figure 6.22). From the xanthan adsorption results at various salinities which are shown in Table 6.10, three points are evident:

(i) for 100 ppm concentration systems (at various salinities), the polymer adsorption level generally is about 5 μg/g (40 $\mu g/m^2$);

(ii) at higher concentration (400 ppm), the polymer adsorption level is 21 μg/g (170 $\mu g/m^2$), much higher than those for the 100 ppm cases;

(iii) the permeability reduction is relatively small after polymer flooding.

The adsorption level increases with increasing concentration, which is in conformity with the principle of Langmuir-type behaviour. A plot of adsorption level (Γ) versus salinity for 100 ppm xanthan concentration both before and after a shut-in period is shown in Figure 6.21. Both plots exhibit a plateau value in the experimental salinity region but, although the adsorption level after the shut in is ~5 times higher, the total adsorption level is still fairly low. The experimental results indicate that, at low xanthan concentration, the salinity effect on polymer adsorption is negligible. We also note that the dynamic adsorption process appears to take some time to reach full adsorptive capacity.

6.7 The Effect of Xanthan Dynamic Adsorption on In Situ Rheology

High molecular weight polymer adsorption is often almost irreversible, which may lead to modified in situ rheological behaviour. Chauveteau et al (1984) found that, for HPAM, if the wall is attractive, the apparent solution viscosity inside the pore may be greater or less than the corresponding bulk value, depending on the concentration of the flowing polymer solution. To the authors' knowledge, no data have been published in the literature for the corresponding xanthan case (or for the case of scleroglucan - see Chapter 7).

Table 6.11 shows the viscosities of xanthan solution in bulk, in the effluent and in the porous medium at various salinities during polymer flooding. Xanthan apparent viscosities (η_{app}) were measured after 2 PV of polymer injection in regime 1 and after 4 PV of injection in regime 2 as shown in Figure 6.22 and as explained above. Note that, in a normal experiment, we cannot measure the in situ apparent viscosity in the period immediately after the shut in (regime 2a in Figure 6.22).

Figures 6.25 and 6.26 illustrates some of the experimental results for 100 ppm xanthan solution in 0.1 and 35 g/l NaCl brine both before (regime 1) and some time after (regime 2b) the shut in period. The effluent viscosity after polymer breakthrough appears to be slightly lower than that of the bulk for all samples, which implies that there may be a

small effect of dissolved species discussed above section. After full adsorption, the effluent viscosity markly decreases and then recovers to normal bulk viscosity as the flood proceeds. Table 6.11 and Figures 6.25 and 6.26 clearly indicate that the in situ apparent viscosities both before and after full adsorption are very similar.

Table 6.11

The Viscosity of Xanthan Solutions in Porous Media before and after Shut in

Salinity (g/l NaCl)	Concentration (ppm)	Condition	Inlet (Bulk) Viscosity η_{in} (cp)	Outlet Viscosity η_{out} (cp)	Apparent Viscosity η_{app} (cp)
0.1	100	before shut in	2.58	2.54	1.98
		after shut in	2.58	2.24	
		before postflush	2.58	2.58	1.97
5.0	100	before shut in	2.17	2.13	1.87
		after shut in	2.17	1.91	
		before postflush	2.17	2.17	1.88
35	100	before shut in	2.22	2.17	1.87
		after shut in	2.22	1.96	
		before postflush	2.22	2.22	1.89
35	100	before shut in	2.24	2.20	1.93
		after shut in	2.24	1.94	
		before postflush	2.24	2.24	1.94
35	400	before shut in	12.80	12.00	7.14
		after shut in	12.80	7.65	
		before postflush	12.80	12.20	6.68

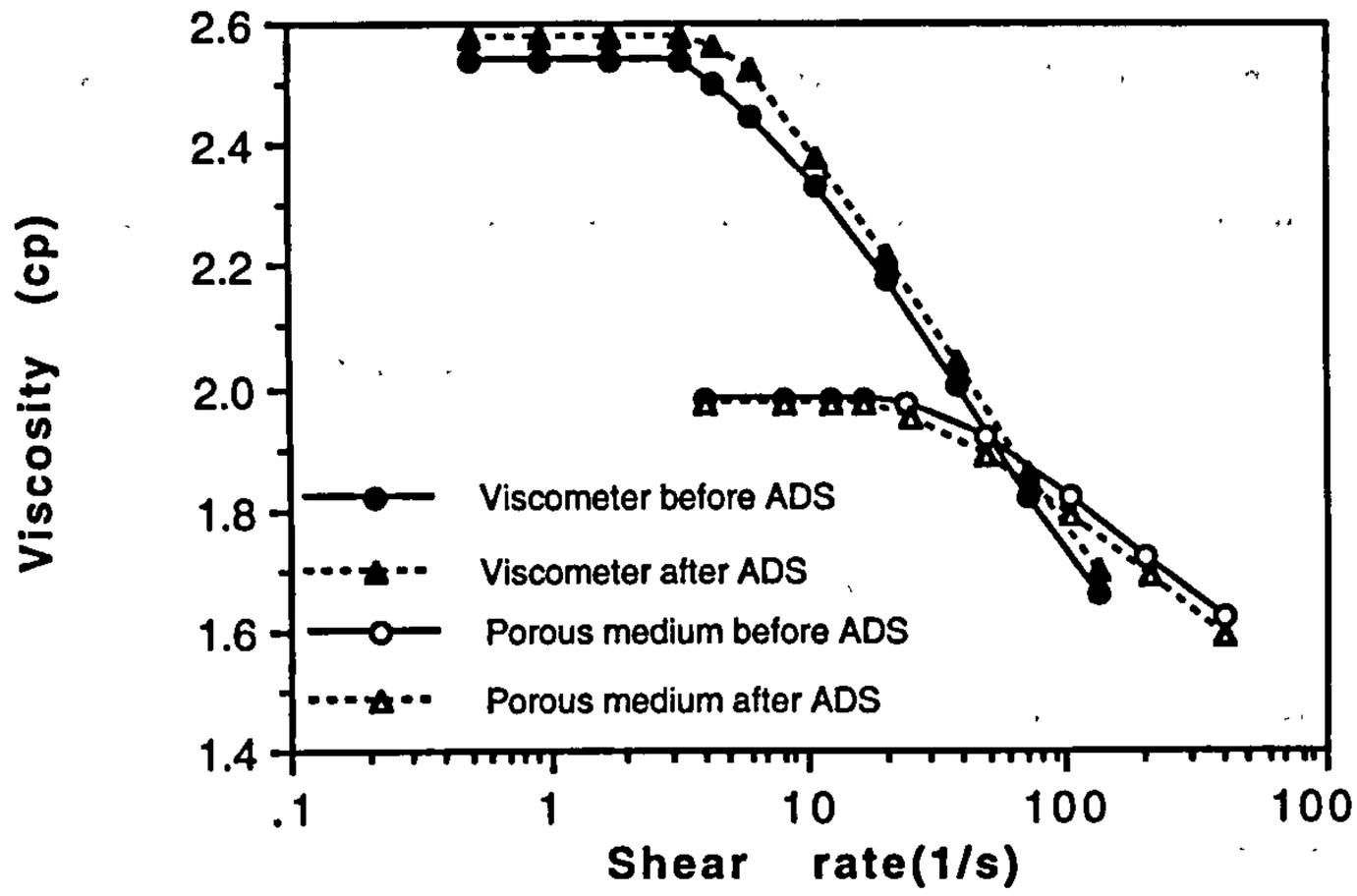

Figure 6.25 The comparison of porous medium and viscometer rheologies for 100 ppm xanthan / 0.1 g/l NaCl system with and without xanthan adsorption

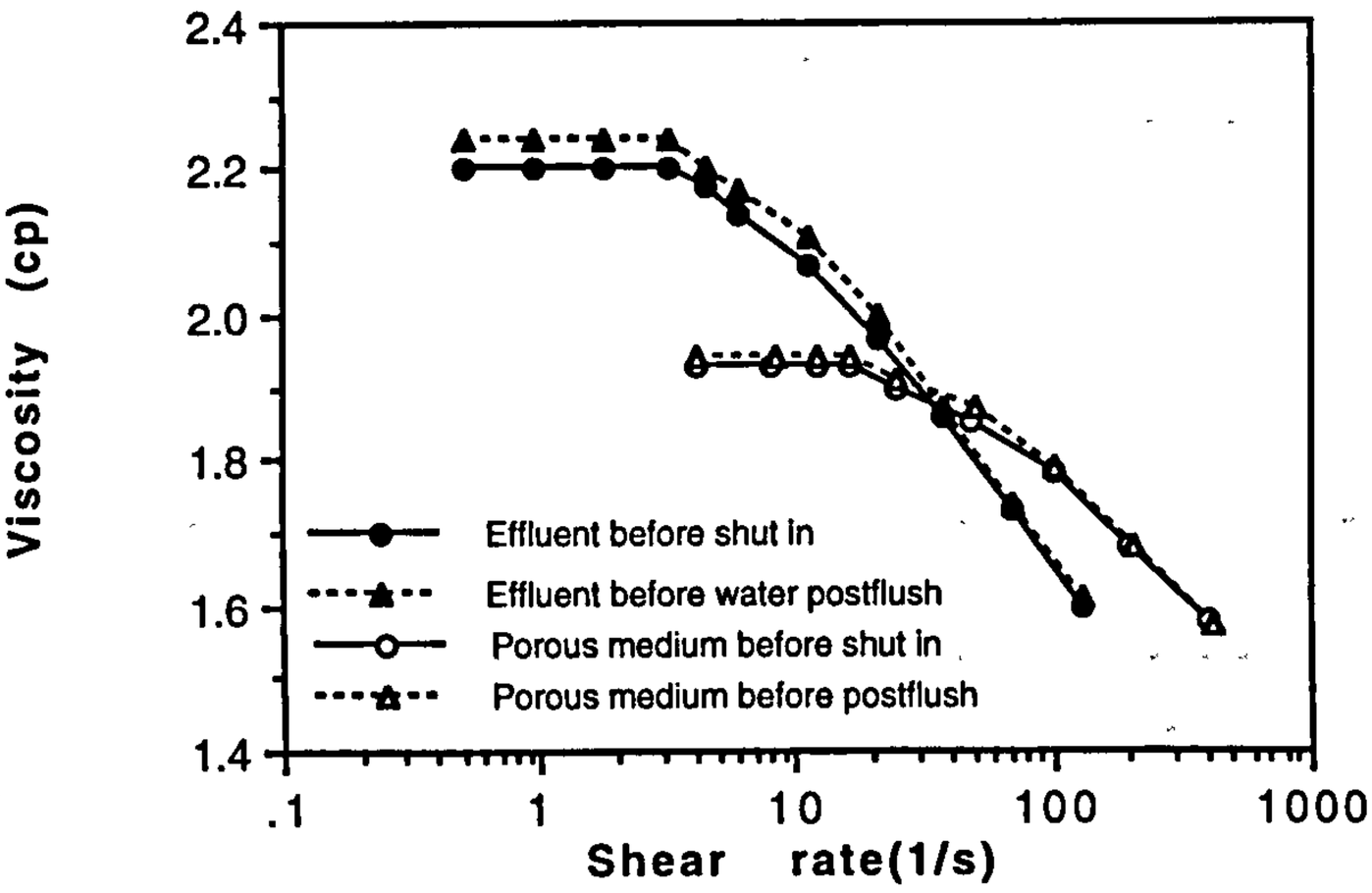

Figure 6.26 The comparison of porous medium and viscometer rheologies for 100 ppm xanthan / 35 g/l NaCl system with and without xanthan adsorption

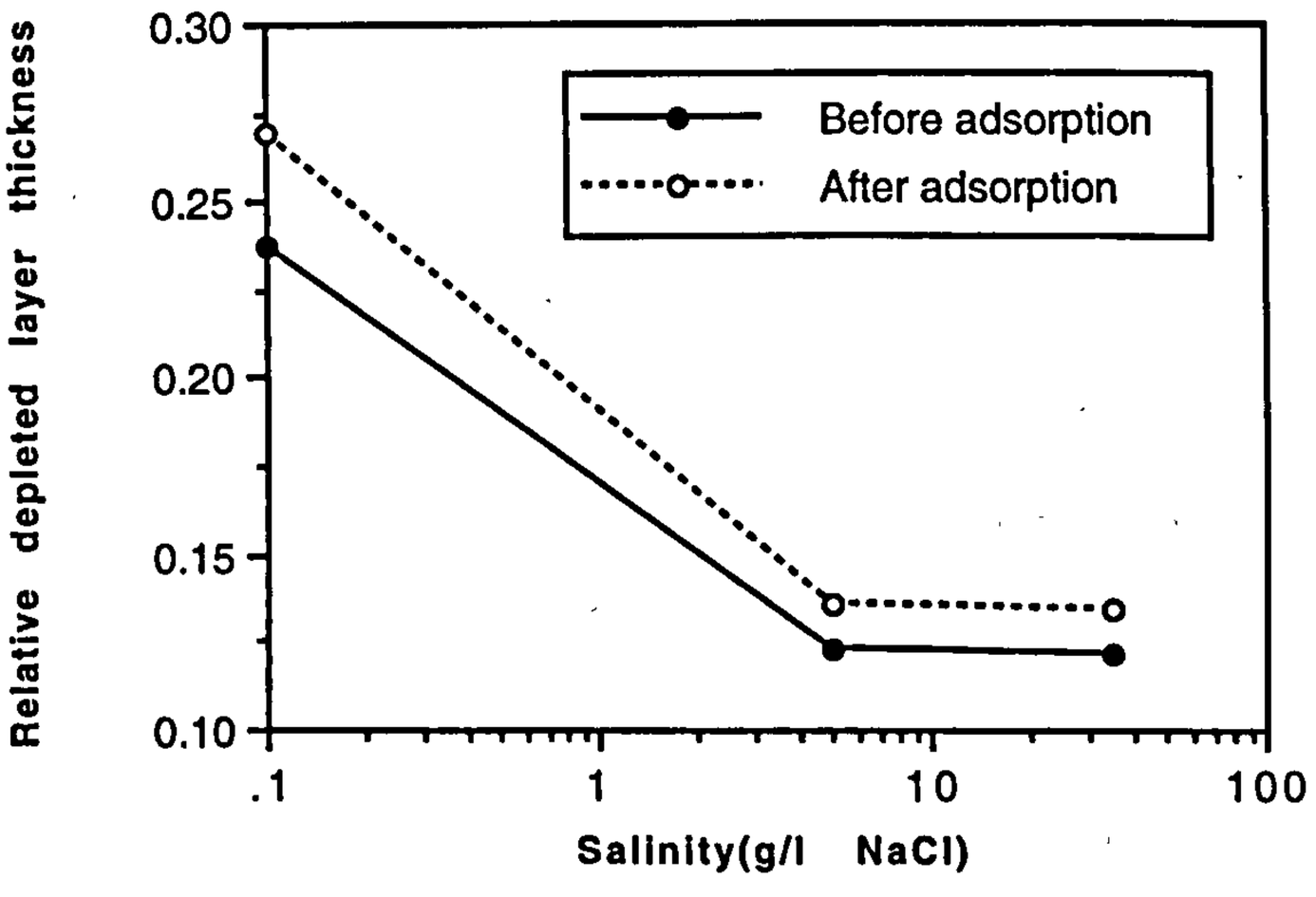

Figure 6.27 A comparison of relative depleted layer thickness as a function of salinity before and after 100 ppm xanthan adsorption

Table 6.12

Depleted Layer Thickness of Polymer Solution in Porous Media

Concentration (ppm)	Salinity (g/l NaCl)	Condition*	Relative Depleted Layer Thickness (δ/r) (Two fluid model A1)	(Linear Layer model A3)	Permeability k (Darcy)
100	0.1	(A)	0.238	0.153	1.16
		(B)	0.269	0.166	1.13
100	5.0	(A)	0.123	0.096	1.16
		(B)	0.136	0.104	1.13
100	35	(A)	0.148	0.112	1.17
		(B)	0.159	0.118	1.14
100	35	(A)	0.122	0.094	1.16
		(B)	0.134	0.102	1.12
400	35	(A)	0.343	0.110	1.18
		(B)	0.651	0.134	1.11

* Experimental condition (refer to Fig. 6.22); Xanthan concentration 100 ppm

(A) After initial 2PV injection of biopolymer solution, before shut in

(B) After succeeding 2PV injection of biopolymer solution after about 5 days shut in, before postflush

The calculation of the relative depleted layer thickness, (δ/r), before and after adsorption is shown in Table 6.12. A comparison of depleted layer thicknesses before and after adsorption calculated using the linear layer model is shown in Figure 6.27. Both curves in Figure 6.27 have a similar tendency; (δ/r) decreases with increasing salinity and tends to level out at high salinity (more than 5 g/l NaCl). This result is consistent with the results reported above (see Section 5.7). From different experiments, we obtained the same conclusion concerning the salinity effect. However, here we are more interested in the effect of xanthan adsorption on the depleted layer thickness. The experimental results

shown in Figure 6.27 indicate that this effect is small. After full adsorption, the (δ/r) seems to be a little higher than that before adsorption although this effect is small.

Table 6.13

The Effect of Xanthan Adsorption on the Relative Depleted Layer Thickness

Period when measured*	Outlet Viscosity η_{out} (cp)	Apparent Viscosity η_{app} (cp)	Relative Depleted Layer Thickness (δ/r)	
			Two Fluid Model [A1]	Linear Layer Model [A3]
regime 1	2.20	1.93	0.122	0.094
regime 2a**	1.90	1.71	0.117	0.096
regime 2b	2.24	1.94	0.134	0.102

* See Figure 6.22 for flow regimes.

** Measured in a separate experiment using ballotini which was pre-equilibrated with xanthan solution along with the corresponding supernatant polymer solution (see text for details)

In order to examine the effect of xanthan adsorption on (δ/r) immediately after the shut in (regime 2a, Figure 6.22) in more detail, the following experiment was carried out. The ballotini glass beads were fully equilibrated with xanthan in 100 ppm solution in a bulk static adsorption experiment and were then packed in the column. The equilibrated xanthan supernatant which had approximate concentration C ≈ 85 ppm was then injected into the column and apparent viscosity was measured and compared with effluent viscosity. Results are shown in Table 6.13 where they are compared with results from the other regimes (as defined in Figure 6.22). In regime 2a, the experimental result shows that (δ/r) is close to the others although the effluent viscosity is much less than those in regime 1 and 2b. Here, the total xanthan dynamic adsorption level is low indicating that the attractive interactions between polymer and interfaces are weak. Theoretically, even at this weak attraction between polymer and pore wall, it may cause a reduction of depleted layer thickness which appears as a higher apparent viscosity. But

in our observation, it is very difficult to find this phenomenon even for the high adsorption case, such as at 400 ppm. When xanthan biopolymer propagates through the porous medium, the dynamic adsorption process takes a long time to equilibrate. Depleted layer thickness is affected mainly by polymer/interface interactions which are strictly repulsive at short distances. The apparent viscosity in porous media mainly depends on the effluent viscosity which may change considerably because of the polymer dynamic and static adsorption in porous media.

6.8 Summary and Conclusions

In this chapter, the static and dynamic adsorption and in situ rheological behaviour of xanthan biopolymer flowing through porous media have been investigated. The long term static adsorption level is much higher than short term dynamic adsorption level. It also is found that the adsorption strongly dependens on the solid/liquid ratio in experimental systems. This may be due to the aggregation of small beads; the collision of large beads; or, more likely, the dissolved species. Experimentally, the apparent viscosities of xanthan solution flowing in the ballotini glass bead packed columns were measured under various conditions and compared with the corresponding bulk viscosities. The experimental data were analysed using simple analytical models (two-fluid model and linear layer model) in order to estimate the apparent depleted layer thickness. The main new results presented in this chapter concern the effect of xanthan dynamic adsorption on the in situ polymer rheology and depleted layer thickness. The general conclusions reached in this chapter may be summarized as follows:

(1) The static adsorption of xanthan solution onto ballotini glass beads is a function of xanthan concentration. Adsorption levels increase linearly with increasing xanthan concentration in the range 10 to 400 ppm. An adsorption isotherm model with depleted layer effect is developed which indicates that the actual adsorption level is more or less higher than the apparent observed adsorption level while the depleted layer is present.

(2) Xanthan adsorption increases with the decrease in solid/liquid ratio for the ballotini system, but not for sand system. Using sand, a fast adsorption equilibrium with concentration can be obtained. The effect of solid/liquid ratio on adsorption may be explained by taking account of the aggregation of small beads or the collision of large beads using Chaveteau's models; however some doubt still remains. The effect of dissolved species from the particle surface on adsorption is observed experimentally and is more readily used to interpret the observed experimental results. The corresponding dissolved species model can also be used for interpreting the solid/liquid ratio effect.

(3) The xanthan dynamic adsorption process within the porous medium used in this work is fairly slow. For the short time flood (within one day), the adsorption level is very low at about 1 μg/g (or 8 $\mu g/m^2$). For the longer flooding period of 7 days, including a 5 day shut in, the total adsorption amount is about 5 μg/g (or 40 $\mu g/m^2$) for 100 ppm xanthan solution. These adsorption levels are not significantly changed with salinity. However, the adsorption level is much higher for higher concentration xanthan solutions i.e. up to 21 μg/g (or 170 $\mu g/m^2$) for 400 ppm polymer solutions.

(4) The effect of xanthan dynamic adsorption on in situ rheological behaviour is not very significant. The plots of relative depleted layer thickness vs. salinity for 100 ppm xanthan solution with and without full adsorption have the same tendency and the in situ apparent viscosities for both cases are very similar. This indicates that, when xanthan molecules adsorb onto the pore walls, the hydraulic radius of the porous medium is not very significantly affected and, therefore, that the rigid xanthan molecules are adsorbed very flat up against the pore wall.

CHAPTER 7

SCLEROGLUCAN BEHAVIOUR IN FLOW THROUGH POROUS MEDIA: COMPARISON OF ADSORPTION AND IN SITU RHEOLOGY WITH XANTHAN

7.1 Introduction

Scleroglucan is a non-ionic polysaccharide produced by the fermentation of a plant pathogen fungus of genus sclerotium. The backbone of the molecule consists of linearly linked β-1, 3-D-glucose residues with a β-1, 6-D-glucose side chain attached to every third residue along the backbone. This biopolymer has a rigid rod-like triple helical structure in aqueous solutions (Yanaki et al, 1981). Due primarily to these molecular properties, dilute scleroglucan solutions have exceptional temperature-stability and show pseudoplastic behaviour. In addition, scleroglucan shows very good shear and chemical stability and is compatible with many brines, which make it of great interest for polymer flooding application. Davison and Mentzer (1982) found that scleroglucan had the best application potential out of 140 polymers tested in terms of its viscosity retention and mobility reduction performance in porous media at high temperature (90°C) and salinity. However, to date, only a limited amount of data has been reported on scleroglucan adsorption in porous media and on its in situ rheological behaviour.

Rivenq et al (1989) presented an evaluation of an industrially manufactered scleroglucan which showed an improved quality on the basis of viscosity and filterability measurements, as well as in its flow behaviour in porous media. They found that the adsorption level of this biopolymer onto Berea cores decreases when the teperature increases down to a low value of about 30 μg/g at 90°C. Stokke et al (1992) compared the rheological properties of xanthan and scleroglucan at various solution shear rates and

temperatures. They indicated that chain stiffness is the basic molecular parameter altered by changes in temperature. Fletcher et al (1991) found that scleroglucan and xanthan exhibit comparable effective viscosities at high flow rates in porous media. At ultra low flow rates, the scleroglucan displayed far greater in-situ viscosity than xanthan, consistent with a higher bulk viscosity value.

This chapter focuses on the flow of scleroglucan through porous media and follows previous studies on the adsorption, transport and in situ rheology of xanthan. Scleroglucan solution used in this work has a salinity 20 g/l NaCl and the experiments were performed at room temperature. The main subject studied here is the in situ rheological behaviour of scleroglucan solution, as it compares with the corresponding behaviour of xanthan biopolymer. This involves the effects on in situ rheology of polymer concentration, pH, dynamic adsorption and retention. The experimental in situ rheological data are analysed using simple analytical models (two fluid flow model and linear layer model) as shown in previous chapters in order to estimate the apparent depleted layer thickness, (δ/r). In addition to presenting a comparison of the rheological and transport characteristics of (nonionic) scleroglucan and (anionic) xanthan, a comparison of the polymer behaviour in the two porous media used in our experiments (ballotini glass bead packs and sandpacks) is also presented.

7.2 Ballotini Glass Bead Packed Columns

7.2.1 Transport and Dynamic Adsorption

A series of polymer flooding experiments was carried out in pretreated ballotini glass bead packed columns using scleroglucan solutions at various concentrations. The total flooding process was carried out in two stages. The first stage is similar to that described in Section 6.6 in which, after full breakthrough of polymer, the packed column was shut in for 4-5 days and then was reopened to continued polymer flooding followed by a water postflush. The second stage is to repeat the whole first stage process, except for the shut-in process, within the same pack.

Some of typical effluent profiles for 100 ppm scleroglucan solution are shown in Figures 7.1 to 7.7. These results shows different behaviour from that previously observed for xanthan biopolymer solution. Figure 7.1 is the polymer breakthrough during first stage. A delay in the effluent polymer profile compared with the tracer is observed which is different from the corresponding xanthan profiles in previous work. In Figure 7.1, the scleroglucan dynamic adsorption is immediately evident, whereas, for xanthan, the first effluent profile showed little retardation compard with the tracer in this porous medium. After full polymer adsorption and postflush, the second polymer injection shows a negligible frontal adsorption level and earlier breakthrough of polymer relative to that of tracer as shown in Figure 7.2. This result is consistent with the corresponding results for xanthan. The advancement in the polymer profile is due to the presence of a surface exclusion effect where the polymer molecules are more likely to pass through the faster streamlines close to the centre of the pore. The first and second scleroglucan breakthrough profiles are compared in Figure 7.3. It is clear that there is a competitive process of retention and exclusion between the polymer molecules and the ballotini pore wall. The difference between the two profiles in Figure 7.3 implies a pure adsorption level.

Figures 7.4 and 7.5 demonstrate the effluent profiles of both polymer and tracer during water postflush in the first stage and the second stage respectively. It appear to be a longer tailing for both stages. Viscous fingering is more obvious in the final postflush where the water breakthrough occurs as early as 0.5 PV injection in Figure 7.5 compared with the first postflush where breakthrough occurred at 0.7 PV water injection as shown in Figure 7.4.

Figure 7.6 shows whole polymer effluent profile in the first stage flooding sequence. Further scleroglucan adsorption in the porous medium is clearly visible immediately after the 5 day shut in. It may be that there are two different adsorption processes occurring during polymer flow through the porous medium; one is a fast physical adsorption and

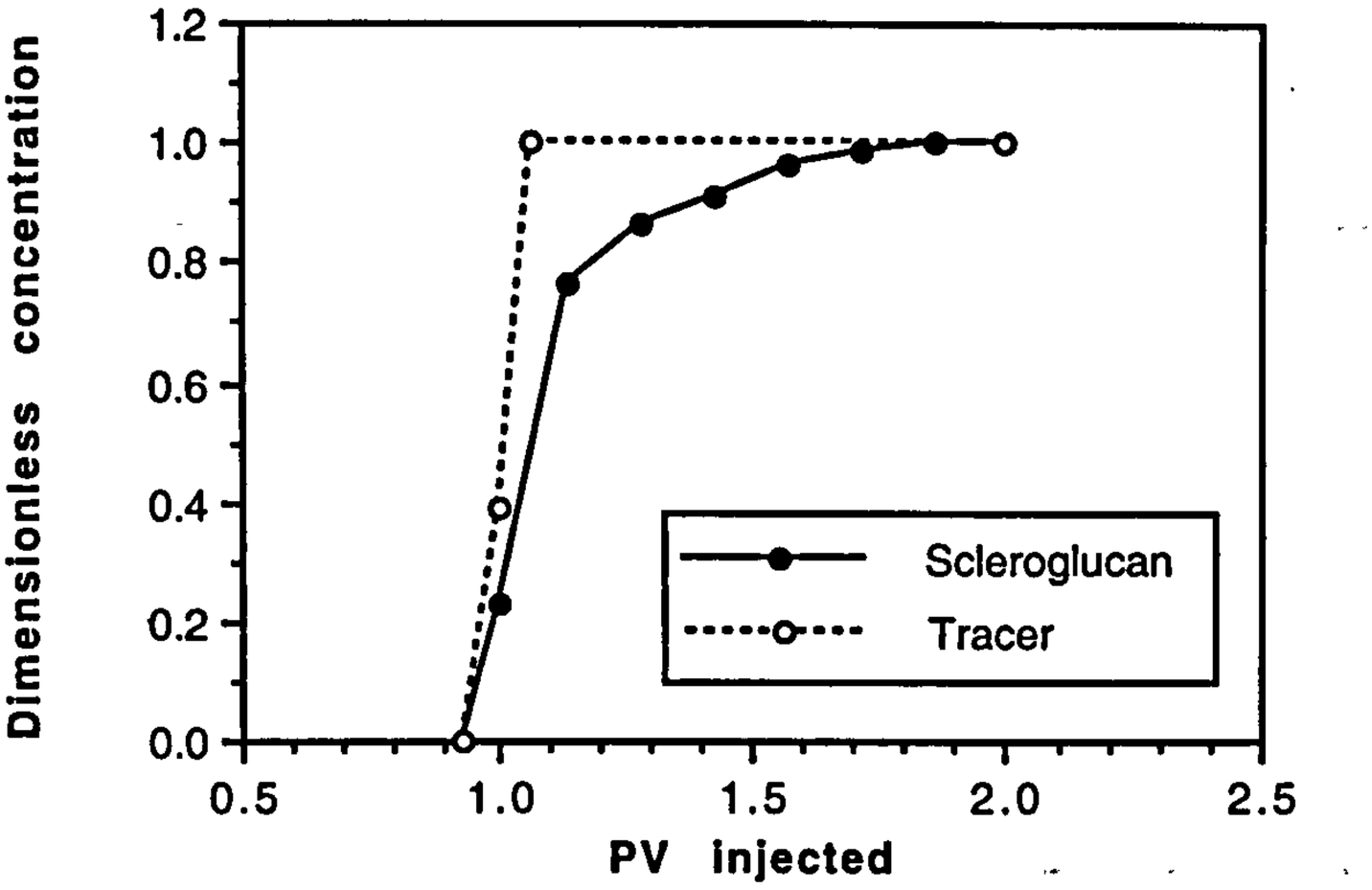

Figure 7.1 Frontal effluent profiles for 100 ppm scleroglucan solution and lithium tracer in first polymer injection stage

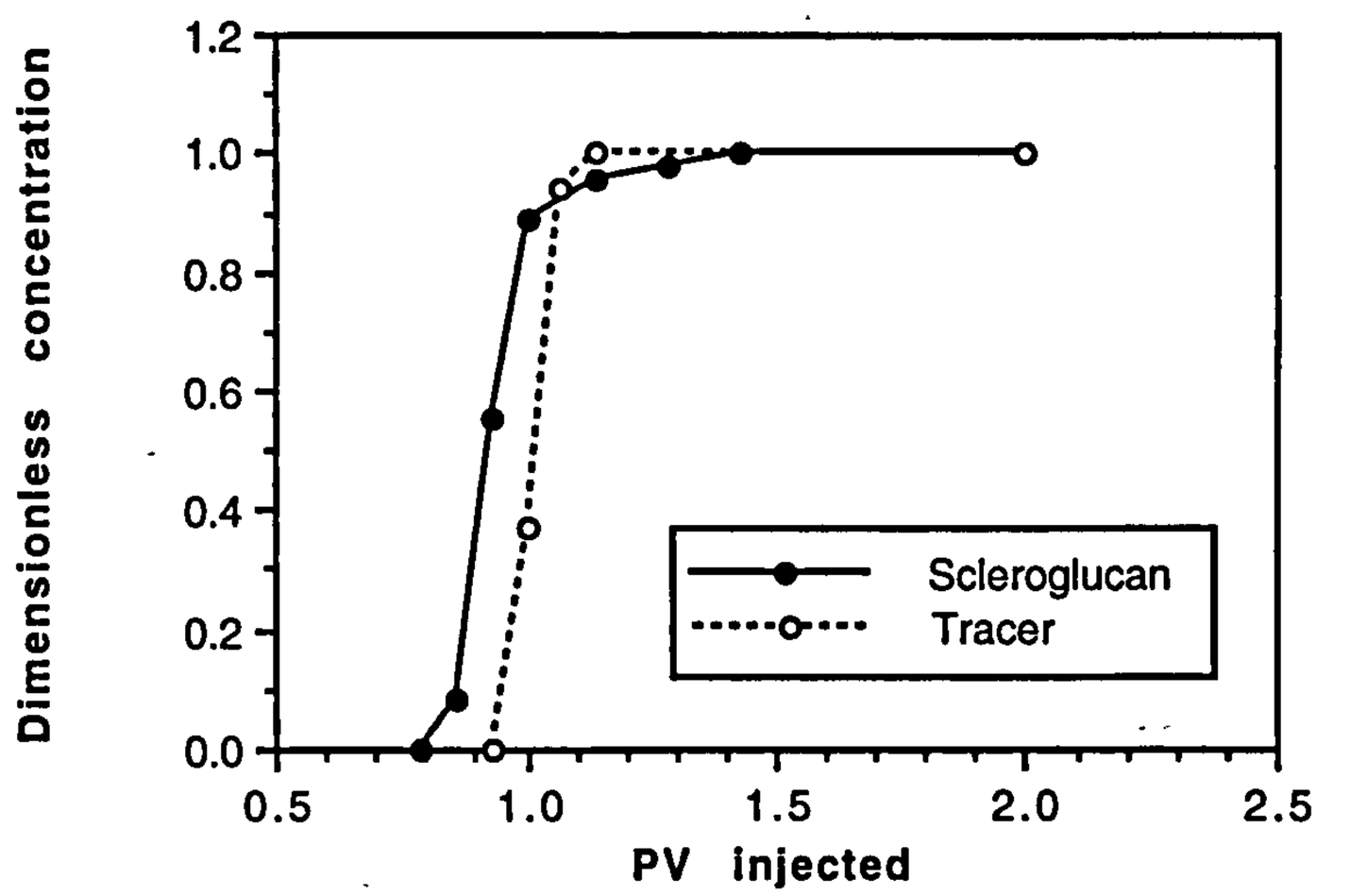

Figure 7.2 Frontal effluent profiles for 100 ppm scleroglucan solution and lithium tracer in second polymer injection stage

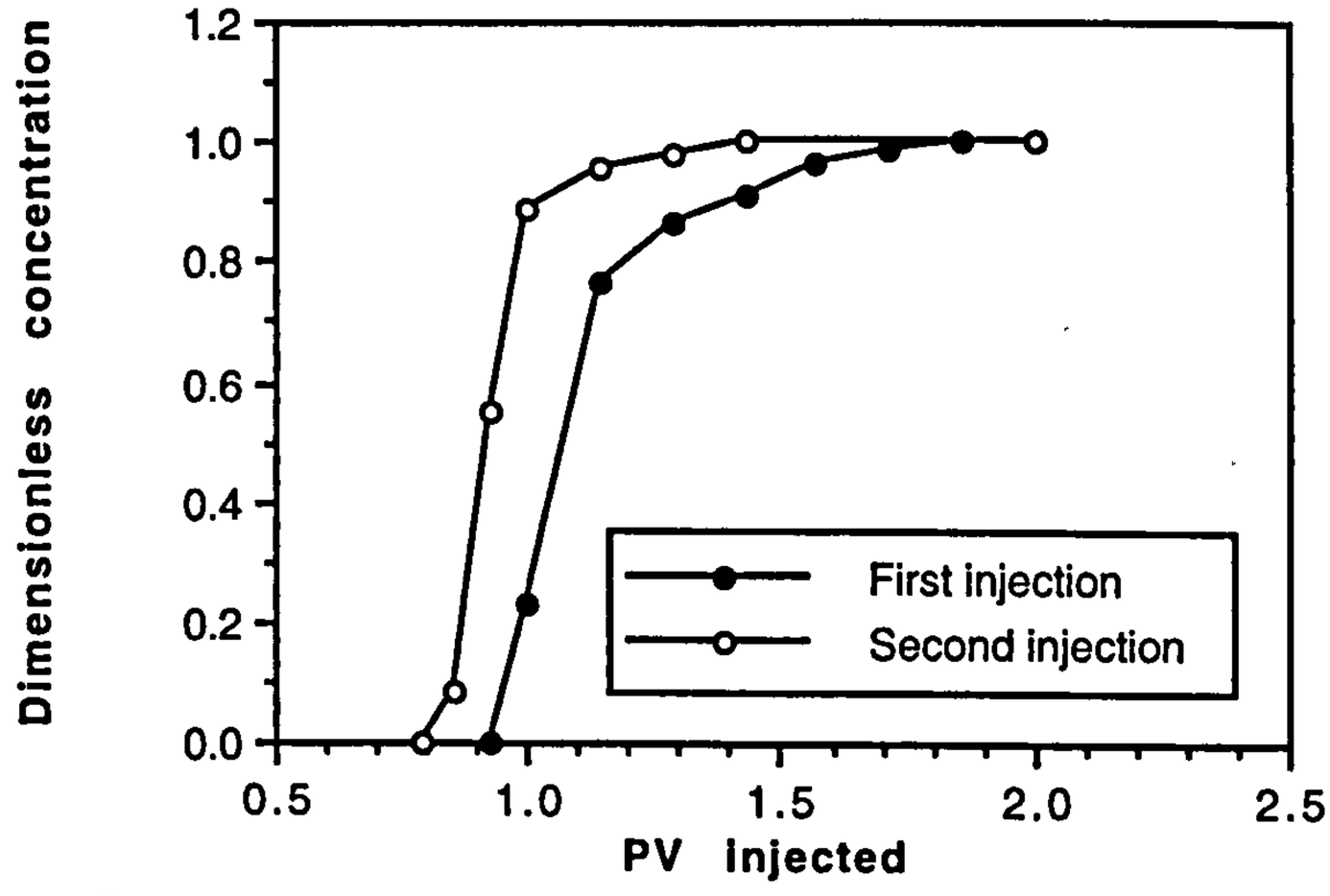

Figure 7.3 A comparison of frontal effluent profiles of first and second injections for 100 ppm scleroglucan solution

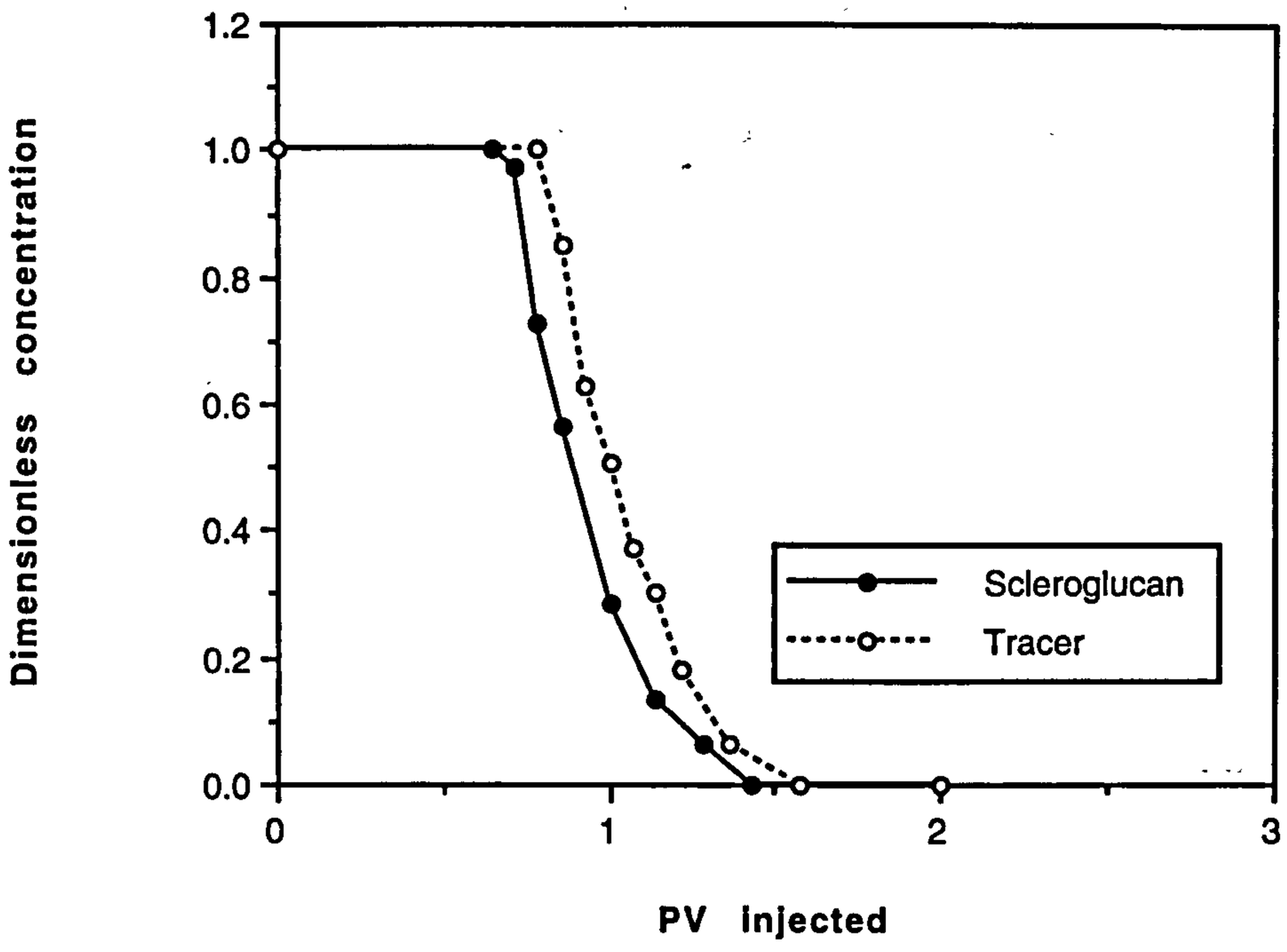

Figure 7.4 Trailing effluent profiles for 100 ppm scleroglucan solution and lithium tracer during first brine postflush

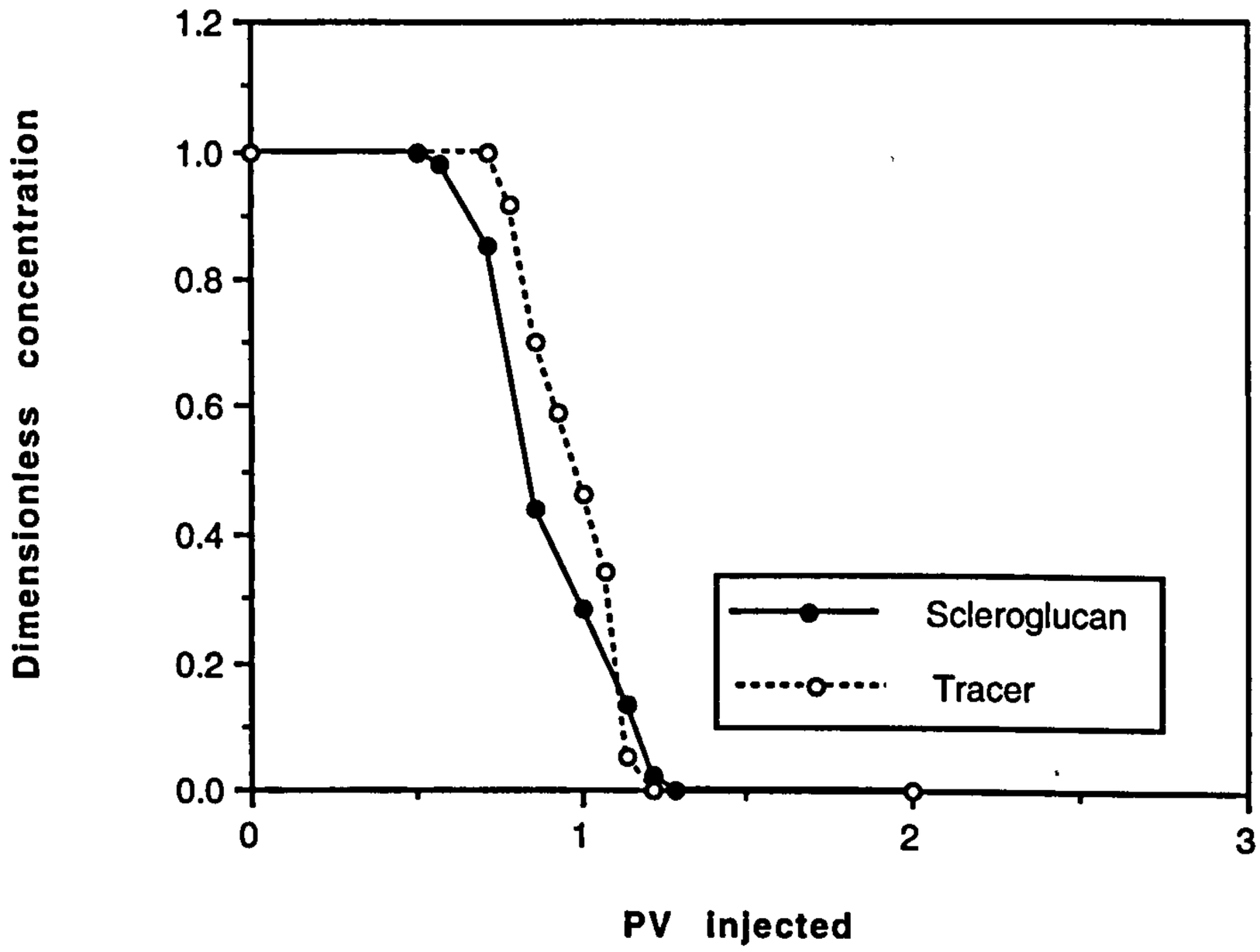

Figure 7.5 Trailing effluent profiles for 100 ppm scleroglucan solution and lithium tracer during second brine postflush

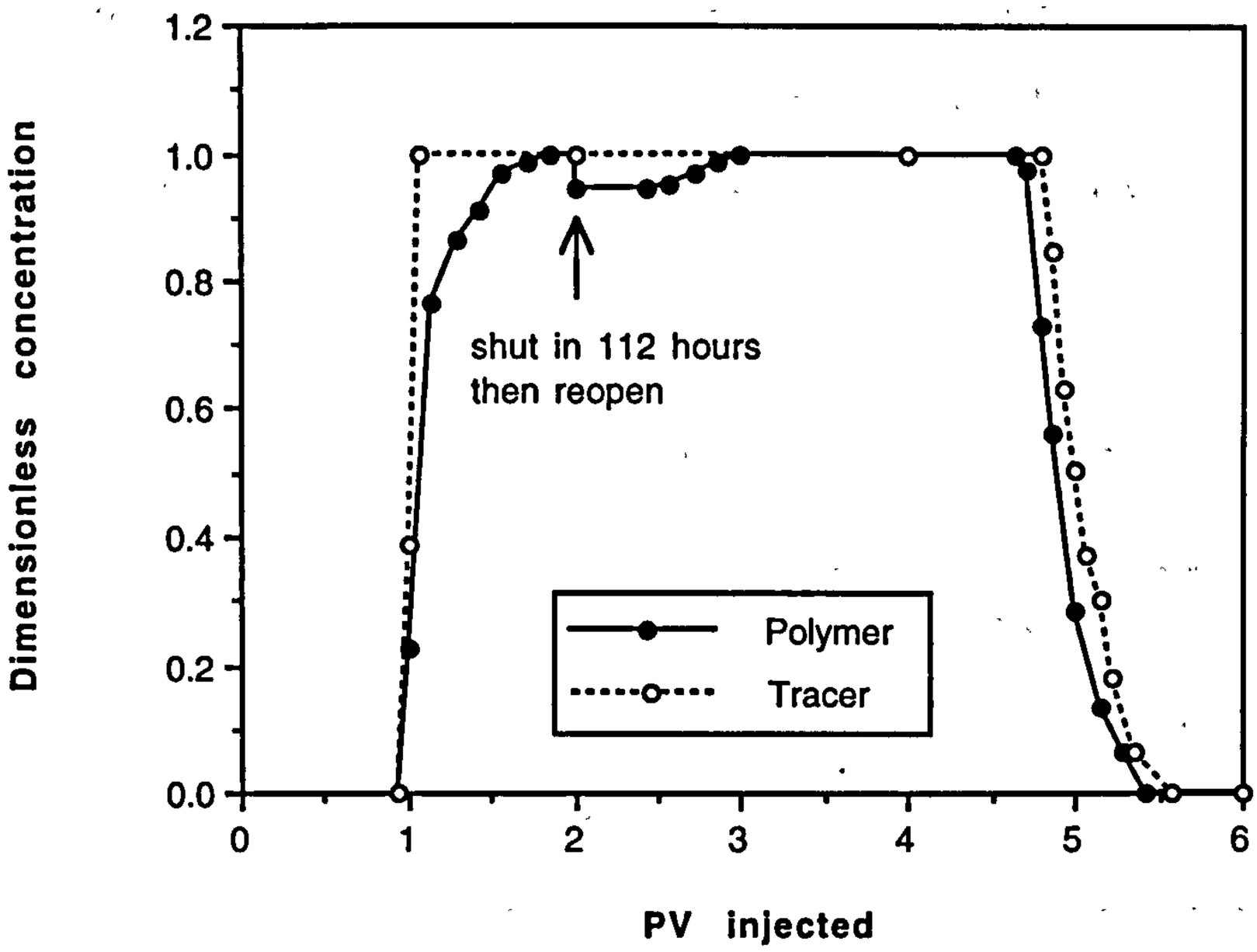

Figure 7.6 Effluent profiles for 100 ppm scleroglucan and lithium tracer in first full flooding

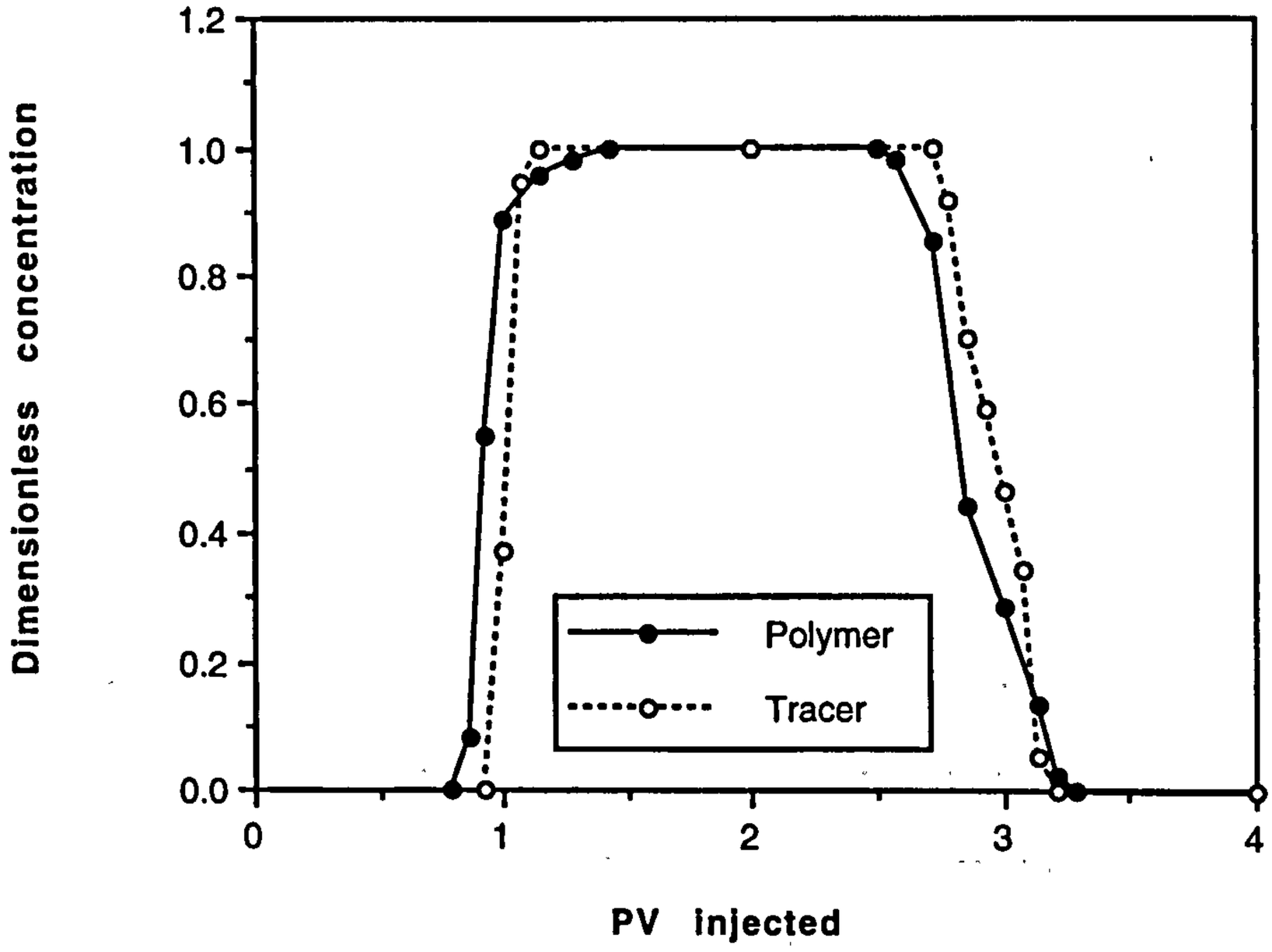

Figure 7.7 Effluent profiles for 100 ppm scleroglucan and lithium tracer in second full flooding

another slow chemical adsorption. From the effluent profiles during the postflush, irreversible losses of polymer are evident. The polymer effluent profiles in the second flooding stage are shown in Figure 7.7. The material balance indicates that only a small additional amount of polymer adsorption occurs after the first stage flood.

Table 7.1

The Dynamic Adsorption of Scleroglucan Solution in Ballotini Packed Columns

Concentration (ppm)	Polymer mass losses (μg)		Total adsorption	
	First stage	Second stage	(μg/g)	(μg/m^2)
50	468.09	53.56	8.21	66.7
100	488.09	66.36	8.73	71.0
200	609.61	133.96	11.71	95.2

Using material balance, the polymer loss in each flooding stage and the total adsorption level for each concentration of scleroglucan solution used, are estimated and the results are shown in Table 1 from which it is concluded that:

(i) the total adsorption level increases with increasing scleroglucan concentration;

(ii) after full adsorption during the first injection stage, the additional adsorption level in the second injection stage is much lower;

(iii) compared with xanthan dynamic adsorption reported in Section 6.6 and Table 6.10, the scleroglucan dynamic adsorption process within the porous medium used in this work is relative fast and the adsorption level is higher. For example, it was found previously that for a 100 ppm xanthan solution, the adsorption level at 35 g/l NaCl salinity is 5.0 μg/g whereas for scleroglucan in 20 g/l NaCl brine the corresponding adsorption level is 8.7 μg/g;

(iv) even though a relative higher dynamic adsorption level is observed for scleroglucan compared with xanthan, the total adsorption level is still relatively low in these ballotini packed columns.

Surprisingly, for the relatively low adsorption levels observed here, the permeability change is quite significant. Figures 7.8 and 7.9 show typical results for permeabilities at different flow rates, before and after polymer flooding, for 50 ppm and 100 ppm scleroglucan solutions repectively. Three points are evident from these results: (a) the permeability reduction is quite significant e.g. from k ≈ 1.3 Darcy before polymer flooding to < 1 Darcy after polymer flooding; (b) no further permeability reduction is found during the second flooding stage which is consistent with the adsorption results discussed above; (c) after polymer flooding, the permeability to brine in the porous medium appears to decrease with decreasing flow rate, especially in very low flow rate region. This latter result is quite reproducible and has been observed in many floods.

The phenomena listed above were also observed for scleroglucan solutions at a range of concentrations and the results are very different from those obtained for xanthan solutions (see Section 6.6). The observed results in this work may be related to the filterability of scleroglucan during its flow through porous medium. Some polymer aggregation tendency at laboratory temperatures (21°C) may be leading to a reduction in permeability at the inlet end of the packed column in these experiments. This may be more evident at very low flow rates which appears as an apparent permeability decrease with flow rate. This kind of polymer retention is much more marked in fine sand packed columns which are discussed later in next section.

7.2.2 Concentration Effect on In Situ Rheology

In situ xanthan rheology at both low and high polymer concentration has been discussed in details in Chapter 4. This section will concentrate on results for scleroglucan solution. In addition, xanthan concentration effect is only considered at very low dynamic adsorption, i.e. before full adsorption, which shows about 1 μg/g adsorption level. In

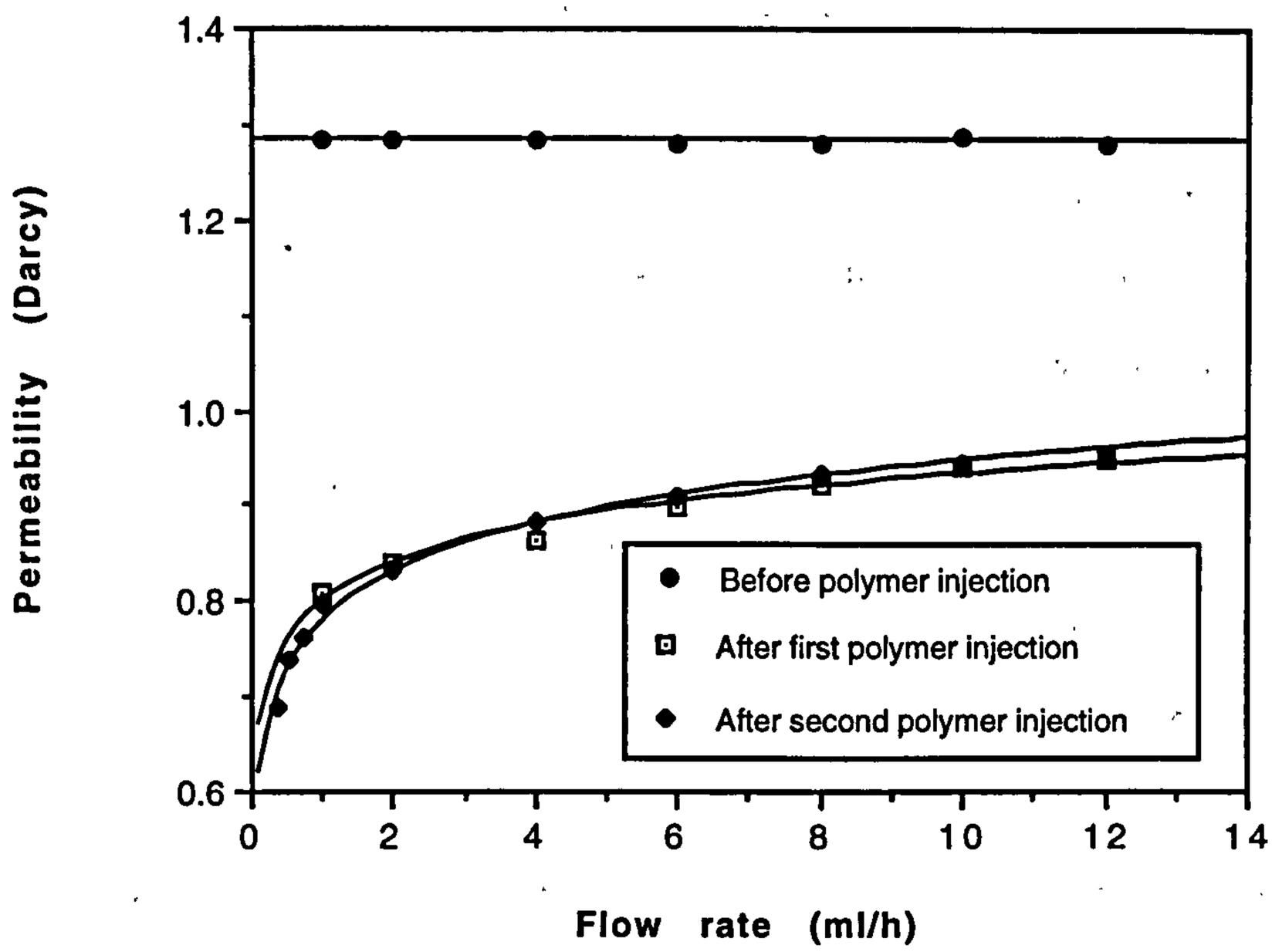

Figure 7.8 Permeability reduction and flow rate dependence after 50 ppm scleroglucan flooding

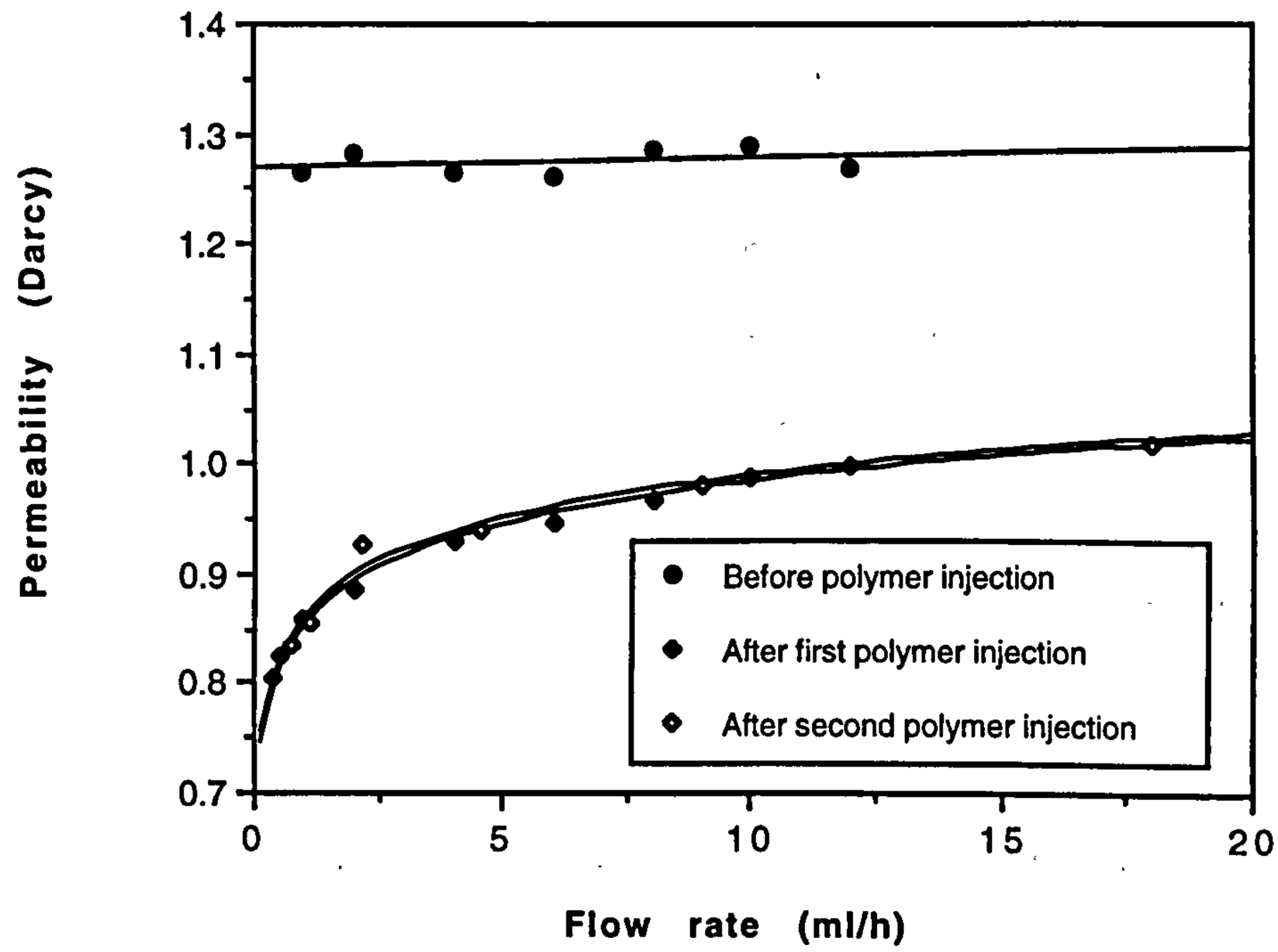

Figure 7.9 Permeability reduction and flow rate dependence after 100 ppm scleroglucan flooding

the scleroglucan case, the in situ rheological behaviour of scleroglucan, both before and after full adsorption in ballotini packed columns, is investigated.

Figures 7.10 to 7.13 demonstrate both the in situ and bulk rheological behaviour of 50, 70, 100, and 200 ppm scleroglucan solutions. All of the experimental concentration systems except 100 ppm solution show the in situ rheological results both before and after full adsorption. Clearly the in situ Newtonian apparent viscosity is always less than the corresponding bulk viscosity in all cases. This results from the apparent slip phenomenon due to the surface exclusion/depleted layer effect near the wall of the porous medium and this has been discussed in detail previously for xanthan. Figures 7.10, 7.11 and 7.13 also indicate that the in situ apparent viscosities both before and after full adsorption are very similar. The fact that the effect of adsorption of scleroglucan on the in situ rheology is very small implies that the adsorption of these molecules is very flat against the pore wall as was found for xanthan. These are consistent with the results presented in chapter 6.

For scleroglucan solutions, the in situ apparent viscosities were obtained using in situ permeability data which depends on the corresponding flow rates as shown in Figures 7.8 and 7.9. This is different from the xanthan case which showed a lower but constant permeability value with flow rate after full adsorption. Figure 7.14 shows an example of the dependence of in situ apparent viscosity on the assumptions concerning the pack permeability. This figure shows results for a 100 ppm scleroglucan solution where the apparent viscosities were obtained using: (i) an initial permeability, k = 1.27 Darcy, before polymer flooding; (ii) an average permeability, k = 0.94 Darcy, at relative high flow rate (1-12 ml/h) after polymer adsorption; and (iii) the in situ permeability, k = 0.80-1.02 Darcy at each corresponding flow rate (0.36-18 ml/h) after polymer flooding. It is interesting to note that, compared with the bulk viscosity behaviour shown in Figure 7.14, if the constant value of permeability is used, no Newtonian apparent viscosity is observed even at very low flow rate. Also, the apparent viscosity is much *higher* than the bulk Newtonian viscosity when the initial permeability is used; this is very similar to the

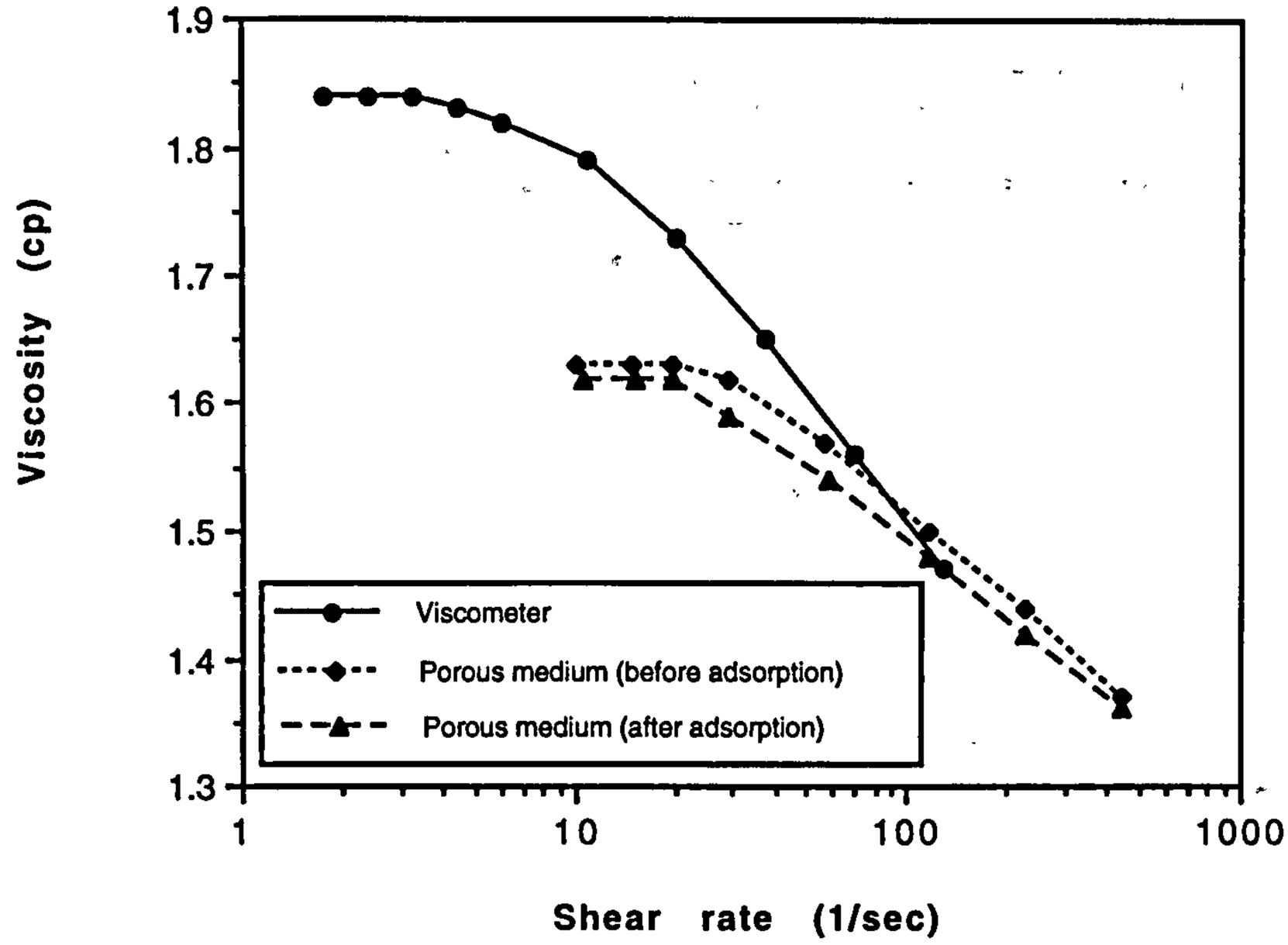

Figure 7.10 The comparison of bulk and in situ apparent viscosities for 50 ppm scleroglucan solution

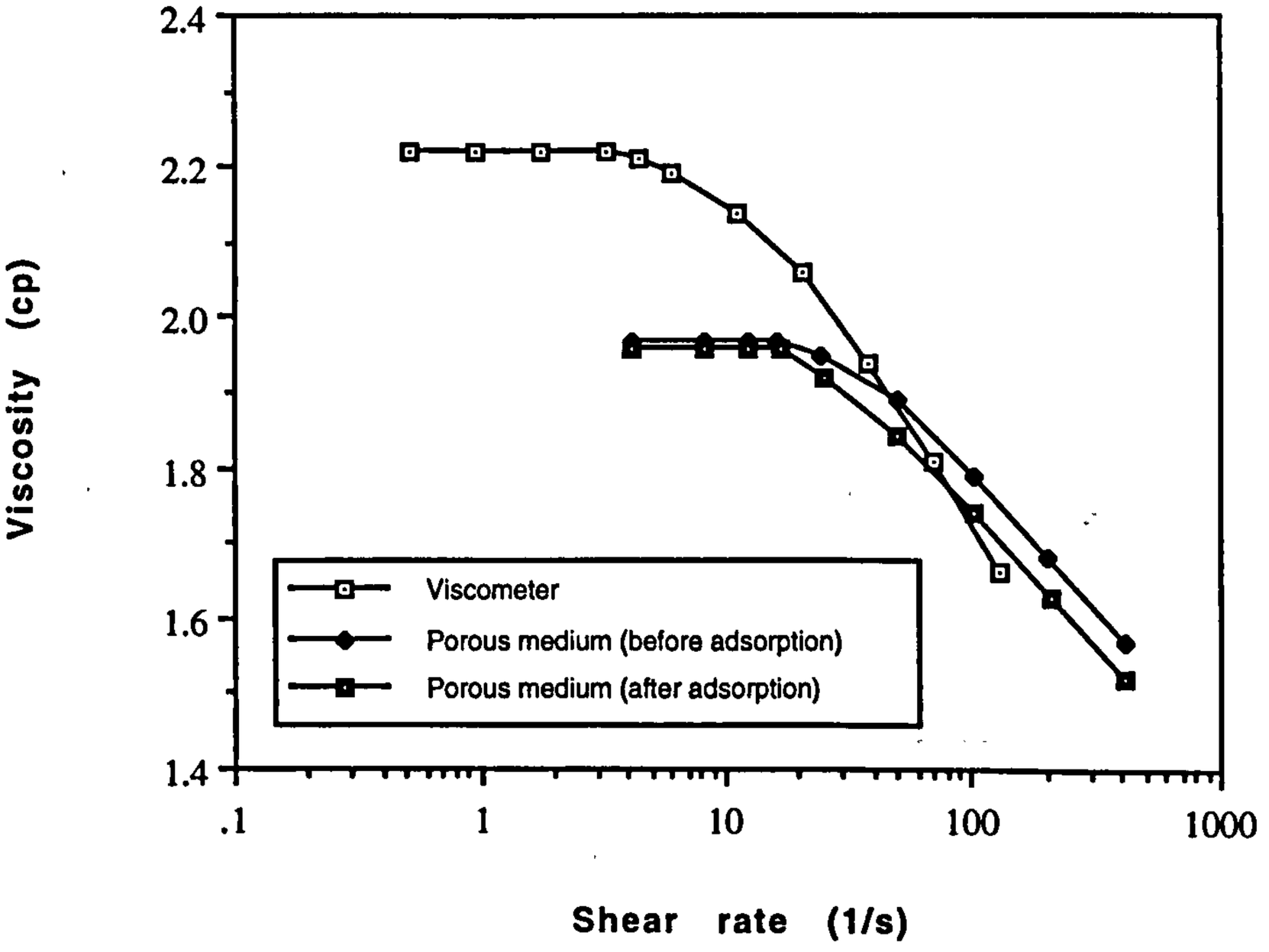

Figure 7.11 The comparison of bulk and in situ apparent viscosities for 70 ppm scleroglucan solution

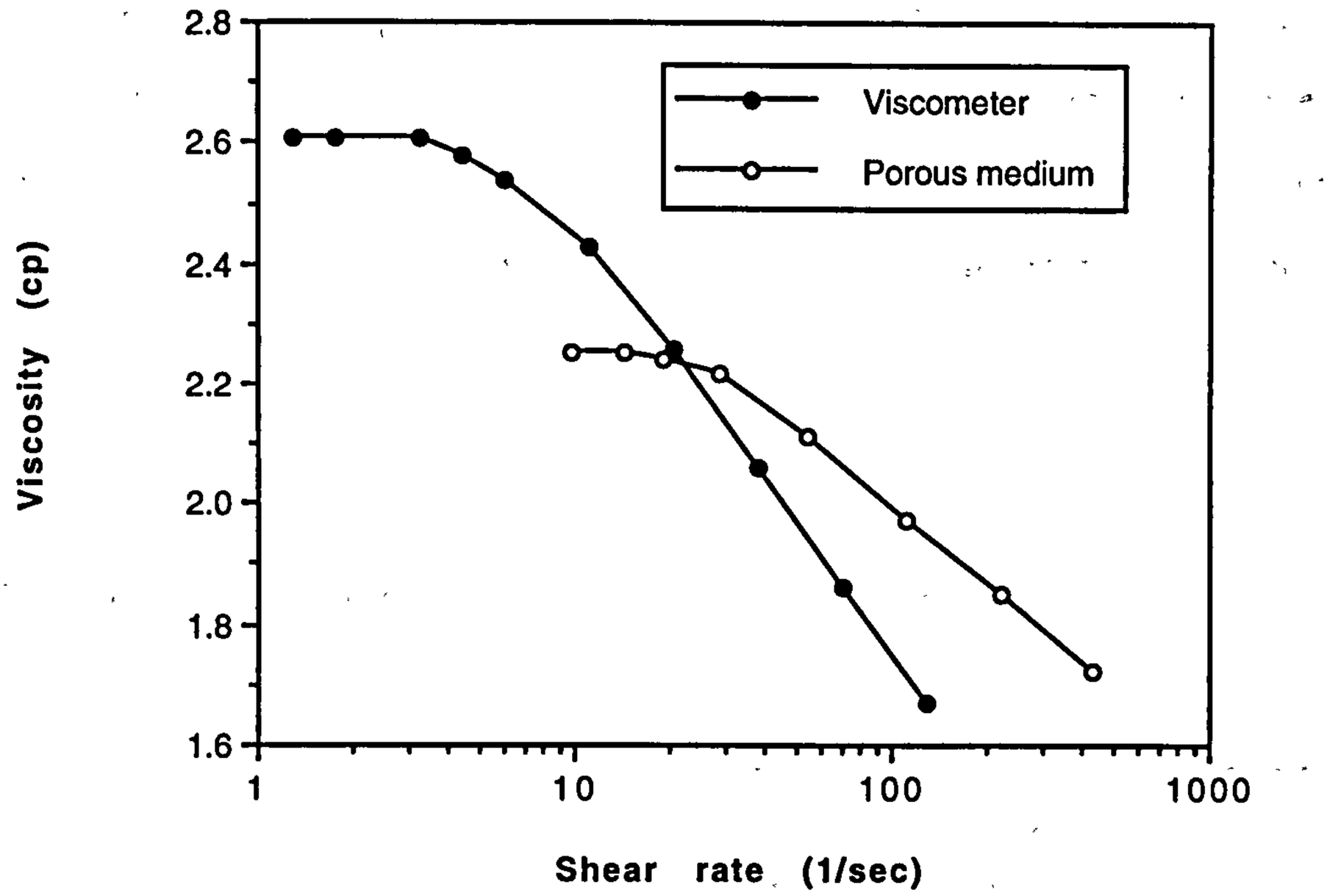

Figure 7.12 The comparison of bulk and in situ apparent viscosities for 100 ppm scleroglucan solution

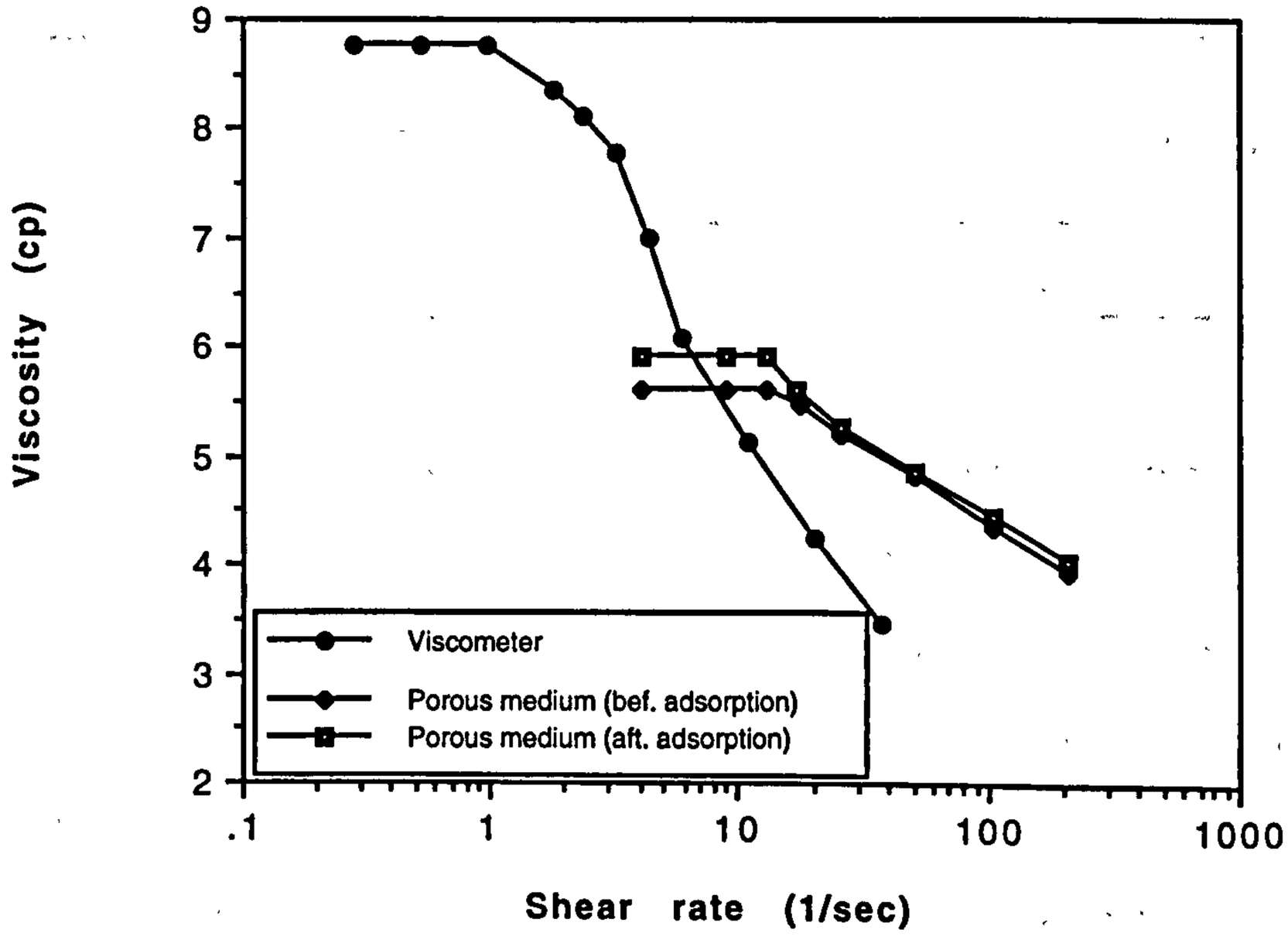

Figure 7.13 The comparison of bulk and in situ apparent viscosities for 200 ppm scleroglucan solution

results reported by Cannella et al (1988). Using the average permeability after adsorption (k = 0.94 D), for the whole range of the experimental shear rate region, almost the same in situ and bulk Newtonian plateau values of apparaent viscosity are found. In our view, the most reliable values of apparent viscosity are obtained by considering the actual (varying) in situ permeability at various flow rates. However, we recommend that further work be carried out on this flow rate dependent behaviour.

Table 7.2

Relative Depleted Layer Thickness (δ/r) of Scleroglucan in Porous Media
- Concentration and Adsorption Effects

Conc. (ppm)	η_b (cp)	η_{app} (cp)	δ/r (TF-A1)	δ/r (TF-A2)	δ/r (LL-A3)	Condition
50	1.84	1.62	0.158	0.189	0.124	After full adsorption
70	2.22	1.96	0.109	0.132	0.085	
100	2.61	2.25	0.111	0.111	0.082	
200	8.76	5.60	0.271	0.196	0.107	
50	1.84	1.63	0.147	0.179	0.117	Before full adsorption
70	2.22	1.97	0.104	0.126	0.081	
200	8.76	5.92	0.210	0.167	0.090	

The relative depleted layer thickness, (δ/r), has been calculated using the "two fluid" and "linear layer" analytical models of the depletion layer as discussed extensively in previous chapters. The calculated values for the scleroglucan solutions at various concentrations in the ballotini packs before and after full adsorption are presented in Table 7.2. The results using these analytical models are also compared in Table 7.2. For scleroglucan, it appears that the relative depleted layer thickness, (δ/r), is virtually constant over the concentration region studied here (50 - 200 ppm) as shown in Figure 7.15. This contrasts with the corresponding results for xanthan in situ rheological behaviour. For xanthan, (δ/r) is *apparently* markedly higher in the low concentration region (25 -

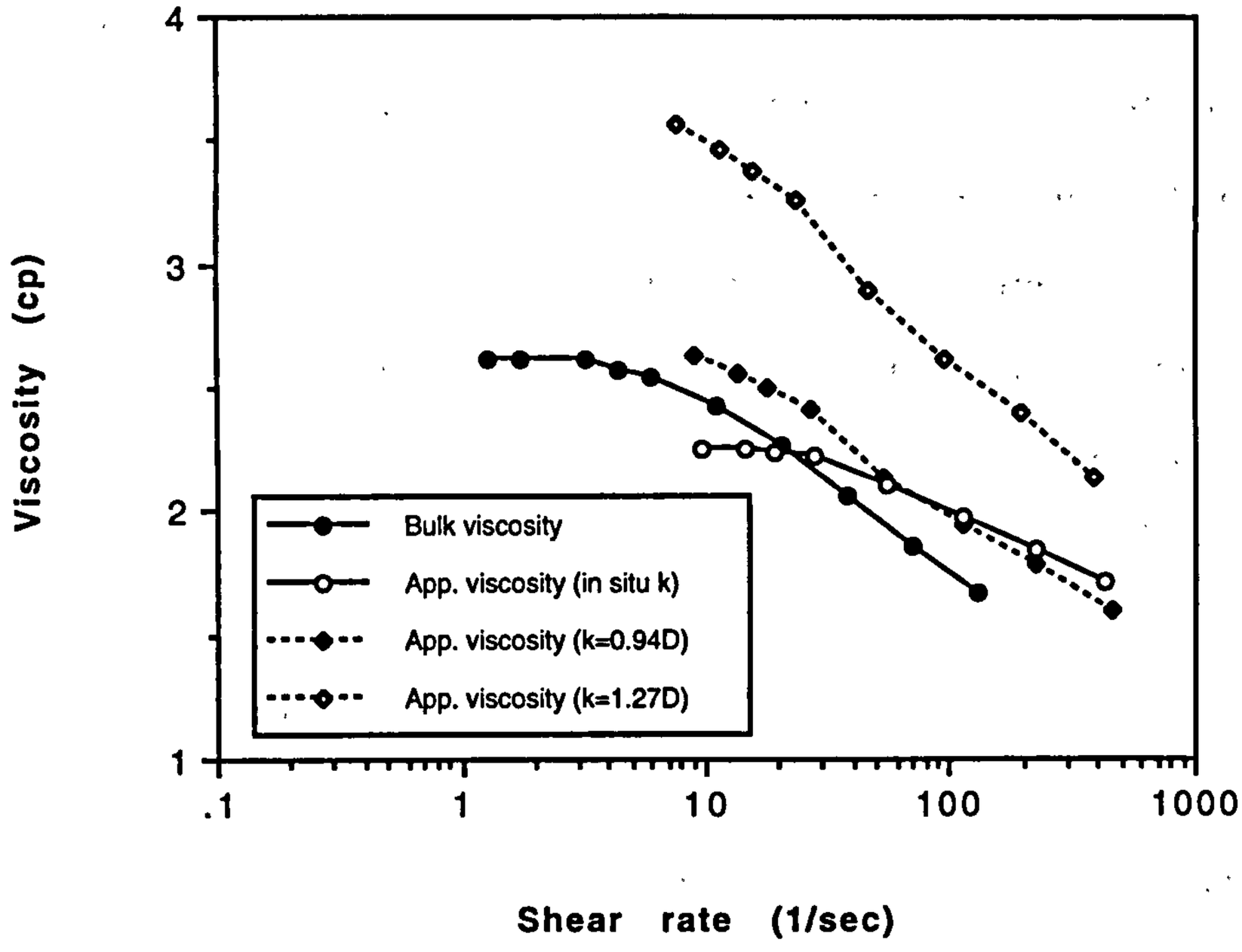

Figure 7.14 In situ permeability effect on apparent viscosity value

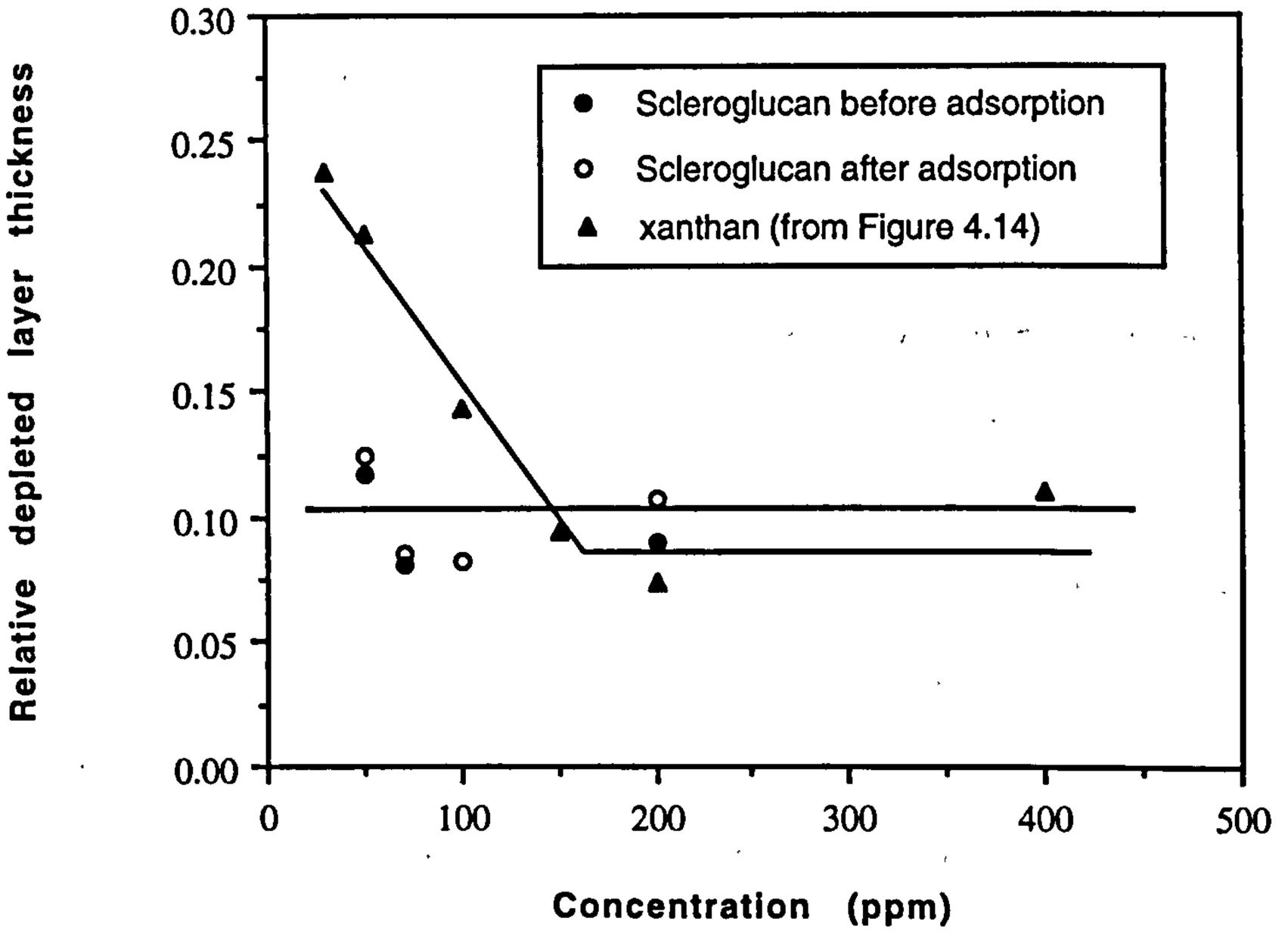

Figure 7.15 A comparison of relative depleted layer thickness for scleroglucan and xanthan

150ppm) and tends to level off at concentrations above 150 ppm as shown in Figure 7.15. An explanation and model for this phenomenon is currently being developed (Huang et al 1993, Appendix B). The data in Table 7.2 and Figure 7.15 also indicates that the value of (δ/r) for scleroglucan is very close before and after dynamic adsorption at each concentration which is consistent with the behaviour observed for xanthan as reported in Chapter 6.7. The concentration effect on (δ/r) for scleroglucan is demonstrated in this work using data for four concentration values and further experiments should be performed in order to verify the conclusion presented here.

7.2.3 pH Effect on In Situ Rheology

We noted above that both xanthan and scleroglucan biopolymers possess a number of similar characteristics. However, they also display some distinctly different properties due to differences in their molecular conformations and ionic characteristics. One property which arises quite directly from the contrasting molecular properties of these two species, is their rheological behaviour as a function of solution pH. In Chapter 5, it has been shown that the pH effect on xanthan rheological behaviour is very obvious, especially in the low pH regime. In this section, we present results on the effect of pH on the rheological behaviour of scleroglucan.

The scleroglucan solution used in these experiments has a concentration of ~ 70 ppm and salinity 20 g/l NaCl. The bulk viscosity of this solution is ~ 2.2 cp, which, for comparison, is close to the viscosity of 100 ppm xanthan solution at salinity 35 g/l NaCl. The pH values of the scleroglucan solutions used are pH 7 and pH 1.2, respectively. The polymer injection sequence is the same as in the first flooding stage described in section 7.2.1. After full polymer breakthrough (about 2 pore volume injection), the apparent viscosity of the polymer solution in the porous medium was measured at a range of flow rates. The pack was then shut in for 5 days and, after reopening, a further 2 pore volumes of polmer was injected and the in situ rheology was remeasured over the same range of flow rates. Figure 7.16 shows the experimental results for the in situ apparent

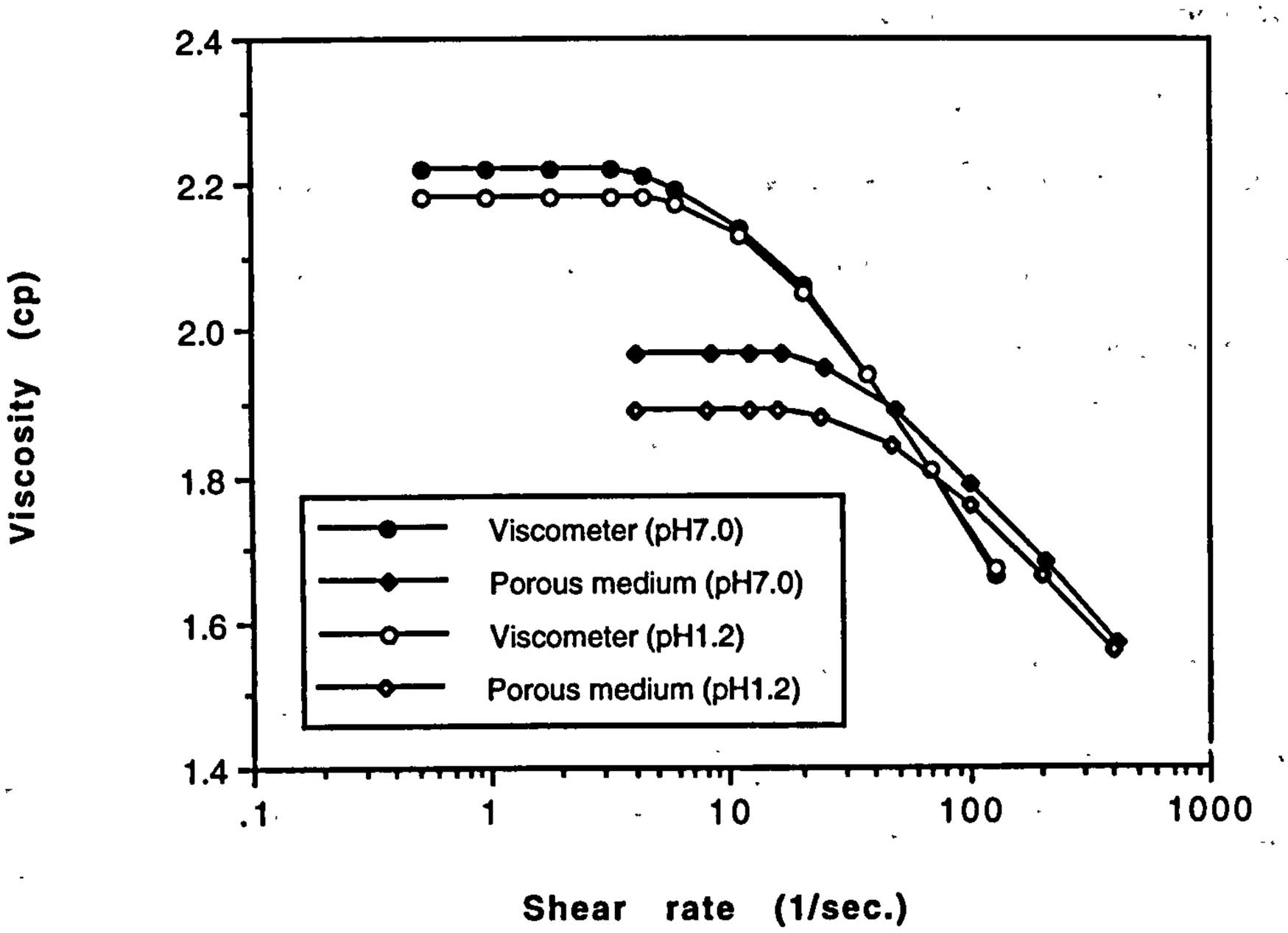

Figure 7.16 The comparison of 70 ppm scleroglucan rheological behaviours at pH 7.0 and pH 1.2

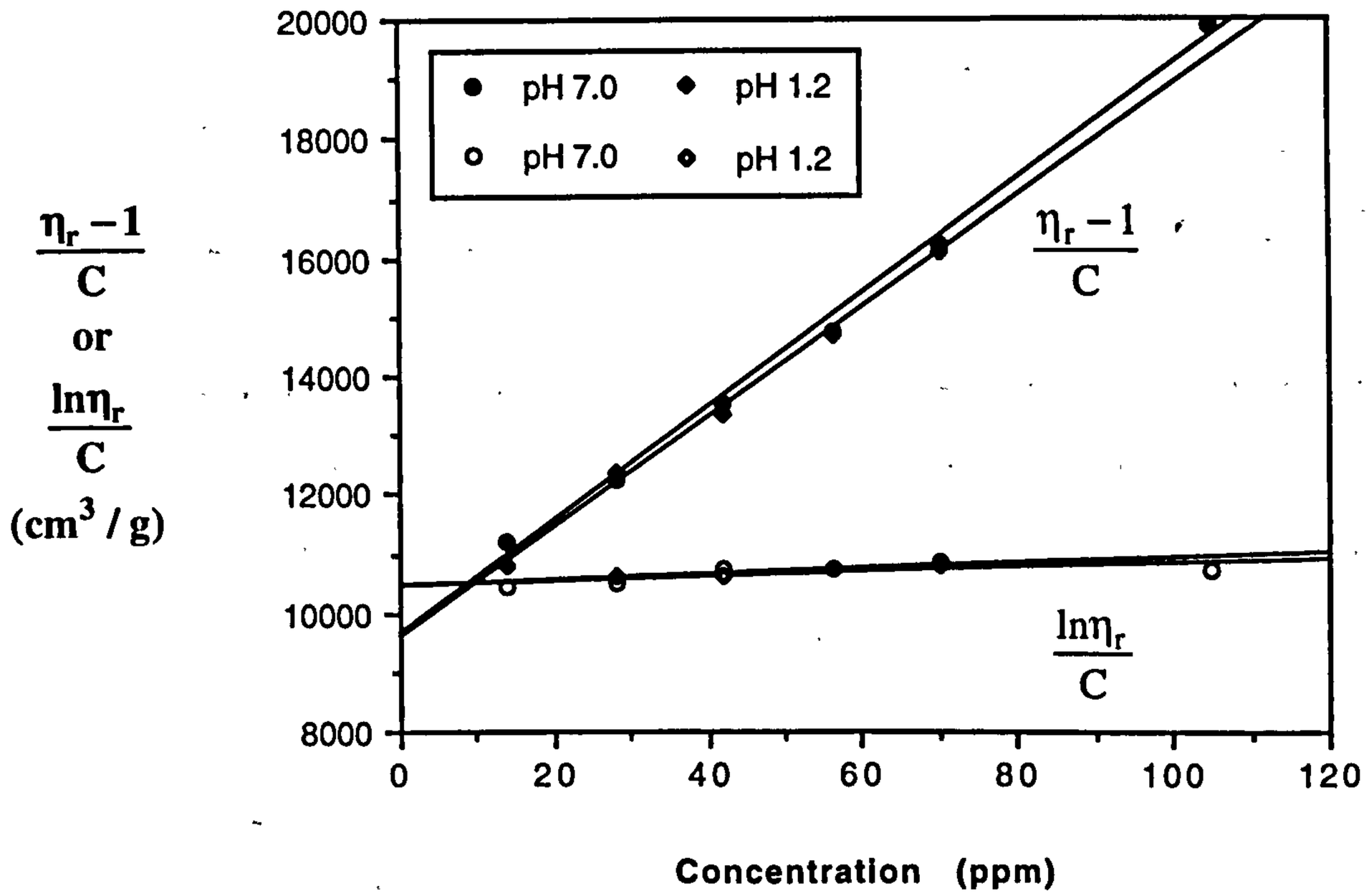

Figure 7.17 Scleroglucan intrinsic viscosities at pH 7.0 and pH 1.2

viscosity and bulk viscosity for pH 1.2 and pH 7 scleroglucan solutions. The experimental data for scleroglucan are shown and are compared with those for xanthan in Table 7.3. Note that the in situ Newtonian apparent viscosity obtained is below the bulk value as measured in a viscometer which we again interpret as being due to a surface exclusion/depleted layer effect. However, it is also interesting to note that the data and the plots of the apparent viscosity curves for the two pH values appear to be very similar i.e. there is not a major effect of pH on the scleroglucan in situ rheology.

Table 7.3

The In Situ Newtonian Apparent Viscosity of Biopolymer Solutions

Polymer solution	pH	Condition	η_b (cp)	η_{app} (cp)
Scleroglucan 70 ppm in 20 g/lNaCl	1.2	before shut in	2.18	1.89
	1.2	before postflush	2.14	1.85
	7.0	before shut in	2.22	1.97
	7.0	before postflush	2.22	1.96
Xanthan 100 ppm in 35 g/l NaCl	1.2	no shut in	1.55	1.49
	7.0	before shut in	2.17	1.87
	7.0	before postflush	2.22	1.89

The corresponding experimental data on the relative depleted layer thickness, (δ/r), are shown in Table 7.4 where the scleroglucan results are compared with those for xanthan. It can be seen that the low pH (~ 1) effect both on the bulk and in situ Newtonian viscosities is much smaller for scleroglucan solution than for xanthan. At low pH, the molecular structure or conformation of scleroglucan shows no significant change and the exclusion between polymer molecules and pore wall is not affected by the change of surface charge on the pore wall as might be expected from the non ionic character of this molecule. This conclusion is further supported by the results in Table 7.4 on the intrinsic viscosities, $[\eta]$, of the various scleroglucan and xanthan solutions at both low and normal

pH. Figure 7.17 also illustrates the intrinsic viscosities of scleroglucan solution at both very low and normal pH. A constant value for scleroglucan is found with changing pH which is very different from the behaviour of xanthan. These results are thus due to the totally non-ionic character of the scleroglucan molecule.

Table 7.4

The pH effect on depleted layer thickness of biopolymer solution

Polymer	Intrinsic viscosity (cm^3/g)	pH	Condition	δ/r TF model [A1]	δ/r TF model [A2]	δ/r LL model [A3]
scleroglucan	10,000	1.2	before shut in	0.134	0.152	0.102
	10,000	1.2	before postflush	0.142	0.156	0.108
	10,000	7.0	before shut in	0.104	0.126	0.081
	10,000	7.0	before postflush	0.109	0.132	0.085
xanthan	3,600	1.2	before postflush	0.057	0.077	0.051
	6,300	7.0	before shut in	0.148	0.177	0.112
	6,300	7.0	before postflush	0.159	0.192	0.118

7.3 Sand Packed Columns

7.3.1 Transport and Retention

The work reported above was carried out in ballotini glass bead packs which were fairly homogeneous and had relative high permeability. In this section, some results from floods in sand pack systems are presented. The scleroglucan solution in these experiments has a constant 100 ppm concentration in 20 g/l NaCl salinity brine.

Three samples of smaller size sands, from Sifraco, were used in this work and the properties of these are listed in Table 7.5 where they are compared with the ballotini used previously. Figure 7.18 shows typical data on the particle chemical composition, size, distribution, and specific surface area, etc of the C7 sand sample which indicates a much wide size distribution compared with that shown for ballotini glass beads in Figure 3.4.

Table 7.5

The Permeability Change of Sand Pack in Scleroglucan Flooding

Sample No.	Average size (μm)	Specific surface area (m2/g)	Permeability (initial k_0) (mD)	Permeability (final k) (mD)	PRF (k/k_0)
C4	53	0.15-0.18	300	57.4	0.19
C7	30	0.20-0.35	61.2	8.45	0.14
C10	19	0.35-0.40	22.6	~3	0.13
Ballotini	52	0.123	1270	894	0.70

It is interesting to compare the properties of the C4 sand sample in Table 7.5 with ballotini; although they have same average particle size and very similar specific surface areas (SSA), their initial brine permeabilities are different by a factor of ~4. This implies that these sand filled column had a much closer packing than ballotini pack due to the wide size distribution. This may affect the polymer transport behaviour in porous media of this type.

The experimental polymer flooding cycle was similar to that described above. However, in some cases, we had to reduce the injection flow rate in order to keep the experimental column at safe operating pressures. The effluent profiles of polymer and tracer in the C10 and C7 sand packs are shown in Figures 7.19 and 7.20 respectively where very high polymer retention is clearly observed. The polymer was detected 3 PV beyond the tracer and it then kept at a very low concentration level in the effluent; for example, about 30 % of the bulk concentration for the C10 pack (Figure 7.19) and 55 % of the bulk

composition chimique (Fluo. X)

SiO_2	sup. à	99,3	%
Fe_2O_3	inf. à	0,025	%
Al_2O_3	inf. à	0,33	%
CaO	inf. à	0,023	%
K_2O	inf. à	0,28	%
TiO_2	inf. à	0,022	%

réactivité acide-base ..... inerte

caractéristiques physiques

densité réelle (Pycnomètre)	2,65
dureté (Mohs)	7
indice de réfraction	1,54 à 1,55
densité apparente ("Proctor")	≈ 1,00
surface spécifique ("Blaine")	2000 à 3500 cm²/g
absorption d'huile (ISO 787/5 - 1980)	≈ 21,4 g/100 g
humidité (sortie usine)	maxi 0,05 %
perte au feu (à 1000° C)	maxi 0,1 %
pH	7 à 8
blancheur ("Garner")	≈ 77 à 81

GRANULOMETRIE MOYENNE STATISTIQUE

(Valeurs indicatives)

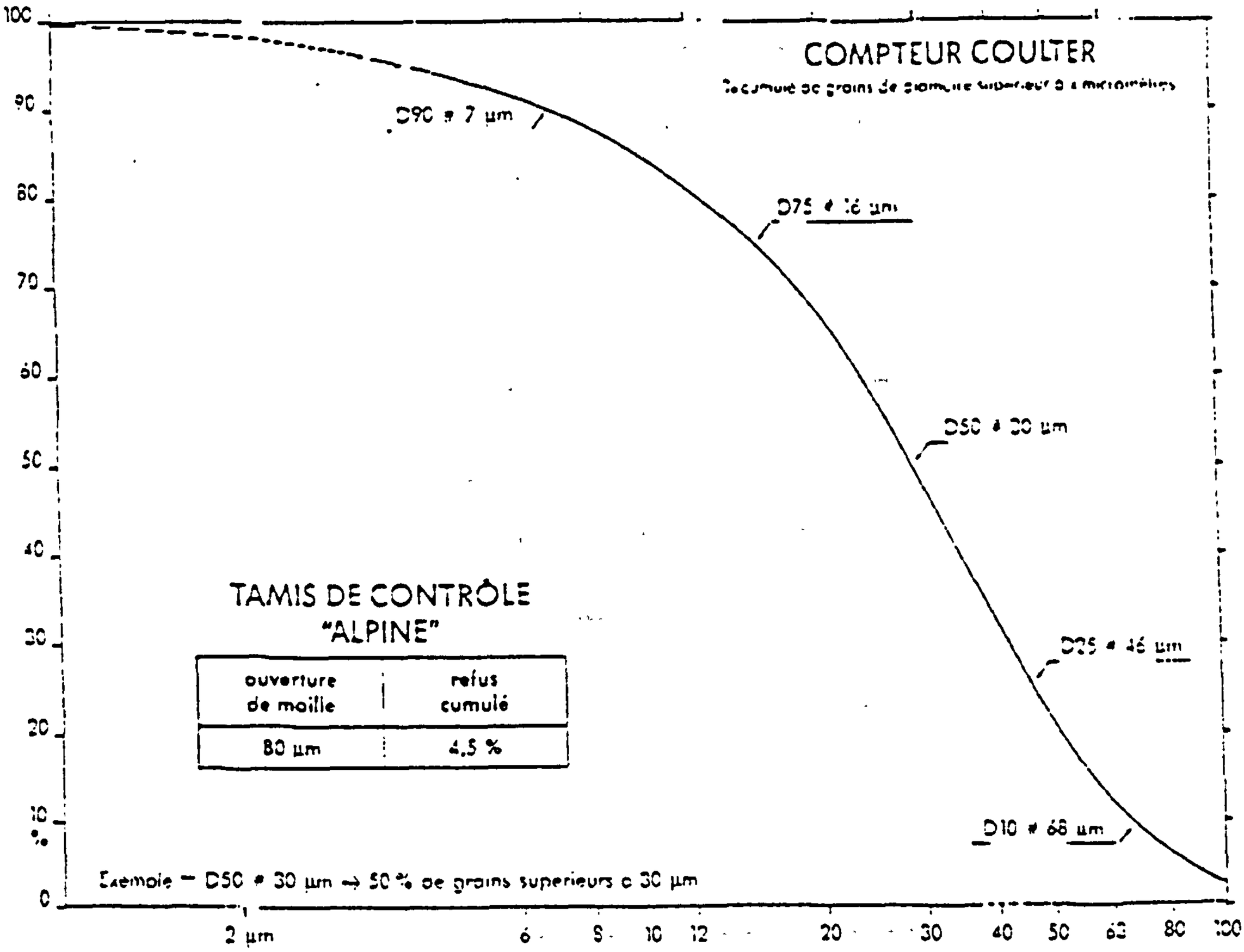

TAMIS DE CONTRÔLE
"ALPINE"

ouverture de maille	refus cumulé
80 µm	4,5 %

Exemple — D50 ≈ 30 µm → 50 % de grains supérieurs à 30 µm

Figure 7.18 The particle chemical composition, size, distribution, and specific surface area for C7 sand sample supplied by Sifraco

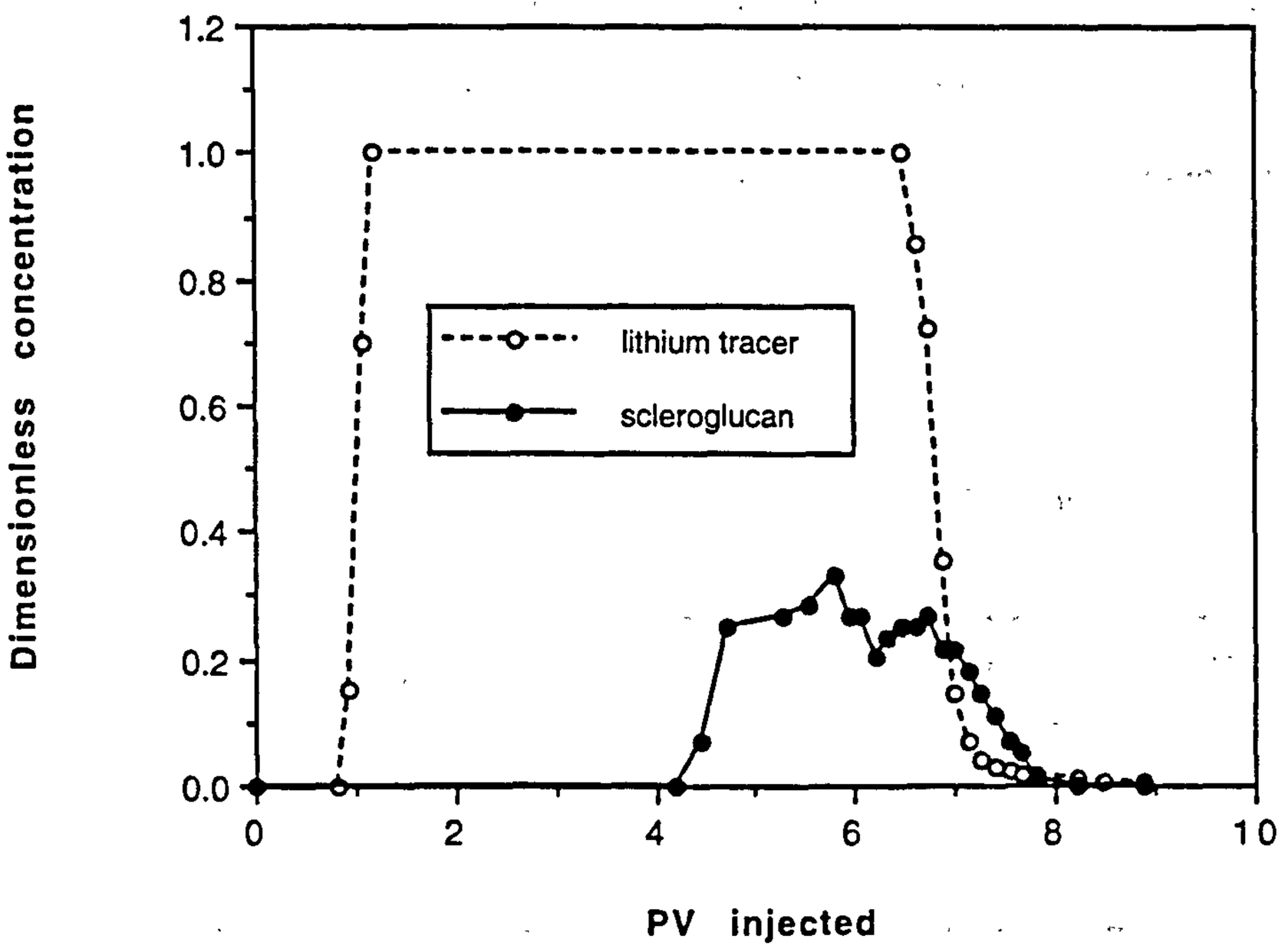

Figure 7.19 The effluent profiles for 100 ppm scleroglucan solution through C10 sand packed column

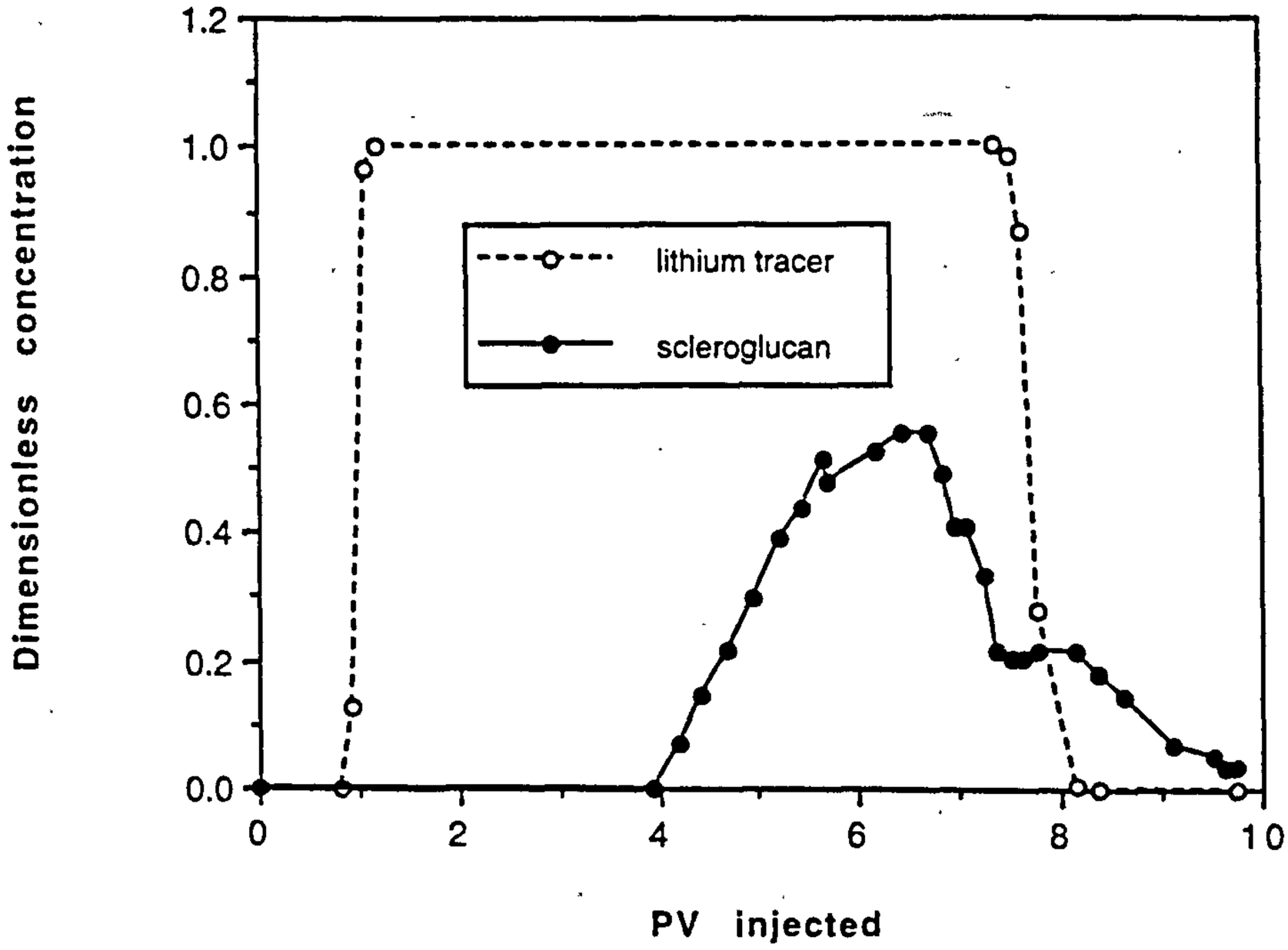

Figure 7.20 The effluent profiles for 100 ppm scleroglucan solution through C7 sand packed column

concentration for the C7 pack (Figure 7.20). In these packs, the polymer never reached full (100 %) breakthrough concentration before the columns were damaged. After brine postflush, the permeabilities for both the C10 and C7 packs were again measured. The C10 pack was almost plugged and the permeability of the C7 pack was severely reduced as shown in Table 7.5.

Table 7.6

Scleroglucan Retention in C7 Sand Packed Column

Section No.	Column region from inlet	Sand weight (g)	Supernatant viscosity (cp)	Total mass of polymer loss (μg)	Apparent adsorption (μg/g)
1	0 - 0.203	13.43	2.55	1121.4	83.5
2	0.203 - 0.393	12.59	2.26	910.0	72.3
3	0.393 - 0.587	12.84	1.58	486.5	37.9
4	0.587 - 0.784	13.06	1.33	286.7	22.0
5	0.784 - 1	14.30	1.13	90.2	6.3
Total	0 - 1	66.22		2894.8	43.7

Finally, each packed column was dismantled and sand samples were collected at several locations along the pack. Each collected fraction was then immersed in brine at a solid/liquid ratio 1/1 (by weight) for a few days; the supernatant fluid was then withdrawn and the viscosity of each sample was measured. Figure 7.21 shows one of the results for a pack made up of sand sample C7 and further data is presented in Table 7.6. The experimental results indicate quite clearly that significant retention occurs closer to the inlet section of the pack. The viscosity of the supernatant from the treatment of the sand from the inlet section is as high as the bulk polymer viscosity, and the viscosity from the sand at the outlet section is much closer to brine viscosity. Thus, it appears that this sample of scleroglucan shows poor filterability in these low permeability sand packs at room temperature. A lower bound estimate of the apparent polymer retention level is

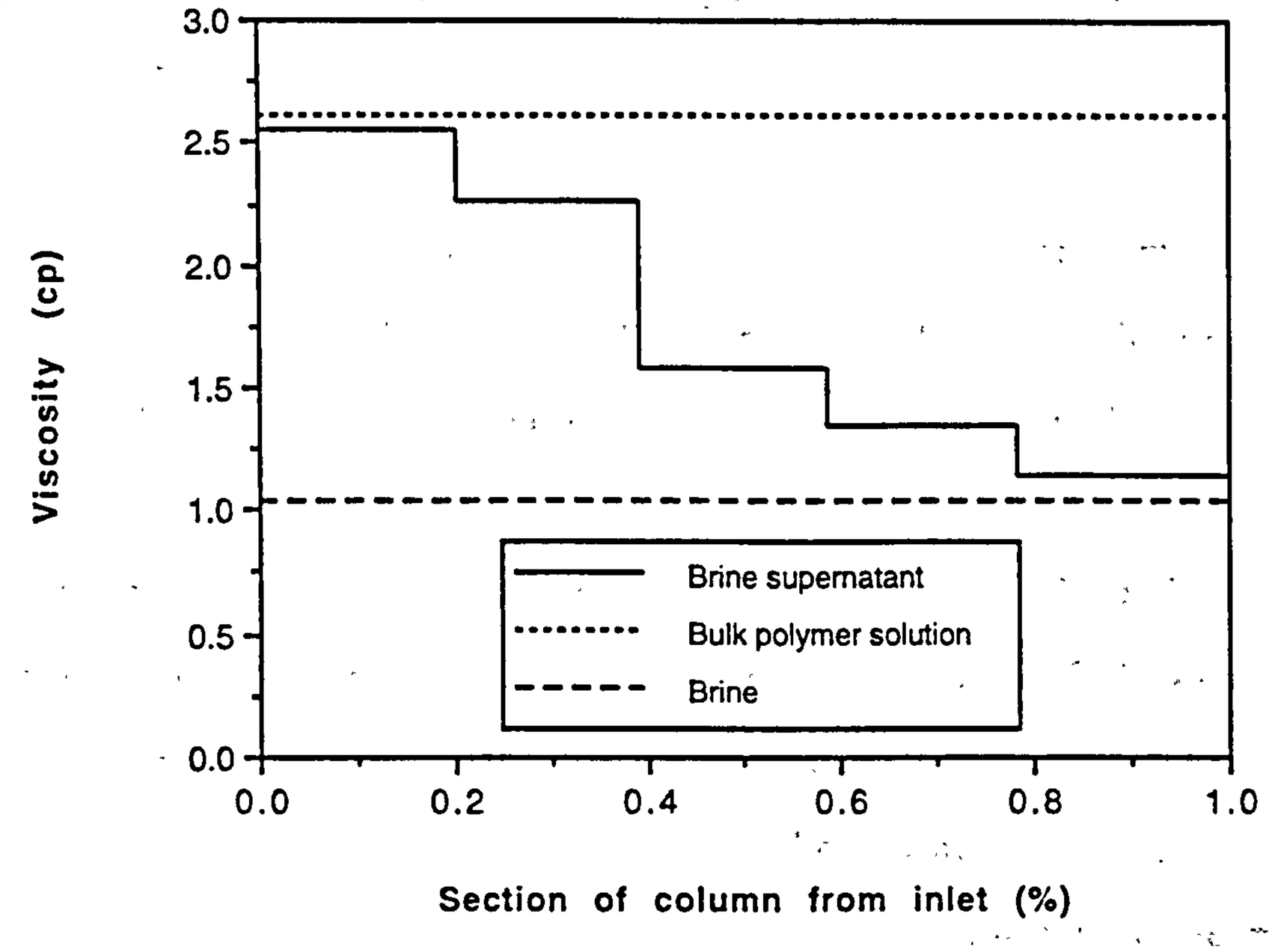

Figure 7.21 Scleroglucan retention in different sections of C7 sand packed column

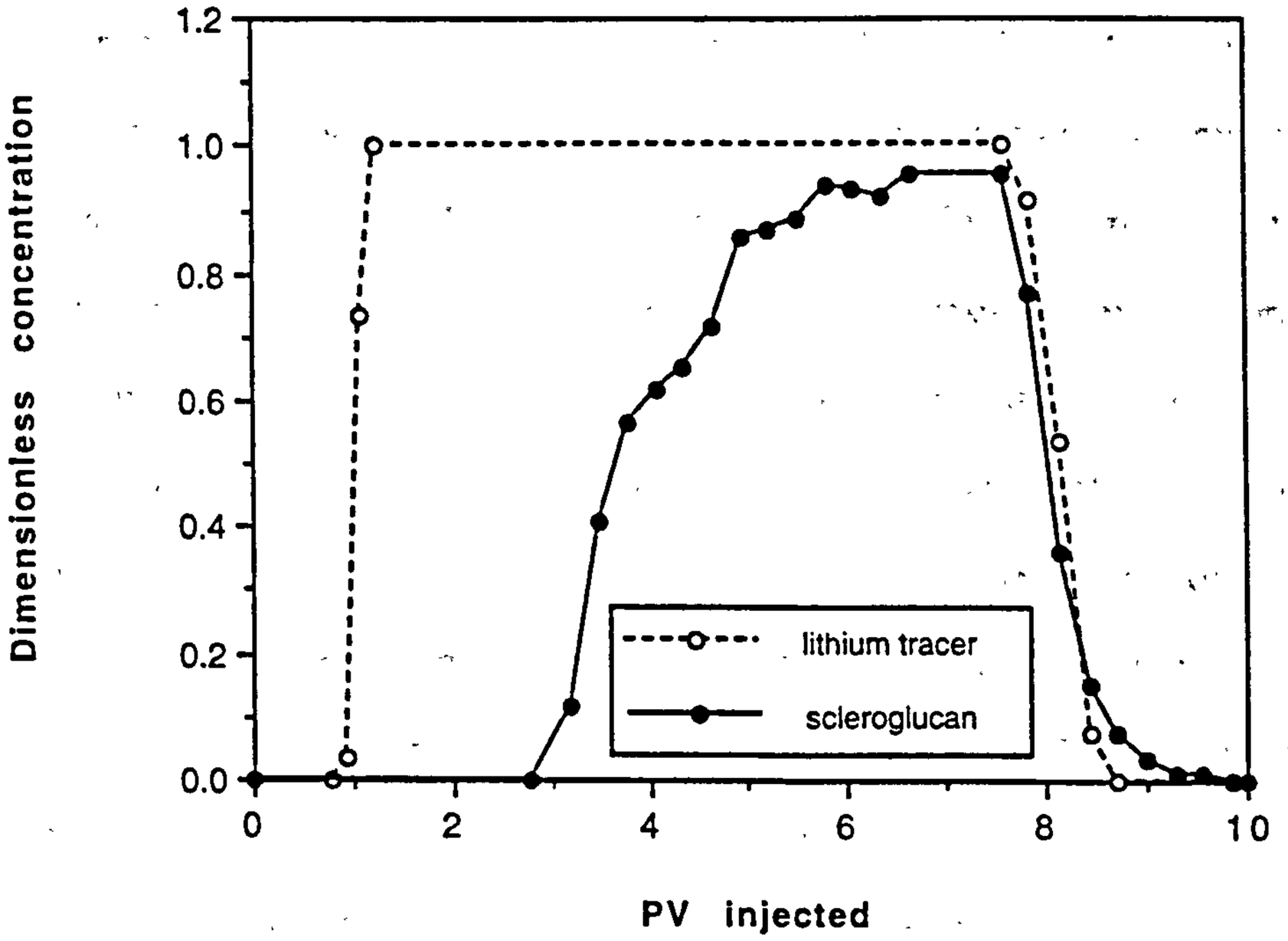

Figure 7.22 The first effluent profiles for 100 ppm scleroglucan solution through C4 sand packed column

listed in Table 7.6 although the real retention level is much higher and unknown. The retention value of ~84 μg/g close to the inlet is extremely high and would be totally unacceptable for field application of polymer flooding.

The packed column made up using the C4 sand sample had a higher permeability (300 mD) than those packs described above. The experimental flood cycle for this pack involved three 100 ppm scleroglucan polymer slugs being injected into the pack. In each stage, polymer injection was carried out until the effluent concentration appeared to be approximately constant and then a brine postflush was performed. The effluent profiles for these floods are shown in Figures 7.22, 7.23 and 7.24. Figure 7.22 shows that initial polymer breakthrough occurred after ~ 2.5 PV injection of polymer solution and reach almost input concentration at ~4 PV of injection. Following the first postflush, the polymer solution was injected again and Figure 7.23 shows that the polymer breakthrough is almost at the same time as for the appearance of tracer which indicates that the most significant adsorption process occured in the first injection stage. Polymer retention is still very obvious in the second polymer injection stage. The brine permeability was measured after the second postflush and it shows a considerable big reduction from the initial permeability as shown in Table 7.5. From this case, it can be expected that continuing polymer injection should cause more serious polymer retention, even if the pack has already reached adsorption saturation. To confirm this, a third slug of polymer solution was injected into the same pack and the resulting effluent profiles are shown in Figure 7.24 for comparison. The largest polymer losses occurred during the first stage of polymer injection. In the third stage, the polymer effluent profile only reached a maximum of ~ 80 % of the injected concentration. It seems that only a fraction of the small size molecules can pass through the high retention pore channels. The final permeability indicates a much lower level as shown in Figure 7.25. After the third polymer injection, the average permeability of the sand pack was about 31 mD compared with 57 mD after the second stage and with an original permeability of 300 mD before polymer flooding. The final brine permeability in this pack again showed a dependence

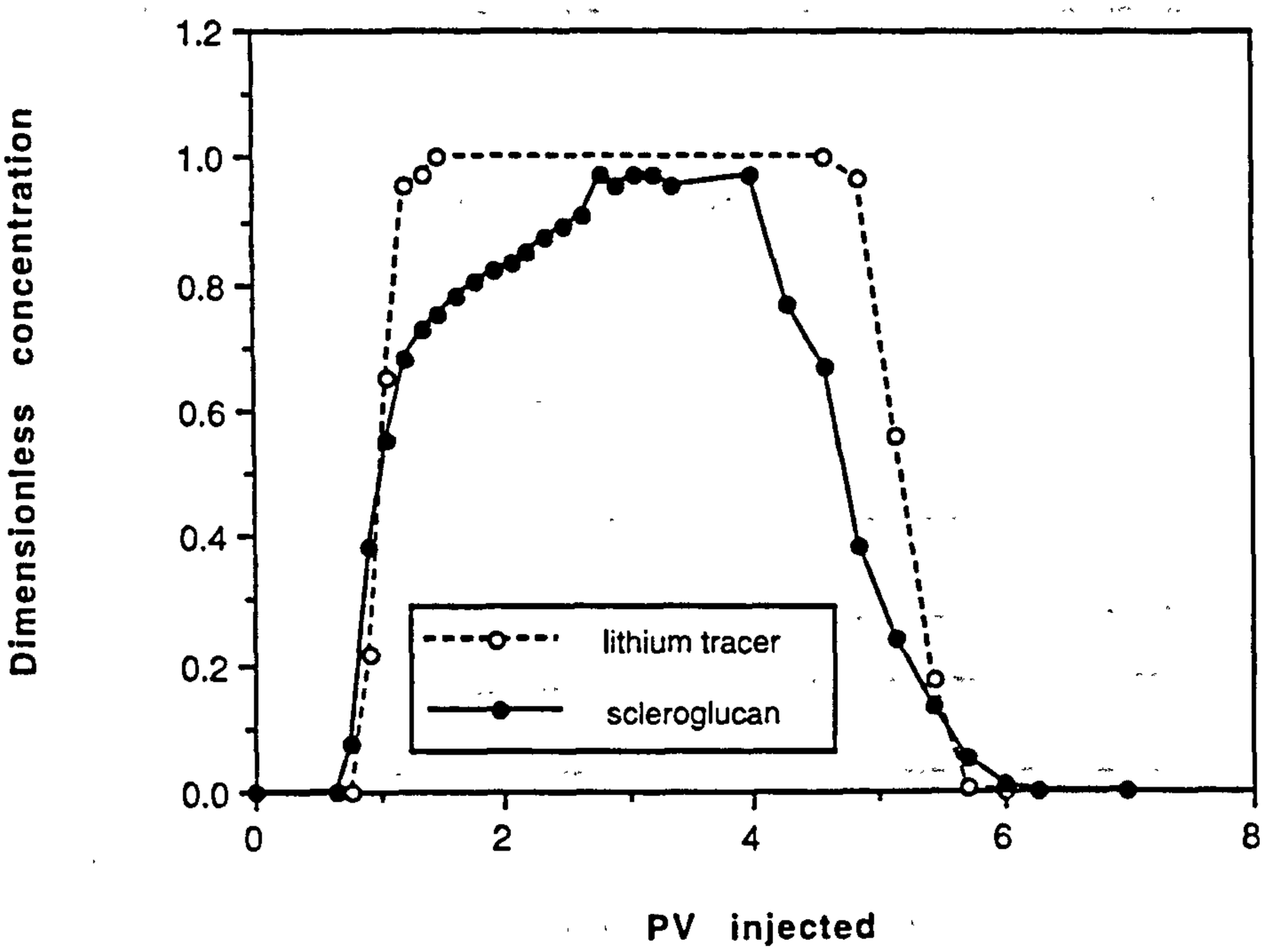

Figure 7.23 The second effluent profiles for 100 ppm scleroglucan solution through C4 sand packed column

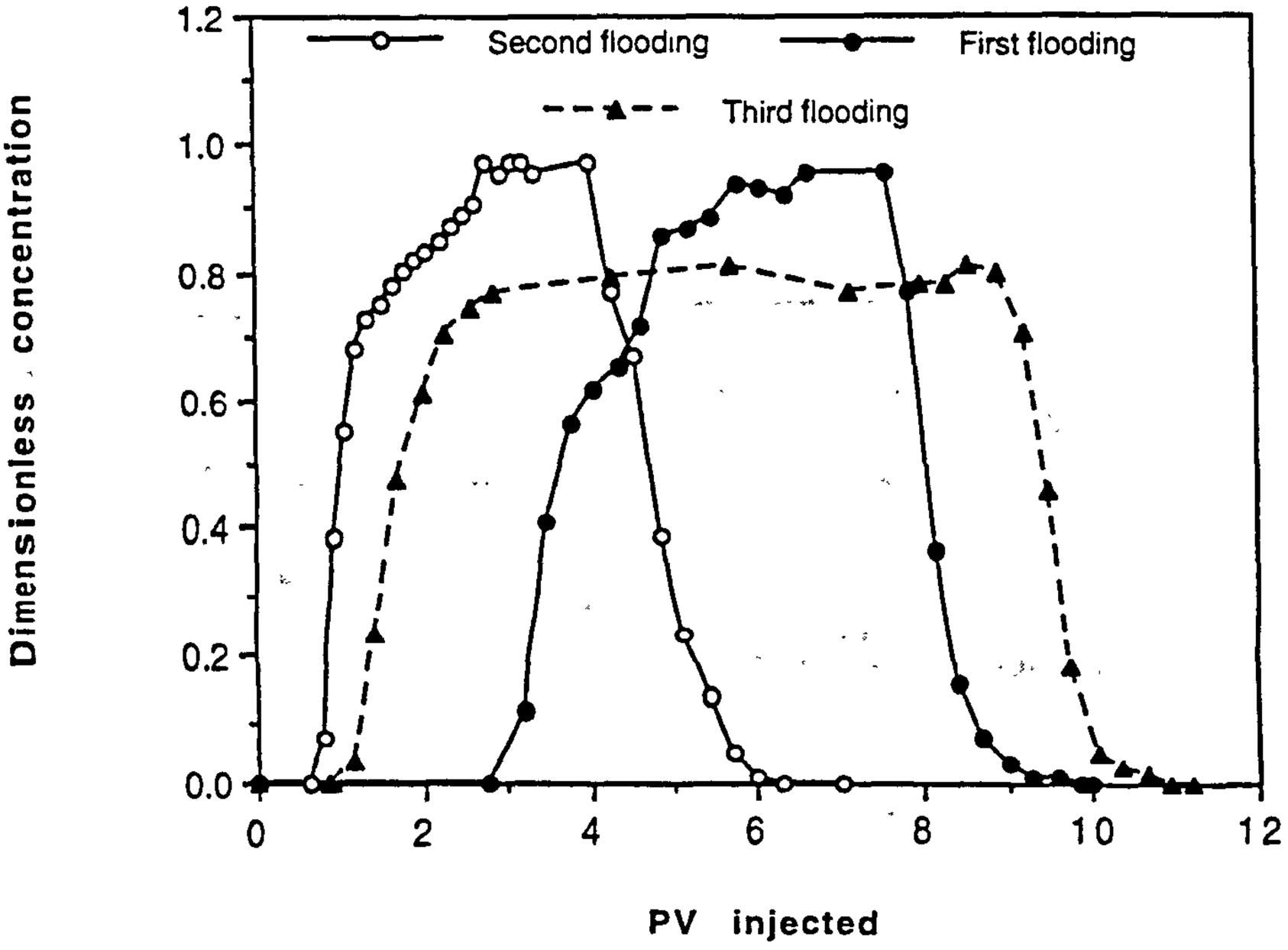

Figure 7.24 A comparison of the three-stage effluent profiles for 100 ppm scleroglucan solution through a C4 sand packed column

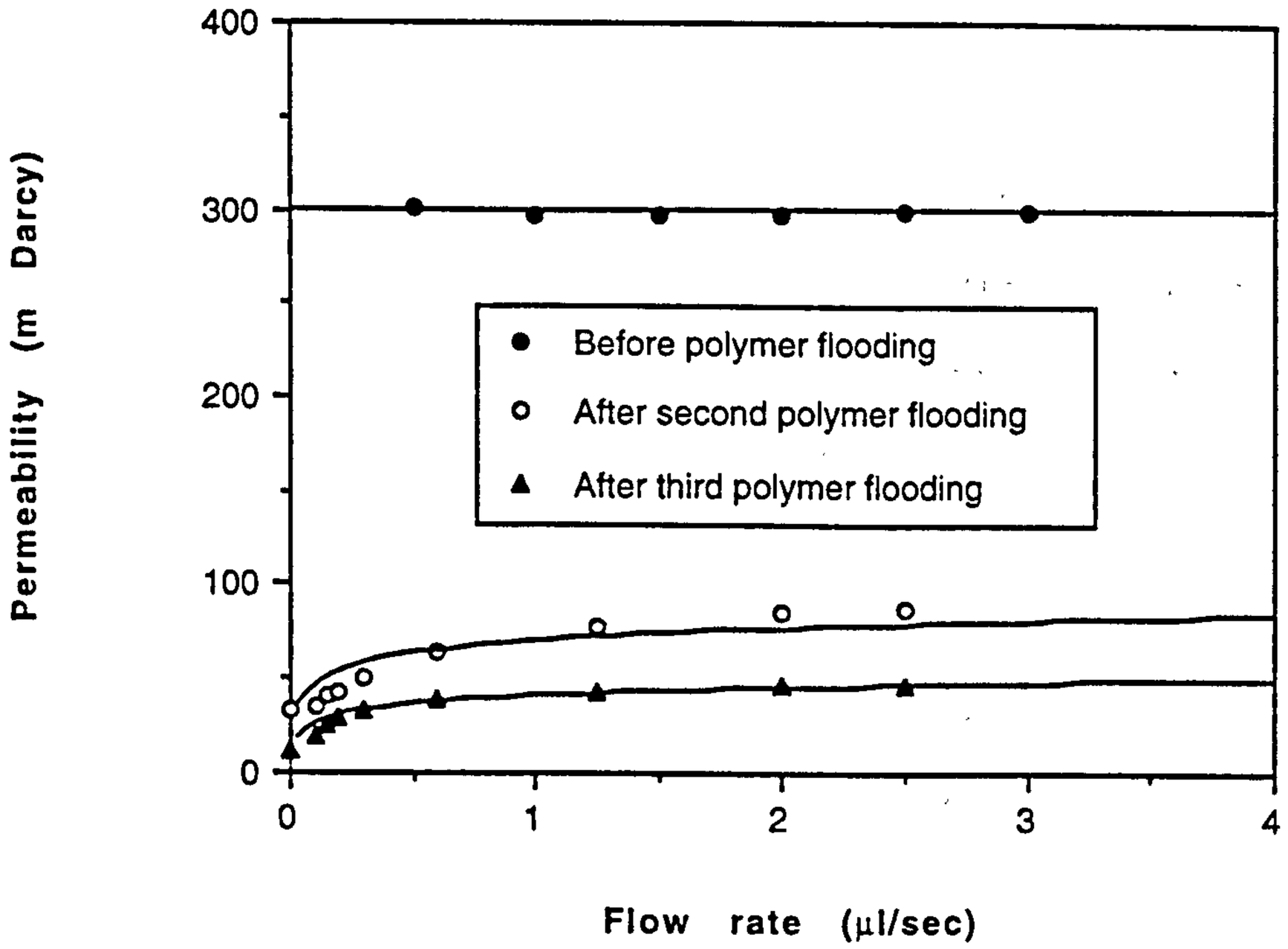

Figure 7.25 Comparison of permeabilities before and after scleroglucan flooding in C4 sand packed column

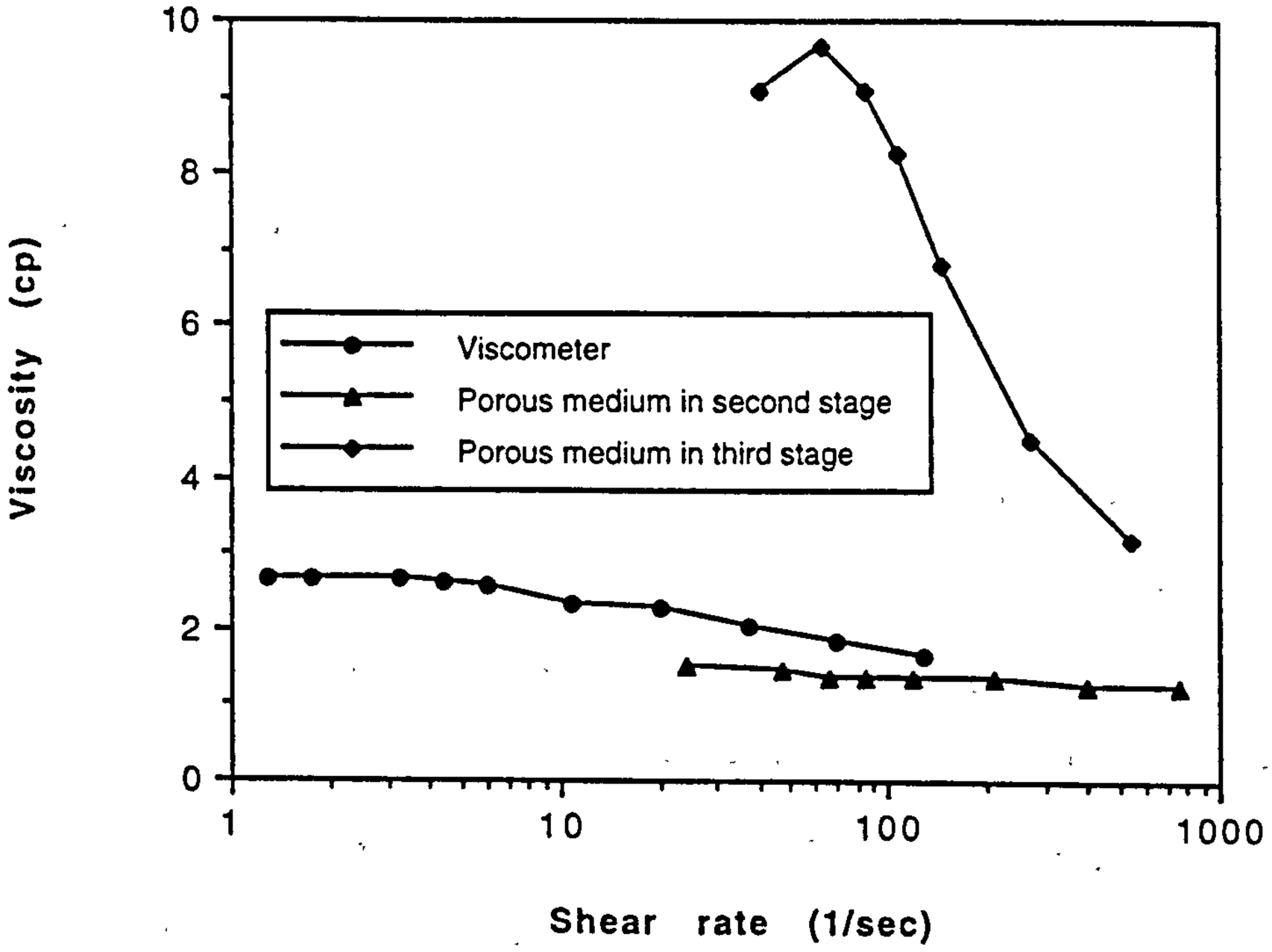

Figure 7.26 A comparison of bulk and in situ apparent viscosities for 100 ppm scleroglucan-C4 sand pack system

on flow rate after polymer flooding which is consistent with the results presented previously in Section 7.2.1.

Comparing the results in this section with those shown in Section 7.2.1, we find that the general adsorption level of scleroglucan is lower and the adsorption effect on the in situ rheology is negligible for relatively homogeneous, higher permeability ballotini packed porous media. However, the behaviour is very different for the lower permeability sand packed porous media where scleroglucan shows very high levels of retention and a clear effect of this retention on polymer in situ rheology is evident. The latter case indicates that there are still concerns on the propagation (filterability) of scleroglucan although these may not be a problem at higher temperatures under field flooding conditions.

7.3.2 In situ Rheology in C4 Sand Pack

Some in situ rheological results for scleroglucan solution flowing through the low permeability/high retention C4 sand packed porous medium are presented here. The in situ apparent viscosity of this polymer solution was measured after the second polymer injection stage, as well as before the final brine postflush (i.e. after the third polymer injection). The data are listed in Table 7.7 and Table 7.8 respectively. A comparison of the in situ apparent viscosity obtained from the calculation using Darcy' law and bulk viscosity measured in the viscometer for 100 ppm scleroglucan solution is shown in Figure 7.26. These results, are not straightforward to understand and explain. They show that, for the Newtonian region, the bulk viscosity is 2.65 cp; the apparent viscosity in the second polymer flooding stage is about 1.4 cp with corresponding effluent viscosity 2.4 cp; and the apparent viscosity in the third stage is around 9 cp with corresponding effluent 2.2 cp. The apparent viscosity in the porous medium appears to be quite low in the second stage but too high in the third. These results are certainly being complicated by the effect of retention and permeability reduction as discussed above.

Table 7.7

Scleroglucan In Situ Rheology after Second Polymer Injection in C4 Sand Pack

Flow rate (µl/sec)	Shear rate (1/sec)	ΔP polymer (mbar)	η_{app} (cp)	ΔP brine (mbar)	k (mD)
2.5	747	1922	1.26	1589	88.1
2.0	610			1324	84.6
1.25	399	1108	1.28	904	77.4
0.6	206	671	1.34	520	64.6
0.3	119	435	1.35	336	50.0
0.2	85.5	336	1.34	260	43.1
0.15	66.5	278	1.37	210	40.0
0.1	47.1	219	1.44	158	35.4
0.05	24.2	121	1.51	83.5	33.5

Table 7.8

Scleroglucan In Situ Rheology after Third Polymer Injection in C4 Sand Pack

Flow rate (µl/sec)	Shear rate (1/sec)	ΔP polymer (mbar)	η_{app} (cp)	ΔP brine (mbar)	k (mD)
2.5	1017			2862	47.5
2.0	814			2288	47.5
1.25	538	5149	3.22	1613	42.2
0.6	269	3787	4.53	844	38.7
0.3	147	3368	6.81	499	32.7
0.2	106	3150	8.24	386	28.2
0.15	84.0	2921	9.08	325	25.1
0.1	62.4	2575	9.67	269	20.2
0.05	40.7	2050	9.07	228	11.9

The best explanation of the above results relates to the influence of pore size on rheological behaviour as shown by Chauveteau et al (Chauveteau and Zaitoun, 1981; Chauveteau, 1982). They found in their study of xanthan flow through fine cylindrical pores that the Newtonian apparent viscosity in these pores is always less than the bulk viscosity and decreases as pore size decreases down to pore size 0.69 μm at which apparent viscosity drops to less than 2 cp compared with a corresponding bulk viscosity of 4 cp. On the contrary, for the smallest diameter pores (0.28 μm), there is no Newtonian plateau and the apparent viscosity increases sharply as shear rate decreases. This was interpreted as being due to the polymer size being larger than the average pore size which then resulted in pore blocking. This is probably what is happening in these experiments and this is supported by the approximate analysis below.

We can roughly estimate the pore size in the sand packs used in this work by using an equivalent capillary bundle model of the porous medium as in Eq. [3.8]. For example, in the second flooding stage (average k ≈ 38 mD), the apparent pore radius is ~ 1.35 μm, a little larger than polymer molecular length where the largest influence of steric hindrance on the polymer molecules is expected to lead to a high slip effect. During the third flooding stage (average k ≈ 19 mD), the pore radius is estimated to be ~ 0.95 μm, a little smaller than the molecular size. Thus, we would expect most of the largest macromolecules to have some difficulty in passing through the pore throats. This would cause an increased pressure drop which should be proportionately higher at lower flow rates. When the shear rate increases, the orientation by shear and elongational flow enables the molecules to pass more easily through the pores.

7.4 Summary and Conclusions

The in situ flow behaviour of the nonionic biopolymer, scleroglucan, has been studied in this work and compared with the anionic biopolymer, xanthan. Experimental results are presented on the transport, retention, and in situ rheology of scleroglucan flow through

ballotini and sand packed porous media. The main conclusions from this work are summarised as follows:

(1) Scleroglucan dynamic adsorption level is higher than xanthan, although it is still quite low in a ballotini pack. The transport behaviour of scleroglucan is clearly affected by the competitive processes of retention and exclusion between the polymer molecules and the pore wall which lead either to a retardation or early breakthrough of polymer relative to tracer.

(2) The effect of concentration on the relative depleted layer thickness, (δ/r), of scleroglucan is much smaller than that of xanthan. This quantity appears to be effectively canstant with scleroglucan concentration.

(3) The low pH effect on both the intrinsic viscosity and in situ rheology (and hence, (δ/r)) of scleroglucan solution is negligible compared with the corresponding effect of pH on xanthan behaviour. This is, as we expect, due to the nonionic nature and triple helix conformation of this polysaccharide.

(4) Scleroglucan shows very high retention levels in low permeability sand packed porous media. This retention process occurs mainly towards the inlet of the packed columns indicating poor filterability of polymer solution at experimental conditions.

(5) The permeabilities both in ballotini and in sand packed porous media appear to be a function of flow rate after polymer flooding. It seems that the final brine permeability decreases with decreasing flow rate especially in the low flow rate regime. This phenomenon is clearly related to the polymer retention but the explanation for this is, as yet, unclear.

(6) The in situ Newtonian apparent viscosity of polymer solution in the C4 sand packed porous medium changes from very low (1.4 cp) to very high (9 cp) compared with

bulk value (2.6 cp) depending on the in situ condition of the porous medium e.g. levels of previous scleroglucan retention.

CHAPTER 8

CONCLUSIONS AND RECOMMEDATIONS

8.1 Conclusions

A wide range of studies relating to several aspects of the flow of biopolymer solution through porous media has been carried out experimentally and analysed theoretically. Nearly one-hundred independent packed column experiments along with many supporting ancillary experiments have been performed and a number of interesting results have been obtained. Results on transport, adsorption, and in situ rheological behaviour of both xanthan and scleroglucan biopolymers within unconsolidated porous media have been presented. These results clearly indicate the existence of a layer depleted in polymer close to the pore wall which results in an apparent slip effect in the observed polymer in situ rheology. The rheological results have been analysed using both a linear layer and a two fluid model for the distribution of the polymer concentration in the region of the pore wall. The behaviour of scleroglucan biopolymer has been compared and contrasted with the behaviour of xanthan.

Many specific technical conclusions from this work are summarised at the end of each chapter. A brief summary of the more important or more general conclusions is presented as follows:

1. The in situ polymer viscosity is usually below the bulk fluid viscosity in the low shear rate Newtonian regime for nearly all cases in the experiments due to a surface-exclusion effect between the polymer molecule and the pore wall.

2. Early breakthrough of the polymer relative to the tracer is clearly visible for most of the experiments because of the presence of a slip effect where the polymer molecules are more likely to pass through the faster streamlines close to the centre of the pore, which is consistent with the results on polymer in situ rheology.

3. The magnitude of the observed slip effect for xanthan is a function of the polymer concentration. It appears that the relative depleted layer thickness, (δ/r), apparently decreases with increasing xanthan concentration over the low concentration range and tends to a constant value at higher concentrations. This observation may be interpreted either by the effect of polymer-polymer interaction at higher concentration or possibly as being due to a wall adsorption effect (Appendix B). However, further work is required in order to understand this observation.

4. The apparent depleted thickness, (δ/r), was found to increase markly with increasing bulk pH of xanthan solution. This result may be interpreted in terms of the pH dependence of the xanthan conformation (charge and molecular size) and the surface charge on the porous medium. It is found that the extension of the xanthan molecule over the lower pH range (1 - 5) contributes more significantly to the thickness of the depleted layer than does the additional electrostatic repulsion at higher pH values.

5. The relative depleted layer thickness, (δ/r), decreases with increasing salinity, which is mainly related to the intrinsic viscosity of xanthan or the stiffness of the molecule. The salinity effect is smaller than the pH effect on the in situ rheological behaviour.

6. The static adsorption level for xanthan is much higher than the dynamic adsorption level measured in the pack floods. Adsorption increases with the decrease in the ballotini solid/liquid ratio. Several theorical models have been proposed to explain

solid/liquid ratio effect on adsorption; the most probable explanation is that it is due to the effect of dissolved species from the particle surface.

7. The effect of xanthan dynamic adsorption on in situ rheological behaviour is not very significant. Experimental results imply that, when xanthan molecules adsorb onto the pore wall, the hydraulic radius of the porous medium is not very significantly affected and, therefore, that the rigid xanthan molecules are adsorbed very flat up against the pore wall.

8. Scleroglucan shows a higher dynamic adsorption level than xanthan in ballotini packed porous media. A delay profile of effluent polymer to tracer in the first polymer injection and a earlier breakthrough of polymer relative to that of tracer are clearly observed due to a competitive effect between attraction and exclusion. For sand packed low permeability systems, the scleroglucan demonstrates very high retention level and poor filterability.

9. The apparent slip effect is still clearly visible when scleroglucan solution flows through ballotini packed porous media. The quantity δ/r is almost constant with scleroglucan concentration unlike the behaviour seen for xanthan. The low pH effect on scleroglucan rheology is negligible, which is very different from the behaviour of xanthan owing to the nonionic nature of the scleroglucan molecule.

8.2 Recommedations for Future Research

Biopolymer solution flowing through a porous medium is a very complicated process even in a well defined pore system such as the ballotini glass bead packed column. Based on the systematic experimental and theoretical studies in this work, some improved understanding of biopolymer flow behaviour in porous media has been obtained. Moreover, several new problems and ideas resulting from this work are proposed for future study.

First, the real mechanism of the polymer concentration effect on rheological behaviour or depleted layer thickness closed to pore wall is still not very clear. The observed apparent slip phenomenon in the above experiments is certainly a result of the wall exclusion or depleted layer effect referred to above. However, the explanation of the concentration behaviour of (δ/r) is still rather speculative. We have previously suggested that this may be due to the higher levels of intermolecular interaction at higher polymer concentrations. However, more recently, an alternative mechanism for the apparent reduction in (δ/r) has been suggested by Chauveteau (private communucation, 1991; 1992) and this is currently being evaluated. A more complicated network model has been developing to solve numerically the problem of rheological behaviour for higher polymer concentration, but this has not been applied.

For pH and salinity effects on polymer in situ rheology, there is probably less argument. More work is suggested on the pH and concentration effects at low salinity (comments from Chauveteau, 1990; Muller, 1991) compared with our previous work at high salinity (35 g/l NaCl). It seems that the change in xanthan conformation appears at higher pH when the salinity is decreased (Zhang et al, 1987) which should affect the in situ rheological behaviour of polymer solution. Also, in the high salinity range, some weak reversible, concentration-increasing polymer adsorption is expected to compete with entropy-driven depletion and to decrease the effective depleted layer thickness with polymer concentration, and at low salinity, the concentration effect may be smaller.

Another problem to be tackled is the study of the action of dissolved species on polymer loss or viscosity loss during xanthan adsorption. A real model for describing the polymer flow behaviour should be devolped to take into account hydrodynamic interactions and the whole competitive process of attraction and exclusion between polymer molecules and pore wall.

Scleroglucan has been investigated here in a preliminary manner. further work should be on this biopolymer to investigate its transport behaviour, adsorption and filtration, in situ rheology in a range of different packed systems. The salinity effect on in situ rheological behaviour should also be investigated although this effect is expected to be small (like the pH effect).

Most of our work on polymer flow behaviour has been performed in ballotini packed porous media which is a relative pure packed system. It is good for simplifing the complicated factors in order to make the studies easier and clearer. For further work, it is very important to work in different sand packed and core systems with various wettabilities and oil saturations. Of course, this is much more difficult job, but much more valuable for oilfield application.

Finally, we are developing a clearer understanding of the fundamental physics of flow of macromolecules through simple porous media in order to use polymer molecules as an actual probe of unknown pore structure and phase distributions through rocks (Sorbie and Huang, 1992c). For example, it is known that polymers interact with the porous medium in a number of ways such as through adsorption or surface exclusion as demonstrated in Figure 8.1 and it has long been suspected that these interactions are functions of wettability. Figure 8.2 and 8.3 shown schematically the flow behaviour of polymers and tracers in two phase flow. It is clear that tracers may be used in each phase to characterise the fluid distribution and flow. The additional use of macromolecules where the size gives us an additional property with which to investigate the size and connectivity of the flow channels. Much further experimental and theoretical work is required on this issue.

As noted above, the depleted layer thickness is a function of both the molecular length, l, (where $l \sim \delta$) and the "pore" radius, r. In fact, the exclusion or depletion zone is a function of how wide the flow channels are in which the polymer molecules are being transported. If, for example as shown in Figure 8.4, polymer were flowing in the aqueous phase in two phase flow in a strongly water wet porous medium, the exclusion

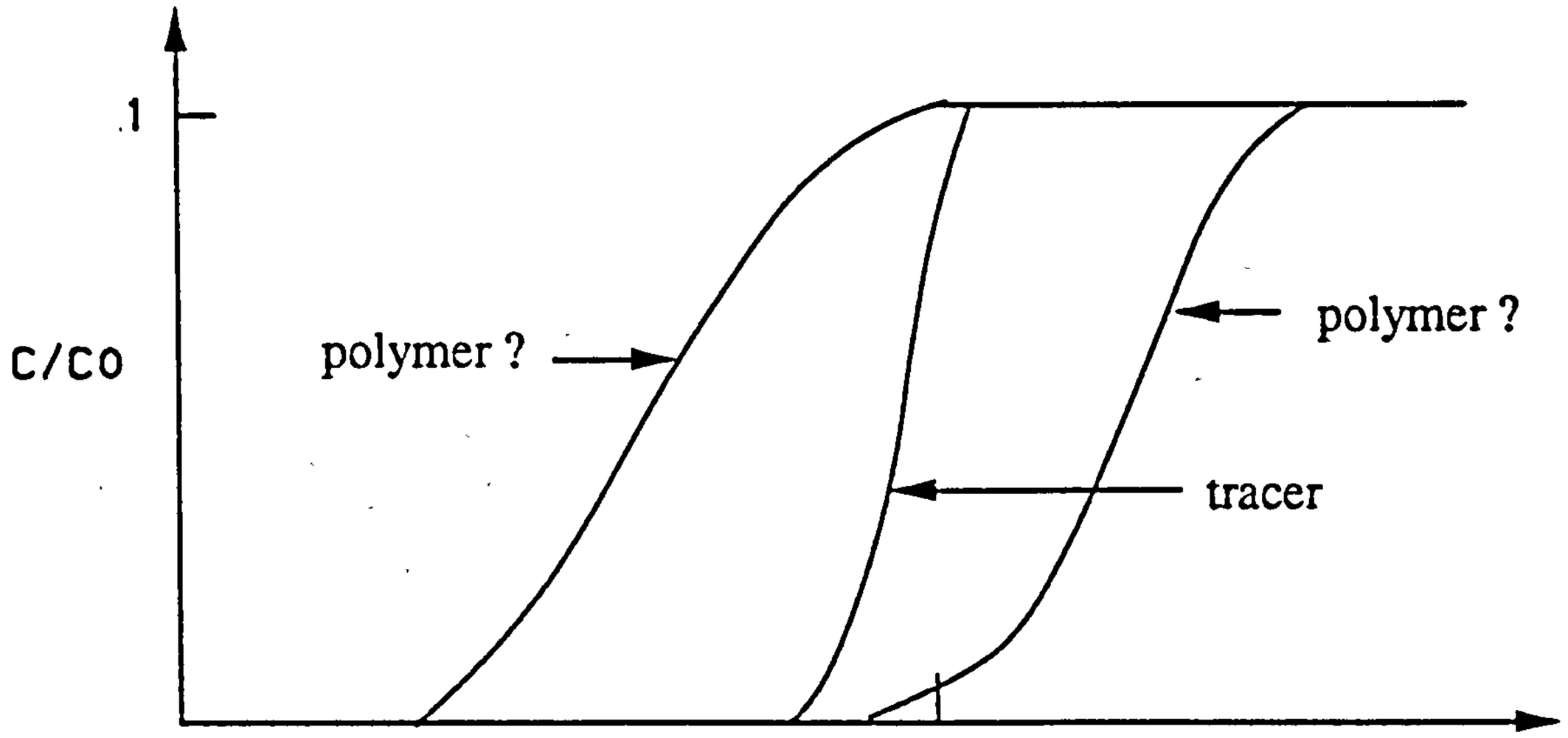

Figure 8.1 A schematical diagram of trecer / polymer transport in two phase flow - effluent behaviours

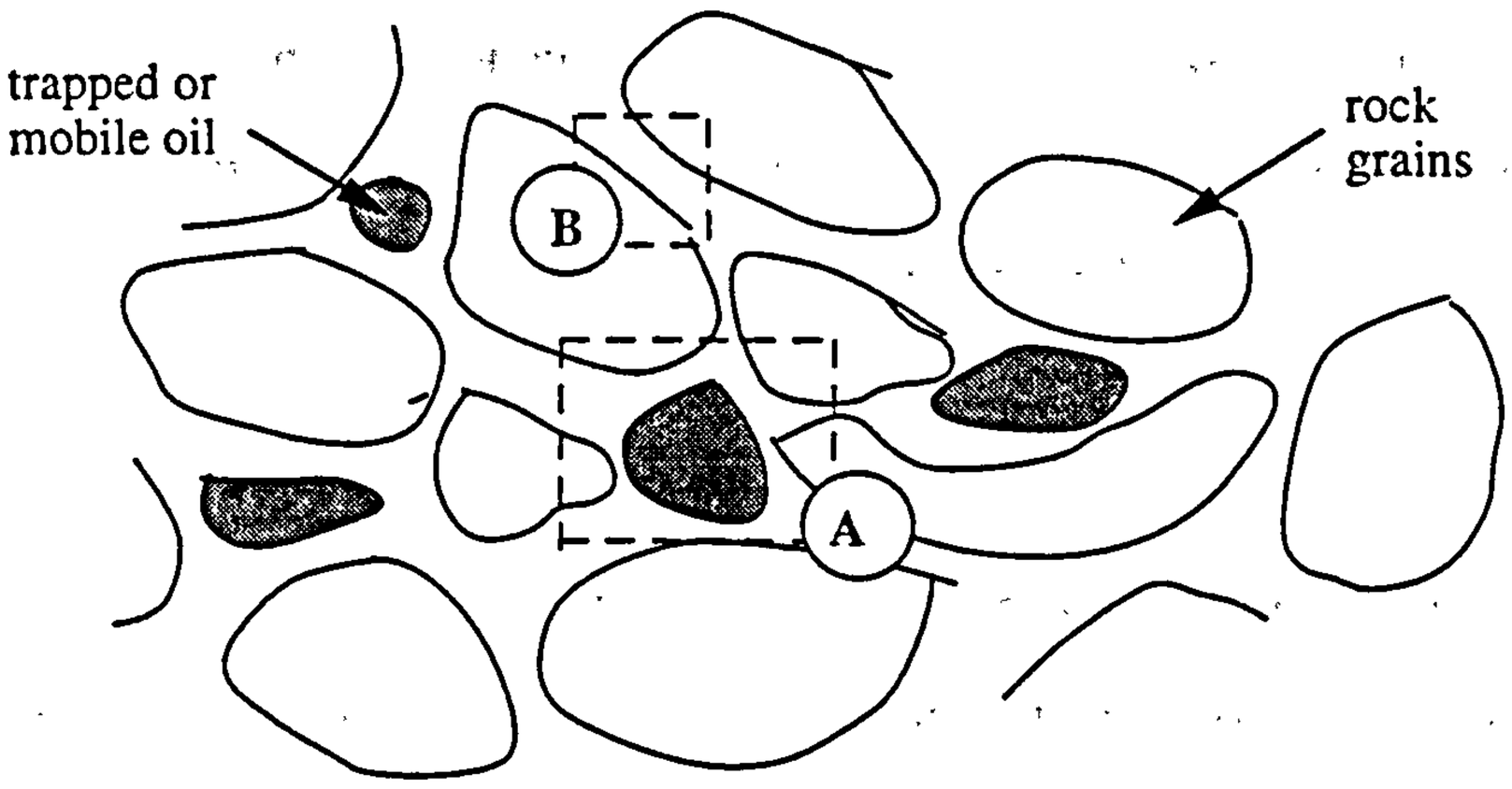

Figure 8.2 Schematical diagram of the porous medium with trapped or mobile oil

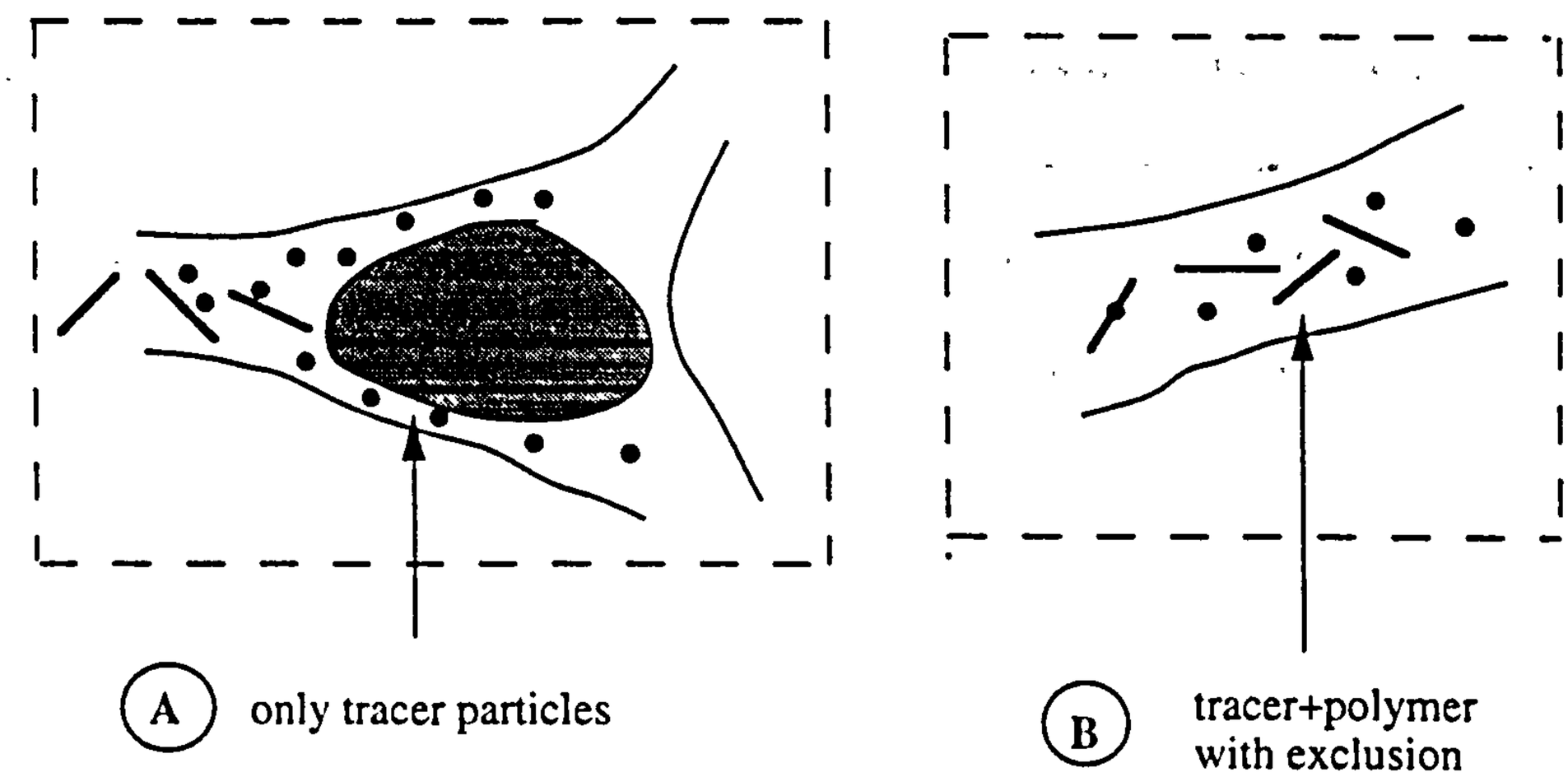

Figure 8.3 Diagram schematically showing the flow behaviours of polymers and tracers in two phase flow

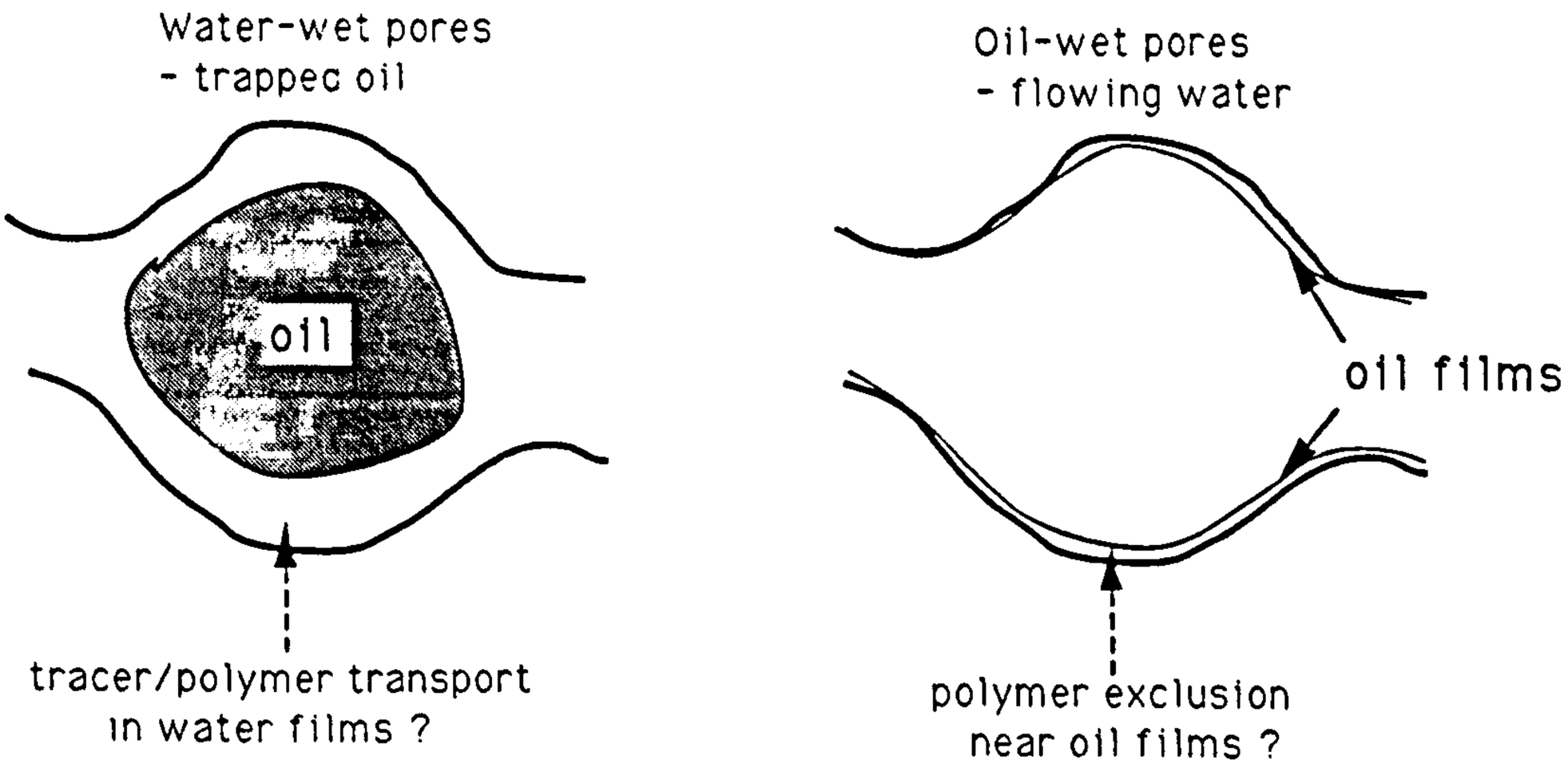

Figure 8.4 Schematical diagram of tracer/polymer transport in different wetttability pores in two phase flow

effect would be much more pronounced than if the medium were oil wet. Thus, if a polymer/tracer slug was injected into the flowing aqueous phase, then quite different transport behaviour is predicted for cases of different wettability (unpublished work, also see Figure 8.1).

In order to establish whether this procedure of using mixed polymer/tracer diagnostic floods will be able to probe the morphology and connectedness of the flowing aqueous phase, a series of very careful experiments must be carried out. These floods will involve setting up the equivalent of a steady state relative permeability experiment with selective polymer/tracer injection into the aqueous phase. The effluents from these floods must be analysed by using network modelling incorporating some of the effects discussed above. Effluent analysis should be directed at assessing this mixed tracer method for probing the pore space occupied by the aqueous phase. If this study is successful, the deliverable will be a new technique for analysing multiphase flow in porous media.

APPENDIX A

DEPLETED LAYER MODELS

The exclusion of macromolecules from the region of the pore wall is an entropic effect driven by the fact that the molecule has many more orientations available to it away from the wall than close to it. This lower viscosity depleted layer close to the pore wall where the shear stress is highest during flow, results in an apparent slip effect causing the apparent viscosity to be *lower* than the bulk viscosity. Two simple models describing this effect - the two fluid and linear layer models - for the concentration distribution in a cylindrical pore are shown in Figure 2.8. There are also two variants of the linear layer model depending on certain ancillary assumptions concerning the wall viscosity, η,The apparent viscosity in the low flow rate (Newtonian) regime can be derived analytically for these simple models (Two Fluid I, Two Fluid II, and Linear layer) and are as follows (all terms are listed at the end of this Appendix):

(i) **Two Fluid Model I** (Chauveteau et al, 1981; 1982; 1984; 1989)

$$\eta_{app} = \eta_w[1-(1-\frac{\eta_w}{\eta_b})(1-\frac{\delta}{r})^4]^{-1} \qquad [A1]$$

$$\text{where } \eta_w = \frac{(\eta_b+\eta_s)}{2}$$

(ii) **Two Fluid Model II** (Chauveteau et al, 1981; 1982; 1984; 1989)

$$\frac{\eta_b}{\eta_{app}} = 1+4(1-\beta)\frac{\delta}{r}C_b[\eta]_0 + 0(\frac{\delta}{r}C_b[\eta]_0)^2 \qquad [A2]$$

$$\text{where } \beta = 0.64$$

(iii) The Linear Layer Depletion Model (Sorbie et al, 1990; 1991)

Using the notation in Figure 2.8 (b), the concentration profile in the linear layer model is as follows:

$$C(x) = \begin{cases} C_b & 0 \le x \le R_1 \qquad [A3-1a] \\ C_b\left(\dfrac{R_2 - x}{\delta}\right) & R_1 \le x \le R_2 \qquad [A3-1b] \end{cases}$$

where x is the radial coordinate and we identify the pore radius, r , with R_2, the capillary radius and $\delta = R_2 - R_1$. If the viscosity is linearly dependent on concentration, the corresponding viscosity profile is:

$$\eta(x) = \begin{cases} \eta_b & 0 \le x \le R_1 \qquad [A3-2a] \\ \eta_b - (\eta_b - \eta_s)\left(\dfrac{x - R_1}{\delta}\right) & R_1 \le x \le R_2 \qquad [A3-2b] \end{cases}$$

in the Newtonian flow regime. For this model, it has been shown (Sorbie, 1990a) that the apparent viscosity, η_{app}, in given by:

$$\eta_{app} = \frac{R_2^4}{\xi_1 + \xi_2} \qquad [A3-3]$$

where ξ_1 and ξ_2 are expressions associated with flow in the inner and outer (depleted layer) regions as follows:

$$\xi_1 = \frac{R_1^2}{\eta_b}[R_1 - 2\kappa] \qquad [A3-4]$$

and

$$\xi_2 = \frac{8\tilde{\beta}\eta_s^2}{A^2}\left[b - \frac{1}{4} - \frac{1}{2}\left(\frac{\eta_b}{\eta_s}\right)^2\left\{\ln\left(\frac{\eta_b}{\eta_s}\right) - \frac{1}{2}\right\} + b\left(\frac{\eta_b}{\eta_s}\right)\left\{\ln\left(\frac{\eta_b}{\eta_s}\right) - 1\right\}\right]$$

$$-\frac{8}{A}\left[\frac{R_2R_1^2}{2} - \frac{R_1^3}{3} - \frac{R_2^3}{6}\right] \qquad [A3-5]$$

The ancillary variables $\tilde{\beta}$, A, κ and b are given by:

$$A = -\frac{(\eta_b - \eta_s)}{\delta} \qquad [A3-6]$$

$$\tilde{\beta} = \frac{\eta_b - AR_1}{A^2} \qquad [A3-7]$$

$$\kappa = 2\eta_b\left\{\frac{\delta^2}{(\eta_b - \eta_s)} - \tilde{\beta}\ \ln\left(\frac{\eta_b}{\eta_s}\right)\right\} \qquad [A3-8]$$

and

$$b = \frac{\eta_b - AR_1}{\eta_s} \qquad [A3-9]$$

Although the total expression for η_{app} in the linear layer model is quite complex compared with Eq. [A1] and [A2] for the two fluid model, it only depends functionally on η_b, η_s and δ. No additional models are required such as that to find η_w in the two fluid model. The above expressions are also very easily programmed and very straightforward to apply in practice. For further discussion of the linear layer and other related models , see references (Sorbie, 1990).

Nomenclature for the Depleted layer Models

C_b bulk polymer concentration

C_w wall polymer concentration

r cylindrical pore radius or average hydraulic radius

β concentration ratio, C_w/C_b

δ depleted layer thickness

δ/r relative depleted layer thickness

η_{app} apparent viscosity

η_b bulk viscosity

η_s solvent viscosity

η_w wall viscosity

$[\eta]_o$ intrinsic viscosity at low shear rate

APPENDIX B

A MODIFIED TWO-FLUID FLOW MODEL FOR THE DEPLETED LAYER EFFECT

B.1 Introduction

When xanthan solution flows through various porous media, a depleted layer effect is observed. The simple analysis of some previous results by Huang and Sorbie, using the Chauveteau two-fluid model or Sorbie linear-layer model (Appendix A) showed that the relative depleted layer thickness, δ/r, **apparently** decreased with increasing polymer concentration over a low concentration region of 30 to 160 mg/l (ppm) (Chapter 4). The observed apparent slip phenomenon in the experiments is certainly a result of the wall exclusion effect. However, the explanation of the concentration behaviour of (δ/r) is still speculative.

In this Appendix, we present a possible model of this behaviour based on a semi-empirical relationship between the wall and bulk fluids. If the relative depleted layer thickness (δ/r) is really *constant* as a function of polymer concentration, then we will show that this has implications for the form of the C_w - C_b relationship; that is, it will affect the calculation of the effective near-wall concentration in the depletion layer, C_w. This matter was first discussed by Chauveteau and an approximate relation was proposed. The later linear-layer model of Sorbie attempted to get round this issue but was still an approximation. In the presence of adsorption as well as surface exclusion, it is not clear exactly what the form of the C_w - C_b relationship should be. Here, we simply explore the consequences of one particular analytical form which is consistent with the experimental observations. However, we note that this *may* be related to the simultaneous adsorption effect but the model cannot be attributed to this unambiguously.

B.2 Statement of the Problem

There is a competitive process of attraction and exclusion between the polymer molecules and the pore wall when polymer flows through porous media. However, the original models used for estimating the relative depleted layer thickness did not consider the effect of polymer adsorption which is, in turn, related to the polymer concentration. The central problem of the simplest model for adsorption is as follows: If polymer concentration in the wall region, C_w, is just directly proportional to the bulk concentration, C_b, i.e.

$$C_w = \beta C_b \qquad [B1]$$

as shown in Chauveteau's two-fluid flow model (see Eq. [B4] below), then this predicts a decreasing (δ/r) with concentration.

B.3 The Modified Model

We may summarise all of the complexity of adsorption and depletion by the following simple extension of Eq. [B1],

$$C_w = \beta' C_b^x \qquad [B2]$$

where x is a constant, $1 \le x \le 2$. We will explore the physical consequences of this assumption below. First we write the relationship in Eq. [B2] as:

$$C_w = kC_b^{1+a} \qquad [B3]$$

where $0<a<1$. Now let us return to Chauveteau's two-fluid flow model (two fluid model II in Appendix A) as shown below,

$$\frac{\eta_b}{\eta_{app}} = 1 + 4(1-\beta)\frac{\delta}{r}C_b[\eta] \qquad [B4]$$

where η_b and η_{app} are polymer bulk viscosity in viscometer and apparent viscosity in porous medium respectively. $[\eta]$ is the intrinsic viscosity of the polymer solution. β is a constant given by C_w/C_b. Under our condition, (Eq. [B3]), we have

$$\beta' = \frac{C_w}{C_b} = \frac{kC_b^{1+a}}{C_b} = kC_b^a \qquad [B5]$$

Eq. [B5] may now be substituted into [B4] to give

$$\frac{\eta_b}{\eta_{app}} = 1 + 4(1 - kC_b^a)\frac{\delta}{r}C_b[\eta] \qquad [B6]$$

or

$$\frac{\eta_b}{\eta_{app}} = 1 + 4\frac{\delta}{r}[\eta]C_b - 4k\frac{\delta}{r}[\eta]C_b^{1+a} \qquad [B7]$$

We can regard Eq. [B7] as an "extended" two-fluid flow model.

B.4 Comparison with Experimental Results

The easiest way to evaluate the constants, k and a, in Eq. [B7] is to rearrange by taking the log of each side as follows:

$$\log\left\{C_b + \frac{1}{4\frac{\delta}{r}[\eta]} - \frac{(\eta_b/\eta_{app})}{4\frac{\delta}{r}[\eta]}\right\} = \log k + (1+a)\log C_b \qquad [B8]$$

From previous work in Chapters 4 and 5, we know $[\eta] = 6.3 \times 10^{-3}$ l/mg (or 6,300 cm^3/g). Here the (δ/r) is now taken to be a *constant* which expresses the relative depleted layer thickness as pure exclusion from the pore wall. It can be obtained by

extrapolating the bulk concentration to zero in the curve of apparent δ/r as a function of C_b as shown in Figure 4.11; from these results, we find that δ/r = 0.342.

So Eq. [B8] can be written

$$\log\left\{C_b + 116\left(1 - \frac{\eta_b}{\eta_{app}}\right)\right\} = \log k + (1+a)\log C_b \qquad [B9]$$

The experimental data of C_b, η_b and η_{app} are listed in Table B.1. Figure B.1 shows the plot of log{f} vs logC_b with f defined as follows,

$$f = C_b + 116\left(1 - \frac{\eta_b}{\eta_{app}}\right) \qquad [B10]$$

Figure B.1 shows a very good linear relation between log{f} and logC_b. From the results in Figure B.1, we obtain that

lg k = -0.36026, and k = 0.436;

1+a = 1.124, and a = 0.124.

Therefore, Eq. [B3] may be rewritten

$$C_w = kC_b^{1+a} = 0.436C_b^{1.124} \qquad [B11]$$

Eq. [B11] enables us to evaluate the wall concentration, C_w. The results are listed in Table B.1. These data are compared with data obtained by using Eq. [B1] (β = 0.64 from Chauveteau) in Figure B.2. It is clear that, in the pore wall region (depleted layer) the wall polymer concentration, C_w, is increasing *slightly* faster than linearly with bulk concentration, C_b. This is one possible explanation for why the apparently relative depleted layer thickness seems to be decreasing with bulk concentration from the old model calculations. We also found that constant k = 0.436 in Eq. [B3] is less than β =

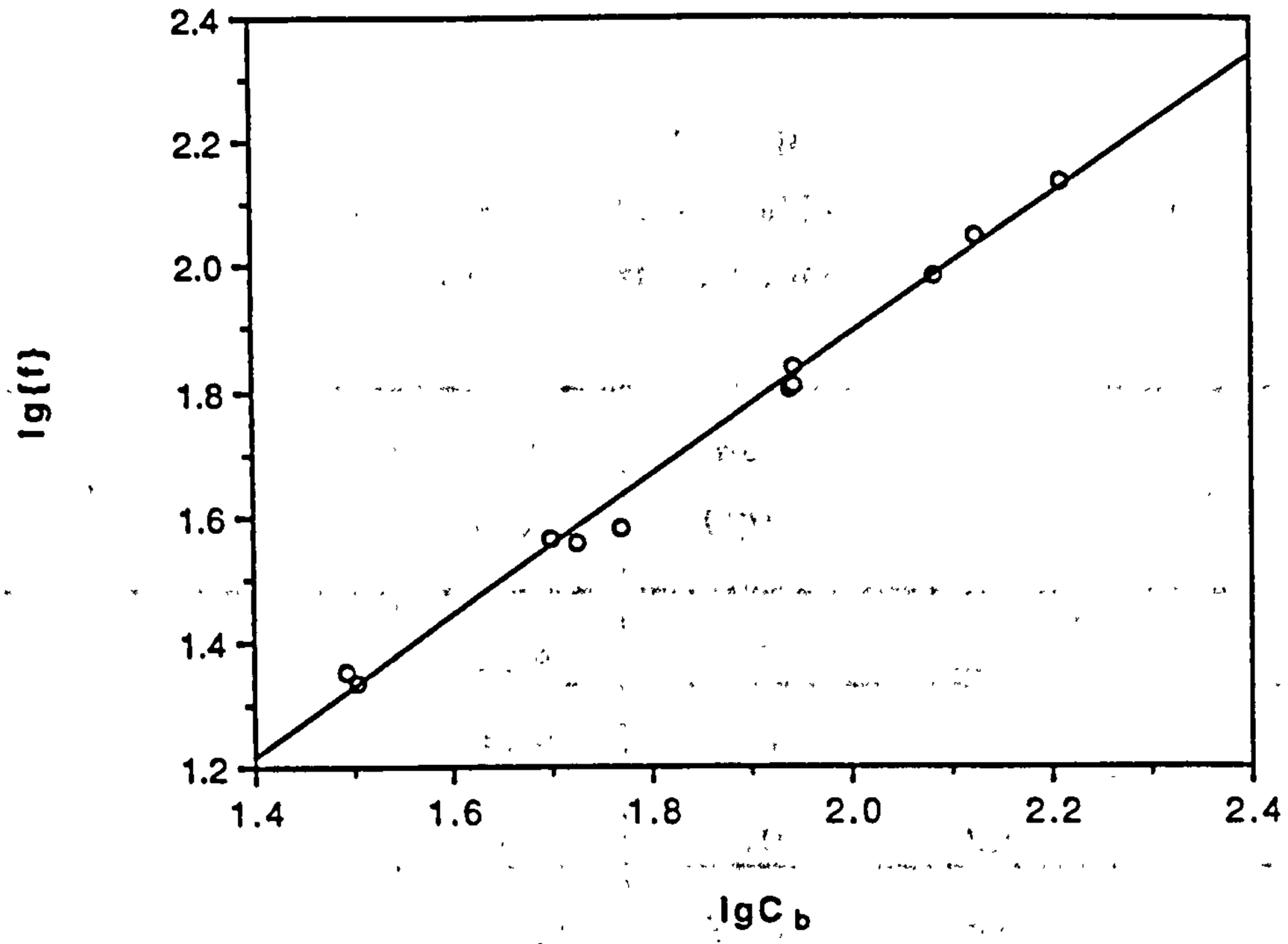

Figure B.1 log{f} as a function of log C_b based on Eqs. [B9] and [B10]

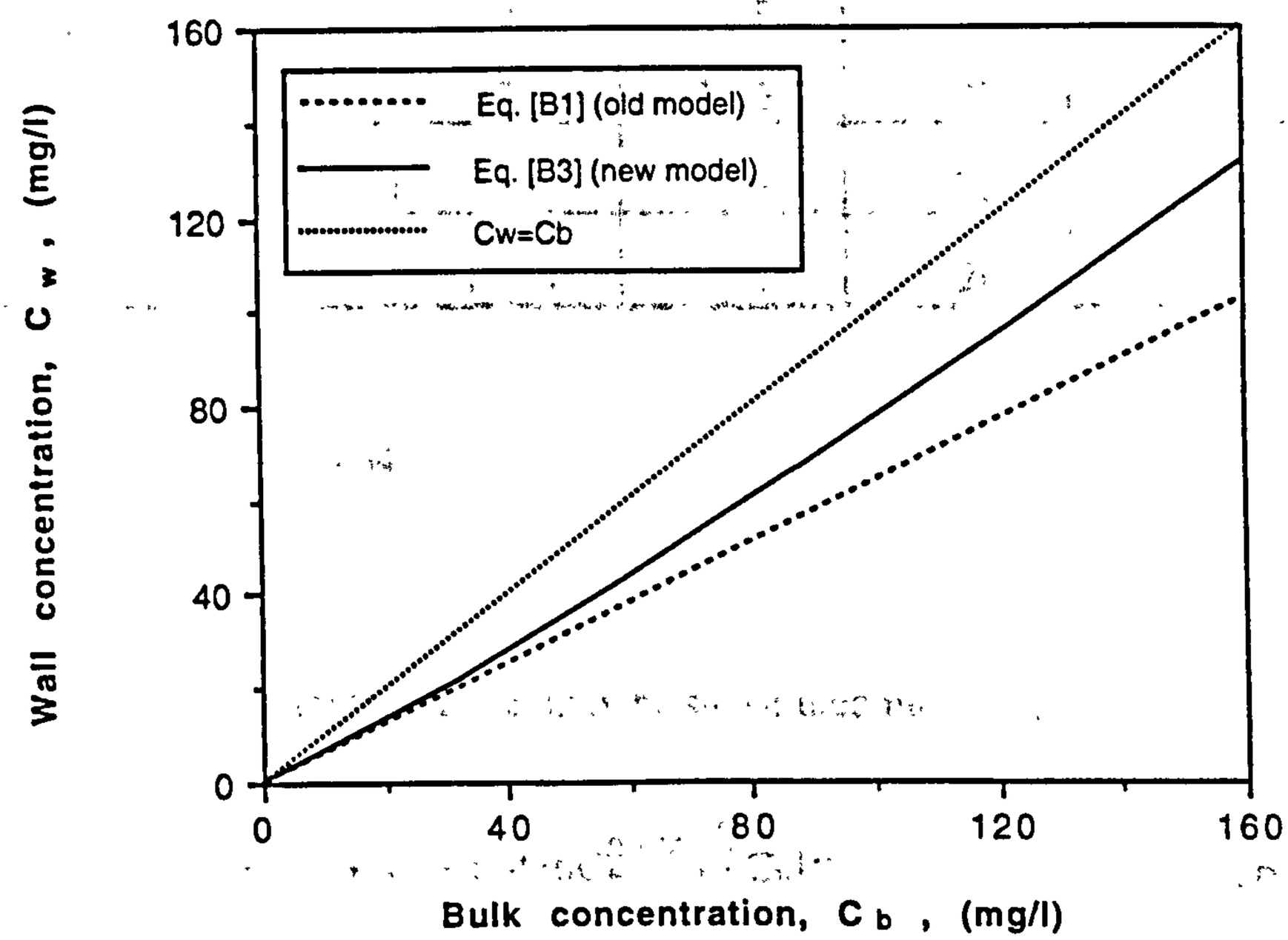

Figure B.2 A comparison of xanthan concentration, C_w in depleted layer region evaluated by old model (Eq. [B1]) and modified model (Eq. [B3]

0.64 in Eq. [B1] implying that real C_w in Eq. [B3] at very low C_b (say $C_b < 22$ mg/l) may be less than the apparent C_w in Eq. [B1].

Table B.1
Comparison of the Original Two-Fluid Depleted Layer Model (Eq. [B4])
with the Extended Model (Eq. [B7])

Exp. No	C_b (mg/l)	C_w* (mg/l)	η_b (cp)	η_{app} (cp)	δ/r**	δ/r***
1	32	21.4	1.32	1.21	0.308	0.342
	53	37.8	1.57	1.37	0.299	0.381
	88	66.8	2.10	1.80	0.205	0.313
	134	107.2	3.06	2.57	0.154	0.283
2	31	20.7	1.31	1.22	0.258	0.284
	59	42.7	1.65	1.40	0.328	0.433
	88	66.8	2.10	1.74	0.254	0.388
	122	96.5	2.76	2.27	0.192	0.336
3	50	35.4	1.53	1.37	0.253	0.318
	87	66.0	2.08	1.73	0.252	0.382
	163	133.7	3.90	3.20	0.146	0.296

* Eq. [11]
** Eq. [4], $\beta = 0.64$
*** Eq. [12]

The obtained constants, k and a, may be substituted into Eq. [B6] to give

$$\frac{\eta_b}{\eta_{app}} = 1 + 4(1 - 0.436C_b^{0.124})\frac{\delta}{r}C_b[\eta] \qquad [B12]$$

for our experimental system. Eq. [B12] may be written

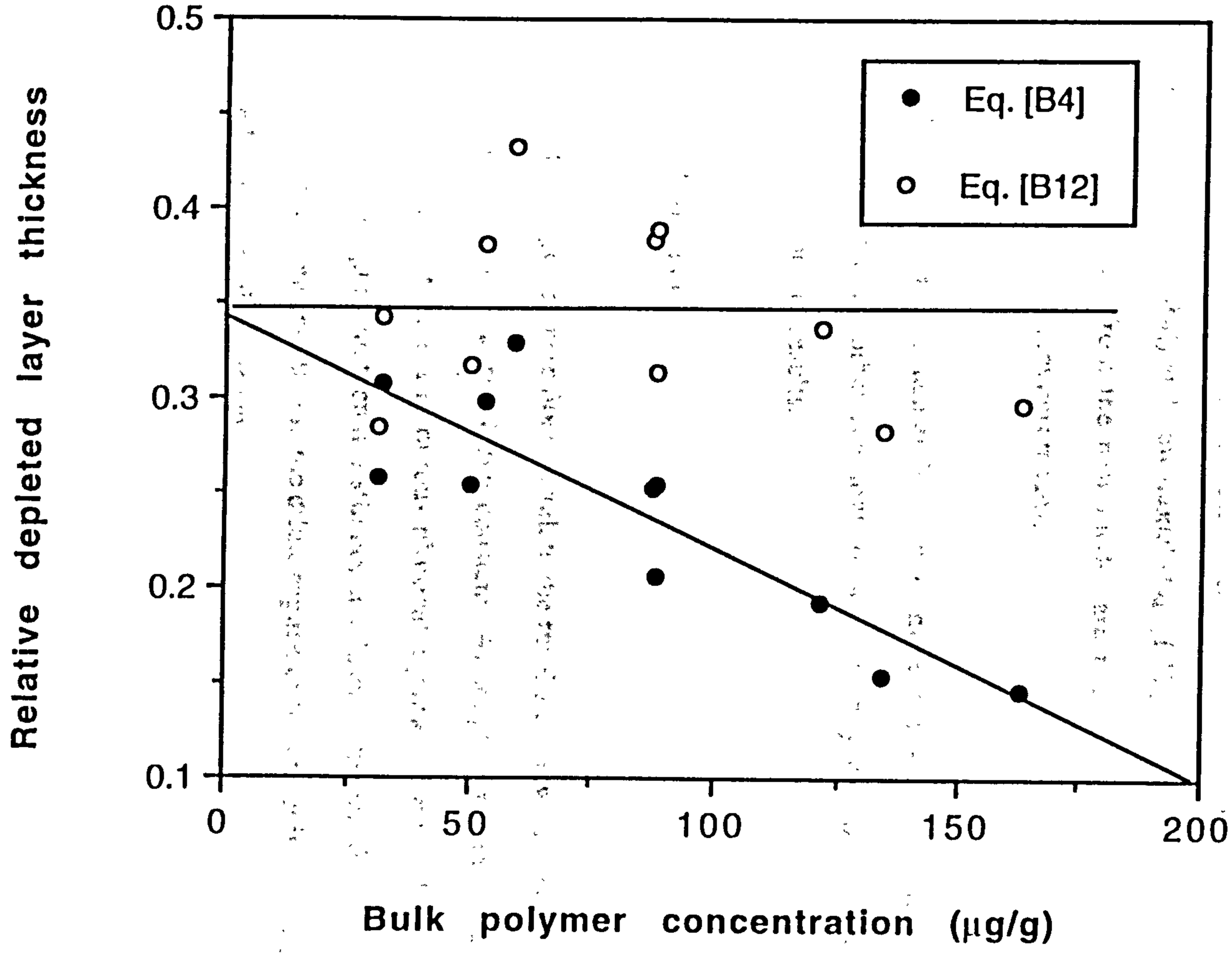

Figure B.3 A comparison of the plots of $\delta'r$ vs C_b as calculated using both the old and modified two-fluid flow models

$$\frac{\delta}{r} = \frac{(\eta_b / \eta_{app}) - 1}{4\left(1 - 0.436 C_b^{0.124}\right) C_b[\eta]} \qquad [B13]$$

Based on Eq. [B13], the relative depleted layer thickness are evaluated and are shown in Table I, where they are also compared with previous results calculated using Eq. [B4]. A comparison of relative depleted layer thickness, δ/r, as a function of bulk concentration, C_b, using old model (Eq. [B4]) and new model (Eq. [B12]) is also shown in Figure B.3. The δ/r values calculated from the new model are nearly constant with increasing concentration compared with previous results.

At high xanthan concentration, such as 400 ppm or more, the polymer flow behaviour is more complicated. That is, other rheological non-linearity can be observed which confuses the interpretation of results.

B. 5 Closing Remarks

The simple model suggested here does correlate the results quite well if we assume that the relative depleted layer thickness (δ/r) is constant. Although this model is satisfactory in this respect, we do not have a rigourous physical argument for it. Unless we can some up with such an argument, then it is still not conclusive whether (δ/r) does *actually* decrease with polymer concentration in the dilute regime or the effect is a consequence of adsorption and (δ/r) is really constant.

REFERENCES

Ash, S. G., Clarke-Sturman, A. J., Calvert, R. and Nisbet, T.M., Paper SPE12085, Proc. of the 58th SPE Annual Technical Conference and Exhibition,San Francisco, CA, 1983

Aubert, J.H., Tirrell, M., and Chauveteau, G., " The Concentration Dependence of the Effective Viscosity of Polymer Solutions in Small Pores", Abstracts of Papers of American Chemical Society, Vol. 184, (1982) 15-16

Ausséré, D., Hervet, H. and Rondelez, F., "Concentration Dependence of the Interfacial Depletion Layer Thickness for Polymer Solutions in Contact with Nonadsorbing Walls", Macromolecules, Vol. 19, (1986) 85-88

Ausséré, D., Edwards, J., Lecourtier, J., Hervet, H. and Rondelez, F., "Hydronamic Thickening of Depletion Layers in Colloidal Solutions", Europhys. Lett., Vol 14, No. 1 (1991) 33-38

Auvray, L., "Solutions de macromolecules rigides: effets de paroi, de confinement et d'orientation par un ecoulement", J. Physique, Vol. 42 (1981) 79

Bagassi, M., Chauveteau, G., Lecourtier, J., Englert, J., and Tirrell, M., "Behavior of Adsorbed Polymer Layers in Shear and Elongational Flow", Macromolecules, Vol. 22 (1989) 262-266

Baviére, M., "Basic Concepts in Enhanced Oil Recovery Processes. Critical Reviews in Applied Chemistry", Elsevier Applied Science Publishers Ltd., London, 1991

Berge, L. I., Feder, J. and Jossang, T., "Rheology of Particles in Xanthan Solutions Flowing through a Single Pore", J. Colloid and Interface Science, Vol. 139, No. 1 (1990) 295

Bird, R.B., Armstrong, R.C. and Hassager, O., "Dynamics of Polymeric Liquids - Volume 1: Fluid Mechanics", Second Edition, John Wiley and Sons, New York, 1987

Bird, R. B., Stewart, W. E. and Lightfoot, E. N. "Transport Phenomena", Wiley, New York (1960)

Bolt, G. H., "Determination of the Charge Density of Silica Sols", J. Phys. Chem., Vol. 61, (1957) 1166

Broseta, D., Medjahed, F., Lecourtier, J., and Robin, M., "Polymer Adsorption/Retention in Porous Media: Effects of Core Wettability and Residual Oil", Paper SPE 24149, Proc. of the 8th SPE/DOE Symposium on EOR, Tulsa, OK, 1992

Brown, W. D., and Sorbie, K. S., "Dispersion and Polydispersity Effects in the Transport of Xanthan in Porous-Media", Macromolecules, Vol. 22, No. 6 (1989) 2835

Bryant, K. C., J. Chem. Soc., 3017 (1952)

Cannella, W.J., Huh, C. and Seright, R. S., "Prediction of Xanthan Rheology in Porous Media" Paper SPE18089, Proc. of the 63rd SPE Annual Technical Conference and Exhibition, Houston, TX, 1988.

Carreau, P. J., Trans. Soc. Rheol. Vol 16, (1972) 99-127

Chang, H. L., "Polymer Flooding Technology - Yesterday, Today and Tomorrow", J. Pet. Tech., (August 1978) 1113

Chauveteau, G., "Rodlike Polymer Solution Flow through Fine Pores: Influence of Pore Size on Rheological Behavior", J. Rheology, Vol. 26, (1982) 111-142

Chauveteau, G., "Fundamental criteria in polymer flow through porous media and their relative importance in the performance differences of mobility control buffers", in "Water Soluble Polymer", ed. J. E. Glass, *Advances in Chemistry* Series of the American Chemical Society, Vol. 213 (1986) 227-268

Chauveteau, G. and Kohler, N., "Influence of Microgels in Xanthan Polysaccharide Solutions on Their Flow through Various Porous Media", SPEJ (June 1984) 361-368

Chauveteau, G., and Lecourtier, J., "Propagation of Polymer Slugs through Adsorbent Porous Media", in "Water Soluble Polymers for Petroleum Recovery", Eds. G. A. Stahl and D. N. Schulz, Plenum Publishing Corp., New York, 1988

Chauveteau, G. and Zaitoun, A., "Basic Rheological Behaviour of Xanthan Polysaccharide Solutions in Porous Media: Effects of Pore Size and Polymer Concentration", Proc. of the First European Symposium on Enhanced Oil Recovery, Bournemouth, England, Elsevier, Ed. F.J. Fayers, 1981.

Chauveteau, G., Delaplace, Ph., Argillier, J.F., Bagassi, M., and Léger, L., "Mechanisms of Flow-Induced Polymer Retention in Porous Media", Proc. of the 6th IFP Research Conference on Exploration and Production, Saint-Raphael, France, 4-6 September, 1991

Chauveteau, G., Tirrell, M., and Omari, A., "Concentration Dependence of the Effective Viscosity of Polymer Solutions in Small Pores with Repulsive or Attractive Walls", J. Colloid and Interface Science, Vol. 100 (1984) 41

Claridge, E. L., "A method for designing graded viscosity banks", Soc. Pet. Eng. J. (October, 1978) 315

Davison, P. and Mentzer, E., "Polymer Flooding in North Sea Reservoirs", Soc. Pet. Eng. J. (June 1982) 353-362

Dawson, R., and Lantz, R.B., "Inaccessible Pore Volume in Polymer Flooding", Soc. Pet. Eng. J. (October 1972) 448-452

de Gennes, P. G., "Scaling Concepts in Polymer Physics", Cornell University Press, Ithaca and London, 1979.

Elaissari, A., and Pefferkorn, E., "Polyelectrolyte Induced Aggregation of Latex Particles: Influence of the Structural Relaxation of Adsorbed Macromolecules on the Colloid Aggregation Mode", J. Colloid and Interface Science, Vol. 141, No. 2 (1991a) 522-533

Elaissari, A., and Pefferkorn, E., "Polyelectrolyte Adsorption at Solid / Liquid Interfaces: A Simple Model for the Structural Relaxation and Excluded Area Effects", J. Colloid and Interface Science, Vol. 143, No. 1 (1991b) 85-91

Elaissari, A., and Pefferkorn, E., "Aggregation Model of Colloids in the Presence of Block Copolymer Micelles", J. Colloid and Interface Science, Vol. 143, No. 2 (1991c) 343-355

Fletcher, A.J.P., Flew, S.G., Lamb, S.P., Lund, T., Bjørnestad, E.O., Stavland, A., and Gjøbikli, N.B., "Measurements of Polysaccharide Polymer Properties in Porous Media", Paper SPE 21018, Proc. of the SPE International Symposium on Oilfield Chemistry, Anaheim, California, 20-22 February, 1991

Fried, J. J., and Combarnous, M. A., "Dispersion in Porous Media", Adv. Hydrosci., Vol. 7 (1971) 170

Fried, J. J., "Groundwater Pollution", Elsevier Scientific Publishing Company, Amsterdam, 1985

Gogarty, W. B., "Mobility Control with Polymer Solutions", Soc. Petroleum Engineers J., Vol. 7 No. 2 (1967) 161

Goodyear, S. G., Johnston, J. D., Lawless, T. A., and Woods, C. L., "Measurement of Polymer Retention Levels Representative of the Formation", Paper SPE/DOE 24155, Proc. of the 8th SPE/DOE Symposium on Enhanced Oil Recovery, Tulsa, OK, 1992

Greaves, M., and Patel, K., "Flow of Polymer-Solution in Porous-Media", Chem. Eng. Res. Des., Vol. 63, (1985) 199

Gupta, S. P., and Trushenski, S. P., "Micellar Flooding - The Propagation of the Polymer Mobility Buffer Bank", Soc. Petroleum Engineers J., (February, 1978) 5-12

Haring, R. E. and Greenkorn, R. A., AIChE J., Vol. 16 (1970) 477

Hejri, S., Willhite, G.P., and Green D.W., "Development of Correlations to Predict Flocon 4800 Biopolymer Mobility in Porous Media", Paper SPE/DOE 17396, Proc. of the 6th SPE/DOE Symposium on Enhanced Oil Recovery, Tulsa, OK, 1988

Heston, W. M., Iler, R. K., and Stears, G. W., "The Adsorption of Hydroxyl Ions from Aqueous Solution on the Surface of Amorphous Silica", J. Phys. Chem., Vol. 64, (1960) 147

Hoagland, D. A., "Concentration Profiles of Rod-like Polymers in Narrow Channels", J. Colloid and Interface Science, Vol. 123, (1988) 117

Holzwarth, G., "Conformation of the Extracellular Polysaccharide of Xanthomonas campestris", Biochemstry , Vol. 15, (1976) 4333

Huang, Y., and Sorbie, K. S., "The Adsorption and In Situ Rheological Behaviour of Xanthan Solution Flowing through Porous Media" Paper SPE/DOE 24153, Proc. of the 8th SPE/DOE Symposium on Enhanced Oil Recovery, Tulsa, OK, 1992

Huang, Y., and Sorbie, K. S., "Scleroglucan Behaviour in Flow through Porous Media: Comparison of Adsorption and In Situ Rheology with Xanthan" Paper SPE 25173, Proc. of the SPE International Symposium on Oilfield Chemistry, New Orleans, Louisiana, 2-5 March, 1993

Huang, Y., Sorbie, K. S. and Chauveteau, G., "A Modified Two-Fluid Flow Model for the Depleted Layer Effect", work in progress, 1993

Huang, Y., Yang, P., and Qin, T., "A Study on the Dynamic Interfacial Tension of Acidic Crude Oil/Alkali (Alkali-Polymer) Systems", In Situ, Vol. 13, No. 4 (1989) 259

Huh, C., Lange, E. A., and Cannella, W. J., "Polymer Retention in Porous Media", Paper SPE/DOE 20235, Proc. of the 7th SPE/DOE Symposium on EEnhanced Oil Recovery, Tulsa, OK, 1990

Iler, R. K., " The Chemistry of Silica", John Wiley & Sons, New York, 1979

Jansson P. E., Kenne, L., and Lindberg, B., "Structure of the Extracellular Polysaccharide from Xanthomonas campestris", Carbohydrate Research, Vol. 45 (1975) 275-282

Kohler, N., and Chauveteau; G., "Xanthan Polysaccharide Plugging Behavior in Porous Media - Preferential Use of Fermentation Broth", J. Pet. Technol. Feb., (1981) 349

Kolodziej, E. J. , "Mechanism of Microgel Formation in Xanthan Biopolymer Solutions", Paper SPE 16730, Proc. of the 62nd SPE Annual Technical Conference and Exhibition, Dallas, TX, 1988a.

Kolodziej, E. J. , "Transport Mechanisms of Xanthan Biopolymer Solutions in Porous Media", Paper SPE 18090, Proc. of the 63rd SPE Annual Technical Conference and Exhibition, Houston, TX, 1988b

Lake, L. W., "Enhanced Oil Recovery", Prentice Hall, New Jersey, 1989

Layec, Y., and Wolff, C., "Sur la Viscosite Intrinseque non-Newtonienne de Solutions d'ellipsoides Rigides", Rheol. Acta., Vol. 13 , (1974) 696

Lecourtier, J., and Chauveteau, G., "Xanthan Fraction by Surface Exclusion Chromatography", Macromolecules, Vol. 17, No. 7 (1984a) 1340-1343

Lecourtier, J., and Chauveteau, G., "Propagation of Polymer Slugs Through Porous Media", Paper SPE 13034, Proc. of the 59th SPE Annual Technical Conference and Exhibition, Houston, TX, 1984 b

Lecourtier, J., and Chauveteau, G., "Adsorption des Polyacrylamides et des Xanthane sur des Surface Minerales", Proc. of the 3rd European Symposium on Enhanced Oil Recovery, Rome, Italy, 16-18 April 1985

Lecourtier, J., Chauveteau, G., and Muller, G.,"Salt-induced Extension and Dissociation of a Native Double-Stranded Xanthan", Int. J. Biol. Macromol., Vol. 8, (1986) 306-310

Lecourtier, J., Rivenq, R., Delaplace, P., Lemonnier, P., Hagry, J. P., and Lefevre, D., "An Innovative Polymer Flooding Simulator Based on Advanced Concepts in Polymer Physics", Paper SPE/DOE 24150, Proc. of the 8th SPE/DOE Symposium on Enhanced Oil Recovery, Tulsa, OK, 1992

Liauh, W. C., Duda, J. L., and Klaus, E. E., "An Investigation of the Inaccessible Pore Volume Phenomenon", AIChE Symposium Series 212, Vol. 78, (1982) 70-76

Littmann, W., Kleinitz, W., Christensen, B. E., Stokke, B. T., and Haugvallstad, T., "Late Results of a Polymer Pilot Test: Performance, Simulation Adsorption, and Xanthan Stability in the Reservoir", Paper SPE/DOE 24120, Proc. of the 8th SPE/DOE Symposium on Enhanced Oil Recovery, Tulsa, OK, 1992

Lund, T., Bjφrnestad, E. Φ., Stavland, A., Gjφvikli, N. B., Fletcher, A. J. P., Flew, S. G., and Lamb, S. P., "Polymer Retention and Inaccessible Pore Volume in North Sea Reservoir Material", Proc. of the 6th European Symposium on Enhanced Oil Recovery, Stavanger, 21-23 May, 1991

Marle, C. M., "Oil Entrapment and Mobilization", in "Basic Concepts in Enhanced Oil Recovery Processes", Ed. M. Baviere, Elsevier Applied Science, London and New York, 1991

Muller, G., Anrhourrache, M., Lecourtier, J., and Chauveteau, G., "Salt Dependence of the Conformation of a Single-Stranded Xanthan", Int. J. Biol. Macromol., Vol. 8, (June 1986) 167-172

Muller-Mohnssen, H., Weiss, D., and Tippe, A., "Concentration Dependent changes of Apparent Slip in Polymer Solution Flow", J. Rheol. Vol 34, No 2 (1990) 223-244

Omari, A., Moan, M., and Chauveteau, G., "Hydrodynamic Behavior of Semirigid Polymer at a Solid-Liquid Interface", J. Rheology, Vol. 33, (1989) 1-13

Pefferkorn, E., and Elaissari, A., "Adsorption-Desorption Processes in Charged Polymer / Colloid Systems; Structural Relaxation of Adsorbed Macromolecules", J. Colloid and Interface Science, Vol. 138, No. 1 (1990) 187-194

Pye, D. J., "Improved Secondary Recovery by Control of Water Mobility", J. Petroleum Technol., Vol. 16 (August 1964) 911

Reppert, T. R., Bragg, J. R., Wilkinson, J. R., Snow, T. M., Maer, N. K. Jr., and Gale, W. W., "Second Ripley Surfactant Flood Pilot Test", Paper SPE/DOE 20219, Proc. of the 7th SPE/DOE Symposium on Enhanced Oil Recovery, Tulsa, OK, 1990

Richards, E. G. "An Introduction to Physical Properties of Large Molecules in Solution" IUPAB Biophysics Series, Cambridge University Press, Cambridge, UK

Rinaudo, M., and Milas, M., "Polyelectrolyte Behavior of a Bacterial Polysaccharide from Xanthomonas campestris: Comparison with Carboxymethylcellulose", Biopolymers Vol. 17, (1978) 2663

Rivenq, R., Donche, A., and Noik, C., "Improved Scleroglucan for Polymer Flooding under Harsh Reservoir Conditions", Paper SPE19635, Proc. of the 64th SPE Annual Technical Conference and Exhibition, San Antonio, TX, 1989

Sandiford, B. B., "Laboratory and Field Studies of Waterfloods Using Polymer Solutions to Increase Oil Recovery" Petroleum Trans. AIME, Vol. 231 (1964) 917

Sato, T., Norisuye, T., and Fujita, H., "Double-Stranded Helix of Xanthan in Dilute-Solution-Evidence from Light-Scattering", Polym. J., Vol. 16, No. 4 (1984) 341-350

Savins, J. G., "Non-Newtonian Flow Through Porous Media", Ind. Eng. Chem. Vol. 61, (1969) 18

Seright, R. S., and Henrici, B. J., Paper SPE/DOE 14946, Proc. of the SPE/DOE 5th Symposium on Enhanced Oil Recovery, Tulsa, OK, 1986

Shah. B. N., Willhite, G. P. and Green. D. W., Paper SPE7586, Proc. of the 53rd SPE Annual Technical Conference and Exhibition, Houston, TX, 1978

Shatwell, K. P., Sutherland, I. W., and Ross-Murphy, S. B. "Influence of Acetyl and Pyruvate Substituents on the Solution Properties of Xanthan Polysaccharide", Int. J. Macromol., Vol. 12 (April, 1990) 71-78

Shatwell, K. P., Sutherland, I. W., Dea, I. C. M. and Ross-Murphy, S. B. "The Influence of Acetyl and Pyruvate Substituents on the Helix-Coil Transition Behaviour of Xanthan", Carbohydrate Research, Vol. 206 (1990) 87-103

Sho, T., Sato, T., and Norisuye, T., "Viscosity Behaviour and Persistence Length of Sodium Xanthan in Aqueous Sodium Chloride", Biophysical Chemistry Vol. 25, (1986) 307-313

Sorbie, K.S., "A Critical Analysis of Models Describing the In-Situ Rheology of Polymers in Porous Media", Proc. of the 5th European Symposium on Enhanced Oil Recovery, Budapest, Hungary, 25-27 April, 1989a.

Sorbie, K.S., "Network Modelling of Xanthan Rheology in Porous Media in the Presence of Depleted Layer Effects" Paper SPE19651, Proc. of the 64th SPE Annual Technical Conference and Exhibition, San Antonio, TX; 1989b.

Sorbie, K.S., "Depleted Layer Effects in Polymer Flow through Porous Media: I. Single Capillary Calculations", J. Colloid and Interface Science, Vol. 139, (1990a) 299-314

Sorbie, K.S., "Depleted Layer Effects in Polymer Flow through Porous Media: II. Network Calculations", J. Colloid and Interface Science, Vol. 139, (1990b) 315-323

Sorbie, K.S., "Polymer Improved Oil Recovery", Blackie and Son, Glasgow, 1991

Sorbie, K. S., and Clifford, P. J., "The Inclusion of Molecular-Diffusion Effects in the Network Modeling of Hydrodynamic Dispersion in Porous-Media", Chem. Eng. Sci. Vol. 46, No. 10 (1991) 2525-2542

Sorbie, K.S., and Huang, Y., "Rheological and Transport Effects in the Flow of Low-Concentration Xanthan Solution Through Porous Media ", J. Colloid and Interface Science, Vol. 145, No. 1 (1991) 74-89

Sorbie, K.S., and Huang, Y., "Depleted Layer Effects on the In Situ Rheological Behaviour of Xanthan Biopolymer", in "Physical Chemistry of Colloids and Interfaces in Oil Production", Eds. H. Toulhoat and J. Lecourtier, Editions Technip, Paris 1992a

Sorbie, K.S., and Huang, Y., "The Effect of pH on the Flow Behaviour of Xanthan Solution though Porous Media", J. Colloid and Interface Science, Vol. 149, No. 2 (1992b) 303-313

Sorbie, K.S., and Huang, Y., "Fundmentals of Macromolecular Flow in Porous Media" 1992 PSTI Technical Forum, Aberdeen, Scotland, 12-13 May, 1992c

Sorbie, K.S., Clifford, P.J., and Jones, E.R.W., "The Rheology of Pseudoplastic Fluids in Porous Media Using Network Modeling", J. Colloid and Interface Science, Vol. 130, (1989) 508-534

Sorbie, K. S., Parker, A. and Clifford, P. J., "Experimental and Theoretical Study of Polymer Flow in Porous Media", Soc. Pet. Eng. (Reservoir Engineering), (August 1987) 281-304

Southwick, J. G., Jamieson, A. M., and Blackwell, J., "Conformation of Xanthan Dissolved in Aqueous Urea and Sodium Chloride Solutions", Carbohydrate Research, Vol. 99 (1982) 117-127

Stokke, B. T., Elgsaeter, A., Bjφrnestad, E. Φ., and Lund, T., "Rheology of Xanthan and Scleroglucan in Synthetic Seawater", Carbohydrate Polymers Vol. 17 (1992) 209

Teeuw, D., and Hesselink, F. T., "Power-Law Flow and Hydrodynamic Behaviour of Biopolymer Solutions in Porous Media", Paper SPE 8982 Proc. of the 5th SPE International Symposium on Oilfield and Geothermal Chemistry, Stanford, CA, 1980

Tinland, B., and Rinaudo, M., "Dependence of the Stiffness of the Xanthan Chain on the External Salt Concentration" Macromolecules, Vol. 22, (1989) 1863-1865

van Genuchten, M. T., Research Report 119. U.S. Dept. of Agriculture Salinity Laboratory, Riverside, CA, (February 1981)

van Genuchten, M. T. and Alves, W. J., Tech. Bull. 1661, U.S. Dept. of Agriculture, Riverside, CA, (June 1982)

Wellington, S. L., "Biopolymer Solution Viscosity Stabilization - Polymer Degradation and Antioxidant Use", Soc. Pet. Eng. J., (December 1983) 901-912

Whitcomb, P. J., and Macosko, C. W., "Rheology of Xanthan Gum", J. Rheology, Vol. 22, No. 5 (1978) 493-505

Willhite, G.P., and Uhl, J.T., "Correlation of the Mobility of Biopolymer with Polymer Concentration and Rock Properties in Sandstone", Proc. ACS Division of PMSE, Vol. 55, September, (1986) 577

Yanaki, T., Kojima, T. and Norisuye, T., "Triple Helix of Scleroglucan in dilute aqueous solutions", Polymer J., Vol. 13 (1981) 1135

Zaitoun, A., and Kohler, N., "The Role Adsorption in Polymer Propagation through Reservoir Rocks", Proc. of the SPE International Symposium on Oilfield Chemistry, San Antonio, Texas, 4-6 February, 1987

Zhang, L., Liu, W., Norisuye, T., and Fujita, H., "Double-Stranded Helix of Xanthan: Rigidity in 0.01 M Aqueous Sodium Chloride Containing 0.01 N Hydrochloric Acid", Biopolymers, Vol 26, (1987) 333-341